A N N U A L R E P O R T

2007

and list of publications

Bayerisches Forschungsinstitut
für Experimentelle Geochemie und Geophysik
Universität Bayreuth

Bayerisches Geoinstitut
Universität Bayreuth
D-95440 Bayreuth
Germany

Telephone: +49-(0)921-55-3700
Telefax: +49-(0)921-55-3769
e-mail: bayerisches.geoinstitut@uni-bayreuth.de
www: http://www.bgi.uni-bayreuth.de

Editorial compilation by: Stefan Keyssner and Petra Buchert
Section editors: Andreas Audétat, Tiziana Boffa Ballaran, Leonid Dubrovinsky, Dan Frost, Florian Heidelbach, Hans Keppler, Catherine McCammon, Nobuyoshi Miyajima, Dave Rubie, Gerd Steinle-Neumann, Nicolas Walte

Staff and guests of the Bayerisches Geoinstitut in **July 2007**:

Die Mitarbeiter und Gäste des Bayerischen Geoinstituts im **Juli 2007**:

First row, from left (1. Reihe, v. links) Catherine McCammon, Polina Gavrilenko, Micaela Longo, Vincenzo Stagno

Second row, from left (2. Reihe, v. links) Sabrina Nazzareni, Lesley Rose-Weston, Eva Holbig, Elisabeth Herrmann, Enikő Bali, Olga Narygina, Juliane Hopf, Sophie Berthet, Ute Mann, Ashima Saikia, Jun Liu

Third row, from left (3. Reihe, v. links) Tiziana Boffa Ballaran, Anastasia Kantor, Nobuyoshi Miyajima, Dan Frost, Ahmed El Goresy, Karen Roscher, Uwe Dittmann, Holger Kriegl, Heinz Fischer

Fourth row, from left (4. Reihe, v. links) Petra Buchert, Shantanu Keshav, Florian Heidelbach, Falko Langenhorst, Kyusei Tsuno, Diego Bernini, Lydia Kison-Herzing, Alexander Kurnosov, Leonid Dubrovinsky

Fifth row, from left (5. Reihe, v. links) David Dolejš, Gudmundur Gudfinnsson, Lora Armstrong, Innokenty Kantor, Dave Rubie, Hans Keppler, Patrick Cordier, Thomas Locherer, Fabrizio Nestola

Sixth row, from left (6. Reihe, v. links) Stefan Keyssner, Gerd Ramming, Sven Linhardt, Stefan Übelhack, Toni Groß, Svyatoslav Shcheka, Andreas Audétat

Absent (Es fehlten) Omar Adjaoud, Ulrich Böhm, Gertrud Gollner, Kurt Klasinski, Alexander Konschak, Detlef Krauße, Oliver Rausch, Hubert Schulze, Gerd Steinle-Neumann, Zhengning Tang, Xiaolin Xiong

Contents

Foreword

When Bayerisches Geoinstitut was founded, experimental studies were the only possibility to understand the properties of materials in the Earth's interior. In recent years, computational methods have opened up new ways for predicting structures and properties of minerals from first principles of quantum mechanics. At the same time, modeling convection processes in Earth's interior has progressed enormously, not only because of the increase in computing power, but also through a deeper physical understanding of flow laws and deformation mechanisms of minerals. A sound understanding of the dynamics of our planet requires the combination of experiments and computer models. It therefore appears natural to supplement the experimental capabilities at Bayerisches Geoinstitut through the addition of a group performing geodynamic modeling. In 2007, we have made a major step in this direction. With the financial support of the *Stifterverband für die Deutsche Wissenschaft*, an industry-based foundation, a new tenure-track junior professorship in geodynamic modeling was established at the institute. In fall, Henri Samuel, previously at ETH Zürich, took over the new professorship.

Bayerisches Geoinstitut is a center for research. However, closely related to research is the education of graduate students. Many young scientists who received their Ph.D. from Geoinstitut used this as a starting point for a successful career in academics or industry. In 2007, we expanded the activities of our institute by offering a new masters course in experimental geoscience. This course, intended for a small number of highly motivated young people, integrates the students into small research groups right from the beginning. Due to the exceptional facilities and the broad scientific expertise at Geoinstitut, the new course offers a kind of training in experimental methods in Earth and materials science that cannot be found anywhere else in Europe.

Among the scientific results of the previous year, a study of melting phase relations of carbonate-bearing mantle rocks is perhaps particularly remarkable. The study shows a very sharp and pronounced minimum of melting temperature in the wadsleyite stability field at 16 GPa. Also, the melt compositions become very calcium-rich in this pressure range. Possibly, this observation is the key for understanding the origin of calcio-carbonatite melts in nature. These melts are believed to be major agents of chemical transport in Earth's mantle. Moreover, the experimental observations may also imply that low seismic velocities, sometimes observed in the transition zone of Earth's mantle, may be related to small degrees of partial melt in a carbonated reservoir. If so, these local low-velocity zones may identify parts of the mantle that are enriched in carbonate.

The study of melting phase relations mentioned above was only possible because melting temperatures could be measured in multianvil experiments with very high precision. This again is related to the great precision in the machining of ceramic components for multianvil assemblies that is carried out in our institute machine shop. Only a perfect reproducibility in

the dimensions and properties of these parts makes reproducible measurements possible. This is just one example for the outstanding support offered by the technicians at our institute – a kind of technical support that many colleagues from other countries find difficult to imagine.

As in previous years, and also on behalf of my colleagues, I would like to thank the *Free State of Bavaria* as represented by the *Bayerisches Staatsministerium für Wissenschaft, Forschung und Kunst* as well as the *Kommission für Geowissenschaftliche Hochdruckforschung* of the *Bavarian Academy of Sciences* for their continuing support and strong commitment to the Bayerisches Geoinstitut. The *President of Bayreuth University,* Prof. Dr. Dr. h. c. Helmut Ruppert always had an open ear for the needs of our institute. We also gratefully acknowledge generous support from external funding agencies, in particular the *Alexander von Humboldt Foundation*, the *European Union*, the *German Science Foundation*, and the *European Science Foundation,* which have also contributed greatly to the development and success of the Institute.

Bayreuth, March 2008 Hans Keppler

Vorwort

Als das Bayerische Geoinstitut gegründet wurde, konnten Materialeigenschaften im tiefen Erdinnern nur durch Hochdruckexperimente untersucht werden. In den letzten Jahren haben jedoch quantenmechanische *ab-initio*-Methoden große Fortschritte gemacht. Diese Methoden erlauben die Vorhersage der Struktur und der Eigenschaften von Mineralen ausgehend von quantenmechanischen Prinzipien. Gleichzeitig gab es enorme Fortschritte in der Modellierung von Konvektionsprozessen im Erdinnern. Diese Fortschritte beruhen nicht einfach auf größerer Rechenkapazität, sondern auch auf einem tieferen physikalischen Verständnis der Fließgesetze und der Deformationsmechanismen von Mineralen. Ein wirkliches Verständnis der Dynamik unseres Planeten ist nur möglich durch die Kombination von experimentellen Studien und Computer-Modellen. Es erscheint daher als natürlicher Schritt, die experimentellen Kapazitäten des Geoinstituts zu ergänzen durch eine Arbeitsgruppe, die sich mit geodynamischer Modellierung beschäftigt. Das Jahr 2007 hat hier einen wichtigen Fortschritt gebracht. Mit der Unterstützung des *Stifterverbandes für die Deutsche Wissenschaft* wurde eine tenure-track Junior-Professur für geodynamische Modellierung am Geoinstitut eingerichtet. Im Herbst hat Henri Samuel von der ETH Zürich die neue Professur übernommen.

Das Bayerische Geoinstitut ist ein Zentrum für Forschung. Eng verknüpft mit der Forschung ist jedoch die Ausbildung von Doktoranden. Für viele junge Wissenschaftler, die ihren Doktortitel vom Geoinstitut bekamen, war dies der Ausgangspunkt für eine erfolgreiche Karriere in der Wissenschaft oder der Industrie. In 2007 haben wir die Aktivitäten unseres Instituts in der Lehre erweitert durch einen neuen Master-Studiengang in "Experimental Geoscience". Dieser Studiengang wendet sich an eine kleine Gruppe von hochmotivierten Studenten, die von Anfang an in kleine Forschergruppen integriert werden. Durch die hervorragenden experimentellen Einrichtungen und die breite wissenschaftliche Expertise am Geoinstitut bietet der neue Studiengang eine Ausbildung, wie man sie in Europa sonst wohl kaum irgendwo finden kann.

Unter den wissenschaftlichen Resultaten des vergangenen Jahres sind neue Untersuchungen zur Schmelzbildung in Carbonat-haltigen Mantelgesteinen vielleicht besonders interessant. Die Untersuchungen zeigen ein ausgeprägtes, scharfes Minimum der Schmelztemperatur im Stabilitätsfeld von Wadsleyit bei 16 GPa. Gleichzeitig werden die Schmelzen in diesem Druckbereich sehr reich an Calcium. Möglicherweise ist diese Beobachtung der Schlüssel zum Verständnis des Ursprungs von calcio-carbonatitischen Schmelzen in der Natur. Diese Schmelzen spielen wahrscheinlich eine wichtige Rolle beim Stofftransport im Erdmantel. Die experimentellen Beobachtungen bedeuten möglicherweise auch, dass anomal niedrige seismische Geschwindigkeiten in der Übergangszone des Erdmantels durch geringe Schmelzanteile in einem Carbonat-haltigen Reservoir verursacht werden. Hierdurch könnten eventuell Carbonat-reiche Bereiche des Mantels identifiziert werden.

Die oben erwähnten Untersuchungen waren nur möglich, weil Schmelztemperaturen in den Multi-Anvil-Pressen des Geoinstituts sehr genau bestimmt werden können. Dies hängt wiederum zusammen mit der hohen Präzision bei der Herstellung von Teilen für Multi-Anvil-Experimente in der Werkstatt unseres Instituts. Nur eine absolute Reproduzierbarkeit in den Dimensionen und Eigenschaften dieser Teile ermöglicht reproduzierbare Messungen. Dies ist nur ein Beispiel für hervorragende Unterstützung durch das technische Personal an unserem Institut – eine Unterstützung, die für viele Kollegen aus anderen Ländern kaum vorstellbar ist.

Wie in den vorangegangenen Jahren möchte ich auch im Namen meiner Kollegen dem *Freistaat Bayern*, vertreten durch das *Bayerische Staatsministerium für Wissenschaft, Forschung und Kunst*, als auch der *Kommission für Geowissenschaftliche Hochdruckforschung* der *Bayerischen Akademie der Wissenschaften* danken für ihre fortwährende Unterstützung und ihre enge Verbundenheit mit dem Bayerischen Geoinstitut. Der *Präsident der Universität Bayreuth*, Prof. Dr. Dr. h. c. Helmut Ruppert, hatte immer ein offenes Ohr für die Wünsche des Instituts. Wir sind auch sehr dankbar für die großzügige Förderung durch externe Geldgeber, insbesondere durch die *Alexander von Humboldt-Stiftung*, die *Europäische Union*, die *European Science Foundation* und die *Deutsche Forschungsgemeinschaft*, die ebenfalls wesentlich zur Entwicklung und zum Erfolg des Bayerischen Geoinstituts beigetragen haben.

Bayreuth, im März 2008 Hans Keppler

1. Advisory Board and Directorship

1.1 Advisory Board

The *Kommission für Geowissenschaftliche Hochdruckforschung der Bayerischen Akademie der Wissenschaften* advises on the organisation and scientific activities of the institute. Members of this board are:

Prof. Dr. G. BREY	Institut für Geowissenschaften der Johann Wolfgang Goethe-Universität, Frankfurt am Main
Prof. Dr. U. CHRISTENSEN	Max-Planck-Institut für Sonnensystemforschung, Katlenburg-Lindau
Prof. Dr. R. KNIEP	Institut für Chemische Physik fester Stoffe der Max-Planck-Gesellschaft, Dresden
Prof. Dr. H. PALME	Institut für Mineralogie und Geochemie der Universität zu Köln
Prof. Dr. R. RUMMEL	Institut für Astronomische und Physikalische Geodäsie der TU München
Prof. Dr.-Ing. G. SACHS (Chairman)	Lehrstuhl für Flugmechanik und Flugregelung der Technischen Universität München
Prof. Dr. E. SALJE	Department of Earth Sciences, University of Cambridge
Prof. Dr. H. SOFFEL	Emeritus, Institut für Allgemeine und Angewandte Geophysik der Universität München

The Advisory Board held meetings in Bayreuth (20.04.2007) and in Munich (23.11.2007).

1.2 Leadership

Prof. Dr. Hans KEPPLER (Director)
Prof. Dr. David C. RUBIE

2. Staff, Funding and Facilities

2.1 Staff

At the end of 2007 the following staff positions existed in the Institute:

- Scientific staff *: **13**
- Technical staff: **13**
- Administrative staff: **2**
- Administrative officer: **1**

* Including a tenure-track junior professorship in geodynamic modeling initially funded by *Stifterverband für die Deutsche Wissenschaft* for 6 years

During 2007, 16 scientific (113 months) positions were funded by grants raised externally by staff members of the institute. In addition 12 long-term scientific positions (83 months) were funded by the resources of the BGI Visiting Scientists' Programme (see Sect. 8) which also supported short-term visits for discussing future projects or presenting research results (see Sect. 6). Positions for 10 Ph.D. students (120 months) and 1 co-ordinator (12 months) were funded under the BGI International Graduate School under the Elitenetzwerk Bayern "Structure, Reactivity and Properties of Oxide Materials" (see Sect. 4). 5 scientists (24 months) were supported by personal grants (stipends).

2.2 Funding

In 2007, the following financial resources were available from the Free State of Bavaria:

- Visiting Scientists' Programme: 416.000 €
- Consumables/investment: 345.000 €
- Internat. Graduate School/Elitenetzwerk Bayern: 147.000 €

The total amount of national/international external funding ("*Drittmittel"*) used for ongoing research projects in 2007 was 763.000 € (Positions: 450.000 €; equipment, consumables and travel grants: 313.000 €).

	positions	**equipment, consumables, travel grants**	**total**
• AvH	31.000 €	7.000 €	38.000 €
• DFG	202.000 €	48.000 €	250.000 €
• EU	200.000 €	223.000 €	423.000 €
• Stifterverband	9.000 €		9.000 €
• Others	8.000 €	35.000 €	43.000 €
			763.000 €

(AvH = Alexander von Humboldt Foundation; DFG = German Science Foundation; EU = European Union; Stifterverband = Stifterverband für die Deutsche Wissenschaft)

In the following list only the BGI part of the funding is listed in cases where joint projects involved other research institutions. Principal investigators and duration of the grants are listed in brackets. Total project funding refers to the funding over the entire duration of this project.

Funding institution	Project, Funding	Total Project Funding
BCTC [*1)]	Travel funding (G. Steinle-Neumann, S. Akber-Knutson – 7.05 - 12.07) for project "Computer Modelling of Deep Earth Mineralogy and Geochemistry"	6.500 €
DFG	Albert-Maucher-Preis für Geowissenschaften (D. Dolejš)	10.000 €
DFG	Bo 2550/1-1 (T. Boffa Ballaran, D.J. Frost, L.S. Dubrovinsky – 8.05 - 7.07) Positions: BAT IIa/2, 24 months 58.800 € Consumables and travel funding: 6.000 €	64.800 €
DFG	Du 393/4-1 (L.S. Dubrovinsky – 12.05 - 11.07) Positions: BAT IIa, 24 months 117.600 € Consumables and travel funding: 23.000 €	140.600 €
DFG	Du 393/6-1 (L.S. Dubrovinsky, H.F. Braun – 8.06 - 7.08) Positions: BAT IIa/2, 24 months 58.800 € Consumables and travel funding: 8.400 €	67.200 €
DFG	Fr 1555/3-1 (D.J. Frost, D.C. Rubie, F. Langenhorst – 1.06 - 12.07) Consumables and travel funding: 8.000 €	8.000 €
DFG	Fr 1555/4-1 (D.J. Frost, A.B. Woodland, F. Langenhorst, S. Jahn – 10.06 - 9.08) Consumables and travel funding:	10.535 €
DFG	Ke 501/5-3 (H. Keppler) Positions: BAT IIa, 24 months 117.600 € Consumables and travel funding: 18.700 €	136.300 €
DFG	ESF-Verbundprojekt "Hydrogen in Minerals" Ke 1351/1-1 (H. Keppler – 12.05 - 11.08) Positions: BAT IIa/2, 36 months 88.200 € Consumables and travel funding: 15.000 €	103.200 €
DFG	Mc 3/16-1 (C.A. McCammon, L.S. Dubrovinsky – 10.06 - 9.09) Positions: student assistant, (80 h/month), 36 months 22.570 € Consumables and travel funding: 45.800 €	68.370 €
DFG	Ru 437/6-2 (D.C. Rubie, D.J. Frost, F. Langenhorst, A. Holzheid – 4.04 - 9.07) Positions: BAT IIa, 24 months 117.600 € Consumables and travel funding: 12.100 €	129.700 €

DFG	Ru 437/8-1 (D.C. Rubie, D.J. Frost, F. Langenhorst – 9.06 - 11.07) Positions: BAT IIa/2, 24 months 58.800 € Consumables and travel funding: 12.750 €	71.550 €
DFG	Ru 1323/1-1 (D.C. Rubie, D.J. Frost – 5.06 - 4.08) Positions: BAT IIa, 24 months 117.600 € Consumables and travel funding: 12.900 €	130.350 €
EU	Marie Curie Research Training Network "Crust to core: the fate of subducted material" (1.07 - 12.10) G. Steinle-Neumann (coordinator), G. Fiquet (Paris, France), A.I. Beccero (Sevilla, Spain), S. Buiter (Trondheim, Norway), O. Cadek (Prague, Czech Republic), D. Dobson (London, UK), D. Andrault (Clermont-Ferrand, France), F. Langenhorst (Jena, Germany), P. Jochym (Krakow, Poland), S. Poli (Milan, Italy) and M.W. Schmidt (Zurich, Switzerland) BGI funding:	536.000 €
ESF	European Science Foundation Grant for organizing workshop on "Multiscale approach to alloys: advances and challenges"	11.770 €
EU	"Research Infrastructures – Transnational Access" Programme (D.C. Rubie – 1.05 - 12.08)	960.000 €
EU	Marie Curie Host Fellowships for Early Stage Research Training (C.A. McCammon – 01.06. - 12.09) Positions, consumables, equipment, travel:	677.952 €
Stifter-verband	Stifterverband für die Deutsche Wissenschaft Junior-Professur Geodynamische Modellierung Positions: W1, 72 months 245.200 € Consumables and travel funding: 120.000 €	365.200 €
Industry	Unrestricted Industrial grants (N.A. Dubrovinskaia, L.S. Dubrovinsky)	45.000 €

*1) Bavaria California Technology Center

2.3 Laboratory and office facilities

The institute occupies an area of

ca. 1200 m^2 laboratory space

ca. 480 m^2 infrastructural areas (machine shops, computer facilities, seminar room, library)

ca. 460 m^2 office space

in a building which was completed in 1994.

2.4 Experimental and analytical equipment

The following major equipment is available at Bayerisches Geoinstitut:

I. High-pressure apparatus
- 5000 tonne multianvil press (25 GPa, 3000 K)
- 1200 tonne multianvil press (25 GPa, 3000 K)
- 1000 tonne multianvil press (25 GPa, 3000 K)
- 500 tonne multianvil press (20 GPa, 3000 K)
- 500 tonne press with a deformation DIA apparatus
- 4 piston-cylinder presses (4 GPa, 2100 K)
- Cold-seal vessels (700 MPa, 1100 K, H_2O), TZM vessels (300 MPa, 1400 K, gas), rapid-quench device
- Internally-heated autoclave (1 GPa, 1600 K)
- High pressure gas loading apparatus for DAC

II. Structural and chemical analysis
- 2 X-ray powder diffractometers
- 1 X-ray powder diffractometer with furnace and cryostat
- Single-crystal X-ray cameras
- 2 automated single-crystal X-ray diffractometers
- High-brilliance X-ray system
- 1 Mössbauer spectrometer (1.5 - 1300 K)
- 3 Mössbauer microspectrometers
- 2 FTIR spectrometers with IR microscope
- FEG transmission electron microscope, 200 kV analytical, with EDXS and PEELS
- FEG scanning electron microscope with BSE detector, EDS, EBSD and CL
- 2 Micro-Raman spectrometers
- JEOL JXA-8200 electron microprobe; fully-automated with 14 crystals, 5 spectrometer configuration, EDX, capability for light elements
- Cameca SX-50 electron microprobe
- 193 nm Excimer Laser-Ablation ICP-MS
- ICP-AES sequential spectrometer
- Water content determination by Karl-Fischer titration
- GC/MS-MS for organic analyses

III. *In situ* determination of properties
- Diamond anvil cells for powder and single crystal X-ray diffraction, Mössbauer, IR, Raman, optical spectroscopy and electrical resistivity measurements up to at least 100 GPa
- Facility for *in situ* hydrothermal studies in DAC
- Externally electrically heated DACs for *in situ* studies at pressures to 100 GPa and 1200 K
- 1-atm furnaces to 1950 K, gas mixing to 1600 K, zirconia fO_2 probes
- 1-atm high-temperature creep apparatus

Gigahertz ultrasonic interferometer and an interface to resistance-heated diamond-anvil cells
Heating stage for fluid inclusion studies
Impedance/gain-phase analyser for electrical conductivity studies
Apparatus for *in situ* measurements of thermal diffusivity at high P and T
Laser-heating facility for DAC

IV. Computational facilities

19 node linux cluster (2x2.4 GHz Xeon, 1 Gb memory), Gb ethernet
16 node linux cluster (2x3.6 GHz Xeon em64t, 4 Gb memory), Gb ethernet
7 node linux cluster (2x3.0 GHz Xeon Woodcrest Dual Core, 8 Gb memory), InfiniBand
RAID System (6 Tb storage)

The Geoinstitut is provided with well equipped machine shops, electronic workshop and sample preparation laboratories. It has also access to the university computer centre.

(A) SEM-BSE photograph of a portion of a squeezed porphyritic olivine chondrule entrained in a shock-melt vein (upper left) of the Peace River L6 chondrite. Oval objects are former porphyritic olivines embedded in a chondrule matrix consisting of polycrystalline clinopyroxene. Former rounded olivines (Fa_{24-26}) were shock-melted and fractionally crystallized to Mg-rich wadsleyite (dark gray) in their cores and Mg-poor ringwoodite (light gray) at their rims. White grain is metallic FeNi.

(B) A laser microRaman map of the texture shown in (A). Wadsleyite (blue color) encompassed by a ringwoodite belt (red color). The green matrix is low-calcium clinopyroxene. Blue square on the lower right corner is FeNi metal.

(A) REM-BSE-Aufnahme (Ausschnitt) einer gequetschten porphyrischen Olivin-Chondre in einer Schock-schmelzader des L6-Chondriten Peace River. Die ovalen Objekte sind Relikte porphyrischer Olivine, eingebettet in eine Matrix aus chondritischem Klinopyroxen. Die ursprünglichen Olivine bestehen nun aus Mg-reichem Wadsleyit (dunkelgrau im Kern) und ringförmig angeordnetem Mg-armem Ringwoodit (im Rand). Die ringförmige Textur der beiden Hochdruckmodifikationen von Olivin beruht auf fraktionierter Kristallisation aus einer schockinduzierten Olivinschmelze (Fa_{24-26}).

(B) Laser MikroRaman-Mineralkartierung der Paragenese aus der REM-Aufnahme (A). Wadsleyit (blau) ist von einem Saum aus Ringwoodit (rot) umgeben. Die grüne Matrix besteht aus Klinopyroxen mit geringem Kalziumgehalt. Das blaue Viereck nahe der unteren rechten Ecke ist FeNi-Metall.

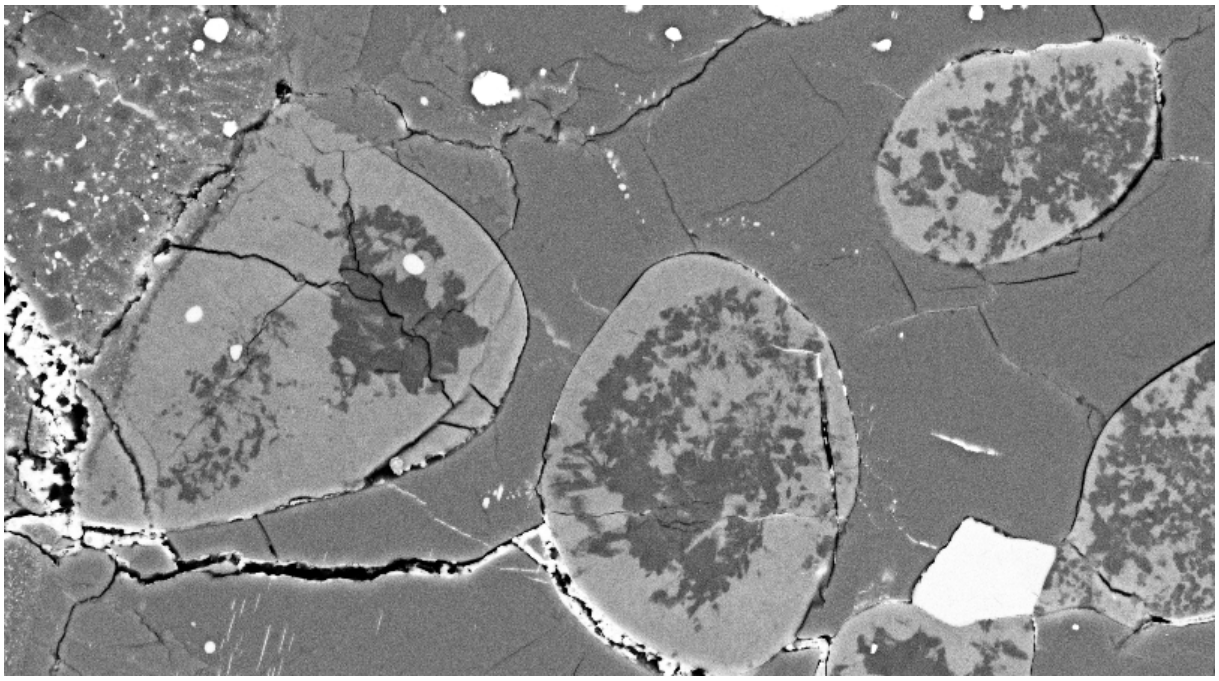

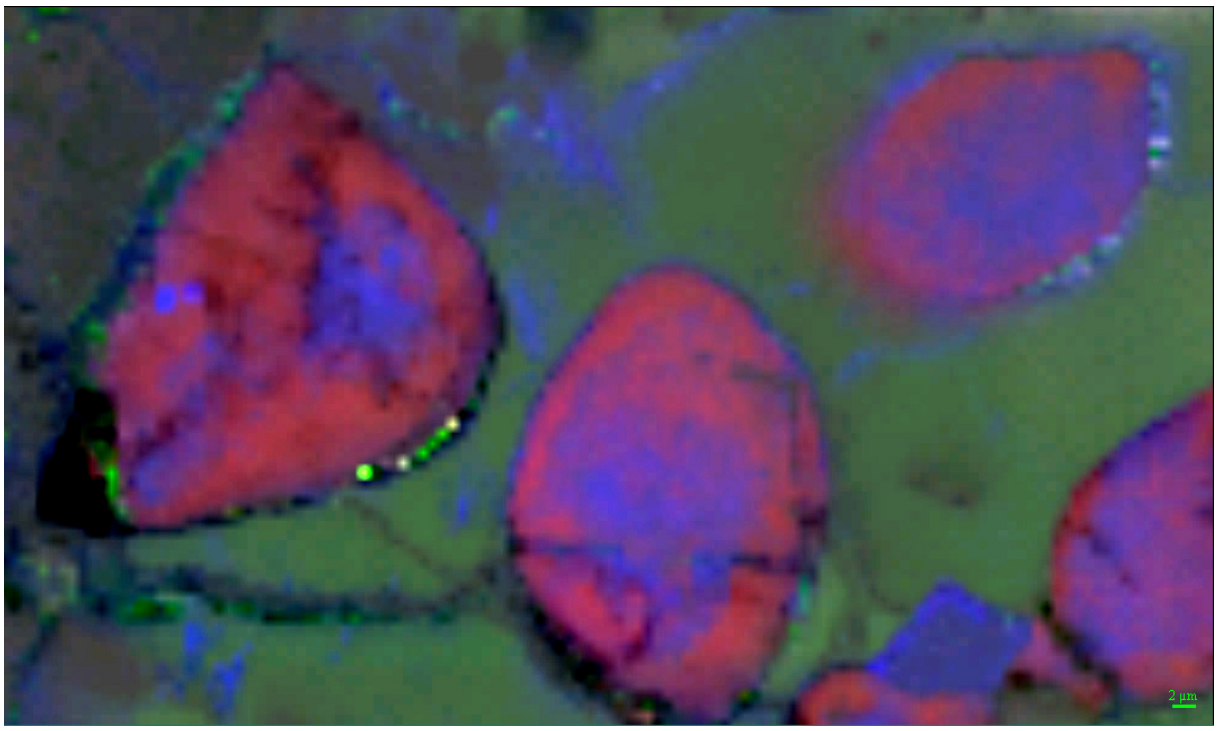
2 µm

3. Forschungsprojekte

Es wird an dieser Stelle nur über die wichtigsten, derzeit laufenden Projekte berichtet. Informationen über abgeschlossene Teilprojekte sind in den Abschnitten 5.1 und 5.2 in Form von Literaturzitaten angegeben. Die Beiträge des Kapitels 3 sollen nicht zitiert werden.

3.1 Aufbau der Erde und Geodynamik

Zahlreiche geologische Prozesse, die auf oder nahe der Erdoberfläche ablaufen, haben ihren Ursprung in der Dynamik des Erdinnern. Dazu gehört neben Vulkanismus, Erdbeben und Gebirgsbildung auch die langfristige chemische Evolution unseres Planeten. Während quantitativ verstanden ist, dass diese Prozesse eine Folge des Wärmeflusses aus dem Erdinneren sind, ist deren detaillierte Aufklärung eines der zentralen Ziele der Geowissenschaften.

Basaltischer Vulkanismus tritt an der Erdoberfläche hauptsächlich entlang der mittelozeanischen Rücken auf, wo neue ozeanische Lithosphäre in Folge von Mantelkonvektion gebildet wird, sowie an *Hotspots*, wo Wärme und Material über eine sekundäre Zirkulation aus dem tiefen Erdinneren an die Oberfläche gebracht werden, möglicherweise sogar von der Kern-Mantel-Grenze. An vielen Orten – so z. B. Island und Afar – treten *Hotspots* an mittelozeanischen Rücken auf. Im ersten Beitrag dieses Kapitels wird die Zusammensetzung von Basaltglas von mittelozeanischen Rücken mit experimentellen Phasenbeziehungen verglichen. Selbst in der Nähe von *Hotspots* erfordern die auftretenden Magmen keine hohen Schmelztemperaturen, wie man sie dort erwarten würde; stattdessen kann die Variabilität der Zusammensetzung durch laterale Heterogenitäten in der Region der Schmelzbildung verstanden werden. Auch im zweiten Beitrag steht die Rolle von Heterogenität im Erdmantel und deren Einfluss auf Schmelzprozesse im Mittelpunkt. In der Form von Magnesit verursachen Karbonate eine starke Abnahme der Solidus-Temperatur in einem peridotitischen Mantel über einen Druckbereich, der der Übergangszone im Erdmantel entspricht. Karbonate können folglich lokal zu partiellen Schmelzen in der Übergangszone führen und sie können damit eine mögliche Ursache für Zonen mit niedrigen seismischen Geschwindigkeiten im Erdmantel sein. Außerdem können partielle Schmelzen zu einem effizienten Transport von Spurenelementen in der Übergangszone führen.

Die Erklärung seismischer Diskontinuitäten im Mantel durch Phasenübergänge stellt einen der wichtigsten Beiträge der Mineralogie zum Verständnis der Struktur des Erdinneren dar. Details dieser Übergänge, insbesondere von Ringwoodit zu Mg-Perowskit und MgO nahe der Diskontinuität in 660 km Tiefe, sind jedoch nach wie vor unklar. Im dritten Beitrag dieses Kapitels wird untersucht, wie sich Fe-haltiger Magnesiumsilikat-Perowskit verhält, wenn er in Bereichen aufsteigender Mantelkonvektion auf die 660 km-Diskontinuität auftrifft.

Über einen langen Zeitraum haben sich mineralogische Studien über den Erdkern auf die Hochdruckphase von Eisen sowie das leichte Element im Erdkern konzentriert. Dabei wurden andere Metalle im Erdkern, insbesondere Nickel vernachlässigt. Im letzten Beitrag dieses Kapitels wird die Kristallstruktur von Fe-Ni-Legierungen unter Druckbedingungen des Erdkerns untersucht. Überraschenderweise verursacht eine Konzentration von ~ 10 mol.% Ni in Eisen bei Drücken über 200 GPa eine Phasenänderung. Dies hat einen starken Einfluss auf die kristalline Struktur des inneren Erdkerns sowie unter Umständen auf die Schmelztemperatur der Fe-Legierung im Erdkern.

3.2 Geochemie

Durch den Parameter Druck wird das geochemische Verhalten zahlreicher Elemente modifiziert; die Elementverteilung zwischen unterschiedlichen Mineralen, Schmelzen und Fluiden ändert sich. Einige in diesem Kapitel aufgeführten Studien zeigen zum Beispiel, welchen Einfluss Druck auf die Verteilung siderophiler (Metalle bevorzugende) Elemente zwischen Metall- und Silikatschmelzen ausübt. Dies ist für das Verständnis der Fraktionierung von Bedeutung, die bei der Trennung von Erdmantel und Erdkern während der Bildung unseres Planeten auftrat. Der Prozess ist sehr kompliziert, da die Elementfraktionierung auch eine Funktion der Sauerstofffugazität ist, die beeinflusst, ob Elemente eher einen oxidischen (z. B. silikatischen) oder einen metallischen Zustand annehmen. Aus einigen Untersuchungen an Meteoriten gibt es Anzeichen, dass die Kernbildung zumindest während des Frühstadiums bei sehr niedrigen Sauerstofffugazitäten stattgefunden hat. Unter derartigen Bedingungen würden zahlreiche Elemente, die normalerweise nicht als siderophil betrachtet werden, im Kern konzentriert werden. Die in diesem Kapitel vorgestellten Experimente und Modellierungen deuten darauf hin, dass die Verhältnisse einiger schwach siderophiler Elemente im Erdmantel nur erklärbar sind, wenn ein Metall/Silikat-Gleichgewicht in großen Tiefen des Mantels herrschte. In weiteren Projekten dieses Kapitels wird gezeigt, wie das Auftreten von S und Ni die Verteilung anderer Elemente beeinflusst. Es gibt somit weitere Einflussfaktoren, die bei Modellierungen zur Erdkernbildung berücksichtigt werden müssen.

Geophysikalische Berechnungen des Wärmeflusses in der Erde sind konsistent mit dem Vorhandensein einer tiefen isolierten Lage, in der wärmeproduzierende Elemente angereichert sind. Diese Theorie wird durch Messungen an Edelgas-Isotopen unterstützt, die auf die Existenz eines primitiven Reservoirs tief im Mantel hindeuten. Ein Projekt untersucht mit Hilfe von *ab-initio*-Methoden die Möglichkeit, ob sich radioaktives Kalium stark in einem derartigen tiefen Reservoir angereichert haben könnte. Dies erscheint jedoch als wenig realistisch. Ein anderer Beitrag beschreibt Untersuchungen zur Löslichkeit von Edelgasen in Mineralphasen bei hohen Drücken. Sofern bei Aufschmelzung in großer Tiefe hohe Anteile dieser Gase im Erdmantel zurückbleiben, wäre das Vorhandensein eines tiefen primitiven Reservoirs für Edelgase nicht unbedingt notwendig.

Der Druckeinfluss auf die Verteilung und die Stabilität anderer leicht-flüchtiger Elemente wie Fluor und Kohlenstoff sind weitere Themen in Beiträgen dieses Kapitels. Während Fluor wahrscheinlich in nominell fluorfreien Mineralen des Erdmantels (z. B. Olivin) residiert, verhält sich Kohlenstoff völlig verschieden, da er überwiegend als separate Mineralphase (Karbonat, Diamant) auftritt. Ein anderer Beitrag befasst sich mit der Bestimmung der Schmelztemperaturen karbonatischer Gesteine unter Bedingungen, die in der Übergangszone herrschen. Die Ergebnisse deuten darauf hin, dass entlang von Subduktionszonen Karbonate tief in den Erdmantel zurückgeführt werden.

TTG-Magmen (Tonalit-Trondjemit-Granodiorit), die einige der ältesten Gesteine auf der Erde repräsentieren, werden allgemein als Aufschmelzungsprodukte ehemaliger subduzierter Ozeankruste betrachtet. Es gibt Hinweise darauf, dass das Mineral Rutil im Verlauf derartiger Aufschmelzungs-Ereignisse im Restmantel verbleibt. Durch Löslichkeitsbestimmungen von Rutil in Schmelzen kann die Temperatur, bei der die Aufschmelzung stattfand, abgeschätzt werden. Der Vergleich von experimentell ermittelten Löslichkeitsdaten mit dem Ti-Gehalt natürlicher Proben deutet auf relativ hohe Temperaturen in archaischen Subduktionszonen.

Ein Beitrag am Ende dieses Kapitels konzentriert sich auf die Verteilung von Spurenelementen zwischen Biotit und granitischen Schmelzen unter Bedingungen der oberen Erdkruste und ihrer Bedeutung für die magmatisch-hydrothermale Erzbildung. Die Untersuchungen ergeben, dass eine Reihe von Übergangsmetallen aus der Schmelze im Verlauf der Biotitkristallisation entfernt werden, jedoch nicht potentiell lagerstättenbildende Elemente wie z. B. Cu und Mo. Dies unterstreicht die Rolle, die Biotit bei der Bildung einiger granitgebundener Erzlagerstätten spielt.

3.3 Kristallchemie

Um Prozesse und Zustände im Erdinneren besser zu verstehen, muss bekannt sein, wie sich Änderungen in Druck, Temperatur, Sauerstofffugazität und chemischer Zusammensetzung auf Kristallstrukturen auswirken. Druck ist hier der wichtigste Parameter da er im Erdinnern über 5 Größenordnungen (von 10^5 bis 10^{11} Pa) variiert. Fünfzehn Beiträge dieses Kapitels befassen sich mit der Reaktion von Mineralen auf die extrem hohen Drücke, die im Inneren der Erde und anderer Planeten herrschen. Zunehmender Druck bewirkt bei Mineralen eine Volumenabnahme, gelegentlich eine Verzerrrung der Kristallstruktur und kann sogar zu einem Übergang in eine dichtere Kristallstruktur führen. Weitere Reaktionen von Mineralen auf hohe Drücke sind zum Beispiel Übergange in andere elektronische Strukturen wie etwa Spin-Übergänge von *3d*-Elektronen in Fe-haltigen Mineralen oder Veränderungen in der elektrischen Leitfähigkeit. Das Verhalten eines Stoffes unter hohem Druck wird nicht allein durch seine Phasenübergänge definiert, sondern auch durch eine genauere Bestimmung seiner Zustandsgleichung mittels verschiedener Methoden der elastischen Streuung, einschließlich Röntgen- und Neutronenbeugung. Starke Reaktionen auf erhöhten Druck äußern sich in veränderten Phasenstabilitäten von Mineralen oder Mineralvergesellschaftungen. Die Unter-

suchung von Phasendiagrammen bei hohen Drücken und Temperaturen ist essentiell für die Erforschung des Erdinneren. Bei Fe-führenden Systemen sind H_2O-Aktivität und Sauerstoff-fugazität weitere wichtige Parameter bei der Ermittlung von Phasenstabilitäten. Jüngste Entwicklungen in der Hochdruck-Experimentiertechnik ermöglichen uns, nahezu alle im Erdmantel herrschenden P-T-Bedingungen experimentell zu erzeugen. Dennoch stellen eine träge Reaktionskinetik von Mineralen in Mischkristallen und chemisch komplexe Systeme noch immer eine Hürde bei der Bestimmung von Phasenstabilitäten dar. Durch einen komplementären Ansatz, nämlich durch thermodynamische Untersuchungen an Endglieder-Mineralen einer Mischkristallreihe und an vereinfachten Systemen, lässt sich dieses Ziel über einen Umweg erreichen.

3.4 Physikalische Eigenschaften von Mineralen

Die Mineralphysik versucht durch die Untersuchung von Materialeigenschaften das Innere unseres Planeten besser zu verstehen. Geophysikalische Messungen liefern Informationen über die räumliche Verteilung von seismischen Geschwindigkeiten, elektrischer Leitfähigkeit und Magnetisierung im Erdinnern. Diese Parameter reflektieren Prozesse im Innern unseres Planeten und sind damit verknüpft mit Plattentektonik, Erdbeben und Vulkanismus. Rückschlüsse aus den Messwerten auf Temperatur, Wärmefluss, Konvektion oder Phasen-übergänge im Erdinnern sind jedoch nur möglich über die Kenntnis der physikalischen Eigenschaften der Materialien im Erdkern und Erdmantel. Hierfür ist eine ständige Verbesserung der experimentellen Methoden erforderlich, um extreme Druck- und Temperaturbedingungen im Labor zu erreichen. Oft ist die Untersuchung von Mineral-eigenschaften unter extremen Bedingungen nur durch eine Kombination experimenteller und theoretischer Methoden möglich.

Wasser hat einen starken Einfluss auf Mineraleigenschaften und Phasenbeziehungen. Mehrere Beiträge in diesem Kapitel befassen sich daher mit Untersuchungen über den Einfluss von Wasser in wasserhaltigen oder in nominell wasserfreien Mineralen. So erfolgt zum Beispiel der Einbau von Wasser in Pyroxen, der nach Olivin das zweithäufigste Mineral des oberen Erdmantels darstellt, nach verschiedenen Mechanismen, die von der Verfügbarkeit von Al im Gesamtsystem abhängen. Der Al-Anteil beeinflusst wiederum die elastischen Eigenschaften des Pyroxens. Jede Substitution von Kationen kann ebenfalls die physikalischen Eigen-schaften wasserhaltiger Phasen verändern, die mögliche Träger von H_2O in den relativ kalten Bereichen abtauchender Krustenplatten sind. Ein weiterer Beitrag beschäftigt sich daher mit dem Effekt von Al und Fe^{3+} auf die physikalischen Eigenschaften der Phase D ($MgSi_2O_6H_2$). Eine *in situ* Raman-Studie an Gips bei hohen Drücken und Temperaturen zeigt sowohl eine Verschiebung der OH-Bande zu niedrigeren Frequenzen und einen damit assoziierten nicht abschreckbaren Phasenübergang, als auch Einzelheiten des Entwässerungs-Mechanismus. Die Resultate erlauben Aussagen über die strukturellen und chemischen Veränderungen in Gips in der Erdkruste, die beteiligt sein könnten an der Auslösung von Erdbeben.

Ein Forschungsziel der Hockdruck-Mineralphysik ist seit langem das tiefere Verständnis des elastischen Verhaltens von Materie. Zwei Beiträge widmen sich diesem Ziel und präsentieren dazu neue Ergebnisse über Wüstit und Eisen-Nickel-Legierungen. Obwohl das anomale elastische Verhalten von Wüstit seit längerer Zeit bekannt ist, lässt sich dieses Phänomen bisher nicht befriedigend erklären. Simultane Untersuchungen mit inelastischer Röntgenstreuung und Einkristall-Röntgenbeugung an $Fe_{0.94}O$ unter hohem Druck zeigen starke Anelastizität. Die Untersuchungen lassen vermuten, dass die meisten Minerale mit internen Freiheitsgraden (Ordnungs-/ Fehlordnungsphänomenen, mikrostrukturellen Defekten usw.) ebenfalls anelastisches Verhalten bei hohen Drücken zeigen könnten.

Untersuchungen magnetischer Eigenschaften von Mineralen unter hohem Druck sind ein neues und wachsendes Forschungsgebiet. Die Untersuchungen machen eine Kombination hochentwickelter experimenteller und theoretischer Verfahren erforderlich, wie in einigen Beiträgen dieses Jahresberichts am Beispiel von Magnetit, Fayalit, Kobalt und Titanohämatit dargelegt wird. Besonders bemerkenswert ist, dass der theoretische Kenntnisstand mittlerweile so hoch ist, dass quantitative Vorhersagen der magnetischen Eigenschaften von Mineralen unter hohem Druck möglich sind.

3.5 Fluide und ihre Wechselwirkung mit Schmelzen und Mineralen

Fluide lassen sich nicht bei Raumtemperatur von hohem Druck abschrecken. Daher lässt sich die Löslichkeit von Mineralen in Fluiden mit konventionellen Methoden nur schwer bestimmen und publizierte Daten zu Löslichkeiten differieren oft um mehrere Größenordnungen. Lange Zeit wurde angenommen, dass HFS-Elemente wie Titan oder Zirkonium in wässrigen Fluiden unter hohem Druck sehr gut löslich sind. Neuere Arbeiten sowohl des Bayerischen Geoinstituts als auch anderer Laboratorien haben ergeben, dass die Löslichkeit von Rutil (TiO_2) in wässrigen Fluiden unter hohem Druck um mehrere Größenordnungen niedriger ist, als bisher angenommen wurde. In diesem Jahresbericht stellen wir erste Ergebnisse zur Löslichkeit von Zirkon in wässrigen Fluiden bei bis zu 900 °C und 1,5 GPa vor. Hierfür wurde die Auflösung von Zirkon *in situ* in einer extern beheizten Diamantzelle beobachtet. Die Daten zeigen, dass die Löslichkeit von Zirkon noch geringer ist als die von Rutil. Dies bedeutet, dass die Verarmung von HFS-Elementen in Inselbogen-Magmatiten wahrscheinlich einfach darauf beruht, dass wässrige Fluide diese Elemente nicht in die Zone der Schmelzbildung transportieren können.

Den starken Schwefelgeruch bemerkt jeder, der sich einem aktiven Vulkan nähert. Schwefelverbindungen sind in der Tat Hauptbestandteile vulkanischer Gase; sie sind für die globale Abkühlung nach größeren explosiven Eruptionen verantwortlich. Erstaunlich wenig ist jedoch über das Verhalten von Schwefel während einer Eruption bekannt. Zwar weiß man prinzipiell, dass Schwefel in einer wässrigen Fluidphase angereichert wird, die Abhängigkeit des Verteilungskoeffizienten von Schmelz-Zusammensetzung und Fluid-Zusammensetzung wurde jedoch bisher nicht systematisch untersucht. In einer umfangreichen Studie zur

Verteilung von Schwefel zwischen Schmelze und Fluid wurde nun eine erstaunlich komplizierte Abhängigkeit des Verteilungskoeffizienten vom Chemismus des Systems beobachtet, wobei der Einfluss der Zusammensetzung unter oxidierenden und reduzierenden Bedingungen verschieden ist.

Während hohe Fluid/Schmelze-Verteilungskoeffizienten die Injektion großer Mengen von Schwefel in die Stratosphäre begünstigen, führt die Adsorption an Aschepartikeln zu einer Reduktion dieser Menge. Wenn die Ausgangskonzentration von Schwefel im Fluid gering ist, kann dadurch sogar fast der gesamte Schwefel aus der Eruptionssäule entfernt werden. Die hier vorgestellten experimentellen Untersuchungen zur Adsorption von Schwefeldioxid an vulkanischen Aschen verbessern daher die Möglichkeiten, den Einfluss von Vulkaneruptionen auf Klima und Umwelt vorherzusagen. Dieser Effekt muss quantitativ verstanden werden, um natürliche und anthropogene Faktoren des Klimawandels unterscheiden zu können.

Die letzten beiden Beiträge in diesem Kapitel beschäftigen sich mit der Speicherung von Wasser in nominal wasserfreien Mineralen. Der erste Beitrag zeigt, dass die Wasserlöslichkeit in Klinopyroxenen mit dem Aluminium-Gehalt stark zunimmt. Dies bedeutet, dass omphazitische Klinopyroxene in Eklogiten einen wichtigen Beitrag zur Subduktion von Meerwasser als Teil des globalen Wasserkreislaufes leisten. Die zweite Studie zeigt einen dramatischen Einfluss der Sauerstofffugazität auf die Wasserlöslichkeit in Wadsleyit im Gleichgewicht mit C-H-O-Fluiden. Eine wichtige Konsequenz dieser Studie ist, dass möglicherweise selbst bei geringen Gesamt-Wassergehalten Fluide in der Übergangzone stabil sein könnten.

3.6 Physik und Chemie von Schmelzen und Magmen

Magmen entstehen im Erdinneren als Folge von Veränderungen in Druck und Temperatur und/oder durch Zuführung leichtflüchtiger Komponenten. Die anschließende Migration und Kristallisation der Magmen führt zur chemischen Differentiation – ein Prozess, der im Verlauf der gesamten Erdgeschichte immer wieder abgelaufen ist. In der frühen Akkretionsphase des Sonnensystems war die Erde aufgrund von zahlreichen hochenergetischen Impaktereignissen vermutlich zum Großteil geschmolzen. Der resultierende tiefe Magmenozean ermöglichte eine effiziente Differentiation in einen metallischen Kern und einen silikatischen Mantel. Die anschließende Kristallisation des Magmenozeans könnte je nach Konvektionsdynamik und Kristallfraktionierung zu einer weiteren Differentiation und Schichtung des Erdinneren geführt haben.

Der erste Beitrag dieses Kapitels beschreibt die computergestützte Modellierung der Struktur- und Transporteigenschaften von Mg_2SiO_4-Schmelze, die als vereinfachtes Analogsystem für den silikatischen Magmenozean angesehen werden kann. Diese Untersuchungen dienen dem Verständnis der dynamischen Prozesse und thermischen Entwicklung des Magmenozeans. Der zweite Beitrag stellt die Resultate einer ersten experimentellen Untersuchung des Solvus

zwischen Fe-reichen und FeO-reichen Schmelzen im System Fe-FeO bei hohen Drücken vor. Dieses System ist für die Einschätzung des Sauerstoffgehaltes im Erdkern wichtig. Um die erzielten Ergebnisse auf die extremen Druck- und Temperaturbedingungen im Erdkern zu extrapolieren, muss zukünftig ein thermodynamisches Modell entwickelt werden, in das diese präzisen Solvus-Bestimmungen dann eingehen werden.

Der dritte Beitrag behandelt die Herkunft von Diamanten im Erdmantel. Am Bayerischen Geoinstitut durchgeführte Experimente zeigen, dass brasilianische Diamanten aufgrund ihrer diagnostischen Mineraleinschlüsse aus einer CO_2-reichen Schmelze auskristallisiert sein müssen. Ursprünglich entstand diese Schmelze wohl durch partielle Aufschmelzung eines CO_2-haltigen Eklogits, einem metamorphen Hochdruckgestein, das bei der tiefen Subduktion ozeanischer Kruste entsteht.

In der gesamten Erdgeschichte hat Vulkanismus eine wesentliche Rolle hinsichtlich des Austauschs leichtflüchtiger Stoffe zwischen dem Erdinnerem und der Erdoberfläche gespielt. Magmen transportieren signifikante Mengen an Volatilen an die Oberfläche und beeinflussen dadurch die Atmosphärenzusammensetzung und damit das Klima. Außerdem bestimmt der Anteil leichtflüchtiger Bestandteile in Magmen den Eruptionscharakter von Vulkanausbrüchen. Deshalb sind Forschungsarbeiten über Löslichkeiten und Speziation von Volatilen in Silikatschmelzen von großer Bedeutung. Zwei Beiträge zu diesem Themenkomplex befassen sich mit Kohlenstoffdioxid und Chlor.

Der abschließende Beitrag dieses Kapitels präsentiert erste Ergebnisse einer neuen *in situ*-Methode zur Untersuchung des Kristallisationsverhaltens und der Kristallisationskinetik von Basaltgläsern in einer Moissanit-Stempelzelle. Ziel dieser Entwicklungsarbeiten ist es letztlich, Experimente an Silikatschmelzen bei erhöhten Temperaturen durchführen zu können. Die erzielten Daten sollen dann eine Interpretation des Gefüges vulkanischer Gesteine in Bezug auf ihre Abkühlungsgeschichte ermöglichen.

3.7 Rheologie

Das Innere der Erde ist durch dynamische Prozesse geprägt, die sich besonders markant in Phänomenen wie Erdbeben oder Vulkanausbrüchen, aber auch in Verschiebungen von Lithosphärenplatten und in Gebirgsbildung äußern. Das Deformationsverhalten der Erdmaterie wird durch ihre rheologischen Eigenschaften, d. h. durch ihre Reaktion auf mechanische Beanspruchung, bestimmt. Die Rheologie von Mineralen und Gesteinen lässt sich durch Fließgesetze beschreiben, die die aufgebrachte Spannung mit der resultierenden Deformationsrate verknüpfen. Fließgesetze können durch mechanische Versuche im Labor ermittelt werden, jedoch ist die Anzahl der Variablen relativ groß. Neben externen Parametern wie Temperatur, Druck und Fugazität/Aktivität der beteiligten chemischen Komponenten müssen auch stoffabhängige interne Materialeigenschaften wie Kristallbaufehler und bevorzugte kristallographische Orientierungen (Textur) berücksichtigt werden. Plastische

Deformation beeinflusst die physikalischen Eigenschaften von Materie zusätzlich und verändert deren Richtungsabhängigkeit (Anisotropie). Die anisotropen Eigenschaften des Erdinneren werden indirekt mit geophysikalischen Messmethoden detektiert und können schließlich über die Ergebnisse experimenteller Gesteinsdeformation interpretiert werden.

Verformungsexperimente am Bayerischen Geoinstitut konzentrieren sich zurzeit auf die D-DIA Multianvil-Presse, mit der Materialverformungen durch uniaxiale Kompression oder gerichtetes Scheren bei Drücken im Gigapascal-Bereich möglich sind. Das bisher wenig bekannte Verformungsverhalten von Hochdruckmineralen wie Coesit, Aragonit oder Ringwoodit wurde mit dieser Apparatur untersucht. Erste Ergebnisse deuten an, dass Versetzungsgleiten der bevorzugte Verformungsmechanismus unter experimentellen Bedingungen darstellt. Deshalb ist bei Mineralen des oberen Erdmantels und der Übergangszone ein anisotropes Mineralgefüge zu erwarten. Minerale des unteren Erdmantels und im Bereich der Kern-Mantel-Grenze sind dagegen bei Drücken stabil, die mit der D-DIA Multianvil-Presse nicht erreicht werden können. Es ist daher notwendig, analoge Modellsubstanzen zu untersuchen. Aus Scherexperimenten an dem Analogmaterial $CaIrO_3$ ist abzulesen, dass beim Übergang von der Perowskit- in die Post-Perowskit-Phase ein anderes Anisotropiemuster entsteht als bei der Verformung von reinem Post-Perowskit. Dies könnte eine Erklärung für die beobachteten Variationen der seismischen Anisotropie an der Kern/Mantel-Grenze sein.

Die rheologischen Eigenschaften von Eklogit sind sowohl für das Verhalten von abtauchenden Ozeanplatten als auch für die Entstehung von Hochdruck-*Terranes* von großer Bedeutung. Die Festigkeit von Eklogit wird im Wesentlichen vom bislang wenig untersuchten mechanischen Verhalten des Minerals Omphazit bestimmt. Verformungsexperimente an Omphazit in der D-DIA-Presse haben ergeben, dass alle Verformungsmechanismen (Gleitsysteme usw.), die in natürlichem Omphazit auftreten, experimentell reproduziert werden können.

Das Mineral mit dem wahrscheinlich höchsten Stellenwert in der Hochdruckforschung stellt hingegen der Diamant dar. Dennoch ist bisher nur wenig über sein plastisches Deformationsverhalten bei erhöhten Temperaturen bekannt. Aus ersten D-DIA-Experimenten bei 4 und 6 GPa Druck und 1800 °C ist zu erkennen, dass Prozesse plastischer Verformung, wie die Aktivierung von Gleitsystemen, oder Drucklösung und Ausfällung bei diesen Temperaturen in Diamant induziert werden können.

3.8 Metamorphose

Bei der Metamorphose handelt es sich um Umwandlungsprozesse im festen Zustand, die Gesteinsmassen unter dem Einfluss sich verändernder chemischer und physikalischer Bedingungen durchlaufen, wenn sie z. B. an Kontinentalrändern in das Erdinnere subduziert werden oder in den tiefen Wurzelzonen neu aufgefalteter Gebirge begraben werden. Auf diese

veränderten Bedingungen reagieren die Gesteine mit einer Umkristallisation ihres Mineralgefüges und der Bildung von neuen Mineralphasen, die bei den entsprechenden Druck- und Temperaturbedingungen im thermodynamischen Gleichgewicht zueinander stehen. Wenn die metamorphen Gesteine in relativ kurzer Zeit wieder an die Erdoberfläche transportiert werden, bleiben diese Mineralphasen reliktisch erhalten und lassen Rückschlüsse auf die chemischen und physikalischen Prozesse im ansonsten unzugänglichen tiefen Erdinneren zu.

In Subduktionszonen und während kontinentaler Kollisionen werden Schollen der weniger dichten kontinentalen Kruste mit den abtauchenden Lithosphärenplatten in große Tiefen des Erdinneren befördert, bevor sie durch die steigenden Auftriebskräfte wieder zurück in oberflächennahe Krustenbereiche gelangen. Die in großen Tiefen ablaufende Ultrahochdruck-Metamorphose ist Thema des ersten Beitrags. Die Autoren untersuchten diamantführende Metapelite aus Nordgriechenland, die während ihrer Metamorphose eine Tiefe von mehr als 220 km erreicht hatten. Durch die Verwendung verschiedener Geothermometer und -barometer konnten sie Teile des Druck-Temperaturpfades rekonstruieren, den die Gesteine im oberen Erdmantel durchliefen.

Die magnetischen Eigenschaften von norwegischen Granuliten wurden im zweiten Beitrag untersucht. Diese Gesteine sind für regionale geomagnetische Anomalien verantwortlich, die hauptsächlich durch nanoskalige Entmischungslamellen von Hämatit in Ilmenit oder Ilmenit in Hämatit eine starke remanente Magnetisierung erzeugen. In dieser Studie wurde ein Titanohämatit-Einkristall mit elektronenmikroskopischen Verfahren (Raster-, Transmissionselektronenmikroskopie und Elektronenstrahlmikrosonde) analysiert, um den Zusammenhang zwischen Entmischungslamellen unterschiedlicher Zusammensetzung und den magnetischen Eigenschaften von Titanohämatit zu ergründen.

Abgesehen von den Variablen Druck und Temperatur kann die Sauerstofffugazität eine wichtige Rolle für die metamorphen Reaktionen in Gesteinen spielen. In dem dritten Beitrag wurde die Wechselwirkung zwischen Mineralgleichgewichten, Fe^{2+}/Fe^{3+}-Verhältnissen und Entwässerungsreaktionen untersucht, um den Oxidationsgrad von eklogitischen Mineralparagenesen unter Subduktionsbedingungen vorhersagen zu können. Die Untersuchungen zeigen, dass die Sauerstofffugazität in der abtauchenden Lithosphärenplatte deutlich höher ist als in den umgebenden Peridotiten des oberen Erdmantels, wodurch sich frühere Untersuchungsergebnisse an natürlichen Proben erklären lassen.

Während die Regionalmetamorphose sich auf der Erde über Zeiträume von Millionen von Jahren erstrecken kann, wird in dem letzten Beitrag ein impaktmetamorpher Meteorit untersucht, in dem die metamorphe Überprägung in Zeiträumen von wenigen Sekunden auftrat. Diese Meteorite enthalten Hochdruckphasen, die ansonsten nur im tiefen unzugänglichen Erdinnern auftreten. Mit Hilfe chemischer und textureller Verteilungskarten reinterpretieren die Autoren die Entstehung der Hochdruckphasen und zeigen auf, dass bisherige Zeitabschätzungen für ihre Bildung möglicherweise zu lang waren.

3.9 Materialwissenschaften

Die experimentelle Forschung des Bayerischen Geoinstituts ist, bedingt durch die Suche nach neuen Hartmaterialien, eng mit Entwicklungen in den Materialwissenschaften verknüpft. Die einzigartige experimentelle Ausstattung zur Synthese von neuen Materialien unter hohen Drücken und Temperaturen prädestiniert das Bayerische Geoinstituts für dieses Feld der Materialforschung. Die Forschungsarbeiten am BGI konzentrieren sich traditionell auf diamanthaltige oder ähnlich strukturierte Hartmaterialien und Keramiken mit Korngrößen im Nanometerbereich.

Im folgenden Kapitel werden acht Projekte vorgestellt, in denen die experimentellen Möglichkeiten zur Synthese und Charakterisierung von Materialien mit ausgezeichneten Eigenschaften für verschiedenste Anwendungen aufgezeigt werden. Mit Bor dotierter Diamant wird zur Untersuchung des Kohlenstoffisotopen-Effekts auf die Supraleitfähigkeit eingesetzt. Der Isotopeneffekt ermöglicht auch den Einsatz von ^{13}C-Diamant für die Druckkalibrierung in Diamantstempelzellen. Die Erzeugung von Nanomaterialien unter hohen Drücken kann partiell zur Amorphisierung führen. Durch wiederholte Zyklen von Kompression und Dekompression lässt sich dieser Effekt verstärken und der Kompressionsmodul erhöhen. Eine bessere Probenhomogenität von Nanokeramiken kann durch Sinterung bei Drücken im Gigapascal-Bereich in der Multianvil-Presse erreicht werden. Hohe Drücke verändern auch die magnetischen Eigenschaften von Feststoffen. Manganit-Perowskit zeigt einen ferro- zu antiferromagnetischen Übergang, während in Ferrit-Spinellen eine Phasenumwandlung erster Ordnung stattfindet und ein ferromagnetisches Moment erzeugt wird. Ebenso ist gut bekannt, dass der Einbau von Stickstoff in Zirkondioxid Sauerstoff-Leerstellen erzeugt, durch die sich die industriell verwertbare Hochtemperatur-Modifikation stabilisieren lässt; weitaus weniger weiß man jedoch über die möglicherweise interessanten Druckeffekte. Die Hochdruck-Modifikationen verschiedener Hydride (Alanit und Borhydrid) haben sich als interessante Materialien zur Wasserstoffspeicherung erwiesen, was die weitere Untersuchung ihrer Struktur und Eigenschaften motiviert.

3.10 Methodische Entwicklungen

Die Entwicklung neuer experimenteller und analytischer Methoden ist Voraussetzung für bahnbrechende Entdeckungen und Entwicklungen in Wissenschaft und Technik. Das Bayerische Geoinstitut hat eine lange Tradition in der Entwicklung von neuen Techniken, die mittlerweile auch an anderen Labors in der ganzen Welt genutzt werden. Im vergangenen Jahr wurden neue Methoden zur Spannungsmessung in Multianvil-Experimenten, zur Bestimmung des Oxidationszustands von Ferroperiklas, für die Präparation und Beladung von Diamantstempelzellen sowie für das Verschweißen von Probenkapseln entwickelt.

Der erste Beitrag dieses Kapitels beschreibt eine neue Methode zur Spannungsmessung in Multianvil-Experimenten, die auf der Nutzung der piezoelektrischen Eigenschaften von

$GaPO_4$ beruht. Der zweite Beitrag befasst sich mit der Kalibrierung der Flankenmethode zur Bestimmung des Oxidationszustands von Eisen in Ferroperiklas. Diese Methode soll später auf Mikro-Einschlüsse in Diamanten angewendet werden. Die nächsten beiden Beiträge konzentrieren sich auf die Präparation von Dichtungen und auf das Beladen von Diamantstempelzellen für Ultra-Hochdruck-Experimente. Im letzten Beitrag wird eine neue Methode präsentiert, die es ermöglicht, relativ große Fluidmengen in Edelmetall-Kapseln einzuschweißen, ohne dabei die zylindrische Form der Kapseln zu verändern.

3.1 Earth's Structure and Geodynamics

Many geological features near or at the Earth's surface are the result of dynamic processes in the Earth's interior. These include volcanism, earthquakes, or mountain building, as well as the long term chemical evolution of the Earth. While we understand in general terms that these processes are a consequence of the ongoing heat transport from the interior to the surface of the Earth, elucidating further details of the underlying causes and forces is one of the central goals in the solid Earth sciences.

Two major sources of igneous rocks at the surface of the Earth are mid-ocean ridges, where new lithosphere is formed as a consequence of plate tectonics, and hot mantle plumes that are attributed to a secondary heat transport mechanism from the Earth's deep interior, possibly the core-mantle boundary. In many locations – like Iceland or Afar – these two features are related, with a plume interacting with the ridge/rift. In the first contribution of this section this relation is explored by comparing mid-ocean-ridge basalt glasses with experimental phase relations, and it was inferred that even at plume locations the melt extracted does not require high temperatures present in mantle plumes, but can be explained by heterogeneity in the source. The second contribution also deals with mantle heterogeneities, induced by the presence of carbonates in the mantle. In a peridotite mantle composition containing magnesite the solidus drops significantly over a pressure range corresponding to depths of the transition zone, possibly inducing partial melting in the presence of carbonates. Such partial melt could be responsible for local low velocity regions in the mantle transition zone and be an efficient engine for the creation of trace element heterogeneity.

One of the most important contributions that mineralogy has made to the study of the Earth's structure is the identification of phase transitions as the cause of seismic discontinuities. While the first order structure has been resolved, there are still interesting questions, for example the influence of temperature and chemical variations on the breakdown of ringwoodite to Mg-perovskite and MgO at the 660 km seismic discontinuity. In the third contribution of this section the interaction of Fe-bearing Mg-perovskite in mantle upwellings with the discontinuity is considered, as the high temperature in such a feature can give rise different phase relations in the system.

Over the past decades the mineralogical studies on core structure has focused on the high pressure phases of iron and the nature of the light alloying element in the core, neglecting the presence of other transition metals, primarily nickel, in the core. In the final contribution of this section the crystalline structure of Fe-Ni alloys at conditions of the Earth's core are examined, and quite surprisingly the presence of ~ 10 % mol. Ni in Fe leads to a change in the crystal structure at pressures above 200 GPa. Aside from the consequences this has on the structure of the solid inner core, the transition to a different structure can have significant influence on the melting behavior of the core material.

a. *Origin of the oceanic lithosphere (D.C. Presnall/Texas and G.H. Gudfinnsson)*

The range of temperature and pressure appropriate for the extraction of mid-ocean ridge basalts (MORBs) from the mantle has been controversial for several decades. Some models require large temperature variations along ridges and have dominated petrologic thinking for the last 20 years. These models require that as temperature increases along a ridge, axial ridge depth decreases, and as a consequence Fe_8 increases, and Na_8 decreases, where Na_8 and Fe_8 are the concentrations Na_2O and FeO normalized to 8 % MgO. In a reevaluation of these models, we have found that variations of the parameters Na_8 and Fe_8 do not support such a model for any ridge. For example, Fig. 3.1-1 shows, for the Carlsberg Ridge, that there is no correlation of sampling depth with either Fe_8 or Na_8. Instead, we attribute the Na_8-Fe_8 variations to source heterogeneity. Thus, the Red Sea mantle is interpreted as being enriched in Fe relative to the northern Indian Ocean mantle. Globally, the normalized Na_2O-FeO variations of MORBs are consistent with the compositional systematics of melts at the solidus of the system CaO-MgO-Al_2O_3-SiO_2-Na_2O-FeO (CMASNF) in the narrow P-T range of the plagioclase/spinel lherzolite transition at 1250-1280 °C, 1.3-1.5 GPa. In this interpretation, the global Na_8 and Fe_8 systematics support the extraction of melts from the mantle at relatively constant T-P conditions, and the variations of Na_8 and Fe_8 are due to mantle heterogeneity rather than temperature variations. A new model for oceanic lithosphere formation is developed that does not involve plumes, has a uniformly low temperature and pressure of melt extraction, and relies on fracturing of the oceanic lithosphere combined with explosive escape of CO_2. This new modeling is based on the recent observation that strombolian eruptive behaviour always accompanies effusive eruptions along oceanic ridges.

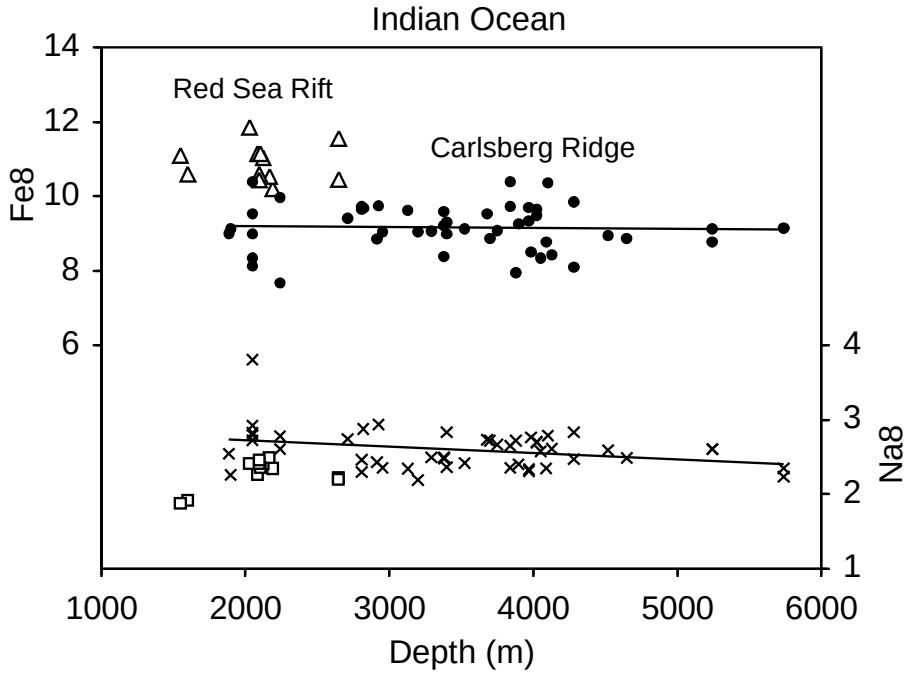

Fig. 3.1-1: Fe8 (upper values and curve, left legend) and Na8 (lower values and curve, right legend) values for the Carlsberg (solid symbols) and Red sea rift (open symbols) as a function of ridge depth.

b. *Precipitous drop in the solidus of carbonated peridotite between 14 and 16 GPa: Calcic carbonatites and seismic low-velocity zones in the Earth's transition zone (S. Keshav, G.H. Gudfinnsson and D.C. Presnall/Texas)*

Carbonatites and kimberlites form part of a spectrum of silica-undersaturated rocks that vary widely in their composition. Even though much less voluminous than basalts, carbonatites and kimberlites have been found on almost every continent, and their presence in the sub-oceanic mantle has been inferred through studies on mantle xenoliths in ocean-island basalt localities, and in the source regions of mid-ocean ridge basalts. Carbonatite-like melts and crystalline carbonates have been found as inclusions in diamonds. And very importantly, the origin of the seismically observed low-velocity zone in the oceanic mantle at ~ 60 km depth has often been ascribed to the presence of a carbonatitic melt. Hence, there is little doubt as to the tremendous importance of carbonatitic melts as agents of introducing chemical heterogeneity at all scales deep in the mantle, and also as melts that have a tremendous influence on the seismic-related properties in the Earth's mantle.

Xenoliths, xenocrysts, and crystalline and melt-inclusions in diamonds recovered in kimberlites are the primary source of information on various petrological, geochemical, and thermal processes that have shaped the Earth's shallow mantle (~ 50-230 km). However, over the last two decades there is growing realization that some diamonds and their inclusions originate from depths well below the continental lithosphere (> 230 km). Dominantly, these inclusions are of majoritic garnet composition originating from depths of 300-500 km. A few diamonds also appear to contain lower mantle silicate crystalline assemblage and carbonate, suggesting that the host kimberlite may come from the Earth's lower mantle (> 660 km), and crystalline carbonate is a stable phase down to these great depths.

Here, we report melting relations in the CaO-MgO-SiO_2-CO_2 (CMS-CO_2) system at pressures of 12-26 GPa (~ 350-750 km). We focus on the part of composition space in the CMS-CO_2 system that is analogous to the natural, carbonate-bearing mantle system with a peridotitic bulk composition. At a fixed pressure in the CMS-CO_2 system, the studied phase relations involving five phases at the solidus are thermodynamically invariant, and it is possible through algebraic methods to determine if the solidus invariant point is eutectic or peritectic. This also means that as long as all the phases at the solidus are present in the experimental runs, the choice of starting composition does not affect the phase compositions, and the bulk compositions can be adjusted so as to maximize the amount of liquid in the experiments. Subsequently, the resulting phase equilibrium data can be used to model very small degrees of melting in a portion of the mantle with the same phase assemblage. Therefore, by studying the CMS-CO_2 system, melts analogous to very small degree mantle melts can be readily analyzed by the electron microprobe, and solidus temperatures as a function of pressure can be determined. This is a huge advantage over experiments that employ multi-component (natural) starting compositions to determine the solidus.

P (GPa)	Phases present
12	liq+fo+cpx+en+mag
14	liq+fo+cpx+maj+mag
16	liq+wad+cpx+maj+mag
20	liq+rw+Capv+maj+mag
26	liq+Mgpv+Capv+per+mag

Table 3.1-1: Phase equilibria at different pressures. Abbreviations for the phases are: melt (liq), forsterite (fo), clinopyroxene (cpx), clinoenstatite (en), magnesite (mag), majorite (maj), wadsleyite (wad), ringwoodite (rw), calcium perovskite (Capv), magnesium perovskite (Mgpv), and periclase (per).

Starting mixtures were made from finely ground silicate glasses and magnesite. About 150 experiments were performed in the multianvil press to locate the solidus at pressures of 12-26 GPa. Phase assemblages as a function of pressure are reported in Table 3.1-1.

The most remarkable feature of the phase relations is the abrupt drop of 115 °C in the solidus of model carbonated peridotite between 14 and 16 GPa (Fig. 3.1-2). The solidus has a positive P-T slope above 16 GPa, and up to at least 26 GPa (Fig. 3.1-2). Simultaneous with the temperature drop between 14 and 16 GPa, the composition of the melt also changes dramatically (Fig. 3.1-3). At 12 and 14 GPa, the solidus melts are magnesiocarbonatites with Ca# (molar Ca/Ca+Mg*100) of 40, while at 16 and 20 GPa, the melts change to become highly calcic with Ca# of 61. This dramatic change within 2 GPa is surprising because the coexisting carbonate continues to be nearly end-member magnesite. Hence, although magnesite contributes all the CO_2 to the melt, the melting reaction must include large amounts of a Ca-rich silicate.

Also shown in Fig. 3.1-2 are boundary lines for the iso-chemical phase transformations for graphite-diamond, fo-wad, wad-rw, and dissociation of rw to Mgpv and per, with the last three thought to be responsible for seismic discontinuities. Creation of cusps in P-T space is required when these boundary lines intersect the carbonated peridotite solidus. At present we do not have sufficient phase equilibrium data for precise determination of the form of these cusps at the solidus, and hence the boundary lines are not extended to the solidus. However, geometrical analysis (through Schreinemakers' constructs) yields a complete set of possible univariant curves at the relevant P-T invariant points. There is compositional, and possibly polytypical degeneracy at all the P-T invariant points. For example, magnesite and liquid

absent-curves cannot be uniquely determined, showing composition degeneracy, making them coplanar. Similarly, at the maj-perovskite transition, there is likely to be polytypical degeneracy. Hence, wherever these degeneracy equilibria exist, the system essentially reduces to CaO-MgO-SiO_2 components, again making them coplanar in this composition space.

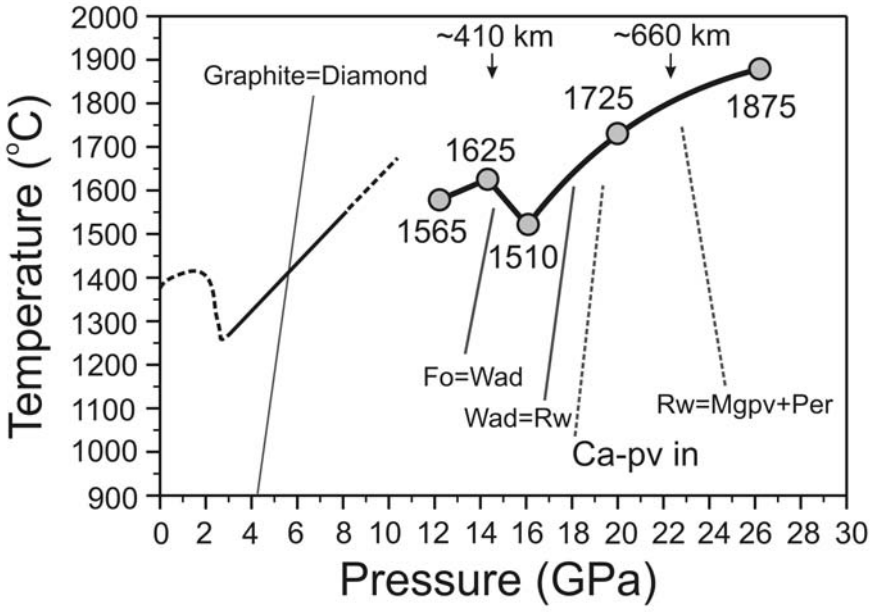

Fig. 3.1-2: The solidus of carbonated peridotite in the CMS-CO_2 system determined in this work (shown as a solid line connecting filled grey circles). Numbers adjacent to the grey circles denote the solidus temperatures. The size of the grey circles represent bracketing runs. At 14 GPa, the run product contains the entire solidus assemblage. The solidus in the CMAS-CO_2 system at lower pressures is shown as solid line. The higher-pressure (> 7 GPa) extension of the solidus in CMAS-CO_2 is shown as a dashed line. In the absence of experimental data, a part of the lower-pressure solidus, near the so-called 'carbonate ledge' is shown as a dashed line. Also shown in this figure are various boundary lines thought to be responsible for causing the seismically observed discontinuities at 410 (fo-wad), 520 (wad-rw), and 660 km (rw to Mgpv and per). Owing to disparate results regarding the slope of the boundary line at 660 km, it is shown as a dashed line. The dotted line denoting 'Ca-pv in' projected onto this diagram shows the approximate P-T limit delineating the stability of Capv in the Earth's mantle.

Changes in the carbonated peridotite solidus between 12 and 26 GPa have fundamental consequences for petrology, geochemistry, and seismology of the mantle at these and greater depths. For example, if interconnection of carbonatitic magmas occurs as readily at transition zone and lower mantle pressures as it does at upper mantle pressures, the magmas are likely to segregate from the source at very low melt fractions, and extraction of these magmas would leave a highly trace-element depleted source. These melts would invariably metasomatize the surrounding mantle, resulting in the development of a variety of geochemical reservoirs over time. Modeling results suggest that the continental kimberlites tap a mantle source that has been enriched in trace elements from melts resembling carbonatites.

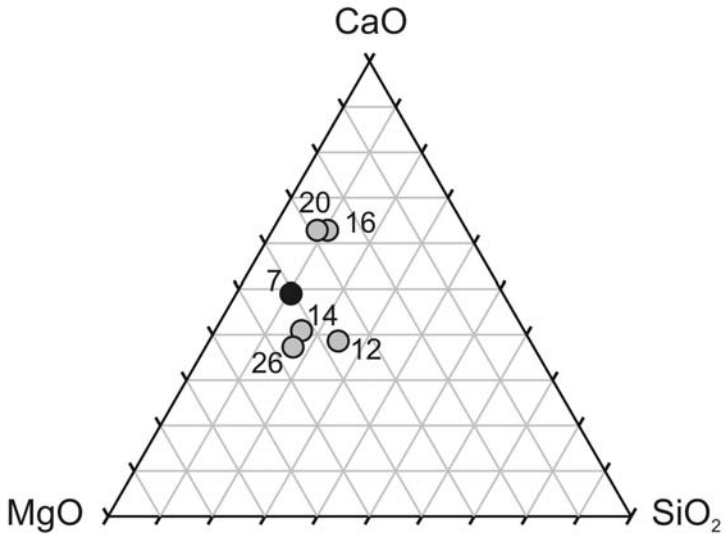

Fig. 3.1-3: Composition of the solidus melts (grey circles) projected from the CO_2 apex onto the CaO-MgO-SiO_2 (CMS) base at all pressures investigated in the present study. Numbers adjacent to grey circles represent pressure in GPa. Also shown is the solidus melt composition in carbonated peridotite in the CMAS-CO_2 system (dark circle) at 7 GPa. Note that melt compositions in the CMS-CO_2 system (this work) lie in the ternary, while those in the CMAS-CO_2 system, since they contain alumina, are slightly off this plane. The melt compositions at 16 and 20 GPa in the CMS-CO_2 system completely overlap each other, and for clarification, they have been slightly separated.

Melting caused by the negative slope of the carbonated peridotite solidus will also influence seismic velocities in the Earth's transition zone. For instance, if two adiabats with a potential temperature (T_p) of 1350 and 1400 °C and a gradient of 13 °C/GPa are drawn through the determined solidus, then intersection of these adiabats with the carbonated peridotite solidus would cause melting at ~ 600 and 550 km, respectively. When these adiabats are just above the solidus, the amount of melting will be very small. At slightly shallower depths, where the adiabats lie at increasingly higher temperatures above the solidus, enhanced melting will take place. We do not have sufficient data above the solidus for precise modeling of the degree of melt that might result, but it could be on the order of ~ 0.2-0.5 %. The depth ranges of some local seismic low-velocity zones (~ 350-600 km) in the mantle correspond almost exactly to the depth range where the solidus of carbonated peridotite abruptly decreases. We propose that these low-velocity anomalies are due to melting associated with the depression of the solidus of carbonated peridotite.

c. *The back reaction and redox relations during mantle upwelling and avalanche (J. Pickles, D.J. Frost, C.A. McCammon and N. Miyajima)*

The mantle constitutes more than half of the Earth's volume, so understanding processes within the mantle is a key to understanding the Earth as whole. Silicate perovskite is the

dominant mineral phase in the lower mantle, *i.e.*, deeper than 660 km, while pyroxene and olivine are the stable minerals in the upper mantle. The project will focus on redox relations involved in the back transformation from silicate perovskite, such as occurs when lower mantle material is displaced, though mantle avalanching or mantle plumes, into the upper mantle. Specifically, the chemistry of Mg perovskite and the change in the Fe^{2+}/Fe^{3+} ratio will be investigated. The work is relevant to dynamic processes within the Earth's mantle and the acquisition of an oxygenated atmosphere around 2.4 billion years ago.

$(Mg, Fe)(Si, Al)O_3$ perovskite will be synthesised in the multianvil press at lower mantle temperatures and pressures (> 26 GPa and 1700 °C), and the Fe^{2+}/Fe^{3+} ratio will be set primarily through the addition of Al into the perovskite. The sample will then be annealed at a lower pressure so that the back reaction can be investigated. To characterise the changes that occur, the samples will be analysed, before and after annealing, using Mössbauer spectroscopy, TEM, XRD and electron microprobe, which will allow the determination of all phases present, the valence state of the iron and its distribution between the phases.

d. *Body-centred-cubic iron-nickel alloy in the Earth's core (L.S. Dubrovinsky, O.Narygina, I.Yu. Kantor, N.A. Dubrovinskaia/Heidelberg, A. Kuznetzov, V.B. Prakapenka/Chicago, A.S. Mikhaylushkin, S.I. Simak and I.A. Abrikosov/Linköping)*

Since the discovery of the Earth's core about a century ago, the idea of iron being the dominant component of the core gained firm support from geochemical observations, seismic data, theory of geomagnetism, and high-pressure studies. Strong support for the idea of iron in the core comes from a reasonably close match between seismologically inferred sound velocities and density of the core and the measured experimental values for iron by shock and static compression. Cosmochemical data and studies of iron meteorites provide evidence that the Earth's core contains significant (5 to 15 %) amounts of nickel. While studying of pure iron at multimegabar pressures draw considerable attention and have provided rich experimental data, the knowledge of the behaviour and properties of Fe-Ni alloys at conditions of the Earth's core is still limited.

The iron-nickel alloy $Fe_{0.9}Ni_{0.1}$ has been studied *in situ* at high pressure and temperature by means of the angle dispersive X-ray diffraction in internally heated diamond anvil cells (DACs). In four experiments out of dozens, pressures over 200 GPa were reached (Fig. 3.1-4). In three of these experiments we employed internal wire-heating technique, allowing for resistivity measurements. At pressure above 230 GPa we observed reversible discontinuous behaviour of resistance as function of temperature in the range of 3300-3400 K. The jump in the resistance can not be associated with melting (because at melting the electrical connection would be broken abruptly) or with chemical reactions (two out of three samples were quenched to ambient conditions and tested using X-ray diffraction and SEM; no sign of chemical reactions was found). This suggests that the anomaly in resistance at pressures above 200 GPa and high temperatures can be associated with a phase transition. In order to

verify the nature of this transition we performed X-ray diffraction experiments with *in situ* laser heating.

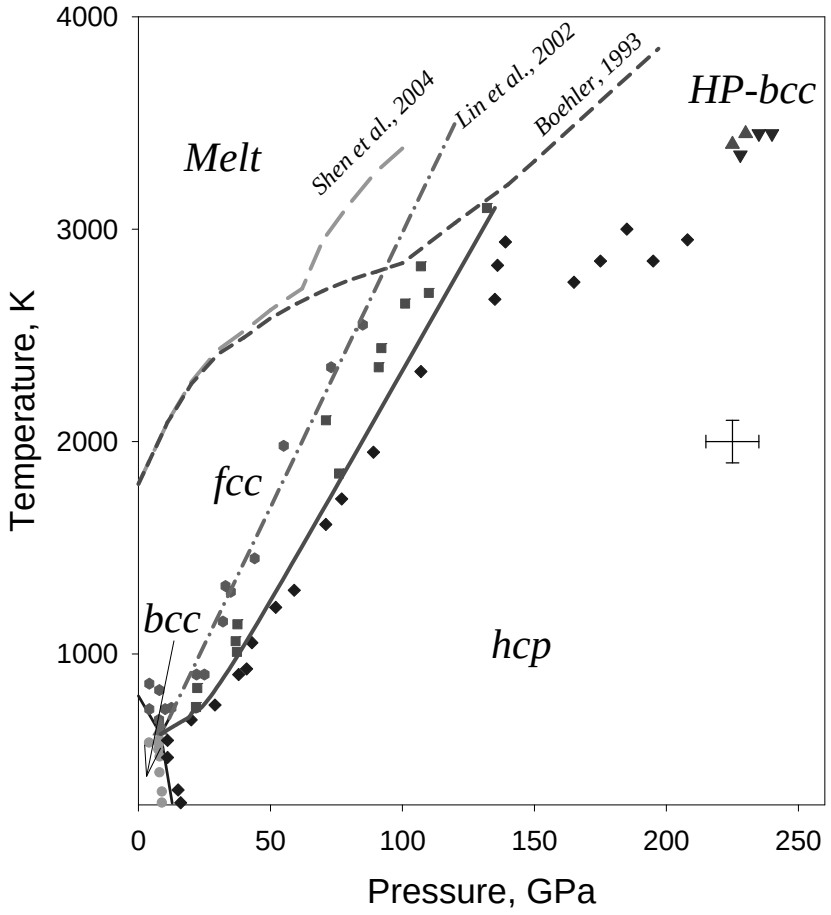

Fig. 3.1-4: Phase relations of the $Fe_{0.9}Ni_{0.1}$ alloy at high pressures and temperatures as determined by *in situ* X-ray diffraction experiments (at pressures below 150 GPa only points closest to the phase boundaries are shown; dots – the low-pressure bcc-phase, diamonds – the hcp-phase, hexagons – the fcc-phase, squares – the mixture of hcp- and fcc-phases, triangles – the coexistence of bcc-, hcp-, and fcc-phases, triangles – the high-pressure (HP) bcc-phase, inverse triangles – conditions at which discontinuity in electrical resistivity was observed; dash-dot line – the phase boundary between hcp and the mixture of hcp+fcc phases according to Lin *et al.* (2003); melting lines for pure iron after Shen *et al.* (*2004*) and Boehler *et al.* (*1993*) are also shown).

In experiments at pressures above 150 GPa with *in situ* X-ray diffraction a double-side near infra-red laser heating system at GeoSoilEnviroCARS at the Advance Photon Source was used. Upon heating the hcp $Fe_{0.9}Ni_{0.1}$ phase at pressures above 200 GPa, it persist at least up to 2900 K (Fig. 3.1-5). At a pressure of 225(10) GPa and temperature of 3400(100) K we observed a complete transformation of the $Fe_{0.9}Ni_{0.1}$ alloy into the bcc phase (Fig. 3.1-5). Note that this structural transition takes place at pressures and temperatures close to the conditions at which the discontinuity in the resistance has been observed (Fig. 3.1-4).

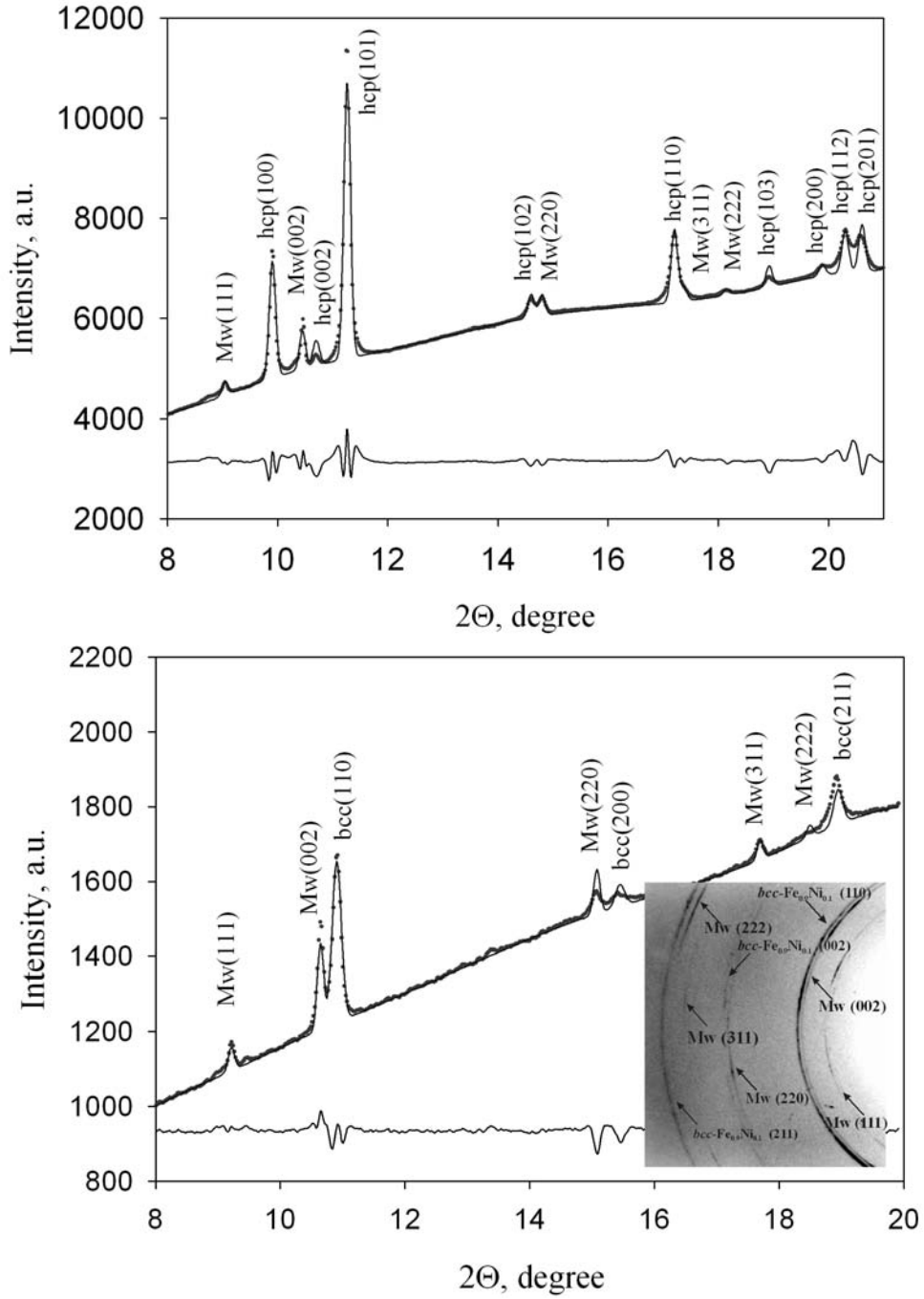

Fig. 3.1-5: Examples of the full-profile treated diffraction patterns collected at 194(10) GPa and 2900(100) K (upper panel) and 225(10) GPa and 3400(100) K (lower panel). The inset in the lower panel shows part of the 2D image (Mw – for $Mg_{0.87}Fe_{0.13}O$, hcp – for hexagonal closed packed $Fe_{0.9}Ni_{0.1}$, bcc – for body centered cubic $Fe_{0.9}Ni_{0.1}$).

The existence of a very high-pressure phase of pure iron has been proposed long ago, but no definitive proof has been obtained so far. We found the hcp-to-bcc phase transition in the $Fe_{0.9}Ni_{0.1}$ alloy at conditions reasonably close to those inferred by shockwave experiments This not only supports the interpretation of Brown and McQueen's (*1986*) shockwave data as

a solid-solid phase transition along the Hugoniout, but also suggests that iron alloys with geochemically reasonable compositions (*e.g.*, with significant nickel, sulfur, or silicon content) adopt the bcc-structure.

Synthesis of bcc $Fe_{0.9}Ni_{0.1}$ at pressures above 230 GPa and temperatures above 3400 K could have implications not only for understanding properties and dynamics of the Earth's solid inner core, but also for the liquid outer core. Changes of the structure of liquids above subsolidus phase boundaries are well known. If changes from "close-packed like" to "bcc-like" type structures occur in molten Fe-Ni alloy at pressures above 200 GPa, it may have implications for the density and rheology of the Earth's outer core as well as partitioning of light elements between differently structured parts of the molten core.

3.2 Geochemistry

Pressure modifies the geochemical character of many elements, forcing changes in the extent to which they partition between different minerals, melts and fluids. Several studies in this section, for example, reveal the effects of pressure on the partitioning of siderophile (metal loving) elements between metallic Fe-rich melt and silicate materials. This is important for understanding the fractionation that occurred as the core and mantle separated during Earth's formation. An additional complexity, however, is that such partitioning is also a function of oxygen fugacity, which controls the extent to which an element prefers the oxide (*i.e.*, silicate) or metallic state. There is evidence from certain meteorites that core formation may have occurred at very low oxygen fugacities, at least during the early stages, and under such conditions many elements that would not normally be considered siderophile would have partitioned into the core. Experiments and modelling described in this section indicate that there are a number of weakly siderophile element ratios in the mantle that could only have been obtained if metal silicate equilibration occurred at great depths within the mantle. A number of further studies in this section, however, also demonstrate how the presence of S and Ni can effect the way other elements partition, broadening the range of influences that must be considered in terrestrial core formation models.

Geophysical heat flow calculations hint at the existence of a deep isolated layer in the mantle, enriched in heat forming elements, and this is apparently supported by noble gas isotope systems, which also require a primordial reservoir. In one study from this section the possibility that potassium, which has a radiogenic heat producing isotope, could have strongly partitioned into such a deep primordial reservoir is examined using *ab initio* calculations, but this is, in fact, found to be unlikely. In another study the possibility that noble gases become more compatible in mineral phases at high pressures, is also being explored. If deep melting causes significant proportions of these gases to be retained in the mantle a deep primordial reservoir for noble gasses may be unnecessary.

The effect of pressure on the partitioning and stability of volatile elements such as fluorine and carbon also features in several studies in this section. While fluorine likely partitions into nominally fluorine-free mantle minerals such as olivine, carbon is quite different as it mainly exists in mineral phases in which it forms a structural component, such as diamond and carbonate minerals. In one study high melting temperatures have been measured for carbonated rocks at transition zone conditions, indicating that the subduction of solid carbonate minerals could recycle carbon deep into the mantle.

Magma types representative of some of the oldest rocks on Earth are widely considered to be the product of melting of subducted oceanic crust, the implications of which are explored in two studies in this section. During such melting events there is evidence that the Ti-bearing mineral rutile remained in the mantle residue. By measuring the solubility of rutile in melts typical of these events the temperature at which melting took place can be estimated. The Ti contents of natural samples when compared with experimental solubility data imply relatively high temperatures in some ancient subduction zones.

The final study in this section focuses on the partitioning of trace elements between biotite and granitic melts at upper crustal conditions with emphasis on its effect on magmatic-hydrothermal ore formation. The results show that while a number of transition metals are effectively removed from melts by biotite crystallisation, ore forming elements such as Cu and Mo are not, underlining the vital role that biotite plays in the formation of some granite-related ore deposits.

a. *Evolution of the enstatite chondrite EH4 Indarch at high pressure and high temperature: new constraints for early planetary differentiation (S. Berthet, V. Malavergne and R. Combes/ Marne-la-Vallée, in collaboration with D.J. Frost)*

Chondrite meteorites are characterized by variations in both bulk chemistry and oxidation state and have long been considered possible building blocks for the terrestrial planets. A number of studies have proposed that enstatite chondrites, highly reduced primitive meteorites, may have potentially participated in the accretion of the Earth. Examination of element ratios in Earth's mantle, which provides a "fingerprint" of the material from which the Earth formed, indicates that no known class of meteorite corresponds to a hypothetical bulk Earth composition in every aspect. To derive constraints on early accretion and differentiation processes and possibly resolve the debate on the formation of the Earth, requires information on the melting phase relations and element partitioning behaviour over a range of pressure, temperature and oxygen fugacity for a variety of chondritic meteorites. P-T melting phase relations for carbonaceous chondrites have been extensively studied experimentally up to pressures and temperatures corresponding to the transition zone and lower mantle. For the more reduced enstatite chondrite compositions only room pressure melting behaviour exits. In this study the melting phase relations of the enstatite chondrite sample known as Indarch have been experimentally investigated at HP-HT.

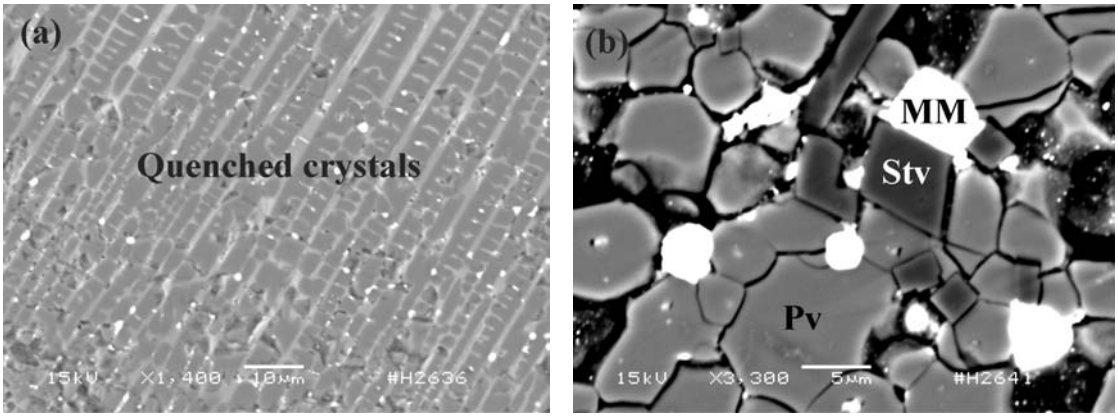

Fig. 3.2-1: Backscattered electron images of the run products: (a) H2636 – 10 GPa – 2000 °C – 20 min. Metallic sub micrometric nuggets are disseminated within the quenched crystals of silicate. (b) H2641 – 25 GPa – 2200 °C – 5 min. Two silicate phases are present: crystals of perovskite (Pv) and of stishovite (Stv). MM: metallic melt.

Natural EH4 chondrite Indarch, doped with a selection of trace elements, was used as the starting material for multianvil experiments. Experiments on the powdered sample were performed between 10-25 GPa and 1500-2400 °C. Figure 3.2-1 shows the texture of a recovered sample and the mineral phases that were present. Depending on the P-T conditions of the experiments, the silicate phase was either all liquid (*i.e.*, quenched crystals) or contained crystals of pyroxene, garnet, perovskite or stishovite in equilibrium with quenched liquid. The first results of this study are presented in Fig. 3.2-2 which shows preliminary P-T phase relations for the Indarch meteorite.

Phase compositions within the natural Indarch meteorite (nearly FeO-free enstatite, Si-rich kamacite FeNi-metal, and various sulphide phases) indicates equilibration under extremely reducing conditions (around IW-6). However, up to 10 wt.% of FeO was observed in the silicate portion of the recovered experimental samples and the metallic phases were Si free. These preliminary results indicate that oxidation of the samples has occurred at HP-HT and the fO_2 of the run products is estimated to be around IW-2. Chemical analyses of the high-pressure phases are currently in progress and the partitioning of major, minor and trace elements will be determined between the different phases in the experiments.

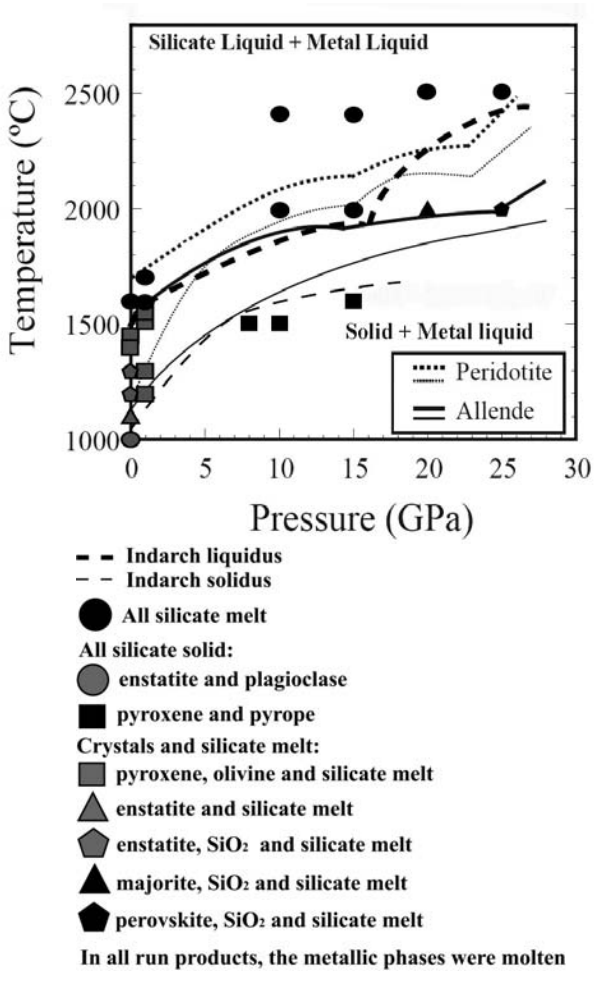

Fig. 3.2-2: P-T phase relations of Indarch with the preliminary liquidus and solidus of the meteorite compared to the ones previously determined for the meteorite Allende and KLB-1 peridotite. The data points at ambient pressure are from the literature. All other points are from this study.

b. *Evidence for high-pressure core-mantle differentiation from the partitioning of lithophile and weakly siderophile elements (U. Mann, D.J. Frost and D.C. Rubie)*

The separation of the Fe-rich metallic core from the silicate mantle was a major differentiation event in the history of the Earth. The metal/silicate element partition coefficients during this process fixed the geochemical signatures of both these reservoirs. A successful model for the core formation process must identify conditions where partitioning of siderophile elements would have led to the present day element abundance pattern of the Earth's mantle. Based on geophysical considerations, large melting events caused by giant impacts are likely to have resulted in metal-silicate equilibration at high pressures and temperatures at the base of a deep magma ocean. In addition, existing core formation models based mainly on the partitioning of Ni, Co, V and Cr argue that the material forming the Earth changed in redox state over the course of accretion, from initially reducing, to more oxidised. If the conditions proposed in such models are correct, the partitioning of other elements not initially included in these models should also be reproduced. In particular, there are a class of elements that can become siderophile at reducing conditions, which are in fact either not at all or only very weakly depleted from the mantle. The partitioning behaviour of such nominally lithophile elements can be used to exclude from core formation models any conditions under which these elements would become strongly depleted from the mantle. Suitable candidates for such studies are for example Ta and Nb or among the least depleted volatile elements Ga, In and Zn.

In high-pressure experiments using multianvil and piston cylinder apparatus we have tested the metal - silicate partitioning behaviour of Nb and Ga in comparison to the weakly depleted elements V and Mn over a large pressure range of 2 - 24 GPa and high temperatures of 1750 - 2600 °C. Under these conditions synthetic peridotite melts were equilibrated with Fe - rich metal melts employing MgO single crystal and graphite capsules. By adding varying proportions of Si to the metal, reducing conditions in the range of -4 to -1 log units below the iron wüstite buffer were obtained. Quenched metal and silicate compositions were analysed with electron microprobe. Partition coefficients were calculated from the metal to silicate concentration ratio of the respective elements. Results from graphite capsules had to be corrected for the change in activity coefficients caused by a relatively high concentration of C that dissolved in the metal liquids. For this we employed the difference between the partition coefficients from MgO and graphite capsules.

From the experimental data we have derived relationships for the dependence of the metal - silicate partition coefficients on P, T and oxygen fugacity and we have simulated the relative behaviour of Nb compared to V and of Ga compared to Mn. Figure 3.2-3 shows the development of the Nb partition coefficient D (Nb) as a function of pressure and calculated for temperatures fixed at the peridotite liquidus and 200 K above. The oxygen fugacity was fixed at the level necessary to match the V concentration of the mantle, which is expressed by a core - mantle partition coefficient D (V) of 1.5. At low pressures D (Nb) is extremely high

and values up to 10 would lead to a much stronger depletion of Nb than that observed for V, which is in contrast to the element abundances in the mantle. In fact, to match the Nb concentration of the mantle, the necessary Nb core-mantle partition coefficient would have to be lower than 0.8. This value is indicated by the horizontal dashed line in Fig. 3.2-3. On the other hand, we observe that D (Nb) clearly decreases with increasing pressure. However, the value of 0.8 is only reached at high pressures in the range of 20 - 30 GPa. This sets a tight constraint on the lower limit of pressure and allows us to exclude core formation scenarios that work at low pressures in the range of a few GPa only. Moreover, the fact that it will have required relatively high pressures for the correct mantle Nb/V ratio to be obtained lends strong support to the idea that a deep magma ocean existed during accretion, with metal silicate partitioning mainly occurring at the base of this ocean.

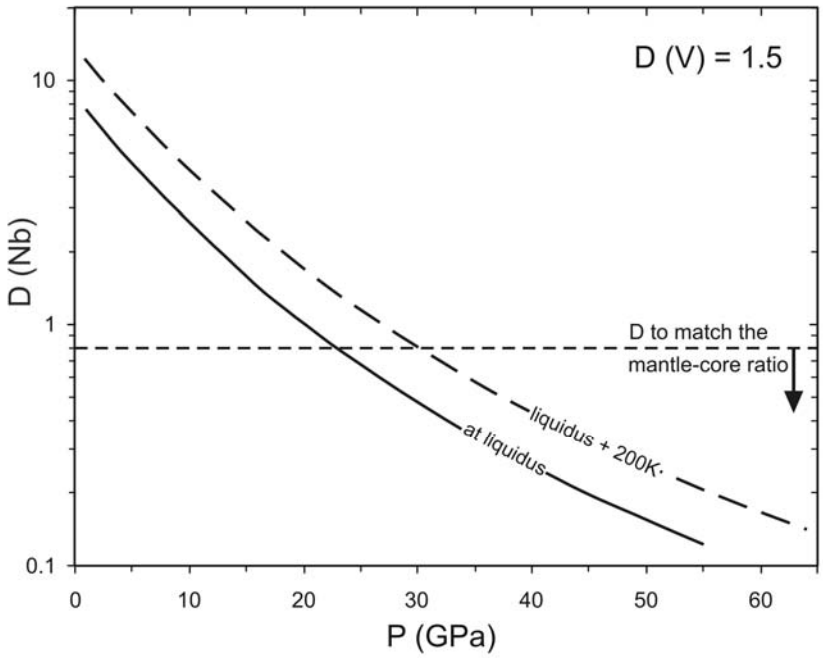

Fig. 3.2-3: The metal-silicate partition coefficient D of Nb as a function of pressure calculated for an oxygen fugacity where the partition coefficient for V (= 1.5) matches the observed present day mantle abundance. The temperature is fixed along the peridotite liquidus (solid line) and 200 K above it (dashed curve). The required D (Nb) for the core/mantle ratio (= 0.8) is indicated with the horizontal dashed line.

A similar conclusion can be reached by considering the relative behaviour of the elements Ga and Mn. These elements are not fractionated from each other in the Earth's mantle and, as Ga is more volatile, one would expect Mn to be more siderophile than Ga to explain their similar degrees of depletion in the mantle. In Figure 3.2-4 we have calculated the ratio of the metal/silicate partition coefficients of Ga and Mn ($K_D = D_{Ga}/D_{Mn}$) over a wide range of pressure from 1 - 80 GPa and with temperatures fixed to conditions at the peridotite liquidus

and in steps of 100 K to 300 K above it. The Ga-Mn partition coefficient decreases strongly with increasing pressure. However, in order for it to reach the a value compatible with the Ga/Mn ratio of the mantle, pressures would have to be at least as high as 60 GPa. At lower pressures, *e.g.*, in the range of 20-30 GPa where Nb and V mantle concentrations can be matched, Ga is much more siderophile than Mn and would consequently be strongly depleted from the mantle to a much larger extent than Mn. This would be in contrast to the near chondritic ratio of the two elements in the Earth's mantle. This further indicates that metal - silicate equilibration required extremely high pressures and temperatures to produce the element abundance pattern that we observe for the present day mantle and such conditions were very likely provided by a deep magma ocean.

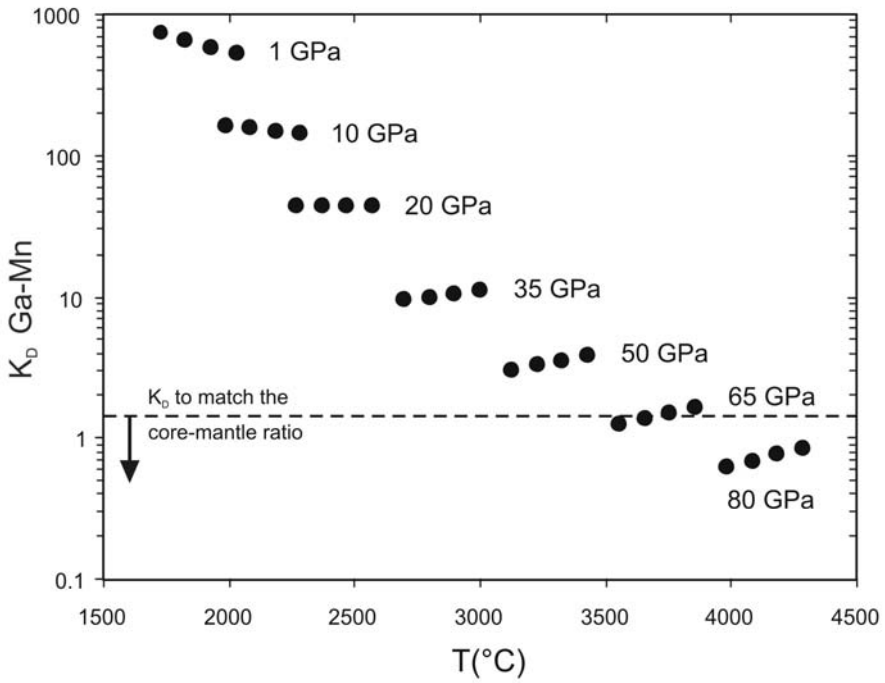

Fig. 3.2-4: The metal/silicate partition coefficient of Ga over that of Mn ($K_D = D_{Ga}/D_{Mn}$) as a function of temperature. Data are plotted at various pressures and temperatures corresponding to the peridotite liquidus and 100 K, 200 K and 300 K above. The required K_D (Ga-Mn) for the mantle (= 1.4) is indicated by the horizontal line.

c. *Oxygen partitioning between magnesiowüstite and liquid Fe-Ni alloy at high pressures and temperatures (K. Tsuno, D.J. Frost and D.C. Rubie)*

The Earth's outer core is believed to be composed of liquid Fe-Ni alloy together with one or more light elements of which oxygen is a possible candidate. Systematic investigations of the partitioning of oxygen between liquid Fe-Ni alloy and silicates/oxides at high pressures and temperatures are scarce, although such studies have been performed on partitioning between pure Fe liquid and silicates/oxides up to core-mantle boundary pressures. The experimental

results and thermodynamic interpretation of the latter studies (Asahara *et al.*, 2007, EPSL, 257, 435) show that the partitioning of FeO into Fe liquid, in equilibrium with silicates/oxides, has a minimum value at a pressure of 15-20 GPa. The partitioning of FeO into Fe-Ni liquid, however, in equilibrium with magnesiowüstite was observed to decrease in the pressure range 5-23 GPa (Rubie *et al.*, 2004, Nature, 2473). However, in this previous study metallic starting materials were used that contained up to 1.5 wt.% of Co, Cr, V, Si, Ti, that might have contributed to some scatter in the results. In order to clarify the effect of Ni on the partitioning of FeO into Fe liquid, we are investigating in this study the partition coefficient of FeO between Fe-Ni liquid and magnesiowüstite, defined as

$$K_d = X_O^{metal} X_{Fe}^{metal} / X_{FeO}^{magnesiowüstite}$$

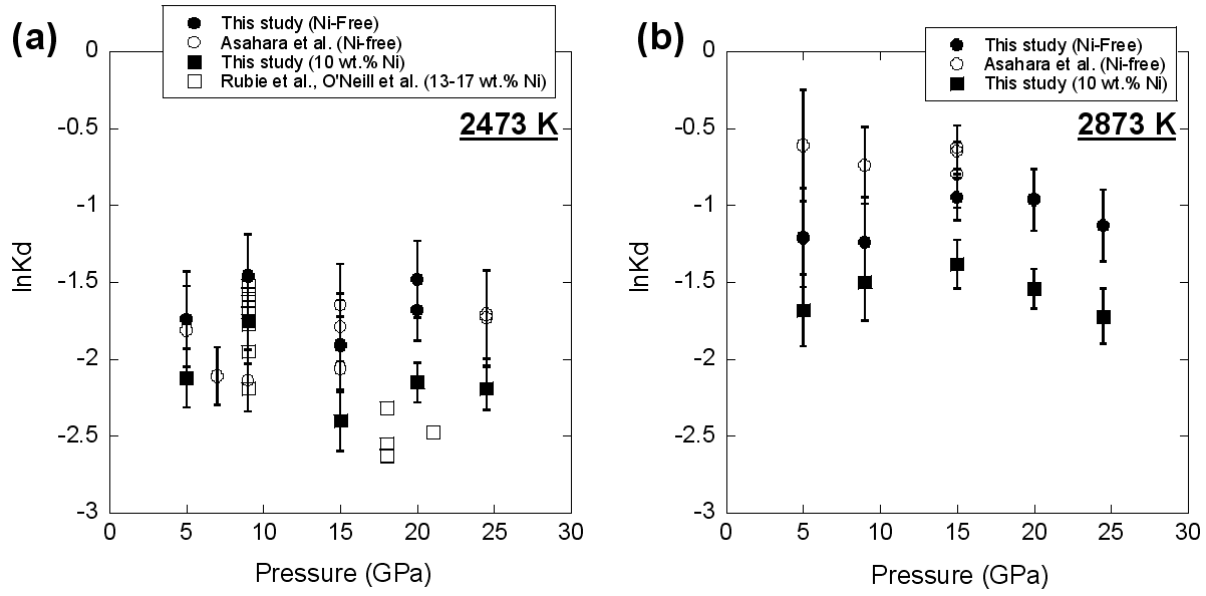

Fig. 3.2-5: The relationship between $\ln K_d$ and pressure at (1) 2473 K and (2) 2873 K. The data from this study are plotted as filled circles ($\ln K_d$ between magnesiowüstite and liquid Fe) and filled squares (magnesiowüstite and liquid Fe-10wt.% Ni). $\ln K_d$ between magnesiowüstite and liquid Fe from Asahara *et al.* (EPSL, 257, 435, 2007) as open circles, and that of magnesiowüstite and liquid Fe-Ni from O'Neill *et al.* (JGR, 103, B6, 12239, 1998) and Rubie *et al.* (Nature, 2473, 2004) as open squares are also shown.

High-pressure experiments were performed using the multianvil apparatus in the pressure and temperature ranges of 5-24.5 GPa and 2473-2873 K, respectively. Metallic starting compositions were (1) Fe-10 wt.% Ni and (2) Ni-free Fe, to which 0.5-1.5 wt.% O were added. Both compositions were run simultaneously in each experiment by containing them in a double-chamber MgO capsule. Our experimental results show that the K_d for Fe-10 wt.% Ni liquid + magnesiowüstite is lower than for pure Fe liquid + magnesiowüstite (Fig. 3.2-5). The

value of K_d for Fe-Ni melt + magnesiowüstite increases with temperature, but the pressure dependence is not yet clearly defined by our results. Based on this study, the concentration of oxygen in the Earth's core could be lower than previously estimated, although the effect of sulphur on oxygen solubility still needs to be investigated systematically.

d. *A new mass balance approach to modelling processes of core formation in terrestrial planets (D.C. Rubie, U. Mann, D.J. Frost and K. Tsuno, in collaboration with Y. Asahara/ Hyogo; P. Kegler and A. Holzheid/Kiel; H. Palme/Köln)*

The concentrations of siderophile ("metal-loving") elements in the Earth's silicate mantle have resulted from chemical interaction between liquid Fe-Ni metal alloy and silicate material during the separation of these phases to form the Earth's core. Thus, elements such as Ni, Co, W and Mo have been extracted from the mantle during this differentiation event and now reside mostly in the core. Recent models of core formation, that have been invoked to explain the concentrations of the siderophile elements that remain in the mantle, are based mostly on metal and silicate equilibrating at the base of a deep magma ocean that results from the energy released by one or more major impacts between the proto-Earth and smaller planetary bodies during accretion. In addition to the high pressures and temperatures of equilibration, oxygen fugacity is a crucial parameter that is generally fixed at about two log units below the iron-wüstite (IW) buffer in order to be consistent with the current FeO content of the mantle.

We are developing new multi-stage models of core formation, based on the partitioning of a range of both siderophile and lithophile elements, which involve the Earth accreting through a series of collisions with smaller bodies that had already differentiated at low pressure. Each impact results in a magma ocean in which the core of the impactor re-equilibrates with silicate liquid at high pressure before merging with the Earth's proto-core. Instead of making assumptions about oxygen fugacity, the bulk composition (oxygen content) of the accreting chondritic material is defined and can be varied for both the proto-Earth and impactors. The compositions of coexisting liquid metal and liquid silicate at high pressure and temperature are calculated using a rigorous mass balance combined with partitioning equations for FeO, Ni, Si and other siderophile and lithophile elements. The oxygen fugacity is determined by the partitioning of FeO between metal and silicate and is a function of pressure, temperature and bulk oxygen content.

An important constraint for core formation is that core-mantle partition coefficients for Ni and Co should both converge to the values of 23-28 that are estimated for the Earth. Based on a recent study of the partitioning of Ni and Co over a wide *P-T* range (BGI Annual Report 2005, pp. 46-48), together with our new data for the metal-silicate partitioning of Si and FeO, this constraint is not satisfied by a single-stage core formation process under any conditions because the partition coefficients for Ni and Co converge at values of < 10 and are therefore much too low. In the present multi-stage model, the appropriate values can be reached if only

some fraction of each impactor core re-equilibrates with silicate liquid in the magma ocean (as proposed previously based on Hf-W isotope studies). Physically, this would mean that only a fraction of impactor cores emulsify as they sink through the magma ocean before merging with the Earth's core. Incorporating other elements (*e.g.*, V, Nb and Cr) in the model requires, in addition, that the bulk compositions of the impactors change during accretion from FeO-poor to FeO-rich. Then, with the resulting increase in oxygen fugacity, incomplete re-equilibration of the cores is required to satisfy the Ni-Co constraint (Fig. 3.2-6). In addition, these models enable the concentrations and identities of light elements (O and Si) in the core to be estimated.

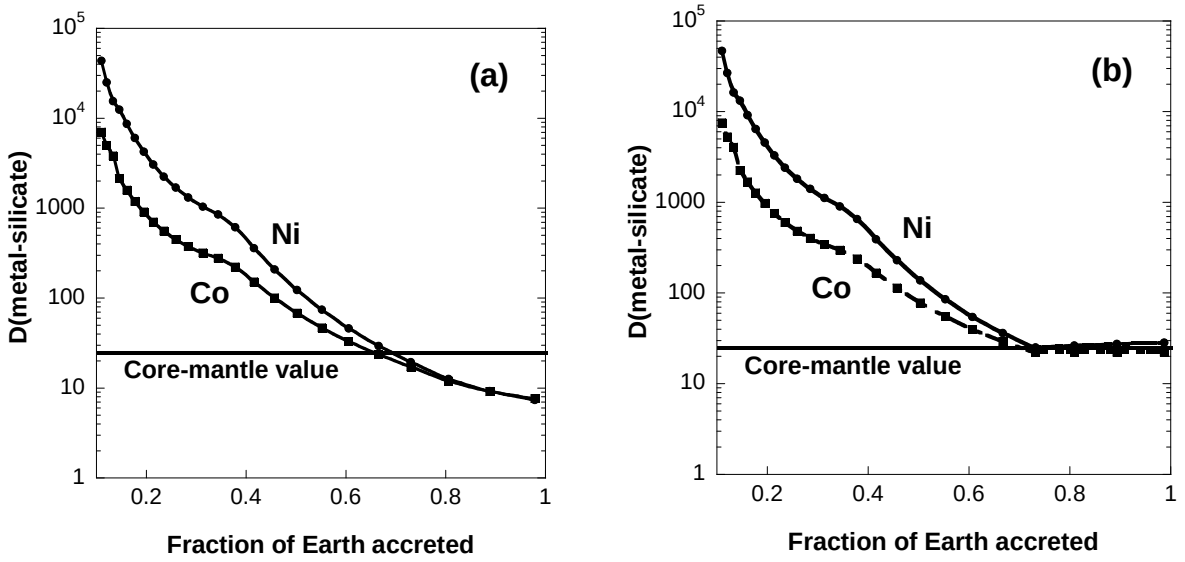

Fig. 3.2-6: Evolution of the partitioning of Ni and Co between the core and mantle as a consequence of multistage core formation during Earth's accretion. Each symbol represents a re-equilibration event following an impact. Both of these results are for heterogeneous accretion in which the initial 70 % of the Earth is formed from chondritic material that has a low oxygen content (1 % FeO) and the final 30 % accretes from more oxidised chondritic material. In (a), the metallic cores of impactors equilibrate completely at high P and T, and the resulting core-mantle partition coefficients for Ni and Co are much too low. (b) disequilibrium is included whereby only a fraction of the impactor cores re-equilibrate with silicate at high P. During the initial 70 % of accretion, 60 % of the impactor core material re-equilibrates whereas in the final stages only 8 % re-equilibrates with the magma ocean. The resulting values of the Ni and Co partition coefficients are close to those required to explain current mantle concentrations.

e. *Consequences of a Hadean sulfide liquid in the aftermath of a giant impact on Earth (L. Rose-Weston, D.J. Frost and D.C. Rubie)*

It is widely accepted that one or more giant impacts occurred in the late stages of Earth's accretion, adding on the order of 10 % of Earth's final mass and causing widespread melting of the previously differentiated planet. If the Earth was relatively oxidized at this stage of

accretion and if the impactor added volatiles such as sulphur to the growing Earth, it is possible that the ensuing silicate 'magma ocean' may have contained a low volume (~ 2 %) FeS-rich liquid. Removal of this 'Hadean matte' to the core would have altered the concentrations of chalcophile (sulphide-loving) elements in the mantle. The chalcophile nature of Pb, and removal of a sulphide liquid after a giant impact has been suggested to explain discrepant ages for the timing of core formation between the U-Pb and Hf-W isotopic systems. Daughter elements Pb and W may have also been fractionated in the mantle during this event, as W is non-chalcophile. Understanding the partitioning behaviour of Pb and W in the metal±sulphide-silicate system at high pressure and temperature is essential for evaluating the validity of this hypothesis. Limited partitioning data suggest that Pb behaves essentially as a lithophile element under conditions most likely for accretion and core formation, whereas W is moderately siderophile. Even in the presence of 10 wt.% S, Pb has been predicted to be lithophile above 35 GPa. Tungsten has been shown to be non-chalcophile, however, its behaviour at high pressure is not well constrained.

The aim of this study is to systematically determine the partitioning behaviour of moderately siderophile elements (Pb, W, Sn, Te, Se, Ni, and Cu) at high temperature and pressure in the presence of varying amounts of sulphur. A series of metal-silicate and sulphide-silicate partitioning experiments were performed using both piston-cylinder and multianvil presses. Experiments were performed at 2000 °C between 3 and 19 GPa. The S content was varied between 0 to 35 wt.% of the metallic phase, the latter corresponding to an FeS composition. Oxygen fugacity conditions were dictated by the experimental S content. Chemical equilibrium between liquids of metal and silicate was established by performing a time series. Run products were analyzed by electron microprobe (major elements and S in both phases), and laser-ablation ICP-MS (trace elements in the silicate phase). A typical run product is shown in Fig. 3.2-7.

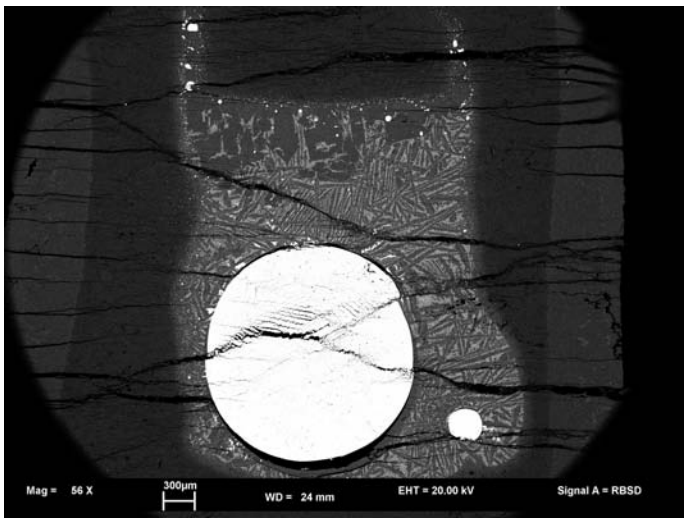

Fig. 3.2-7: Backscattered electron image of a sulphide-silicate partitioning experiment (3 GPa, 2000 °C) containing quenched metal and silicate phases. Some olivine is observed to be nucleating on the roof of the capsule, which was composed of polycrystalline MgO.

Metallic and silicate liquids quench to a coarse-grained texture, necessitating large spot sizes for both electron microprobe (10-50 μm) and laser-ablation ICP-MS (50-100 μm) analysis. A basaltic glass containing Te (60 ppm), Se (490 ppm), and Pb (890 ppm) was synthesized and analyzed by solution ICP-MS at the University of Toronto for use as a laser ablation standard for the silicate phase. Ni, Sn, W, and Cu were standardized against NIST 610 glass.

Partitioning results are displayed in Fig. 3.2-8 for Pb, Te, Se, Sn, Cu, and W. In S-free experiments at 3 GPa and 2000 °C, all six elements partition between metallic liquid and silicate liquid in a predictably siderophile manner. Sulphur is moderately siderophile at these run conditions, and is therefore concentrated in the metallic phase. As the S content increases, element partitioning is affected. Te, Se, and Cu are chalcophile elements, as the addition of S causes the sulphide-silicate partition coefficients (D) to increase. A slight increase in Pb partitioning behaviour is observed between 0 and 40 mol.% FeS in the metal phase, but this trend is reversed closer to an FeS composition, therefore Pb is only slightly chalcophile. W, Sn, and Ni (not shown) on the other hand are not chalcophile, as the addition of S causes partition coefficients to decrease. Both Sn and Ni remain siderophile, however, in contrast to W, which becomes lithophile when the metal phase contains greater than 40 mol.% FeS. Experimental results at higher pressures between 5 and 19 GPa indicate that partition coefficients of Ni and Cu decrease as pressure increases, whereas those of Sn do not change significantly. In contrast, the partition coefficient of W increases as pressure increases.

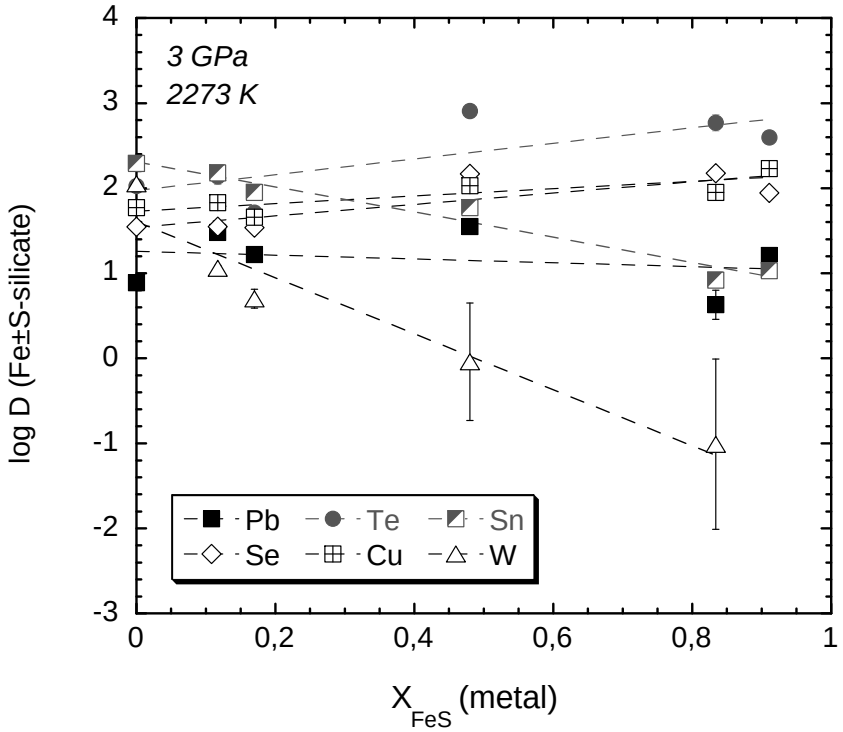

Fig. 3.2-8: Metal- and sulphide-silicate partitioning of siderophile elements at 3 GPa and 2000 °C as a function of mole fraction of FeS in the metal phase. Linear fits are not weighted for error.

The relatively weak siderophile behaviour of Pb over a wide range of S content suggests that partial removal of late-stage 'Hadean' sulphide liquid would not greatly affect the total concentration of Pb in the mantle. With the available experimental data, our findings do not support such a mechanism to fractionate Pb from W after the giant impact, and therefore the U-Pb chronometer was likely not reset by this mechanism. Our partitioning results can also be used in an Earth differentiation model in which initial core formation occurred at high pressure and temperature (simulated by S-free metal-silicate partitioning at 3 GPa), followed by the formation and slight removal of a late-stage 'Hadean' sulphide liquid (simulated by Fe(50mol.%FeS)-silicate partitioning at 3 GPa). The chalcophile nature of Te, Se, and Cu promotes further depletions of these elements from the mantle if such a 'Hadean' sulphide liquid was partially removed from the mantle. The magnitude of this depletion depends on the FeS content of the metal phase, pressure and temperature estimated for the base of the magma ocean, and the amount of sulphide liquid removed to the core. Further experiments at high pressure and temperature will help to refine this model.

f. *New experimental results for the HP-HT partitioning behaviour of the highly siderophile elements (Ru, Rh, Pd, Re, Ir, Pt) (U. Mann, D.J. Frost, A. Audétat and D.C. Rubie, in collaboration with H. Becker/Berlin)*

In this study liquid metal - liquid silicate partitioning data for the highly siderophile elements (HSE's) Ru, Rh, Pd, Re and Pt at pressures up to 18 GPa and high temperatures up to 2500 °C have been determined. At 1 bar HSE are know to have extremely high metal-silicate partition coefficients of $\geq 10^4$. With such a high preference for the metal rather than a coexisting silicate phase these elements should have consequently been completely extracted from the mantle while the Earth was differentiating into mantle and core. However, they are present in the mantle in much higher concentrations than these 1 bar partition coefficients would predict and in approximately chondritic proportions. The main theory to explain this observation is that these elements were strongly depleted from the mantle but were added back by the addition of a late veneer of a highly oxidized, chondritic material (~ 1 wt.% of the Earth's total mass) that occurred after core/mantle differentiation had ceased. Another possibility, however, is that pressure might lower HSE metal/silicate partition coefficients to levels where metal-silicate partitioning alone might explain the abundances in the mantle. To data, however, there is scant high-pressure HSE partitioning data through which to test this possibility.

We have performed liquid - metal liquid - silicate partitioning experiments for Ru, Rh, Pd, Re, Ir and Pt in a range of 3.5 to 18 GPa and 2150-2500 °C using a multianvil apparatus. Performing experiments on this group of elements presents a number of experimental and analytical difficulties. In previous studies at 1 bar it has been observed that concentrations in the silicate melt might be overestimated due to the presence of tiny metal particles, called nuggets, that are mechanically trapped but do not dissolve in the silicate melt. In order to

minimize the risk of incomplete metal separation we chose a rather depolymerized peridotitic silicate melt composition mixed with Fe-metal and added the HSE's as pre-alloyed metal chips that were placed into the middle of the MgO single crystal capsule. By varying the Fe to HSE (50 - 90 wt.%) proportions in the bulk metal phase, redox conditions could be varied in the range of -1.5 to +2.5 log units relative to the iron wüstite buffer. Because of the extremely low concentrations of the HSE's in the quenched silicate phase (ppm to ppb level) they need to be analysed with a microanalytical technique such as LA-ICP-MS. Additionally, there is a lack of appropriate standards for HSE measurements in silicate phases using such techniques and we have therefore synthesized silicate glass standards doped with the HSE's Ru, Rh, Pd, Re, Ir and Pt at concentrations of between 1 - 120 ppm. The quenched metal melt was analyzed using the electron microprobe.

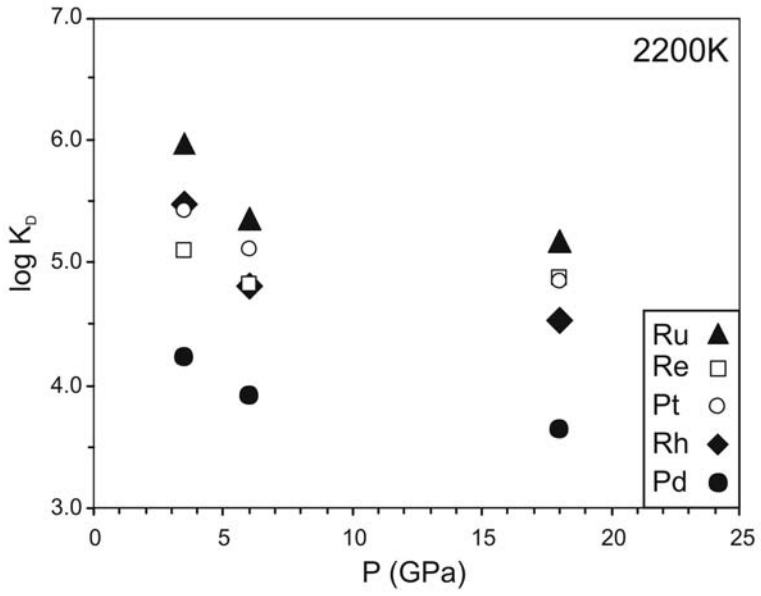

Fig. 3.2-9: Comparison of the pressure dependence of the K_D values of Ru, Rh, Pd, Re, Pt at a common temperature of 2200 K. Compositional effects on the metal activity coefficients were not corrected for.

In general we observe that all studied elements become less siderophile with increasing pressure and temperature. The effect of pressure is more significant than temperature and Fig. 3.2-9 shows the distribution coefficient K_D (*i.e.*, the partition coefficient of the elements relative to the metal-silicate ratio of Fe) for the elements Ru, Rh, Pd, Re, Pt as a function of pressure with all data corrected to a common temperature of 2200 K. In addition to the overall negative pressure trend there may be a change from a strong decrease of the K_D values < 6 GPa to a weak decrease between 6 and 18 GPa. This pressure effect on the partitioning behaviour of the HSE's resembles that recently reported for Ni and Co. In order to test whether this principal trend also applies to natural systems, we must correct our partitioning data for the fact that large concentrations of HSE were present in the metallic phase of our experiment. Metal HSE activities must therefore be corrected to infinite dilution. We have

performed these activity corrections for the Rh data in Fig. 3.2-10. The corrected data clearly confirm the observed pressure effect and the presence of two distinct regimes, especially when 1 bar are considered from the literature. These results imply that even though the partition coefficients for the HSE's do decrease with increasing temperature and pressure, they are still extremely high at 18 GPa and inconsistent with the attainment of mantle HSE concentrations. Considering the weak effect of pressure above 6 GPa, it is unlikely that significantly higher pressures would be sufficient to explain the HSE mantle abundances by metal-silicate equilibration in a deep magma ocean. Additionally, even though some of the HSE partition coefficients are similar in the studied pressure range, there is still a difference of over one order of magnitude between the K_D's of Ru and Pd (Fig. 3.2-9) which is in contrast to the observed chondritic ratios of these elements in the mantle. Therefore, a process such as the accretion of an undifferentiated late veneer seems to be a more plausible explanation for mantle HSE abundances.

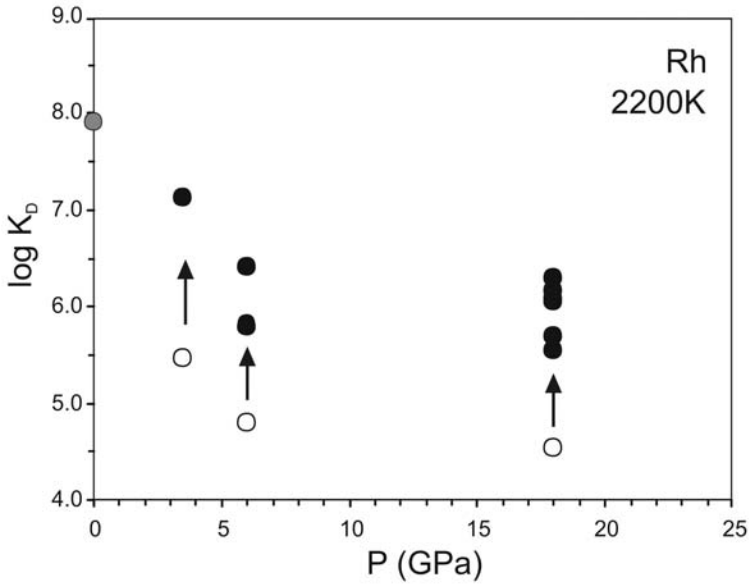

Fig. 3.2-10: The logarithmic values of K_D for Rh (corrected for activities of Rh and Fe in the metal melt) as a function of pressure after correcting to 2200 K (black symbols). The grey symbol shows a 1 bar result from the literature. For comparison, the experimental K_D values, un-corrected for metal activities are shown with the unfilled symbols; the arrows indicate the effect of correction.

g. *Ab initio predictions of potassium partitioning between Fe and Al-bearing $MgSiO_3$ perovskite and post-perovskite (K.K.M. Lee/Las Cruces and S. Akber-Knutson/San Diego, in collaboration with G. Steinle-Neumann)*

Partitioning of radioactive isotopes in the Earth's interior is important to the thermal evolution of the Earth as radioactive decay provides an important source of energy for mantle dynamics. As a consequence, enriched (or depleted) reservoirs in the mantle influence the energy

balance in geodynamics. The recently discovered transition in $MgSiO_3$ from perovskite (pv) to post-perovskite (ppv) in the lowermost mantle, together with its increased density (ppv is ~ 1.5 % denser than pv at lowermost mantle conditions) provides the possibility for an enriched or depleted zone at the base of the mantle. Therefore, the partitioning of radiogenic isotopes among the phases of the lower mantle is of central importance to the geochemistry and geodynamics of the deep Earth.

Where potassium (K) resides in the lower mantle may determine where this potentially important internal heat source is located. The pv-ppv phase transition is the only phase transition known in the lower mantle and the ppv bearing D" layer could consequently provide a distinct reservoir for heat-producing potassium. Here we explore this possibility by means of *ab initio* computations on the incorporation of K into $MgSiO_3$ pv and ppv at lower mantle pressures. In order to incorporate monovalent K into the pv or ppv structures, we choose to charge couple K^+ with Fe^{3+} or Al^{3+}, the most abundant trivalent cations in the lower mantle that are incorporated readily in $MgSiO_3$ pv. In the computations we consider Fe and Al-bearing $MgSiO_3$ perovskites and their corresponding high-pressure polymorphs, Fe and Al-bearing $MgSiO_3$ post-perovskites.

To investigate K partitioning between pv and ppv we consider the following two reactions composed of oxides and 160-atom silicate supercells:

$$(Mg_{30}\mathbf{M}K)Si_{32}O_{96}[pv] + 2MgO \leftrightarrow Mg_{32}Si_{32}O_{96}[pv] + \frac{1}{2}K_2O + \frac{1}{2}\mathbf{M}_2O_3 \qquad (1)$$

$$(Mg_{30}\mathbf{M}K)Si_{32}O_{96}[ppv] + 2MgO \leftrightarrow Mg_{32}Si_{32}O_{96}[ppv] + \frac{1}{2}K_2O + \frac{1}{2}\mathbf{M}_2O_3 \qquad (2)$$

where **M** is Fe or Al. Combining reactions (1) and (2), yields a reaction with only pv and ppv terms:

$$(Mg_{30}\mathbf{M}K)Si_{32}O_{96}[pv] + Mg_{32}Si_{32}O_{96}[ppv] \leftrightarrow (Mg_{30}\mathbf{M}K)Si_{32}O_{96}[ppv] + Mg_{32}Si_{32}O_{96}[pv] \qquad (3)$$

where the oxide terms cancel. For perovskite and post-perovskite, two Mg sites are allowed to have either an iron-potassium or an aluminium-potassium pair that replaces two magnesium atoms, in order to locally charge balance the $MgSiO_3$ based solid solution in pv and ppv.

The electronic structure and energetics of the supercells used have been calculated by density functional theory (DFT)-based electronic structure methods. We use the generalized gradient approximation (GGA) for all of our computations in order to assure compatibility of results as well as to compare with previous computations in the Mg-Fe-Al pv and ppv solid solutions. We use the projector augmented wave method (PAW) as implemented in the Vienna *Ab initio* Simulation Package (VASP). For the iron-bearing silicates, we perform spin-polarized computations.

In order to determine thermodynamic phase stability as well as partitioning, we compute the Gibbs free energy $G = E+PV-TS$ for $(Mg_{30}\mathbf{M}K)Si_{32}O_{96}$, where E is the internal energy computed from the *ab initio* computations, P is pressure determined from the Birch-Murnaghan equation of state, V is volume, T is temperature and S is entropy, composed of two parts: the vibrational S_{vib} and configurational S_{conf}. Enthalpy H comprises the first two terms of the above expression for Gibbs free energy and is used in this study, since the computations are performed under static conditions, *i.e.*, at 0 K.

We compute the difference in enthalpy ΔH between the equilibrium reactions 1 and 2 (Fig. 3.2-11). At 0 K, we find that at all mantle pressures, K prefers the pv over ppv structure for both the Fe and Al-bearing silicate, with Fe making ppv slightly more receptive to K than the Al-bearing counterpart.

Our results imply that potassium is preferentially partitioned into pv in the Earth's mantle, which makes an enriched lowermost mantle layer based on the stability of ppv unlikely. Even if a dense layer of Fe-rich ppv could be maintained at depth due to preferential partitioning of Fe into ppv it would not be enriched in potassium.

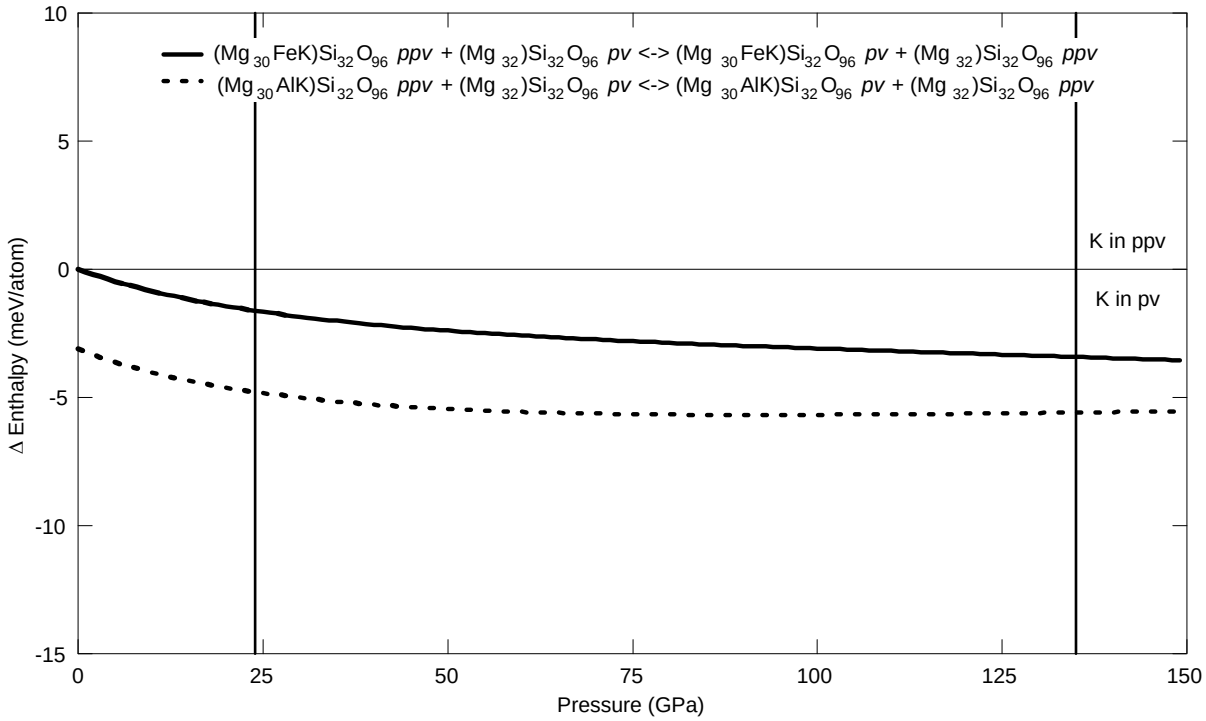

Fig. 3.2-11: ΔH per atom versus pressure for reaction 3. The solid curve corresponds to **M** = Fe and the dashed curve corresponds to **M** = Al. Negative ΔH values correspond to K preferring the pv structures, whereas positive ΔH values correspond to K favoring ppv structures. The two vertical lines correspond to the pressures of the upper-lower mantle boundary (~ 24 GPa) and core-mantle boundary (~ 136 GPa).

h. *Iron partitioning between magnesiowüstite and Mg-perovskite in pyrolite up to 50 GPa (T. Irifune, T. Shinmei, T. Sanehira and Y. Tange/Matsuyama; K. Funakoshi/Hyogo; C.A. McCammon, N. Miyajima, D.J. Frost and D. Rubie)*

The lower mantle has been considered to be a geophysically "quiet" place relative to the upper mantle and mantle transition region except for the lowermost part (the D" layer). However, recent seismological studies have demonstrated that there are some minor discontinuous changes in the seismic velocities in the upper to the middle parts of the lower mantle, which are generally attributed to the presence of subducted slabs or to some unknown phase transitions in the mantle material under the corresponding P, T conditions. In order to address this issue, careful and precise observation of the possible phase transitions and associated chemical changes in mantle materials are needed.

We have developed techniques to produce pressures to ~ 60 GPa and temperatures to 2000 K in a multianvil apparatus using sintered diamond anvils. Using this technique, combined with synchrotron and other radiation sources, *in situ* and *ex situ* observations on the phase transitions and chemical composition changes in a pyrolite composition have been made, with particular emphasis on the variation of partitioning of iron between magnesiowüstite (Mw) and $MgSiO_3$-perovskite (Pv) as a function of pressure.

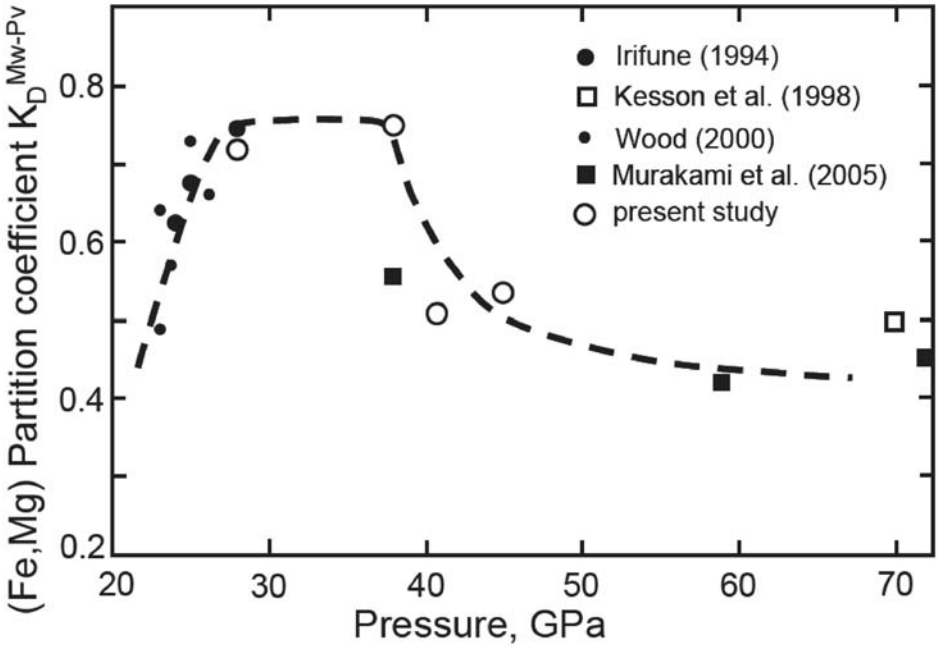

Fig. 3.2-12: Variation of the Fe-Mg partition coefficient (K_D) between magnesiowusitite and $MgSiO_3$ perovskite in pyrolite or peridotite compositions as a function of pressure. Data source: Open circles, present study; Solid circles, Irifune (Nature 370, 131-133, 1994); small solid circles, Wood (Earth Planet. Sci. Lett. 174, 341-354, 2000); Open square, Kesson *et al.* (Nature 393, 252-255, 1998); Solid squares, Murakami *et al.* (Geophys. Res. Lett. 32, L03304, 2005).

Fig. 3.2-12 summarizes the observed changes in the Fe-Mg partition coefficient between Mw and Pv (K_D(Mw/Pv) = (Mg_{Mw}/Fe_{Mw})/(Mg_{Pv}/Fe_{Pv})) in the present study, which are compared with those observed in earlier studies with pyrolite or peridotite compositions up to about 70 GPa. It is seen that K_D increases with increasing pressure up to about 28 GPa, which is interpreted in terms of substitutions of 6- or 8-fold coordination sites by Fe^{3+} in the presence of Al^{3+}, as the Al^{3+} content in Pv increases with pressure in this pressure interval. The K_D value stays essentially constant (K_D = ~ 0.75) at pressures between 28 and 38 GPa, where virtually no changes in both phase assemblage (*i.e.*, Pv + Mw + $CaSiO_3$-Pv) and chemical compositions of the individual phases are observed. However, K_D notably decreases thereafter down to ~ 0.5, consistent with the values observed in earlier studies by other laboratories using the diamond anvil cell. Significant iron enrichment in Mw was observed at pressures above 40 GPa, while Pv became slightly more Mg-rich.

In order to examine the possible changes in Fe^{2+}/Fe^{3+} ratios in Mw and Pv with increasing pressure, EELS and Mössbauer measurements have been made on two samples recovered from the runs at 28 GPa (M439) and 41 GPa (M248), at temperatures of 1600 °C and 1800 °C, respectively. The EELS measurements demonstrated that iron in Mw in both of these samples is essentially Fe^{2+}, with the $Fe^{3+}/(Fe^{2+}+Fe^{3+})$ value being less than ~ 0.02 (Fig. 3.2-13a), which is consistent with Mössbauer spectroscopic analyses on the same sample and those reported previously for a peridotite composition at 26 GPa by EELS measurements. Thus the notable increase of iron in Mw can be attributed to the increase of Fe^{2+} in this phase with pressure.

On the other hand, the EELS measurements on these samples show that the $Fe^{3+}/(Fe^{2+}+Fe^{3+})$ values for Pv at 28 GPa (M439) and 41 GPa (M248) are 0.66 (Fig. 3.2-13b) and 0.71, respectively, while those based on Mössbauer measurements are 0.63 (Fig. 3.2-14) and 0.52. It should be noted that the quality of the collected spectra in both EELS and Mössbauer measurements for the latter sample is not so high, and that these values may have significant uncertainties at 41 GPa. Nevertheless, these values reasonably agree with those estimated from literature values of the systematic relation between $Fe^{3+}/(Fe^{2+}+Fe^{3+})$ and Al content in Al-beraing Pv (~ 0.4-0.7 for X_{Al} = ~ 0.1), and it can be said that $Fe^{3+}/(Fe^{2+}+Fe^{3+})$ in Pv at these pressures may stay in a range of ~ 0.6-0.7. As it seems most likely that the $Fe^{3+}/(Fe^{2+}+Fe^{3+})$ values in both Mw and Pv do not change significantly with increasing pressure, the notable decrease in K_D at pressures above ~ 38 GPa cannot be attributed to the changes in iron content associated with the increase/decrease in solubility of ferric iron in the two phases with pressure.

Recent theoretical and experimental studies suggest that the electronic high-spin to low-spin transition occurs in Mw at pressures in the lower mantle, depending on the iron content of this phase. For instance, one recent study demonstrated that the spin transition in Mw with $Mg^{\#}$=81.25 would occur over a wide pressure interval between ~ 35 GPa and ~ 80 GPa along a geotherm, on the basis of a first-principles calculation. The effective ionic radius of ferrous

iron in the low-spin state is smaller than that of Mg^{2+}, and thus the gradual enrichment of iron in Mw is expected to occur upon the smeared-out spin transition in Mw, provided that no such spin transition occurs in Pv in the corresponding pressure range, which is currently in debate. The notable increase in the iron content in Mw and slight decrease of iron in Pv, and hence the apparent decrease in K_D as shown in Fig. 3.2-12, may thus be attributed to the occurrence of the spin-transition in Mw at pressures near 38 GPa, consistent with the pressures predicted by the first-principles calculation. Additional experiments at higher pressures to ~ 60 GPa are currently being conducted to confirm this interpretation for the variation of the iron partitioning between Mw and Pv with pressure.

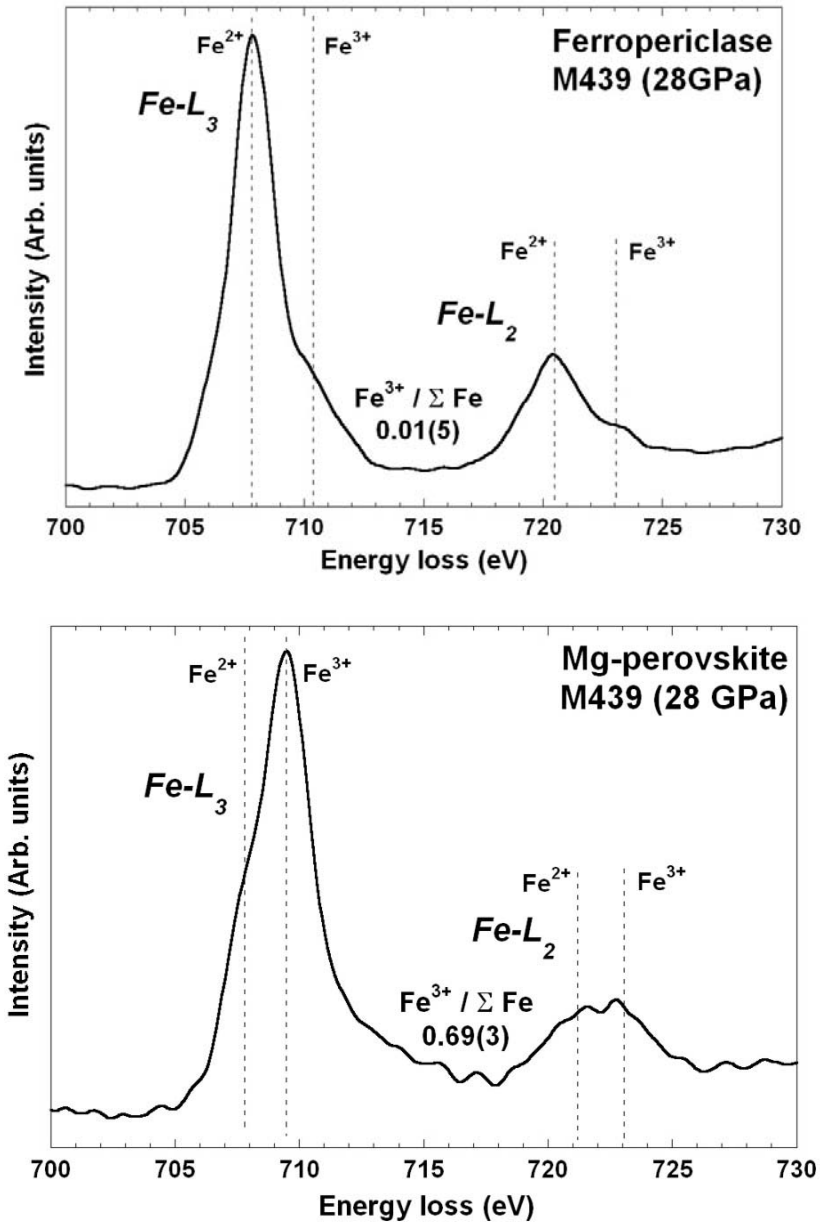

Fig. 3.2-13: Fe $L_{2,3}$-edge electron energy-loss spectra (EELS) from sample M439 (28 GPa) for magnesiowüstite (a) and $MgSiO_3$ perovskite (b).

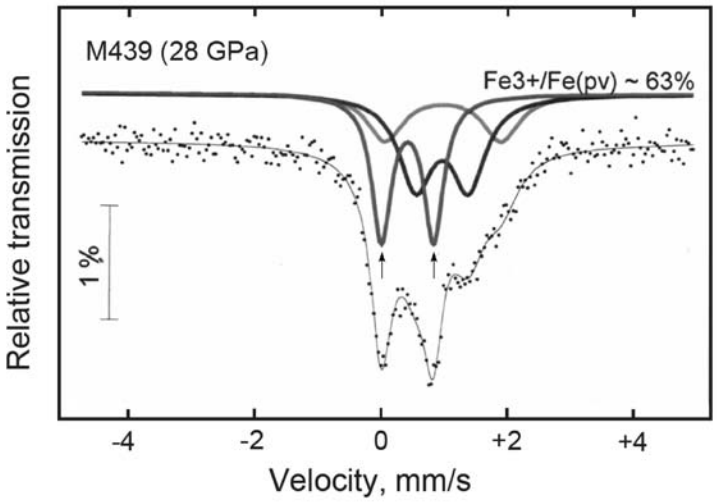

Fig. 3.2-14: Mössbauer spectrum of sample M439 (28GPa) recorded using a point source. The quadrupole doublet due to Fe^{3+} absorption is indicated by arrows.

i. *Partitioning of noble gases during mantle melting (S. Parman/Durham, C. Ballentine/ Manchester, S. Kelley/Milton Keynes, in collaboration with C.A. McCammon and D.J. Frost)*

Due to their unique characteristics, the noble gases (He, Ne, Ar, Kr, Xe) are central to chemical evolution models for the Earth's interior and atmosphere. Despite this importance, surprisingly little is known about partitioning of noble gases between solids and melts. There are only a handful of experiments at near-surface pressures, and only 5 data points from a single study (only for Ar and Kr) at mantle pressures. Models of mantle/atmosphere separation as well as mantle convective structure are based upon the general assumption that noble gases, because they have no charge, are highly incompatible during melting. However, low-pressure experimental data contradict this assumption, and indicate that significant amounts of noble gases can be retained in crystalline solids after melting. If so, the current models of atmospheric separation and mantle convection will need to be revised. However, it is not clear that the low-pressure experimental results (< 0.1 GPa) can be simply extrapolated to the high pressures relevant to mantle melting (> 1 GPa), particularly in light of the large changes in solubility and partitioning exhibited by other volatiles (H_2O, CO_2, S).

Analyzing noble gas concentrations is traditionally performed by crushing and/or melting solid materials (olivine crystals, glass chips). Adapting these methodologies to analyzing crystal-melt partitioning experiments is not straightforward because crystals must be physically separate from the melts. Previous studies have shown that once crystals and melt are in contact, it is difficult to recover crystals that are not melt contaminated. One previously successful method is to separate the melt and crystals during the experiment, by placing the melt in one capsule and the crystals in another. In this case, the gas atmosphere of the furnace allows the noble gases to equilibrate with the melt and crystals, and so the melt and crystals

should themselves be in equilibrium, at least with respect to the species in the atmosphere of the furnace. In this study this technique has been adapted for use in high-pressure experiments. The basic design is shown in Fig. 3.2-15 The bottom of a graphite capsule is filled with a basalt composition (or any other melt). Above that are placed a series of crystal discs. The discs are separated from the melt and each other by layers of diamond. The diamond layers provide an open network for the volatiles to move through (advection) and so equilibrate between the crystal discs and melt, while minimizing the interaction between the melt and crystal.

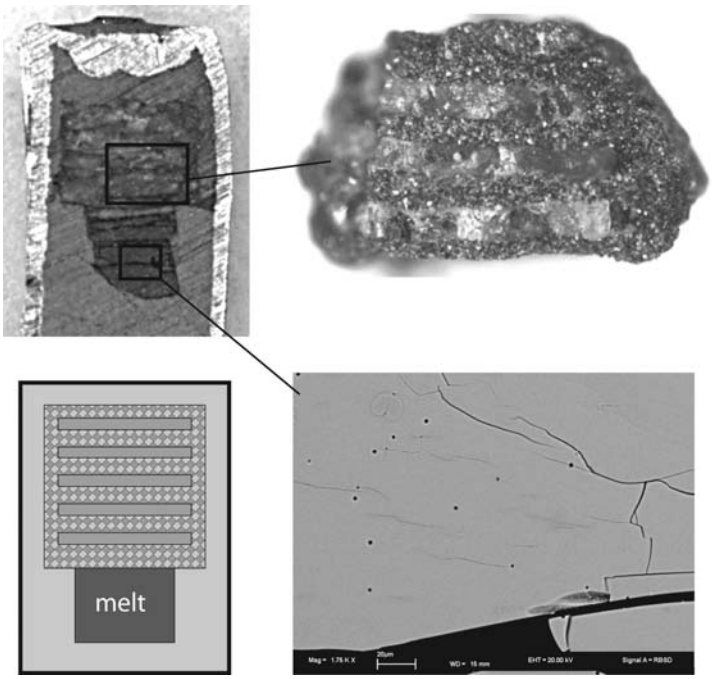

Fig. 3.2-15: Experimental geometry. *Top left* – sectioned experiment showing crystal discs above melt, surrounded by graphite and finally by the Pt outer capsule. *Top right* – three discs of olivine surrounded by diamond, removed from a 2 GPa experiment. *Bottom right* – SEM image of melt from an experiment showing small bubbles, indicating that the melt was saturated with noble gases throughout the experiment. *Bottom left* – idealized geometry of experiments.

The other main difficulty with the experimental design is how to get enough noble gases into the capsule to begin with. Helium, in particular, diffuses rapidly out of the capsules, and so a significant quantity needs to be introduced to the capsule to maintain gas saturation during the run. Thus the capsules are pre-loaded with up to 60 bars of gas, using the capsule-loading device at BGI.

Initial experiments indicate that the geometry described above is viable. The geometry of the experiment was maintained during the run. In particular, the olivine discs undergo minimal deformation (Fig. 3.2-15). They are thoroughly fractured, but large (up to 300 micron) areas

of coherent crystal are preserved (Fig. 3.2-16). The crystals are easily removed from the charge as the diamond adheres only weakly to their surfaces. One minor problem with the technique is that the surface of the discs are indented by the diamonds (Fig. 3.2-16), which will prevent detailed depth profiling measurements, which require flat surfaces. Other geometries, such as using polished discs of glassy carbon, are being investigated to remedy this issue.

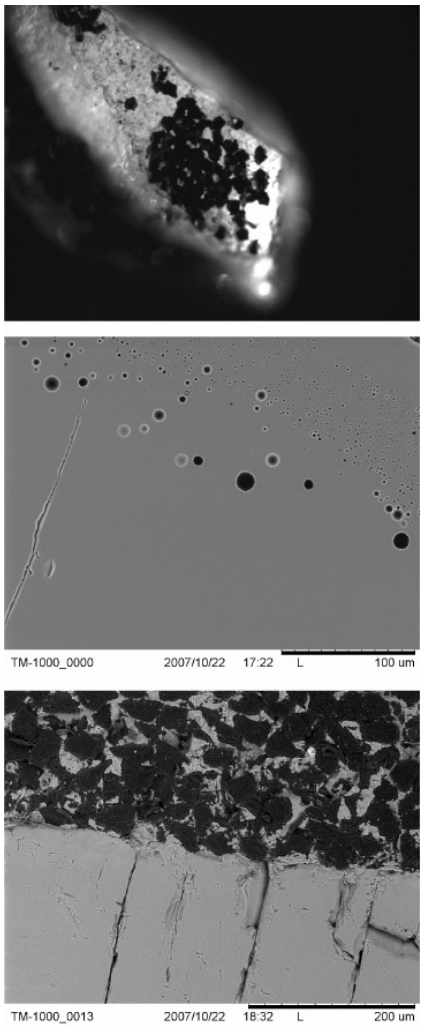

Fig. 3.2-16: (Top) diamond crystals (black) adhering to indented surface of olivine crystal (light area, 300 microns long) after the experiment. (Middle) bubbles in experimental glass. (Bottom) melt (bright areas between dark crystals) in between diamond crystals (dark) above an olivine disc (medium bright lower half of image).

Some of the melts have gas bubbles in them, indicating that they were gas saturated (Fig. 3.2-16-middle). It was expected that the melts would penetrate some distance into the diamond layers, but in fact, they fill all of the available porosity (Fig. 3.2-16-bottom). However, the reduction in contact area between the crystal and melt seems to have prevented the melts from forming melt pockets/inclusions within the crystals.

In addition to traditional crush/melt analyses the noble gas concentrations in the crystals and melts also will be analyzed by laser-ablation. Laser-ablation is a relatively new method and there a still some issues with the detection limits, but it has been used in previous studies of noble gas partitioning (Fig. 3.2-17) and appears promising. By performing laser-ablation

analyses on the same samples that are analyzed by the more established crush/melt method, we will be able to verify the laser technique.

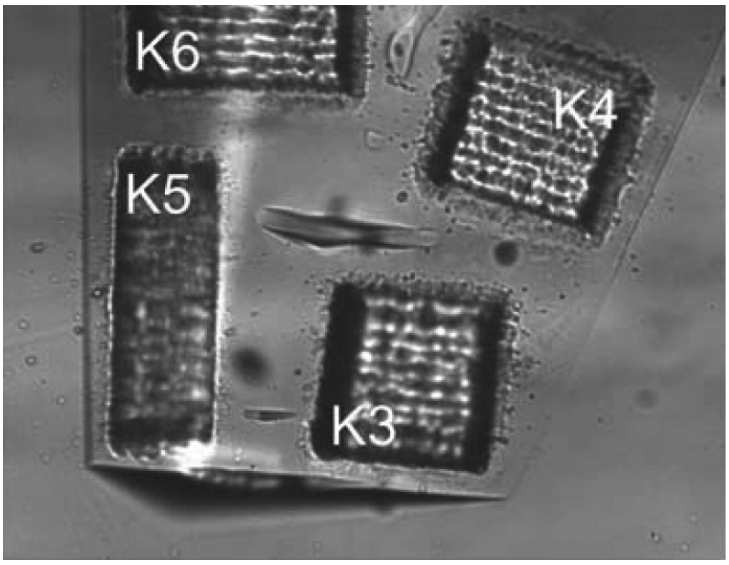

Fig. 3.2-17: Laser-ablation pits (rastered) from noble gas analyses of a pyroxene crystal. Image is 200 microns across. Such rastered areas will easily fit within our 250 x 1000 micron crystals.

j. *Thermodynamic and crystal-chemical constraints on the incorporation of fluorine in upper-mantle minerals (D. Bernini and D. Dolejš)*

Halogens are common constituents of hydrous silicates as well as in sea water but very little is known about their behaviour during slab devolatilization and melting at convergent plate boundaries. Fluorine is often found in metasomatic mantle assemblages (*e.g.*, fluorine-bearing amphiboles and phlogopites) or it forms separate fluoride phases. In order to define storage and transport mechanisms of fluorine in subduction zone settings, we have focused on incorporation of fluorine in nominally halogen-free minerals. In this contribution, we present preliminary thermodynamic and chemical analysis of substitution mechanisms.

Major high-pressure phases (forsterite, enstatite, spinel and pyrope) span the system MgO-Al_2O_3-SiO_2, where the fourth component, F_2O_{-1}, represents an exchange operator maintaining the charge balance. In the MgO-SiO_2-F_2O_{-1} ternary, thermodynamic calculations at 500-1000 °C and 5-20 kbar performed by minimizing the chemical potential of F_2O_{-1} show that sellaite (MgF_2) is a saturating phase in peridotitic assemblages. During deep subduction, the following equilibrium

$$4\ MgSiO_3 + 2\ MgF_2 = 3\ Mg_2SiO_4 + SiF_4$$

proceeds to the right due to the high compressibility of (initially) liquid SiF_4. Above 970 °C, 40 kbar or 800 °C, 50 kbar, siliconfluoride is compatible with mantle silicate phases.

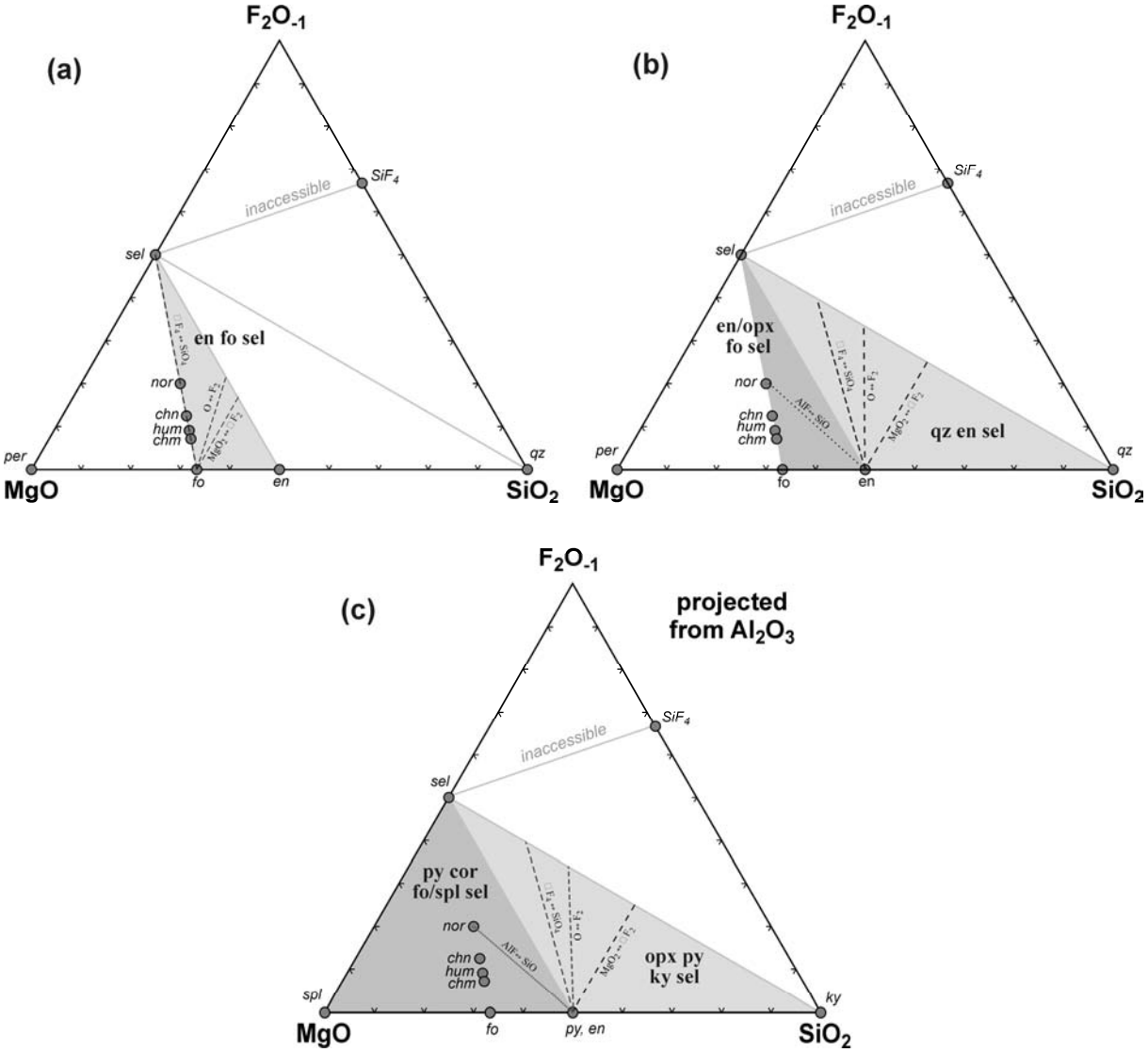

Fig. 3.2-18: Ternary diagrams of the MgO-SiO_2-F_2O_{-1} system illustrating fluorine substitution mechanisms in (a) forsterite, (b) enstatite and (c) pyrope, projected from Al_2O_3. Gray fields are computed compatibility triangles indicating mineral assemblages stable at 800 °C and 10 kbar. Mineral abbreviations: chm – clinohumite, chn – chondrodite, en – enstatite, fo – forsterite, hum – humite, ky – kyanite, nor – norbergite, opx – orthopyroxene solid solution, per – periclase, py – pyrope, qz – quartz, sel – sellaite (MgF_2), and spl - spinel.

Magnesium (alumino)silicates can incorporate fluorine by replacing oxygen *via* four mechanisms: (1) $O \rightarrow F_2$; (2) formation of magnesium vacancy, $MgO_2 \rightarrow \square F_2$; (3) formation of silicon vacancy, $\square F_2 \rightarrow SiO_4$; and (4) charge balance *via* Al-Si exchange, $AlF \rightarrow SiO$. Relevance of these substitutions depends on stereochemical constraints, alumina activity and

silica activity. Figure 3.2-18 illustrates the locations of individual element exchanges in the MgO-SiO_2-F_2O_{-1} ternary space. For forsterite, all substitutions span the forsterite-enstatite-sellaite space. Along the silicon-vacancy join, clinohumite (4:1), humite (3:1), chondrodite (2:1) and norbergite (1:1) are potential intermediate phases and hosts for fluorine; the ratio determines proportions of the forsterite and SiO_4-vacant (sellaite) layers. Recent reports of elevated solubilities of fluorine in forsterite suggest the existence of additional solid solutions along the tetrahedral vacancy join. The $O \rightarrow F_2$ substitution appears less favourable due to size constraints.

In the MgO-Al_2O_3-SiO_2-F_2O_{-1} system, Al-bearing orthopyroxene and pyrope can accommodate fluorine via the $SiO \rightarrow AlF$ substitution related to the excess aluminium in the tetrahedral site. Calculated fluorination vectors of enstatite and pyrope span several compatibility fields at 800 °C and 10 kbar: (1) orthopyroxene, quartz and sellaite, (2) forsterite, orthopyroxene and sellaite, (3) orthopyroxene, pyrope, kyanite and sellaite, and (4) forsterite/spinel, pyrope, corundum and sellaite. The silica activity exerts control on the relative significance of $MgO_2 \rightarrow \square F_2$ and $SiO_4 \rightarrow \square F_4$ substitutions. By the tetrahedral vacancy mechanism, Mg-garnet can accommodate at least 3.4 wt.% F (Smyth *et al*., 1990; Amer. Mineral. 75, 314-318). The AlF-SiO substitution in pyrope has not been documented yet and it is predicted to be compatible with silica-undersaturated, spinel- or corundum-bearing assemblages only (Fig. 3.2-18). Our analysis suggests that fluorine incorporation mechanisms are sensitive to activities of alumina and silica in the system. When a silicate assemblage (olivine, orthopyroxene and pyrope) is saturated by one fluoride phase (sellaite or clinohumite), the substitution mechanisms in silicates are predicted to differ, leading to distinct potential for fluorine storage.

k. *The stability of carbonatitic melts with respect to oxygen fugacity (V. Stagno and D.J. Frost)*

Carbonatitic magmas are frequently cited as potential metasomatic agents in the mantle and significant evidence exists for the presence and passage of such magmas from the study of mantle xenoliths. In addition it has been proposed that the initial melts produced during upwelling of mantle beneath mid ocean ridges may be carbonatitic, and that the solidus of carbonate peridotite may therefore control the onset of melting deep beneath these ridges. Initial, carbonate-rich melts are also implicated in the origin of kimberlitic magmas. On the other hand, there is evidence for the presence of graphite and diamond in a number of mantle xenoliths and peridotite massifs, and it has been proposed that graphite may buffer the oxygen fugacity during mantle partial melting, thus explaining the narrow range of oxygen fugacities reported for mid ocean ridge basalts.

Oxygen fugacity is the main parameter controlling whether graphite/diamond or carbonate minerals and melts are stable in the mantle. While it is possible that the coexistence of carbonate and graphite/diamond may buffer the oxygen fugacity of the mantle, as a result of the relatively low carbon content, ferric/ferrous equilibria probably exert a more dominant

influence and may drive the oxygen fugacity of the mantle down with increasing depth. In this scenario the onset of carbonatite melt production in upwelling mantle will be controlled not only by the solidus but also by the oxygen fugacity, in the sense that carbonate (solid or liquid) will only be stable at oxygen fugacities higher than the appropriate carbon-carbonate equilibria. The simplest of such equilibria is described by the mineral acronym EMOG/D *i.e.*,

$$\underset{\textit{enstatite}}{MgSiO_3} + \underset{\textit{magnesite}}{MgCO_3} = \underset{\textit{olivine}}{Mg_2SiO_4} + \underset{\textit{graphite/diamond}}{C} + O_2$$

the oxygen fugacity of which can be quite accurately calculated, at least at low pressures, using thermodynamic data. A more applicable reaction in the mantle in terms of carbonate chemistry, however, is

$$\underset{\textit{enstatite}}{2Mg_2Si_2O_6} + \underset{\textit{melt}}{CaMg(CO_3)_2} = \underset{\textit{olivine}}{2Mg_2SiO_4} + \underset{\textit{diopside}}{CaMgSi_2O_6} + \underset{\textit{graphite/diamond}}{2C} + 2O_2$$

where the carbonatitic melt phase would become more SiO_2-rich with increasing temperature. Due to the complexity of the melt chemistry this reaction cannot be accurately calculated using thermodynamic data. In this study the oxygen fugacity imposed by a similar equilibrium in the FeO-CaO-MgO-SiO_2-CO_2 system has been studied as a function of pressure and temperature in the multianvil apparatus. Two starting compositions in the Fe-Ca-Mg-Si-C-O and Fe-Mg-Si-C-O systems were assembled from mineral mixes of olivine, enstatite, diopside, graphite, $MgCO_3$ and $CaCO_3$. Because in these experiments carbon is present in far higher amounts than iron, the oxgen fugacity will be buffered by the carbon-bearing phases rather than by the iron-bearing phases. Both compositions were run simultaneously in a single Re foil capsule that enclosed two separate graphite sleeves. 5 wt.% Ir powder was added to both compositions such that the oxygen fugacity could be determined after each experiment using the equilibrium,

$$\underset{\textit{olivine}}{2Fe_2SiO_4} = \underset{\textit{enstatite}}{2FeSiO_3} + \underset{\textit{metal}}{2Fe} + O_2$$

in which the oxygen fugacity is calculated using

$$\log fo_2 = \frac{-\Delta G^o}{\ln(10)RT} + 2\log a^{Ol}_{Fe_2SiO_4} - 2\log a^{enstatite}_{FeSiO_3} - 2\log a^{metal}_{Fe}$$

ΔG^o is the Gibbs free energy of the pure end member equilibrium, and $a^{Ol}_{Fe_2SiO_4}$, $a^{enstatite}_{FeSiO_3}$ and a^{metal}_{Fe} are the activities of the Fe end-member components in olivine, enstatite and the Ir metal, which are determined from microprobe analyses of the run products employing appropriate activity-composition models. During the experiment Fe alloys with the Ir metal to shift the oxygen fugacity of this equilibrium to that imposed by the presence of carbonate melt

and graphite. Experiments were performed between 1250 and 1350 °C at 3 GPa. In the lowest temperature experiment a calcium-rich carbonate melt was produced in the Fe-Ca-Mg-Si-C-O system, while at higher temperature the melts contained more SiO_2. An SEM image of a typical mineral and melt assemblage is shown in Fig. 3.2-20.

In Figure 3.2-21 the oxygen fugacity calculated for the graphite-carbonate melt equilibrium in the Fe-Ca-Mg-Si-C-O system is compared with previous determinations of the EMOG buffer at the same conditions. While the trends are similar, the slight curvature in the Ca bearing system likely results from dilution of the carbonate-rich melt phase by dissolved silicate at higher temperature. Further experiments at higher pressures and in natural mantle peridotite compositions will be used to delimit the stability of graphite/diamond and carbonatitic melt throughout the upper mantle.

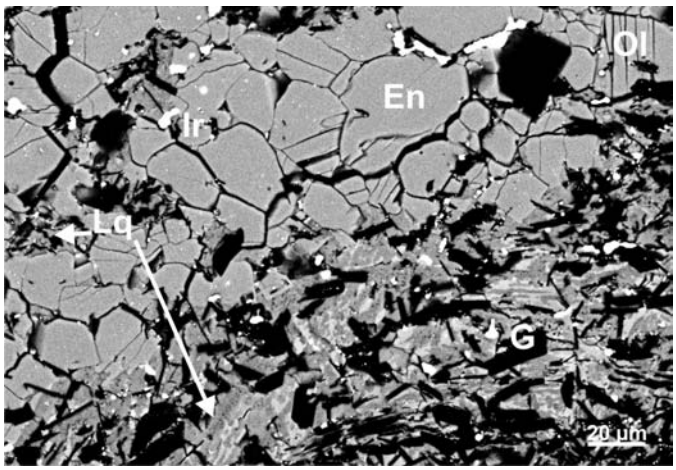

Fig. 3.2-20: Scanning electron microscope images of enstatite (En), olivine (Ol), Ir-Fe alloy (Ir), laths of graphite (G) and quenched carbonatitic melt (Lq) recovered from an experiment at 1300 °C and 3 GPa.

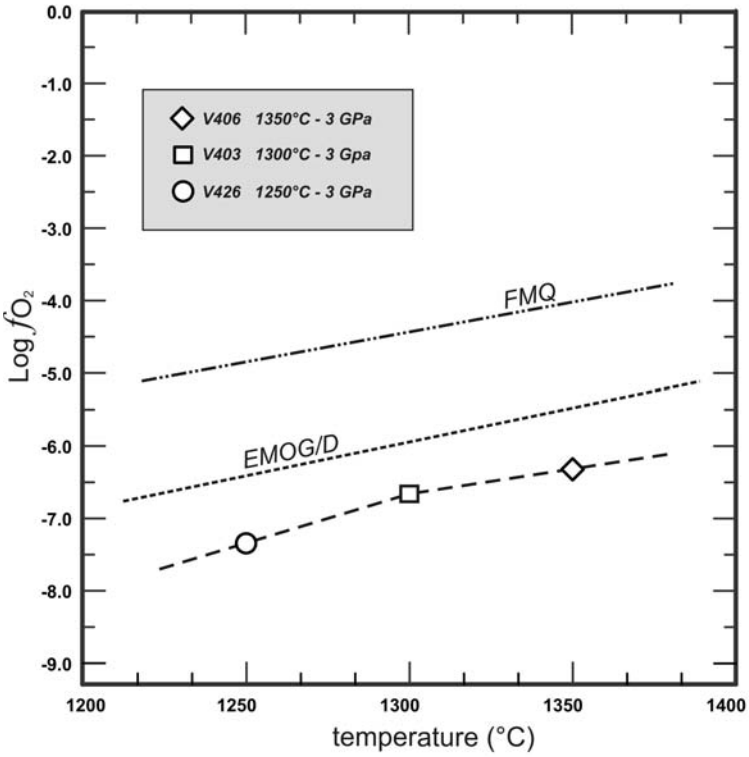

Fig. 3.2-21: Log fO_2 vs. T (°C) for the graphite/ carbonate melt equilibrium in the Fe-Ca-Mg-Si-C-O system, as compared to the FMQ buffer and the EMOG buffer in the Mg-Si-C-O system.

l. *Carbonatites produced by melting of hydrous, carbonate-bearing garnet lherzolite at 3-7 GPa (G.H. Gudfinnsson, S. Keshav and D.C. Presnall/Richardson)*

Small-degree carbonatitic melts are probably widespread in the mantle. Because of their great mobility and enrichment in incompatible trace elements, they could be important agents of metasomatism with a significant influence on the distribution of many incompatible trace elements. In addition, carbonatitic melts may affect velocities of seismic waves in the mantle and could be an important part of the global cycle of carbon, integrally linked with carbon in the atmosphere, the biosphere and the crust. Trace-element chemistry of carbonatites found at the Earth's surface indicates that they are generally derived from the mantle. However, while most documented extrusive carbonatites have calciocarbonatitic composition, melting experiments on anhydrous, carbonated mantle peridotite produce magnesiocarbonatitic melts. Explanations for this discrepancy include derivation of calciocarbonatites from more Mg-rich carbonatite melts by crystal fractionation or wall-rock reactions in the mantle. Generation by melting of a pyroxenitic rather than peridotitic source has also been offered as an explanation for the common occurrence of Ca-rich carbonatites. Furthermore, liquid immiscibility, producing coexisting carbonatitic melt and alkalic silicate melt, has been a popular model for the genesis of carbonatites.

At least in some cases, the emplacement of carbonatites seems to occur at temperatures of considerably less than 1000 °C. This low temperature compared to the melting temperature of pure carbonates can, in part, be explained by the presence of alkalis and halogens in natural carbonatites. However, there is also ample evidence for the presence of significant amounts of H_2O, and melting experiments indicate a high solubility of H_2O in carbonatitic melts. The melting behaviour of carbonated peridotite with H_2O present is therefore of interest for insights into carbonatite genesis. Melting experiments on natural mantle compositions relevant to the generation of carbonatites are problematic because carbonatites must be produced by very small amount of melting, considering their high contents of incompatible elements and CO_2 compared to the mantle. The small amounts of interstitial melt in such experiments are almost impossible to analyze and equilibrium is difficult to attain. One method to circumvent this problem is to conduct experiments in low-variance, simplified systems where the phase compositions are independent of the bulk composition, which can then be designed such as to maximize the amount of any phase, including the melt. In the system CaO-MgO-Al_2O_3-SiO_2-CO_2 (CMAS-CO_2), the garnet lherzolite (garnet + forsterite + enstatite + diopside) phase assemblage coexists with carbonate and carbonatitic melt along a univariant line that extends from pressures < 3 GPa to at least 14 GPa. The stable solid carbonate is dolomite at < 4.5 GPa but magnesite at higher pressures. With H_2O added (CMAS-CO_2-H_2O system), this phase assemblage coexists along a divariant surface that extends from the CMAS-CO_2 univariant line to lower temperatures with increasing amount of H_2O in the melt (Fig. 3.2-22).

We have conducted multianvil experiments to determine these phase relations in the CMAS-CO_2-H_2O system at 3-7 GPa, using the earlier experiments in the CMAS-CO_2 system as an initial guide to phase compositions in the CMAS-CO_2-H_2O system. The starting compositions

contain 3-6 wt.% H_2O, which is added as brucite, whereas magnesite, and in one case also $CaCO_3$, is the source of CO_2. These compounds were added to silicate glasses to form the starting mixtures. The starting compositions were confined in Pt capsules and run at 1000-1450 °C for 2-24 h. A series of three experiments at 4 GPa, 1150 °C of 2, 6 and 24 h duration

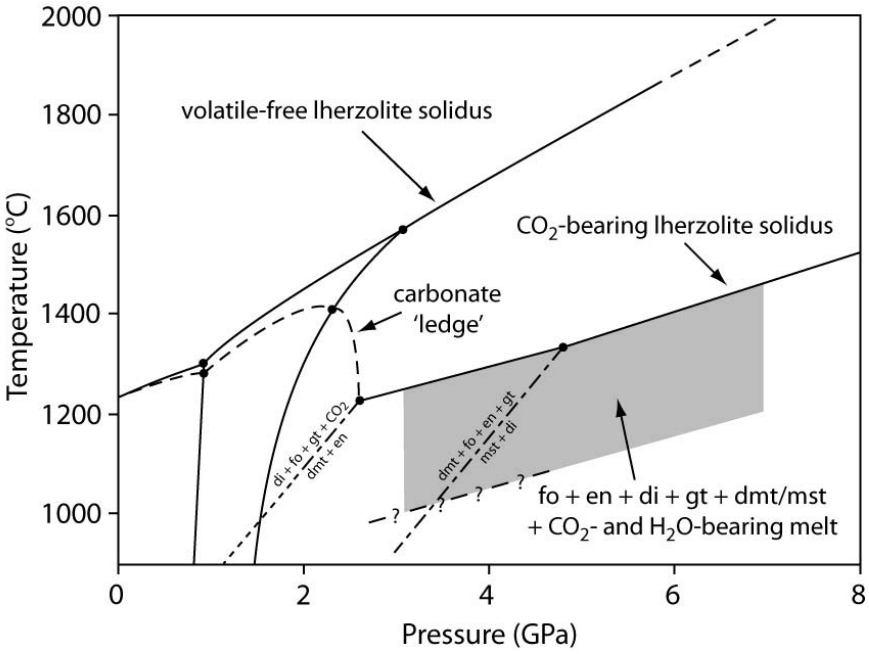

Fig. 3.2-22: Pressure-temperature diagram showing 1) the solidus of volatile-free lherzolite (garnet lherzolite at ≥3 GPa) in the CMAS system, 2) the solidus of CO_2-bearing lherzolite in the CMAS-CO_2 system, and 3) the divariant surface (shaded) containing forsterite (fo), enstatite (en), diopside (di), garnet (gt), and carbonate (depending on pressure, dolomite (dmt) or magnesite (mst)) in equilibrium with CO_2- and H_2O-bearing melt in the CMAS-CO_2-H_2O system at 3-7 GPa. The dashed line with question marks is the provisional solidus for fluid- and carbonate-bearing garnet lherzolite in the CMAS-CO_2-H_2O system. The so-called carbonate ledge marks a rapid increase in the solubility of CO_2 in basaltic melts with increasing pressure, terminating when the subsolidus CO_2-bearing phase changes from vapor to dolomite.

shows that there is continual loss of H_2O from the Pt capsules during the experiments such that estimated half of the H_2O content is lost after 24 h. Provided that all the desired phases are present and chemical equilibrium is maintained, this should not affect the phase relations, but can lead to an overestimation of the H_2O content of the melt. The polished run products were inspected and analyzed in the electron microprobe (Fig. 3.2-23). The quenched melts have highly porous textures, apparently caused by the exsolution of H_2O from the melt on quenching, forming an intergrowth of carbonates (the dominating phase), smaller amounts of silicates, and presumably water-filled, interstitial cavities (Fig. 3.2-24). Accordingly, when the capsules are punctured, small amounts of H_2O are seen streaming out. The crystallization

of the carbonate melt during cooling makes a precise determination of the melt compositions difficult and subject to considerable uncertainties. However, we assume that the quench mats are now essentially H_2O-free and calculate the amount of CO_2 as the difference between microprobe totals and 100 %. The concentration of H_2O in the melt can be calculated from the volume of the melt on the assumption that all the H_2O is retained in the capsule during an experiment and is present only in the melt. Because of the relatively low solubility of H_2O in the crystalline phases, the latter assumption almost certainly causes only a minor error. In contrast, as mentioned above, the first assumption tends to lead to an overestimation of the H_2O content of the melt, as with time an increasing amount of H_2O is lost from the capsule and concurrently the amount of melt decreases. Note, however, that the phase relations demand that the H_2O content of the melt is constant at the same P and T as long as all the same phases are present.

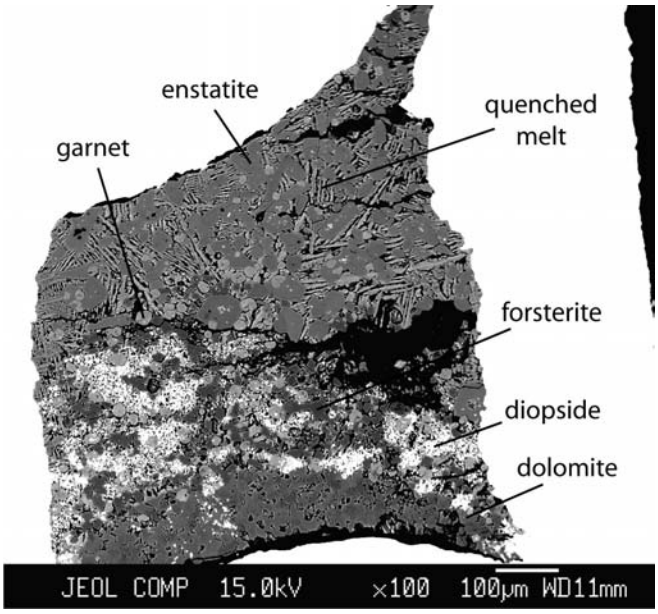

Fig. 3.2-23: Backscattered electron image of the products of an experiment at 4 GPa, 1150 °C showing a cross section of the sample capsule. Five different crystalline phases coexist with a hydrous, carbonatitic melt. The quenched melt forms long laths with cavities in between, which were presumably filled with exsolved H_2O. The estimated H_2O content of the melt is between 5-10 wt.%. The large dark areas are caused by sample loss on polishing.

At pressures ≤4 GPa, the solid carbonate present in the experiments is dolomite. The lowest temperature experiment was performed at 3 GPa, 1000 °C, which is about 245 °C below the solidus of anhydrous, carbonate-bearing garnet lherzolite in the CMAS-CO_2 system. At this temperature, the estimated amount of H_2O in the melt is between 15-20 wt.%. Textural evidence suggests that fluid saturation may have been reached at this temperature, but further experiments are necessary to resolve this uncertainty. With increasing H_2O contents, the melt

composition becomes more calcic to the point that the ratio CaO / (CaO + MgO) is close to that of the boundary between magnesiocarbonatites and calciocarbonatites (0.8). With increasing H_2O content, the amount of SiO_2 decreases from about 5-6 wt.% at anhydrous conditions to about 1 wt.% at the lowest temperature, while the amount of Al_2O_3 decreases from 0.5-1.0 wt.% to < 0.5 wt.%. In experiments at 7 GPa, the solid carbonate is magnesite, and just as at lower pressures, increasing H_2O content depresses the equilibrium temperature significantly. At 1300 °C, about 150-200 °C lower temperature than the CMAS-CO_2 solidus, the estimated amount of H_2O in the melt is 10-15 wt.%. However, the effect of H_2O on the melt composition appears to be smaller than at lower pressures, with more magnesian and less calcic melts. This suggests that calciocarbonatites could be produced in the mantle by the melting of hydrous, dolomite-bearing garnet lherzolite at pressures ranging from the end of the carbonate ledge (about 2 GPa) up to about 4 GPa where magnesite becomes stable.

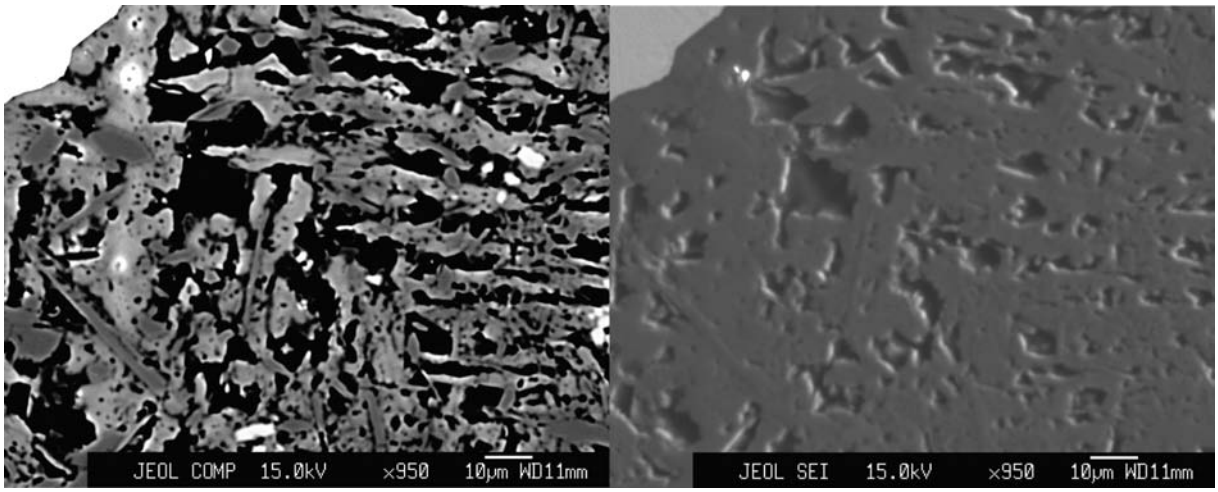

Fig. 3.2-24: On the left, a backscattered electron image of the products of an experiment at 3 GPa, 1000 °C showing an area with quenched melt. The figure on the right is a secondary electron image of the same area. Notice the relatively large cavities that have formed between the quench crystals. These are thought to have developed by H_2O exsolution at the time of quenching. The estimated H_2O content of the melt was about 15-20 wt.%, and may have been close to fluid saturation. The width of each image is about 150 μm.

m. *Carbonate survival at great depths in the Earth: results from the solidus determination of model eclogite in the system CaO-MgO-Al_2O_3-SiO_2-CO_2 (S. Keshav and G.H. Gudfinnsson)*

Eclogite is a major mantle rock-type composed predominantly of clinopyroxene and garnet with a broadly basaltic composition. While opinions vary on the ultimate genesis, a significant proportion of eclogite in the mantle is likely to have originated from subduction of former oceanic crust to various depths. In addition, a considerable amount of this oceanic

crust has been altered and contains crystalline carbonate, and it has been shown that in order to balance the carbon dioxide (CO_2) emissions at active volcanic centers, carbon must be recycled into the Earth's mantle.

Previous phase equilibrium experiments in model systems have established that the carbonation reactions relevant for bimineralic eclogites (dominantly clinopyroxene + garnet) occur at pressures higher than those for a peridotitic assemblage. The intersection of these subsolidus carbonation-decarbonation boundary lines with the appropriate solidus would therefore be at higher pressures than in the corresponding peridotitic systems. This is important because it means that the solubility of CO_2 in incipient solidus melts at high pressures from carbonated mafic rocks (eclogites) will play a larger role than in peridotitic systems. This carbonation-decarbonation reaction offset between carbonated mafic and carbonated ultramafic rocks in pressure-temperature (P-T) space also implies that there will be a depth (pressure) interval in the Earth where CO_2-rich fluid will exist in mafic rocks, while crystalline carbonate will be stable along the peridotite solidus.

Previously, melting phase equilibria have been reported for carbonated mafic rocks on natural, multicomponent (2-15 GPa) as well as simplified compositions (3-8 GPa). While some studies in natural systems report a steep drop (owing to the formation of crystalline carbonate in the subsolidus) in the solidus temperatures of carbonated eclogite in the approximate pressure range of 3-6 GPa (Fig. 3.2-24:), others do not observe any signs of this behaviour (Fig. 3.2-24:). On the other hand, in simplified compositions, only a very gentle negative solidus trajectory, that occurs at ~ 3 GPa, is reported (Fig. 3.2-24).

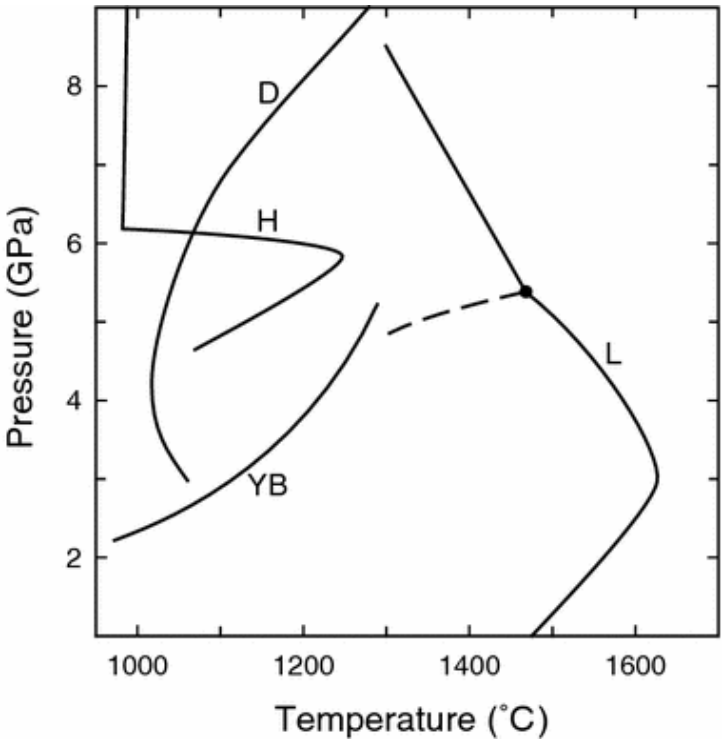

Fig. 3.2-24: Solidi for carbonate-bearing eclogites from four recent experimental studies at various pressures. Abbreviations are: H, Hammouda (*EPSL*, *214*, 357, 2003), D, Dasgupta *et al.* (*EPSL*, *227*, 73, 2004), YB, Yaxley and Brey (*CMP*, *146*, 606, 2004), and L, Luth (*CMP*, *151*, 141, 2006; diopside-CO_2).

Considerable flattening of the solidus curve, after approximately 5-8 GPa is a prominent feature in at least one study that has determined the solidus of carbonated eclogite in natural systems (Fig. 3.2-24). However, most of the solidus temperature determinations differ by as much as ~ 200-300 °C at the highest pressure (Fig. 3.2-24). These experimental studies, therefore, differ in their conclusions as to whether crystalline carbonate can be subducted into the mantle to great depths . To help resolve this question we have determined the solidus of carbonated eclogite between 12 and 20 GPa in a multianvil device. This pressure range corresponds to depths of ~ 350-600 km in the Earth. In this contribution, we have chosen to focus on the part of composition space in the system CaO-MgO-Al_2O_3-SiO_2-CO_2 (CMAS-CO_2), which is analogous to the natural carbonate-bearing mantle system with eclogitic bulk composition. The silicate part of the chosen composition space corresponds to the composition of average mid ocean ridge tholeiite, reduced to CaO-MgO-Al_2O_3-SiO_2 (CMAS). Carbonate was added as $MgCO_3$.

With increasing pressure from 12 to 20 GPa, we have determined the following isobarically invariant points (Fig. 3.2-25):

- Calcite/Aragonite + magnesite + clinopyroxene + majoritic garnet + stishovite + melt at 12-16 GPa
- Magnesite + cpx + garnet + stishovite + CAS (calcium-alumino-silicate) + melt at 18 GPa
- Magnesite + garnet + stishovite + CAS + calcium perovskite + melt at 20 GPa

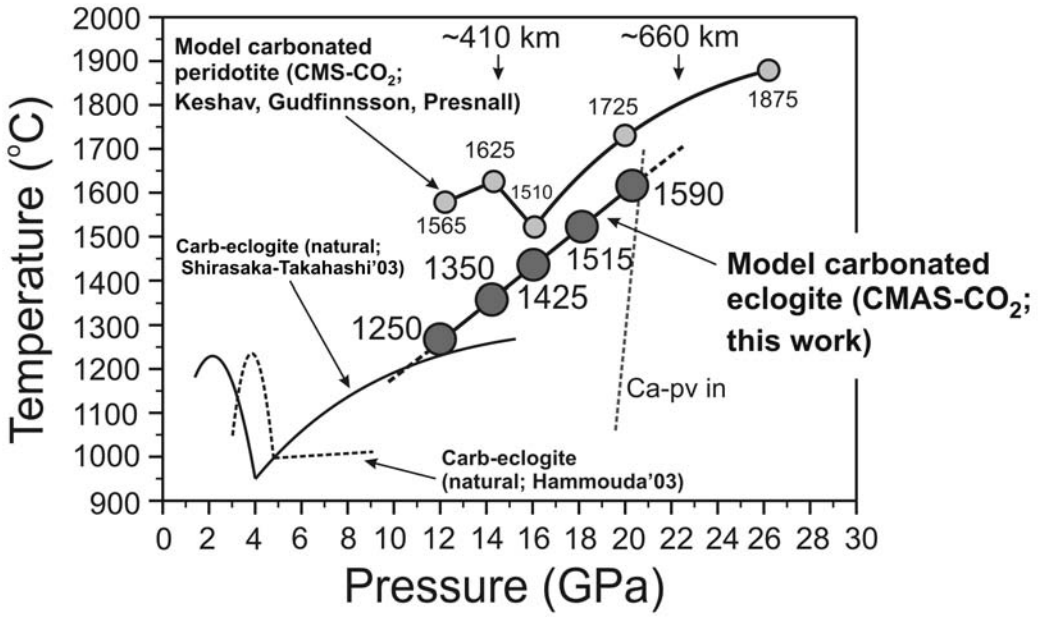

Fig. 3.2-25: The solidus of carbonated eclogite in the CMAS-CO_2 system determined in this work (shown as a straight solid line connecting filled grey circles). Numbers adjacent to the grey circles denote the solidus temperatures. Also shown in this figure are three recently determined solidi for carbonated mantle: Shirasaka and Takahashi (*IKC, FLA-0043*, 2003); Hammouda (*EPSL, 214*, 357, 2003) and Keshav, Gudfinnsson, and Presnall; this yearbook).

At 12, 14, and 16 GPa, both $CaCO_3$ and $MgCO_3$ phases are stable at the solidus. The $CaCO_3$ phase is assumed to be aragonite. Hence, the experiments reported here suggest that in this part of the composition space, relevant to carbonated eclogite at moderate depths in the Earth's mantle, both crystalline carbonates will be stable. By far the most important advantage of using simplified compositions to understand melting phase equilibria in the mantle is that as long as all the relevant phases are present in the experimental run products, the choice of bulk composition does not affect the melting phase relations.

At all pressures investigated, melts in equilibrium with the stated crystalline assemblage are highly calcic in their composition, with Ca# ($Ca/Ca+Mg*100_{molar}$) ranging from 75 to 85. Hence, in this respect, melts in the experiments resemble mantle-derived, true calcio-carbonatites (Ca# > 75) seen on the Earth's surface. However, we are not suggesting that surficial carbonatites erupt from these great depths in the mantle. The similarity simply means that the composition space investigated here is relevant toward understanding melting phase equilibria in the Earth's mantle.

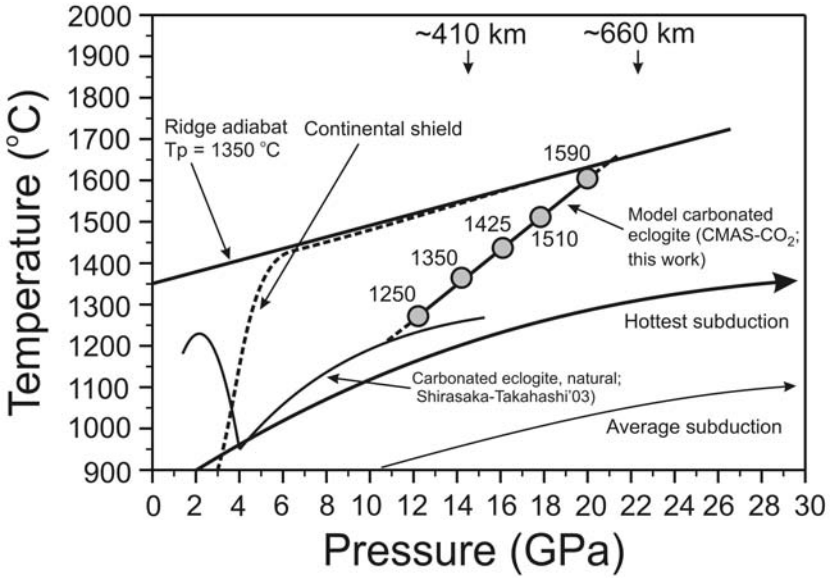

Fig. 3.2-26: Location of carbonated eclogite solidus determined in the system CMAS-CO_2 (this study) shown as solid line connecting filled, grey circles, with respect to mid-ocean ridge geotherm (thick solid line; potential temperature, Tp = 1350°C with an adiabatic gradient of 13 °C/GPa), calculated P-T conditions for subducting crust (shown as two curves with arrows on each: average subduction, thin curve; hot subduction, thick curve), and continental shield geotherm ($40mW/m^2$; dashed line). Also shown is the solidus curve of carbonated eclogite as determined by Shirasaka and Takahashi (*IKC, FLA-0043,* 2003).

Given the constraints on the solidus temperatures of carbonated eclogite, we are in a position to comment on the survival of carbonate during subduction to moderate to great depths in the Earth's mantle. In this respect, the chief concern regarding the delivery of carbonates (CO_2) to

the deep mantle by subducted carbonated eclogite is whether or not the solidus is encountered along plausible subduction geotherms. In Figure 3.2-26, we show the location of the solidus of carbonated eclogite determined in this work (CMAS-CO_2) in relation to an oceanic ridge geotherm (Tp = 1350 °C, with an adiabatic gradient of 13 °C/GPa), calculated P-T conditions (geotherms) for subducting oceanic crust, and continental shield geotherm. As illustrated in Fig. 3.2-26, the two possible (and extreme) subduction geotherms do not intersect the solidus of carbonated eclogite at any pressure, implying that melting of this carbonated eclogite will not be induced. Hence, subduction is likely to introduce carbonated eclogite to significant mantle depths. In addition, although we do not have the solidus temperatures of carbonated eclogite beyond 20 GPa, and unless the solidus of carbonated eclogite shows complications with increasing pressures (depths in the mantle), it is safe to say that carbonated eclogite is the most probable source to introduce vast amounts of carbon into the mantle.

n. *The role of TiO_2 phases during melting of subduction-modified crust: implications for deep mantle melting (G.D. Bromiley and S.A.T. Redfern/Cambridge, R. Hinton/Edinburgh, in collaboration with D.J Frost)*

Subduction of oceanic lithosphere provides the main mechanism for recycling material back into Earth's deep interior, although the role of subduction in geochemical recycling and melt generation in the mantle remains poorly understood. It is a paradigm of mantle geochemistry that melting of ancient, recycled oceanic crust in the Earth's mantle is a key process, either directly or indirectly, in the genesis of ocean island basalts (OIB). It has been demonstrated that partial melting of subduction-modified, Si-poor oceanic crust (garnet-pyroxenite) can produce nepheline-normative melts, and that in terms of major element chemistry, melts from ancient crust are a potential direct source for parental OIB magmas. However, it has proven challenging to explain trace element composition of OIB arrays by direct melting of oceanic crust, and HIMU type sources (commonly assumed to represent melts from ancient crust in OIB mantle source regions) can only be modeled by melting of ancient crust if it has undergone substantial subduction modification and ageing, and if degrees of partial melting are very low (only a few weight percent). Alternatively, it has recently been suggested that melting of ancient crust may act as a secondary source for OIB by providing silica-rich melts which locally metasomatise upwelling regions of the mantle.

We have been conducting a detailed investigation of phase and melt relations in model subduction-modified crust systems. Initial work has focused on understanding the role that TiO_2 phases play during partial melting of ancient crust in the deep mantle. Experiments performed over the pressure range 5-15 GPa demonstrate that rutile, or its high-pressure polymorph TiO_2(II), are stable up to at least 10-15 wt.% melting (Fig. 3.2-27) even in relatively Si-poor systems. This is contradictory to data on TiO_2 solubility in silicate melts at lower pressures which suggest that rutile stability should be constrained to much lower degrees of partial melting due to high TiO_2 solubility in Si-poor melts. Low TiO_2 solubility in high-pressure melts may be due to changes in melt polymerization and Si coordination which occur at elevated pressures. Results from this work demonstrate that for degrees of partial

melting invoked in trace element modeling studies TiO_2 phases should be present in solid residues. This presents a problem, because the presence of rutile during shallow melting of subducting oceanic crust results in a very characteristic Nb and Ta depletion that is not seen in typical OIB arrays. In order to explain this we have preformed rutile/TiO_2(II)-melt partitioning experiments over a large P-T range relevant to deep melting of ancient crust in the mantle source region for OIBs.

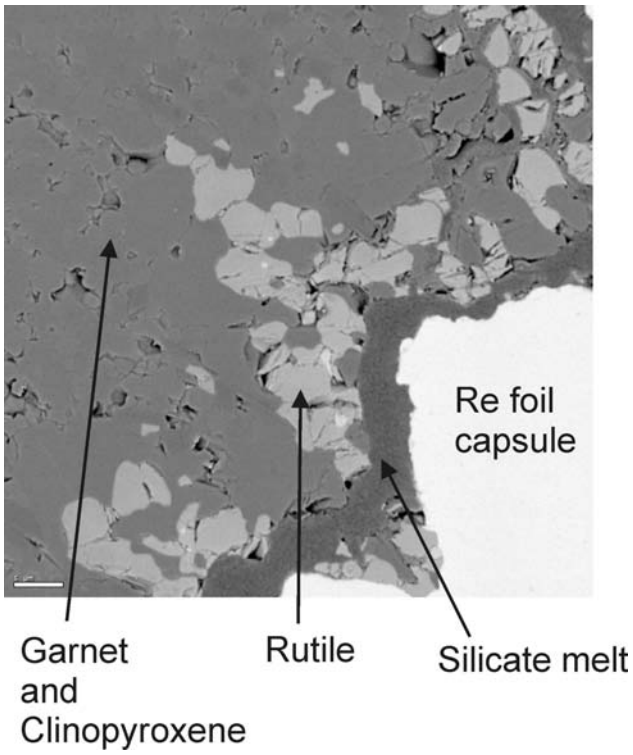

Fig. 3.2-27: BSE SEM image (scale bar = 5µm) of a sectioned capsule showing phase/melt relations in subduction-modified crust at 8 GPa, 1650 °C. Solid residue consists of garnet + clinopyroxene + rutile (no free silica phase is present). Mass balance calculations imply approx. 10 wt.% melting.

Results show that depth of melting has a controlling influence on Nb and Ta partitioning (Fig. 3.2-28), which can again be correlated with systematic changes in melt structure (increase in Si coordination and degree of melt polymerization) with increasing pressure. Changes in melt structure also influence Zr and Hf partitioning, although lattice strain has a greater influence due to the large difference in ionic radius between Zr/Hf and Ti. The influence of the pressure of partial melting on partitioning behaviour of high field strength elements may provide a useful indicator of depth of partial melting vs degree of partial melting in the mantle. Ancient, subduction-modified crust cannot be a major component of OIB unless depth of melting is > 300 km or degree of partial melting is much higher than predicted by trace element modeling (although the degree of partial melting required to remove TiO_2 phases from solid residues is yet to be determined). Likewise, the absence of strong depletion of Nb and Ta in OIB also provides constraints on the degree of partial melting vs depth of partial melting for models where melting of ancient crust acts as an indirect source for OIB by metasomatic interaction with the mantle. However, in this instance silica-rich melts required by metasomatic models necessitate much higher degrees of partial melting of ancient crust to remove TiO_2 phases from solid residues. Furthermore, in order to produce silica-rich partial melts, ancient crust must have remained relatively intact during sub-arc processes.

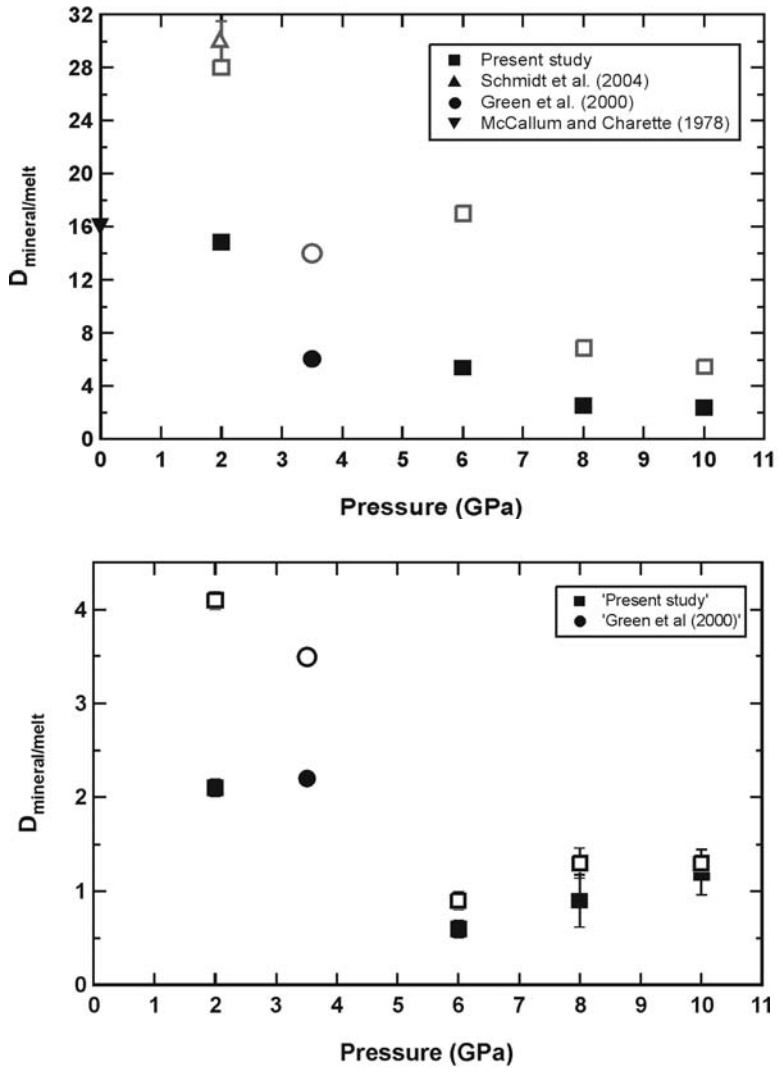

Fig. 3.2-28: Rutile/TiO_2(II)-melt partitioning coefficients for (A) Nb (black) and Ta (gray) and (B) Zr (black) and Hf (gray) as a function of pressure. Solid line marks position of rutile to TiO_2(II) transition. Data are consistent with previous studies at pressures up to 3 GPa. Low partition coefficients for Nb and Ta from Green *et al.* (2000) are probably due to the fact that experiments were performed under hydrous conditions.

The influence of depth of partial melting on Nb and Ta partitioning also has broader implications for constraining deep mantle melting. Because melt structure has a controlling influence on Nb and Ta behaviour similar trends to those shown in Fig. 3.2-28 are expected even when TiO_2 phases are not stable in melt residues. Systematic changes in melt structure are also expected to continue to at least 30 GPa, which implies further decreases in Nb and Ta compatibility at even higher pressures. Therefore, melts from Earth's deep mantle should be relatively enriched in Nb and Ta. Comparative trends in Nb and Zr partitioning also suggest that high-pressure melts should be characterized by low Zr/Nb ratios. As such, depth of partial melting could be as important a constraint as mineral and melt chemistry and degree of partial melting in constraining the composition of partial melts originating in Earth's deep mantle.

o. *Rutile solubility and the temperature of early crust-building magmatism (X. Xiong, H. Keppler, A. Audétat and G.H. Gudfinnsson)*

The TiO_2 content in a natural magma depends on many factors, but in the presence of a Ti-rich phase, it is controlled by the solubility of this Ti-rich phase in the magma. Previous experiments have shown that TiO_2 solubility in silicate melts depends mainly on temperature and melt composition. It is thus possible to determine the temperature of magma generation from TiO_2 solubility experiments if a Ti-rich phase was present during the generation of the magma. Archean TTG (tonalite-trondhjemite-granodiorite) rocks, the early crust-building magmas, are the products of partial melting of metabasalts in the subducted crust and are characterized by strong depletion of Nb-Ta and Ti relative to other elements of similar compatibility. Previous experiments have demonstrated that rutile is a necessary residual phase leading to the Nb-Ta depletion in TTG magmas. We have determined the TiO_2 solubility in TTG melts saturated with rutile over a wide range of P, T and H_2O in order to define the temperature of slab melting that yielded the early crust-building magmas.

Two starting materials were used for the experiments. One is trondhjemitic and the other is tonalitic. 2-5 wt.% TiO_2 was added to these two base compositions to ensure rutile saturation during the experiments. All experiments were conducted with an end-loaded piston-cylinder apparatus at 1.5-3.5 GPa, 750-1250 °C with ~ 5-30 wt.% H_2O for 48-432 hours. Major elements in minerals and melts and Nb and Ta in rutile were analyzed with the electron microprobe. The TiO_2 contents in the melts of all the experiments are very homogeneous, indicating that dissolution equilibrium of rutile in the melts was achieved.

Experimental results are summarized in Fig. 3.2-29 (A, B, C & D). TiO_2 solubility in melt markedly increases with melt basicity as expressed by the melt compositon parameter FM and increasing temperature. It decreases slightly with increasing pressure and increases slightly with increasing H_2O content. By least squares analysis of 31 experiments, the general TiO_2 solubility model is given as:

$$\ln (TiO_2)_{melt} = \ln(TiO_2)_{rutile} + 2.86 - (9735/T) - 0.27P + 0.149FM + 0.01H_2O$$

where TiO_2 and H_2O are in wt.%, T is in Kelvin, P in GPa and FM is given by $FM=(1/Si)\bullet[Na+K+2(Ca+Fe+Mn+Mg)]/Al$, in which the chemical symbols represent cation fractions. The TiO_2 solubility expression provides a good fit to the data with relative error between experimental and calculated values being less than 10-15 % for all the experiments except for two runs.

The TiO_2 solubility in rutile-saturated melts has been used to constrain the temperature range of TTG production. Archean TTG rocks from 25 areas worldwide have average TiO_2 in the range of 0.15-0.88 wt.% and average SiO_2 generally in the range of 65.0-73.0 wt.% (FM=2.65-1.50). The melts in equilibrium with rutile in our experiments have SiO_2 ranging

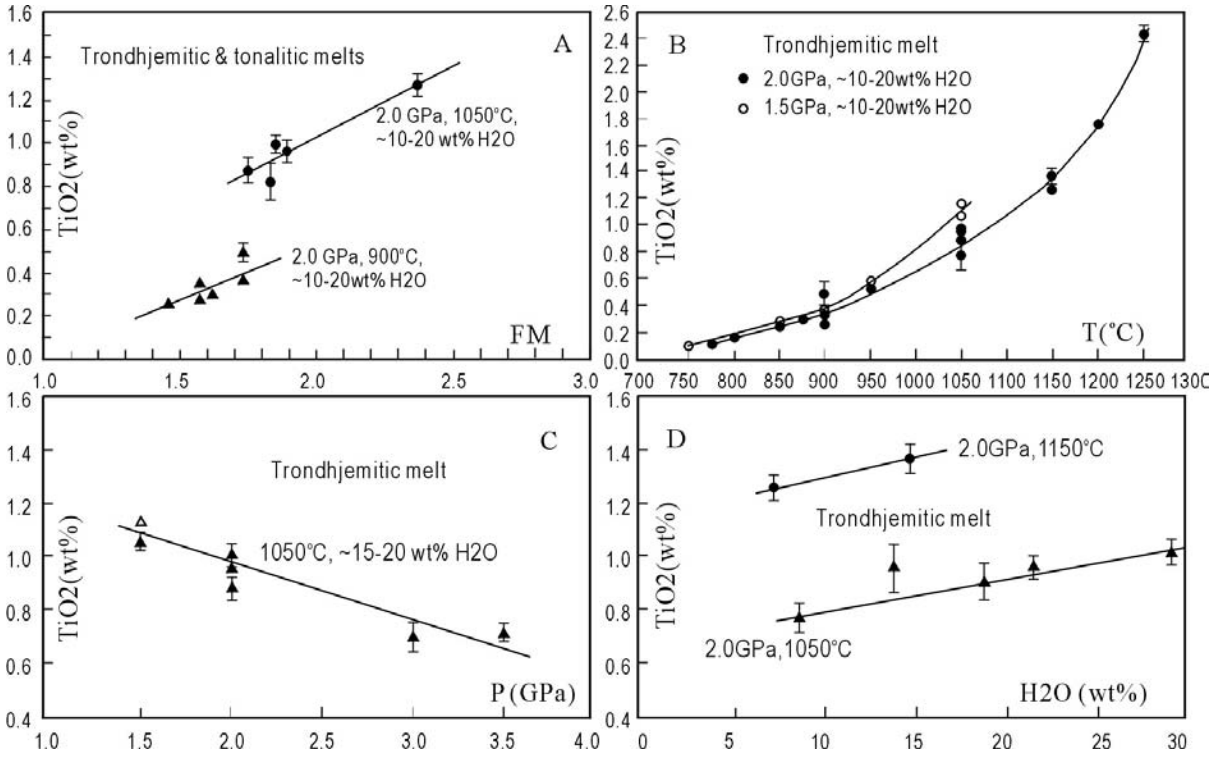

Fig. 3.2-29: TiO_2 solubility in rutile-saturated melts; A: compositional effect; B: temperature effect; C: pressure effect; D: H_2O effect.

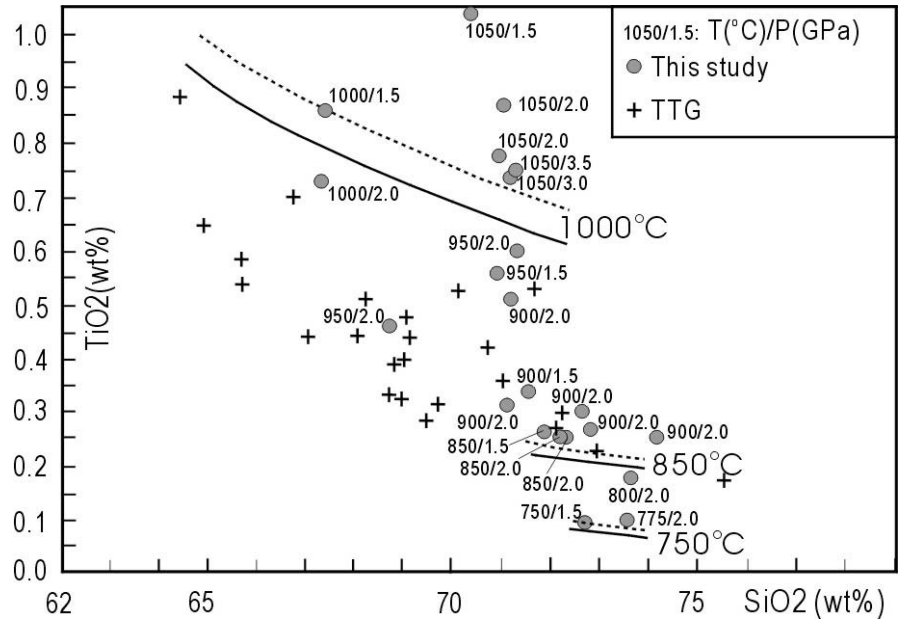

Fig. 3.2-30: TiO_2 vs. SiO_2 in rutile-saturated TTG melts from runs at 1.5-3.5 GPa and 750-1050 °C compared with those of Archean TTG, showing that the TTG data overlap the experimental and estimated data only at temperatures between 850 °C and 1000 °C. Solid lines: estimated isotherms for 2.0 GPa, 10 wt.% H_2O TTG compositions; dashed lines: estimated isotherms for 1.5 GPa, 10 wt.% H_2O.

from 67.0 to 74.0 wt.% (FM=2.37-1.35), very close to the natural TTG compositions. Figure 3.2-30 shows that the TTG rocks in terms of TiO_2 vs SiO_2 overlap only with the experimental melts at temperatures of 850-1000 °C under conditions of realistic pressures and H_2O contents. On the assumption that the TTG magmas did not undergo remarkable fractional crystallization of Ti-rich accessory minerals and that there was no other magma process that has significantly modified the magma composition, the temperature range of the TTG magmatism is confined to 850-1000 °C. Dehydration of serpentine, amphibole and other hydrous phases in subducted oceanic lithosphere may lead to slab melting and modern adakite production at temperatures close to the wet solidus of basalt. However, only amphibole has dehydration temperatures overlapping with 850-1000 °C. This constrains amphibole to be the sole H_2O source for the TTG production and suggests much higher slab melting temperatures in the Archean than today, given that slab melting in modern subduction zones takes place at temperatures close to the wet solidus of basalt.

p. *Mantle redox conditions beneath Antarctica (A. Martin and C.A. McCammon, in collaboration with A. Cooper/Dunedin)*

The oxygen fugacity of the upper mantle can be determined from natural samples using mineral oxybarometers, *e.g.*, olivine-orthopyroxene-spinel, which have been applied to a range of samples from different localities to provide a relatively detailed picture of the redox state of the upper mantle across the globe. One continent is missing from the dataset, however, namely Antarctica, and the purpose of this project is to address this deficiency. Two seasons of fieldwork were conducted on Mount Morning, a 2,723 m high eruptive centre in the Southern Victoria Land region of the Ross Sea, Antarctica. The mantle xenoliths are atypically large (up to 50cm) and abundant compared to localities elsewhere in the world. The project will comprise extraction of single grains of the individual mineral phases (olivine, orthopyroxene, spinel and clinopyroxene) and measurement of Fe^{3+} concentrations using Mössbauer spectroscopy. These data will be combined with chemical compositions, mineral modes and thermobarometer/oxybarometer models to determine both the oxygen fugacity and bulk Fe_2O_3 concentration of the assemblage. Together with data from other studies of the volcanic region, our results will be used to construct a more complete picture of oxygen fugacity relations in the upper mantle beneath Antarctica.

q. *Fractionation of iron isotopes in mantle eclogites (C.A. McCammon, in collaboration with H. Williams and S. Nielsen/Oxford, C. Renac/St. Etienne; N. Pearson, W. Griffin and S. O'Reilly/Sydney)*

Iron isotopes can provide novel constraints on mantle processes as Fe is abundant in mantle rocks and consequently resistant to alteration and contamination. Recent studies have

demonstrated that although there is little variation in the $\delta^{57}Fe$ values of oceanic basalts, significant isotopic variations are preserved in mantle peridotites and pyroxenites, which can be explained by melt extraction and metasomatism. In this study we investigated the composition of bimineralic eclogite xenoliths from the mantle (*i.e.*, pure garnet and omphacitic pyroxene). We collected iron isotope data for eclogite xenoliths originating from the Kaalvallei and Bellsbank kimberlite pipes, South Africa, and correlated the results with Fe^{3+} concentration data derived using Mössbauer spectroscopy. Our data show no correlation between garnet $\delta^{57/54}Fe$ and $Fe^{3+}/\Sigma Fe$ (Fig. 3.2-31a), in contrast to our previous study of spinel in mantle peridotites. There is, however, a good correlation between the garnet Fe^{3+} concentration and degree of depletion as measured by the Mg number (Fig. 3.2-31b), consistent with partial melting. A further study of these eclogites involving oxygen isotopes shows a strong correlation between $\delta^{18}O$ and $\delta^{57/54}Fe$, consistent with disequilibrium partial melting events in the lithosphere, implying that low $\delta^{18}O$ values in ocean-island basalts cannot be used to infer recycled oceanic crust in their source regions.

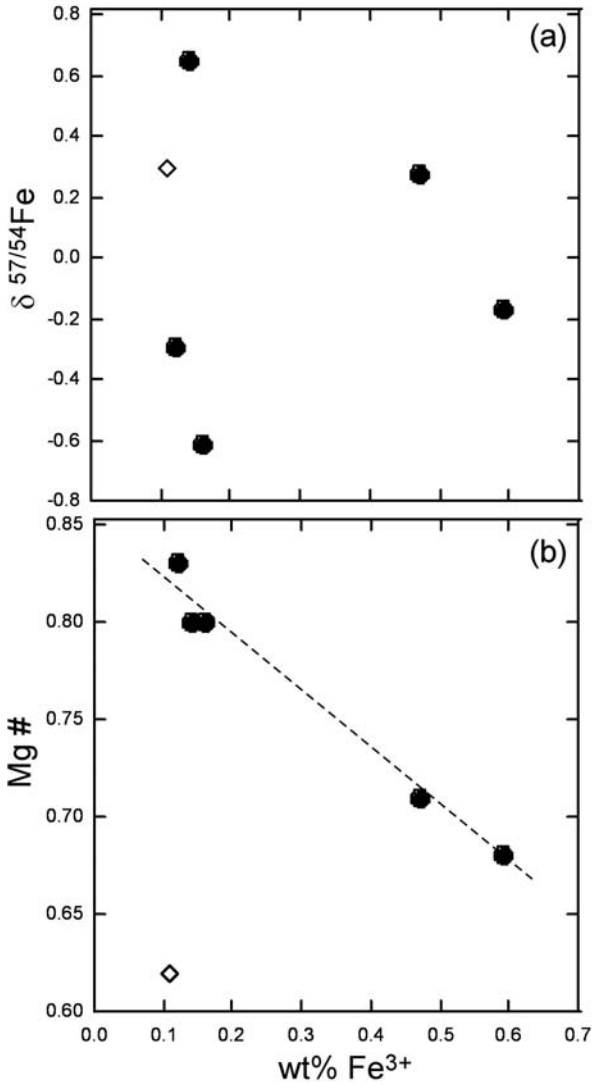

Fig. 3.2-31: (a) Variation of $\delta^{57/54}Fe$ in garnet from Kaalvallei (solid circles) and Bellsbank (open diamond) eclogite xenoliths with wt.% Fe^{3+} determined using Mössbauer spectroscopy. There is no obvious correlation between these parameters. (b) Variation of Mg# with wt.% Fe^{3+} for the above garnets showing a strong inverse correlation, consistent with a partial melting process. The dashed line is a guide for the eye.

r. *The distribution of trace elements between biotite and granitic melts (P. Were/Tübingen and H. Keppler)*

Many hydrothermal and pegmatitic ore deposits are associated with granites and related rocks. These ore deposits are usually the final products of long fractionation processes, involving enrichment of trace elements by fractional crystallization, fluid/melt partitioning and other processes. Biotite is a common mineral that crystallizes early from many granitic magmas. Only those trace elements that are not removed by biotite crystallization at an early stage of magma evolution may ultimately be concentrated in residual melts. Understanding the distribution of trace elements between granitic melts and biotite is therefore essential for predicting the economic potential of granites.

So far, only very limited data on biotite/melt partitioning are available in the literature. One reason for this is probably the difficulty to grow biotite crystals large enough for chemical analysis by microprobe from a granitic melt. We have overcome this problem by experiments with run durations up to 45 days at 700-800 °C and 2 kbar, which produced biotite crystals in equilibrium with a silicate melt (Fig. 3.2-32). Starting materials were glasses of appropriate composition together with about 10 % of water to induce water-saturation. The experiments were done in standard cold seal vessels.

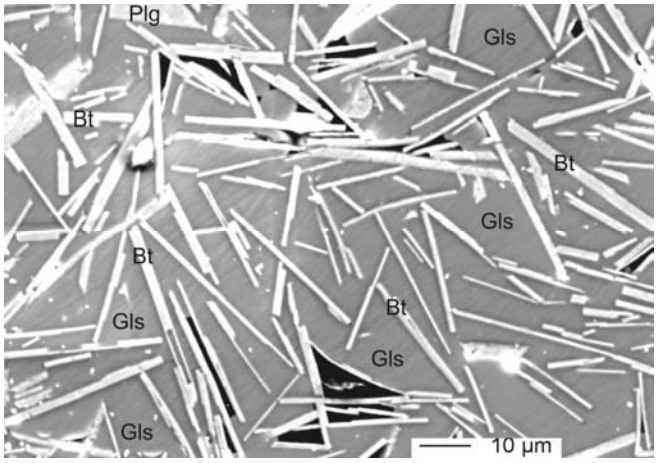

Fig. 3.2-32: Run product of an experiment on biotite/melt partitioning at 2 kbar, 800 ˚C, run duration 45 days. Biotite crystals (Bt) are surrounded by a granitic melt quenched to glass (Gls).

The starting materials of the experiments were doped with a suite of trace elements at the hundred to thousand ppm level. Partition coefficients were determined by microprobe analyses of coexisting biotite and quenched glass. Results for various trace elements are shown in Fig. 3.2-33 and for rare earth elements in Fig. 3.2-34. Inspection of Fig. 3.2-33 shows that most high field strength elements and other transition metals such as Ti, Cr, V, Ni, Co, and Zn are efficiently removed from the melt by biotite crystallization ($D^{biotite/melt}$ >>1). On the other hand, Mo and Cu that are commonly found in porphyry copper deposits, are incompatible or only slightly compatible in biotite. This also applies to Cs, Ta and Zr, which belong to the elements frequently enriched to economic level in granitic pegmatites. These observations confirm that biotite fractionation probably exerts a strong control on metal enrichment in the evolution of granitic magmas.

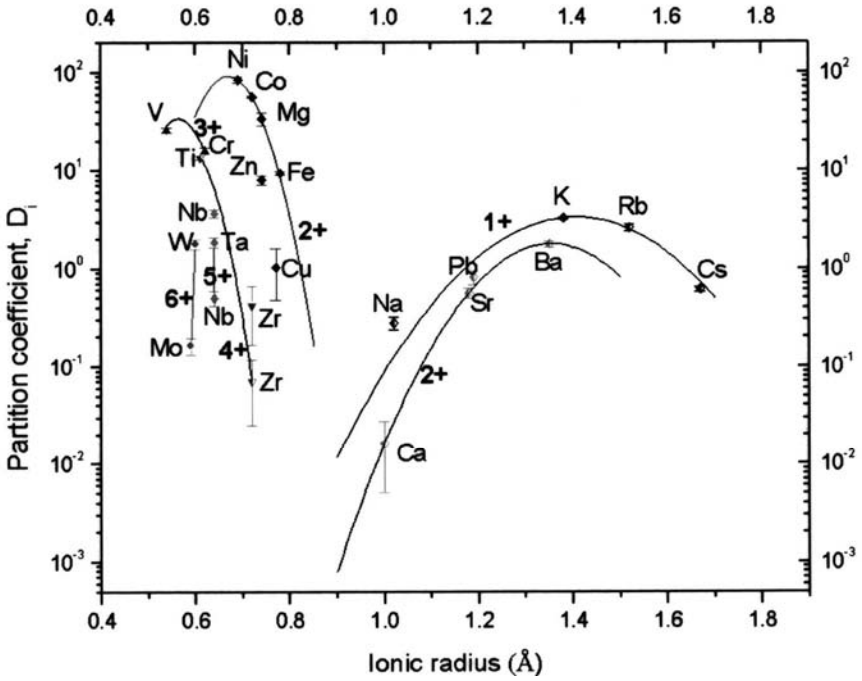

Fig. 3.2-33: Biotite/melt partition coefficients for a suite of trace elements. Curve fits from lattice strain theory are shown for trace elements of different valence entering the Mg site and the interlayer K-site.

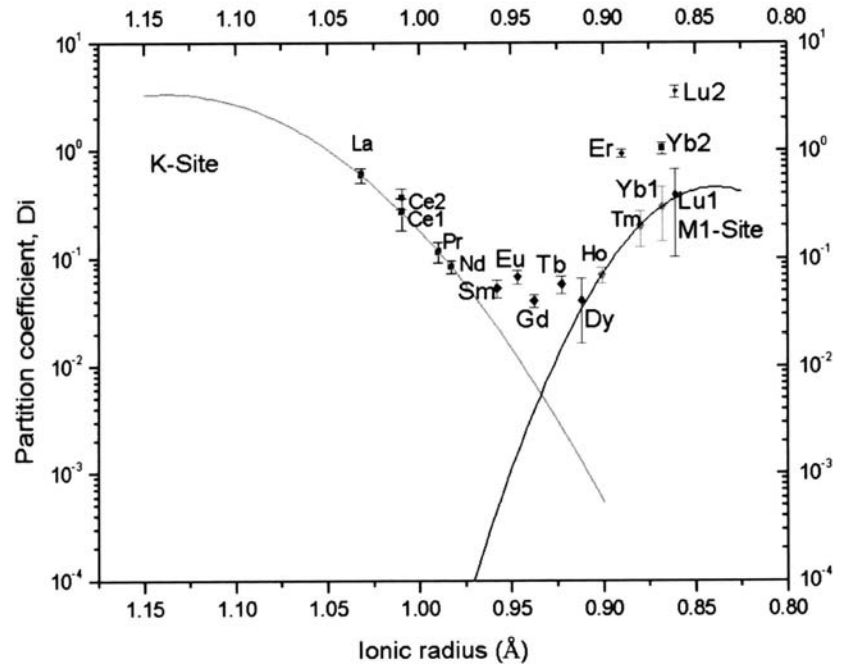

Fig. 3.2-34: Biotite/melt partition coefficients for rare earth elements. Curve fits from lattice strain theory are shown for rare earth elements entering the Mg site and the interlayer K-site. Where two data points are shown for one element (*e.g.*, Lu1 and Lu2), the data point with the higher apparent partition coefficient may be affected by submicroscopic inclusions of allanite in biotite.

The pattern of distribution coefficients observed for the rare earth elements (Fig. 3.2-34) is unusual, as it has a pronounced minimum for middle rare earth. This is probably a result of the light rare earth being incorporated in the interlayer site of biotite, while the heavy rare earths partition into the Mg-site. The middle rare earths are incompatible in both sites and therefore have particularly low partition coefficients.

3.3 Mineralogy, Crystal Chemistry and Phase Transformations

Studying the response of crystal structures to changing pressure, temperature, oxygen fugacity and chemical composition is fundamental to understanding the Earth's interior. Although nearly all materials are affected by these parameters, pressure is one of the most important for describing deep Earth behaviour, because it ranges over more than five orders of magnitude (from 10^5 to 10^{11} Pa). In this chapter, fifteen contributions explore the response of different minerals to the extremely high pressures within the Earth's interior and other planets. Increasing pressure causes not only a volume reduction in minerals, but can also distort the crystal structure, potentially causing a structure transition. Another type of response to pressure involves a change in electronic structure, for example spin transitions of *3d*-electrons in iron-bearing materials, or a change in electrical transport properties. The response of a mineral to high pressure is defined not only by its phase transformations, but also by an accurate determination of its equation of state (EOS) using various elastic scattering techniques, including X-ray and neutron diffraction. One of the most dramatic responses to high pressure is a change in the phase stability of a mineral or assemblage, and determining phase diagrams at high pressure and temperature is a classical yet indispensible approach for exploring the Earth's interior. For systems containing iron, H_2O activity and oxygen fugacity are also important for determining phase stabilities. Recent developments in high-pressure techniques now allow us to generate nearly all *P-T* conditions of the Earth's mantle; however sluggish kinetics of mineral reactions in solid solutions and chemically complex systems remain obstacles that must be overcome to clarify phase stabilities. A complementary approach, namely thermodynamic studies of end-member minerals and simplified systems, provide a bypass for reaching this goal.

a. *High-pressure Raman study of the phase transformation in $K_{0.5}Na_{0.5}AlSi_3O_8$ hollandite (J. Liu, T. Boffa Ballaran and L.S. Dubrovinsky)*

$KAlSi_3O_8$ hollandite, which is isochemical with sanidine and may be a host phase of K in the mantle, undergoes a phase transformation from the tetragonal *I*4/*m* structure to the monoclinic *I*2/*m* structure at about 20 GPa. For K-hollandite containing different Na contents, our experiments showed that all hollandite samples transform to the monoclinic structure at high pressure. The transition pressure decreases with increasing Na content (see BGI Annual Report 2006). Our experiments, conducted with different pressure transmitting media, also showed that the tetragonal to monoclinic high-pressure phase transformation depends strongly on the presence of deviatoric stresses. The transition pressures observed in experiments conducted using LiF as a pressure transmitting medium are much lower than those observed under hydrostatic conditions. The deviatoric stresses have therefore the effect of stabilising the monoclinic phase with respect to the tetragonal one. For example, the transition pressure observed in a Raman experiment using LiF as transmitting medium of a hollandite containing 40 % Na is about 4 GPa; however in a X-ray diffraction experiment conducted at the ESRF with a hollandite sample containing 50 % of Na and He as pressure transmitting medium, no phase transformation was observed up to 12 GPa. It is therefore necessary to use hydrostatic

pressure media to properly define the physical properties of the aluminosilicate hollandite with different K and Na content. Here we take advantage of the gas loading system recently installed at BGI to perform a high-pressure Raman experiment on a $K_{0.5}Na_{0.5}AlSi_3O_8$ hollandite using neon as pressure transmitting medium. Neon has been reported to provide hydrostatic conditions up to 16 GPa.

The experiment was carried out using a Dilor XY Raman spectrometer with a 514.5 nm Ar+ ion laser equipped with a microscope and liquid-nitrogen-cooled CCD detector. $K_{0.5}Na_{0.5}AlSiO_8$ hollandite sample powder was loaded in a diamond anvil cell with neon as pressure transmitting medium and a piece of ruby as pressure standard. The sample was compressed at room temperature up to 15 GPa. Changes in the slopes of the Raman peak positions as well as broadening were observed at around 13 GPa, suggesting that the tetragonal to monoclinic phase transition occurs at such a pressure. The peak position of the Raman signal at ~ 217 cm^{-1} decreases with increasing pressure up to 13 GPa, and then increases for pressures above 13 GPa (Fig. 3.3-1). This behaviour is identical to that described for the B_1 Raman-active mode of stishovite across its high-pressure phase transition. Adding the constraint of the transition pressure of this hollandite composition to our previous results obtained in a He pressure transmitting medium for a $K_{0.8}Na_{0.2}AlSi_3O_8$ hollandite sample (BGI Annual Report 2006) and assuming a linear decrease of the transition pressure with increasing Na content, we suggest a transition boundary at about 7-8 GPa for pure $NaAlSi_3O_8$ hollandite.

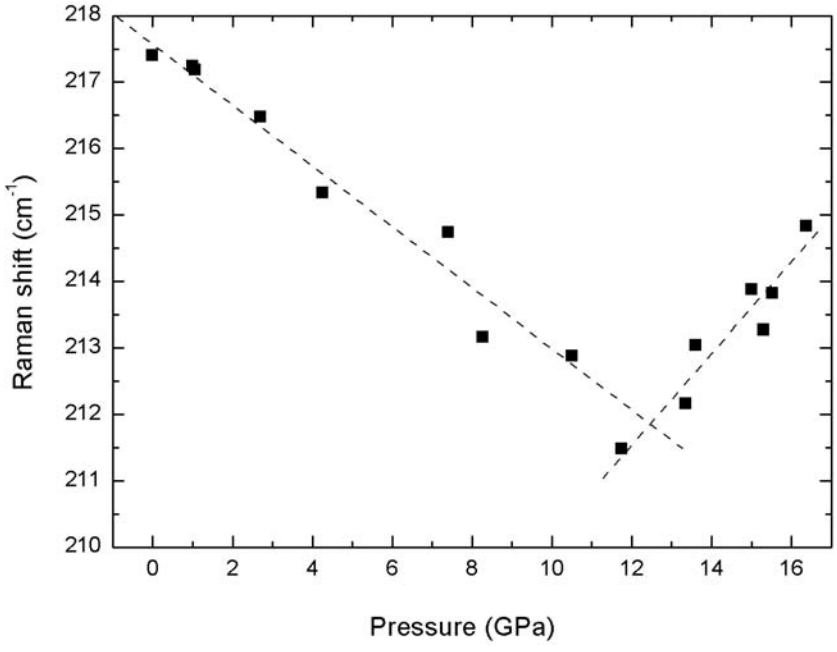

Fig. 3.3-1: Effect of pressure on the position of the Raman peak near 217 cm^{-1}. The change in slope at ~ 13 GPa indicates a phase transition, and the dotted lines are linear fits of the data before and after the transition.

b. *High-pressure C2/c - $P2_1/c$ phase transition along the $LiAlSi_2O_6$-$LiGaSi_2O_6$ solid solution (F. Nestola/Padova and T. Boffa Ballaran)*

The quest for a general quantity (being a structural, chemical or physical feature) to describe the $P2_1/c \leftrightarrow C2/c$ phase transformation occurring in pyroxenes as a function of temperature,

pressure and composition is one of the most pursued in mineralogy. In several studies it has been pointed out that the size of the octahedral M1 site may play a major role in controlling the pressure at which such a transition occurs. Spodumene ($LiAlSi_2O_6$) is not a major mantle phase; however it undergoes a $C2/c \rightarrow P2_1/c$ phase transformation which is closely related to those occurring in other more common pyroxenes, and can therefore be used to better constrain the systematics of this transition. In this study we report new data on the compressibility of two Li-clinopyroxenes with compositions $Li(Al_{0.53}Ga_{0.47})Si_2O_6$ and $LiGaSi_2O_6$ obtained by means of single-crystal X-ray diffraction using a diamond anvil cell. These data show the clear effect of cation substitution on the elasticity of pyroxenes, and the dependence of the transition pressure on the M1 cation size.

Unit-cell lattice parameters were determined at 12 and 10 different pressures up to P = 8.8 and P = 7.3 GPa for $Li(Al_{0.53}Ga_{0.47})Si_2O_6$ and $LiGaSi_2O_6$, respectively. $Li(Al_{0.53}Ga_{0.47})Si_2O_6$ shows a *C*2/c - $P2_1/c$ phase transformation between 1.8 and 2.2 GPa, characterised by a discontinuous decrease in the unit-cell volume and by the appearance of the *b*-type reflections ($h + k$ = odd) typical of a primitive symmetry. In contrast, the Ga end-member transforms to the $P2_1/c$ symmetry as soon as some pressure is applied to the cell. At the lowest pressure data obtained at 0.4 GPa, $LiGaSi_2O_6$ has already the primitive symmetry. A comparison among the data obtained so far for Li-bearing pyroxenes indicates that the *C*2/*c* low-pressure phases are more rigid than the $P2_1/c$ high-pressure ones and that an increase of the M1 cationic radius causes a decrease in the bulk modulus K_{T0}. Moreover the **c** axis which is the most rigid in the *C*2/*c* phases becomes the most compressible after the phase transition to the *P* symmetry.

c. *Spin transition in (Mg,Fe)(Si,Al)O_3 perovskite (C.A. McCammon, I.Yu. Kantor, O. Narygina, J. Rouquette and L.S. Dubrovinsky, in collaboration with U. Ponkratz, I. Sergueev and M. Mezouar/Grenoble, V.B. Prakapenka/Chicago)*

Spin-pairing transitions of iron were predicted to occur within the Earth's interior nearly 50 years ago, but only in the past few years has direct experimental evidence for such transitions at lower mantle conditions been reported. A high-spin to low-spin transition of Fe^{2+} in (Mg,Fe)O is now well established by both experimental and computational data to occur near 50 GPa at room temperature for lower mantle compositions. However in the Earth's most abundant phase, (Mg,Fe)(Si,Al)O_3 perovskite, the picture is not so clear. Previous X-ray emission (XES) and nuclear forward scattering (NFS) data present conflicting results on the location, number and sharpness of the transition(s), and whether Fe^{2+} or Fe^{3+} or both are involved. To reconcile these observations, we undertook the first high-pressure high-temperature study of iron-containing silicate perovskite using combined Mössbauer, NFS and X-ray diffraction techniques to determine the spin state of iron in the dominant lower mantle phase.

We collected 119 ^{57}Fe Mössbauer and 32 NFS data of $Mg_{0.88}Fe_{0.12}SiO_3$ and $Mg_{0.86}Fe_{0.14}Si_{0.98}Al_{0.02}O_3$ perovskite using a resistively-heated diamond anvil cell at pressures up to 110 GPa and temperatures up to ~ 1000 K, combined with high-resolution X-ray diffraction of several of the same sample loadings. All data show the appearance of a new component above 30 GPa with high quadrupole splitting (QS) whose stability is enhanced with increasing pressure, and *in situ* high-temperature data show that this component is also stabilised by higher temperatures (Fig. 3.3-2). The transition involved in the sudden change of QS is purely electronic, since high-resolution X-ray diffraction data show no change in crystal structure up to 110 GPa. The most likely possibility is a spin transition, and a decrease in spin number with pressure in silicate perovskite was already found using XES in data reported in the literature. Using the relative abundance of components derived from our Mössbauer data to calculate the spin number as a function of pressure and temperature, we find that a high-spin to intermediate-spin transition of Fe^{2+} agrees well with all XES data (Fig. 3.3-3ab). Intermediate-spin Fe^{2+} is also consistent with the high quadrupole splitting and large centre shift of the new component, which was observed in previous NFS data reported in the literature. From the observed trend of spin number with temperature, we predict that Fe^{2+} in $(Mg,Fe)(Si,Al)O_3$ perovskite will be predominantly in the intermediate-spin state throughout most of the lower mantle (Fig. 3.3-3c).

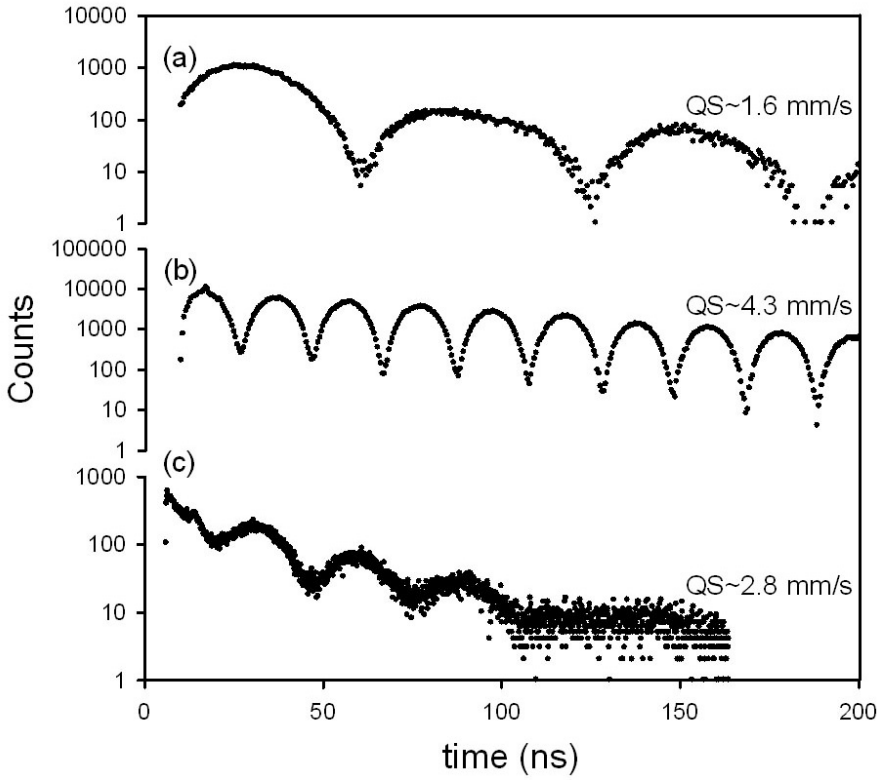

Fig. 3.3-2: NFS data of $Mg_{0.88}Fe_{0.12}SiO_3$ perovskite at (a) 7 GPa, 290 K; (b) 110 GPa, 290 K; (c) 62 GPa, ~ 1000 K. At low pressure only high-spin Fe^{2+} is present, characterised by low QS, while intermediate-spin Fe^{2+} is stabilised by high pressure and high temperature, recognised by high QS. In (c) QS is reduced due to the temperature effect, but is still significantly higher than it would be for high-spin Fe^{2+}.

Spin transitions affect the electronic structure of Fe^{2+}, which in turn influences lower mantle properties such as radiative and electrical conductivity, rheology and iron partitioning. Much of our knowledge of lower mantle behaviour is based on experiments on quenched samples, yet spin transitions are reversible with respect to both pressure and temperature. The stability of intermediate spin-state Fe^{2+} in lower mantle perovskite is not the first surprising revelation for the Earth's most abundant phase, and based on the implications of spin transitions for lower mantle properties, is probably also not the last.

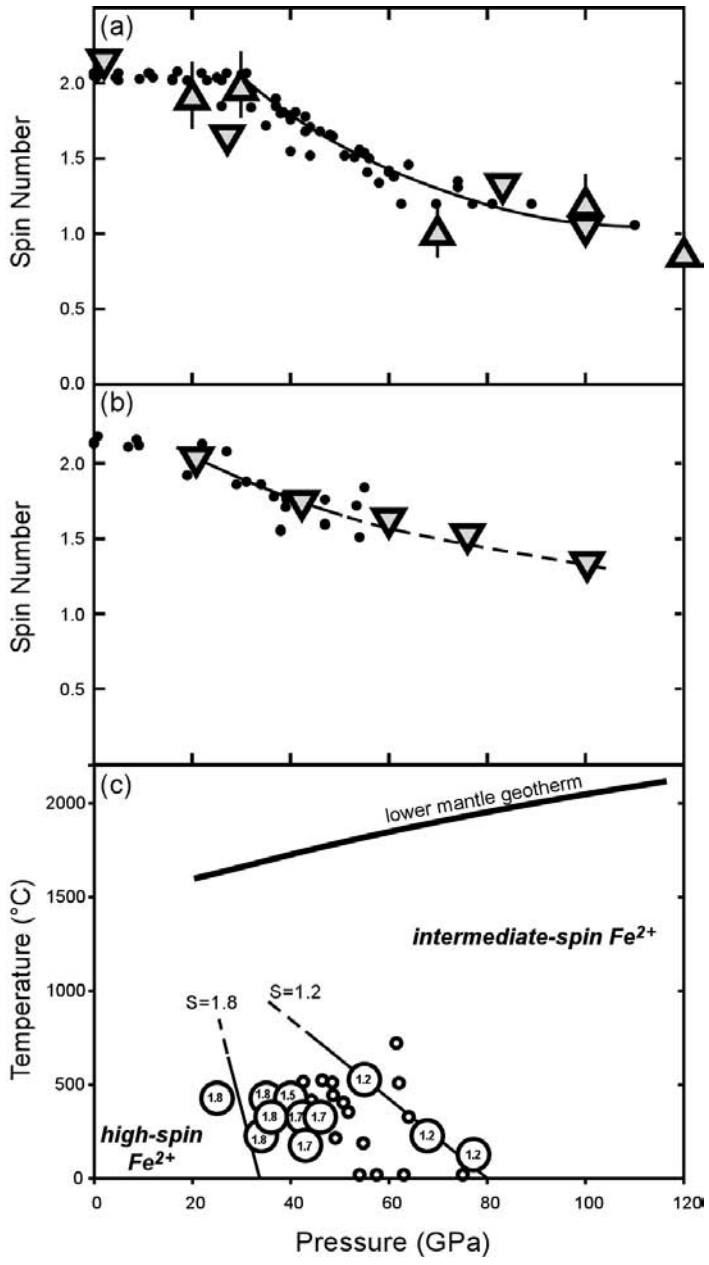

Fig. 3.3-3: Effect of pressure on the average spin number of (a) $Mg_{0.88}Fe_{0.12}SiO_3$ perovskite and (b) $Mg_{0.86}Fe_{0.14}Si_{0.98}Al_{0.02}O_3$ perovskite calculated from room temperature Mössbauer spectra (circles) assuming assignment of the new component to intermediate-spin Fe^{2+}. Previous XES data [J. Badro *et al.*, Science 305, 383, 2004; J. Li *et al.*, Proc. Nat. Acad. Sci. 101, 14027, 2004] are shown as triangles and inverted triangles, respectively. (c) Effect of pressure and temperature on the average spin number of $Mg_{0.88}Fe_{0.12}SiO_3$ perovskite. Large circles (spin number indicated within) indicate Mössbauer data, while small circles correspond to NFS data, and all spin numbers show a consistent decrease with increasing pressure and temperature. Lines of equal spin number have negative slope; hence along the lower mantle geotherm Fe^{2+} is predicted to be predominantly in the intermediate-spin state.

d. *In situ determination of transitions in Fe_3O_4 at high pressures and temperatures using resistivity measurements (A. Woodland and K. Schollenbruch/Frankfurt, in collaboration with D.J. Frost)*

Determining the stability and behaviour of Fe_3O_4 magnetite is essential for understanding the phase relations and thermodynamics of the simple Fe-O system and for referencing the properties of more complex Fe-bearing phases. As a mixed oxide magnetite is a good test material through which to investigate the effects of pressure and temperature on intervalence charge transfer processes, that likely control electrical conductivity throughout the mantle. Magnetite is known to undergo an unquenchable 1st order phase transition at ~ 21 GPa and room temperature. The post spinel *h*-Fe_3O_4 phase has been identified as either a $CaMn_2O_4$-type or $CaTi_2O_4$-type structure. The transformation of magnetite is accompanied by a significant change in density (+ 6 %) and most likely changes in magnetic and electrical properties. The position of the phase boundary in P-T space is very poorly constrained because the transition is extremely sluggish. The previously proposed negative Clapeyron slope for this transition, from externally heated diamond anvil cell experiments, may arise because a large overstep of the reaction boundary is required at low temperatures to nucleate the high pressure phase. Reversed experiments at higher typical mantle temperatures are required in order to determine the stability field of *h*-Fe_3O_4.

The aim of this study is to examine if the *h*-Fe_3O_4 transition can be detected through electrical conductivity measurements, thus providing an *in situ* probe of the phase relations. As the resistance of magnetite is low, four-wire conductivity measurements must be performed in order that the resistance of the leads can be accounted for in the measurement. A sample of magnetite 2 mm in diameter and 2.5 mm long was hot pressed in an initial experiment at 5 GPa and 900 °C. This sample was placed in an 18 mm edge length multianvil assembly with two W_3Re_{97}-$W_{25}Re_{75}$ thermocouples inserted from each end of the assembly making electrical contact with the sample through 0.3mm long Pt electrodes (Fig. 3.3-4). The sample was compressed with 11 mm truncation cubes in the 5000 tonne press. The resistance was measured by applying a constant current of 50 mA across the sample using one set of W_3Re_{97} thermocouple wires. The voltage across the sample was then recorded using the second set of $W_{25}Re_{75}$ wires. The sample measurement also includes the resistance of the Pt electrodes, but this should be negligible.

The sample was first compressed to 9 GPa, during which the resistance of the sample decreases by approximately one order of magnitude (Fig. 3.3-5). As the sample is heated, an additional Seebeck voltage is created across the sample that can be measured and then subtracted from the sample potential by turning the constant current supply off between measurements. During heating to 1100 °C the resistance first increased to a maximum at approximately 540 °C, then decreased to a value at 1100 °C that is comparable with room temperature. During cooling the resistance follows an identical path. This maximum in resistivity occurs at a temperature that is very close to the Curie temperature for magnetite at

ambient pressure (575-585 °C). While many materials are reported to exhibit resistivity maxima at the Curie temperature, previous measurements of the Curie temperatures for titanomagnetites have concluded that the Curie temperature increases linearly with pressure.

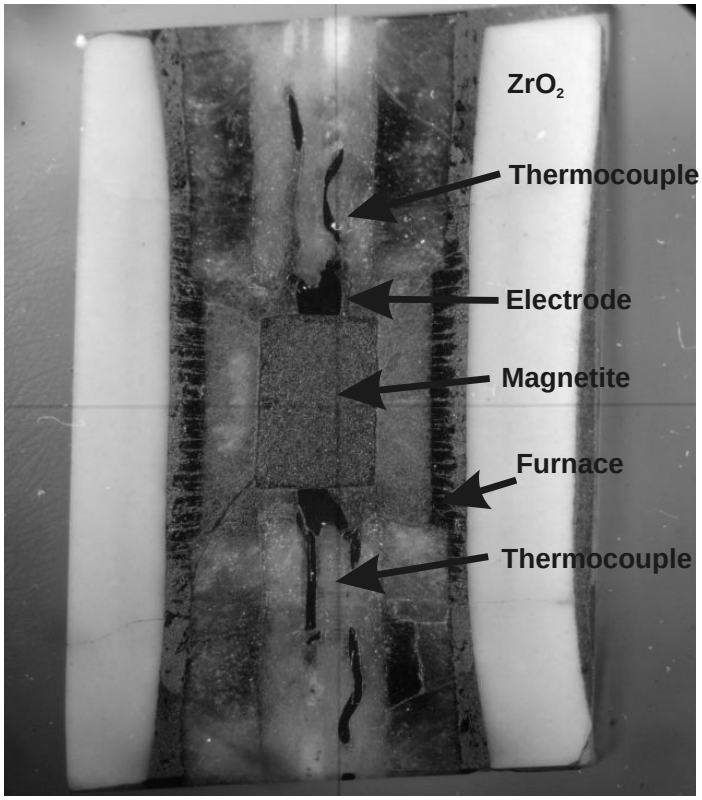

Fig. 3.3-4: Recovered section of a 18/11 multianvil experiment for a four-wire conductivity measurement of magnetite. Two thermocouples on either side of a hot pressed magnetite sample make electrical contact with the sample through Pt electrodes. The sample is surrounded by MgO and is heated with a $LaCrO_3$ furnace inside a ZrO_2 thermal insulating sleeve.

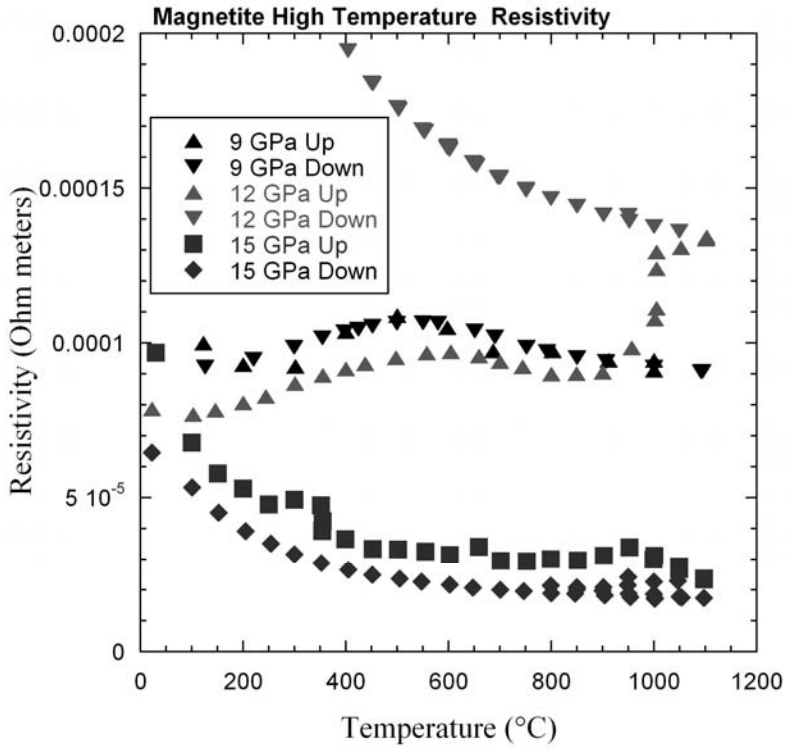

Fig. 3.3-5: Resistivity measurements of magnetite at 9, 12 and 15 GPa to 1100 °C. Up and Down refer to heating and cooling measurements, respectively.

The sample was then further compressed to approximately 12 GPa. During initial heating a similar maximum was encountered between 550-600 °C; however at 950 °C resistivity started to rise again and went through a sharp increase at 1000 °C by approximately 40 % (Fig. 3.3-5). The conditions of this increase are in reasonable agreement with conditions where the *h*-Fe_3O_4 phase might be expected. A different cooling behaviour was then observed with no maximum in resistivity, also indicative of the formation of a phase with different electrical properties to magnetite. After compression to 15 GPa, no resistivity maximum was observed during heating to 1100 °C, implying that the *h*-Fe_3O_4 phase remains stable during heating to these conditions. Although repeat measurements are required to confirm these observations, *in situ* resistivity measurement appears to be a promising technique for mapping high pressure and temperature transitions in Fe_3O_4.

e. *High-pressure behaviour of $CaIrO_3$ perovskite and post-perovskite phases (T. Boffa Ballaran, R.G. Trønnes/Oslo and D.J. Frost)*

At pressures in the range 1-3 GPa and temperatures > 1350 °C $CaIrO_3$, which has the *Cmcm* space group at ambient conditions, assumes a perovskite structure with the space group *Pbnm*. These two phases are isostructural analogues for $MgSiO_3$ post-perovskite and perovskite, respectively, which are likely the dominant phases of the Earth's lower mantle. The phase transition of $MgSiO_3$ perovkite to post-perovskite occurs in the Earth within the D" layer, a mantle region above the core-mantle boundary. The pressure and temperature conditions of this region are extremely high for accurate physical property measurements; whereas *ab initio* calculations, which have proved to be useful in providing information beyond the experimental limits, have often reported contradictory results. The use of low pressure analogue phases may, therefore, help to better understand the high-pressure and high-temperature behaviour of the $MgSiO_3$ phases and to constrain the physiochemical properties of the Earth's lowermost mantle. In this study we report the equation of state of $CaIrO_3$ perovskite and post-perovskite phase determined by means of X-ray single-crystal diffraction and point out similarities and dissimilarities of this compound with its high-pressure high-temperatures analogues.

Unit-cell lattice parameters have been measured to ~ 8 GPa in a diamond anvil cell for two single-crystals of $CaIrO_3$, one with the perovskite (*Pbnm*) and the other with the post-perovskite (*Cmcm*) structure. The $CaIrO_3$ post-perovskite structure is more compressible than the perovskite structure (Fig. 3.3-6). The same applies to the isostructural $MgSiO_3$ phases, as indicated by experimental and computational studies. A third-order Birch Murnaghan equation of state has been used to fit the measured *P*-*V* data with the following refined parameters: V_0 = 229.463 (8) Å^3, K_0 = 198 (3) GPa, K' = 1.2 (8); and V_0 = 226.38 (1) Å^3, K_0 = 181 (3) GPa, K' = 2.3 (8) for $CaIrO_3$ perovskite and post-perovskite, respectively. The larger

value of *K*' obtained for $CaIrO_3$ post-perovskite indicates that this phase become more incompressible with pressure relative to the perovskite phase. This result supports theoretical calculations which indicate that *K*' of $MgSiO_3$ post-perovskite is slightly larger than that of $MgSiO_3$ perovskite. However, such a conclusion had not been supported to date by experimental results, which, given the high pressures required, have always reported *K*' for $MgSiO_3$ perovskite and post perovskite fixed to the value of 4. The compressibility of the unit-cell axes of the perovskite structure is highly anisotropic with $\beta_a >> \beta_c >> \beta_b$. In contrast the *b* axis is the most compressible in the post-perovskite structure; whereas the *a* and *c* axes have similar compressibilities (with *c* slightly less compressible than *a*) and are much stiffer. A comparison between the compressibility of $CaIrO_3$ perovskite and post-perovskite with the isostructural $MgSiO_3$ phases reveals a similar general behaviour, although in detail $CaIrO_3$ perovskite is more and the post-perovskite less anisotropic than the corresponding $MgSiO_3$ compounds.

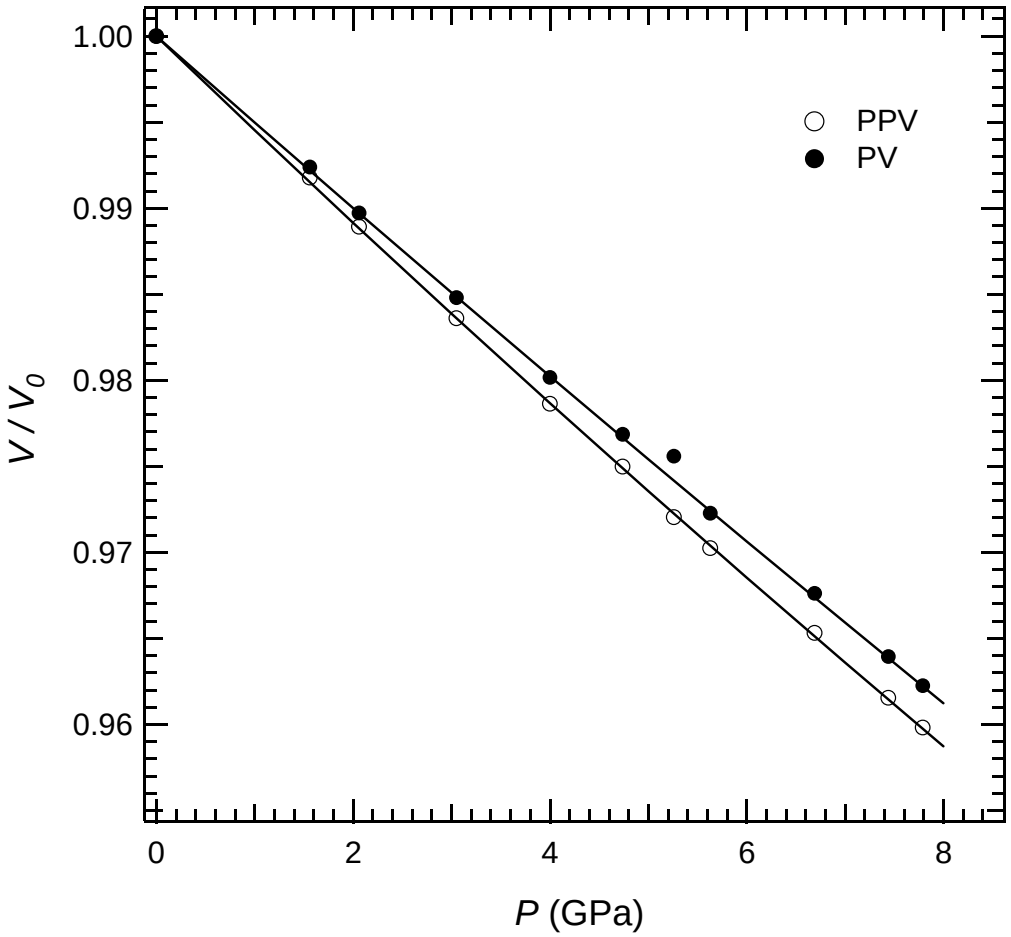

Fig. 3.3-6: Unit-cell volume variation of $CaIrO_3$ perovskite (filled circles) and post-perovskite (open circles) crystals as a function of pressure. Solid lines are third-order Birch-Murnaghan EoS fits through the data. Uncertainties are smaller than the symbols used except for the data point at 5.26 GPa collected for the perovskite sample, whose reflection profiles were quite broad and which falls outside the EoS fit.

f. *The ground-state structure of $Fe_{0.98}O$ (D.P. Dobson, I.G. Wood and L. Vočadlo/London; K.S. Knight and W. Kockelmann/Didcot, in collaboration with C.A. McCammon)*

Magnesiowüstite (Mg,Fe)O, the second most abundant constituent of the Earth's lower mantle, takes the rock-salt structure at ambient pressure and temperature. At elevated pressures and reduced temperatures, the paramagnetic iron end-member, wüstite becomes antiferromagnetically ordered, accompanied by a distortion of the atomic structure. For the iron-defective compositions which are stable at atmospheric pressure ($Fe_{0.96}O$) the antiferromagnetic phase is rhombohedrally distorted, with magnetic moments aligned along the [111] direction of the cubic cell. A previous study from another group investigated the low-temperature structure of $Fe_{0.99}O$ synthesised by metastable decomposition of $Fe_{0.96}O$ and found one split reflection in their neutron diffraction study which could be best fitted by a monoclinic distortion of the FeO cell. However, unambiguous interpretation the data in this study was hampered by the large amount of magnetite which was generated during the metastable decomposition process. In the present study we have synthesised nearly phase-pure $Fe_{0.98}O$ by reaction of $Fe_{0.96}O$ with metallic iron at 18 GPa and determined its atomic and magnetic structure by neutron diffraction between 10 and 298 K.

Commercially available (Alfa Aesar) wüstite was packed in Fe capsules and annealed at 18 GPa and 1073-1173 K for two to four hours using multianvil presses. X-ray powder diffraction confirmed that recovered samples had $Fe_{0.98}O$ stoichiometry and were > 99 % phase pure with only minor Fe impurities. Four synthesis experiments yielded sufficient sample for a neutron diffraction study using the GEM diffractometer at the ISIS pulsed neutron source. Samples were loaded in a standard vanadium can in a closed-circuit refrigerator (CCR) for non-ambient diffraction experiments. The CCR was evacuated and purged with a few mbar He gas pressure to act as a heat-transfer gas, and the temperature was monitored at the top of the sample can, some 1.5 cm away from the sample position. This results in a small offset in absolute temperature which has not been corrected for here.

Time-of-flight neutron diffraction patterns were collected at 5-10 K intervals between 10 and 298 K: the temperature set-point was changed and the temperature was allowed to equilibrate for at least 20 minutes prior to starting data collection. The close agreement between diffraction patterns collected during cooling and heating cycles indicates that the sample had thermally equilibrated in this time. Diffraction patterns were collected for 1 hour, ~ 170μAh, which was ample for Rietveld refinement of the data. Figure 3.3-7 shows a diffraction pattern of $Fe_{0.98}O$ collected at 298 K and another collected at 10 K. The peak splitting due to a monoclinic distortion in $Fe_{0.98}O$ is clear in the 10K diffraction pattern.

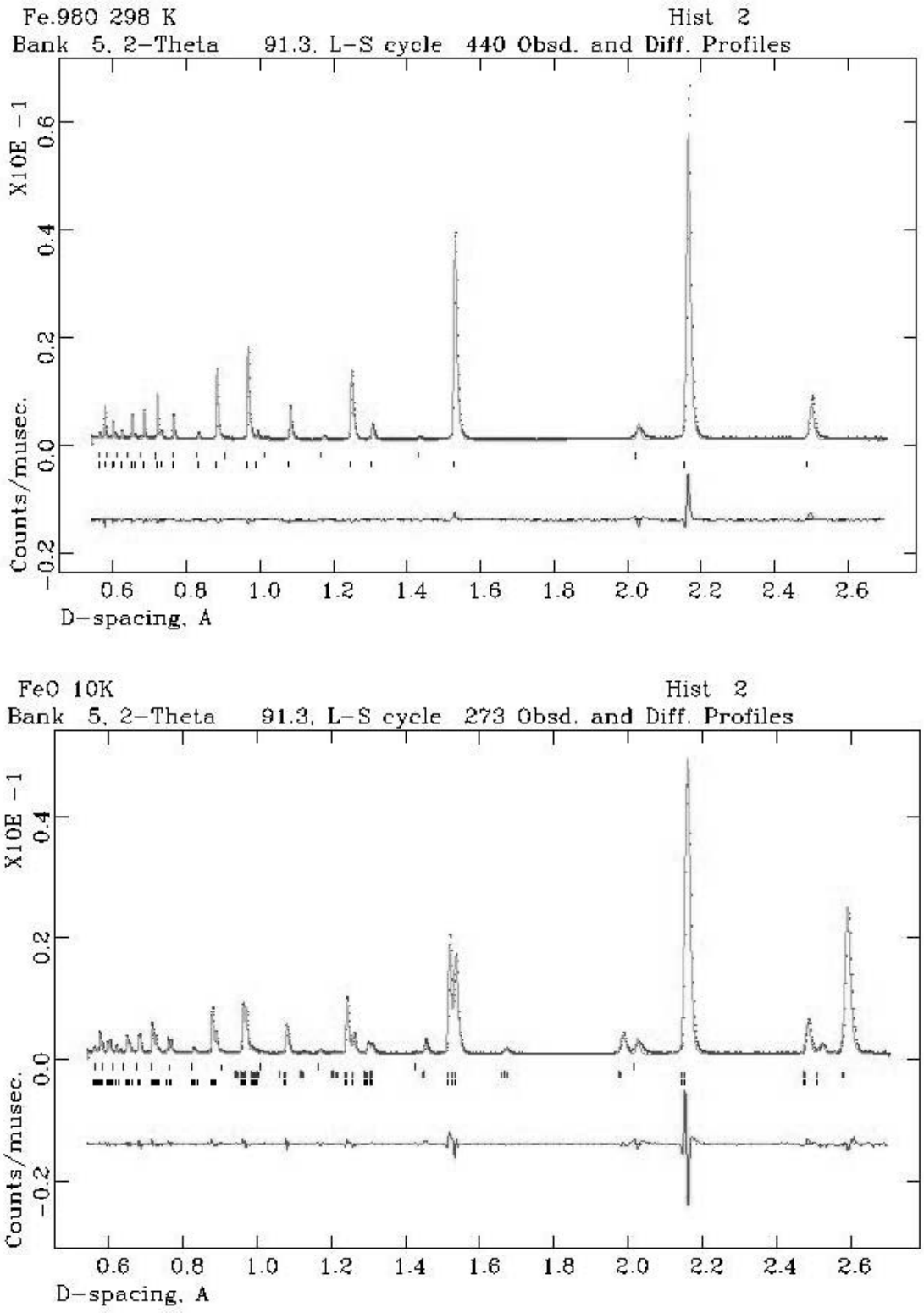

Fig. 3.3-7: Neutron diffraction patterns of $Fe_{0.98}O$ at 298 K (top) and 10 K (bottom) Symbols are the observed data and the lines are the Rietveld fits; the difference between the two is plotted below each pattern. Tick marks indicate reflections for phases included in the refinements and show (from top to bottom) Fe and wüstite (top plot), and Fe, magnetic wüstite reflections and atomic wüstite reflections (bottom plot).

g. *Pressure effect on the crystal structure of columbite minerals (S.C. Tarantino and M. Zema/Pavia, in collaboration with T. Boffa Ballaran)*

Columbite-tantalite minerals $(Fe,Mn)(Nb,Ta)_2O_6$ are the predominant Nb-Ta phases found in granitic pegmatites of the rare elements class. Their structure (Fig. 3.3-8) shows a tri-α-PbO_2-type structure in which the tripling of the *a* cell parameter is due to the ordering of divalent and pentavalent cations between the two available octahedral sites, named A and B, and does not cause a variation in the symmetry of the crystal structure. The degree of cation ordering, as well as the composition within the solid solution reported above, are responsible for sensible changes in the structure which, as we have previously shown, can be rationalized in terms of the different ionic radii of the species involved and of the second-order Jahn-Teller effect affecting the d^0 transition metal cations.

In the completely ordered samples, our work has also shown that increasing the temperature results in a positive and linear expansion of the columbite structure. Such thermal expansion is slightly anisotropic in Fe-rich samples, with *a* and *c* directions showing the largest variations with temperature, and becomes fairly isotropic with increasing Mn content. Columbite lattice constants as a function of the applied pressure were measured by a different research group on samples with different composition and order degree. The compressional behaviour is anisotropic with linear axial compressibility scheme $\beta_b > \beta_c \geq \beta_a$. Such anisotropy increases slightly with increasing Mn content. Comparison of these data shows how there is no "inverse relationship" between axial compressibility and axial thermal expansion in the columbite structure.

In this study structural investigations at high pressure were carried out on two natural columbites, the same samples used for our previous high temperature and high pressure studies: one ferrocolumbite crystal from Raode (Africa) and one manganocolumbite crystal from Kragero (Norway). The samples were preliminarily annealed to attain the complete cation-ordered state and avoid the superimposition of the effects of cation ordering during high-temperature studies. For each crystal, five complete datasets were collected from room pressure up to ca. 7 GPa using the Oxford Xcalibur four-circle diffractometer mounted with a CCD detector. Moreover, at each pressure accurate lattice parameters were measured with the Huber four-circle diffractometer by using eight-position centring of 15-18 Bragg reflections according to protocols described in the literature. For each dataset, all diffracted intensities were checked and only reflections whose intensity was not affected by diffraction effects from diamond or Be from the DAC were used. Structure refinements converged to a final discrepancy factor *R* ranging between 5.2 and 5.8 % for both the crystals.

Structural refinements of X-ray diffraction data at different pressures have allowed us to characterise the different mechanisms by which the columbite structure accommodates variations in pressure. A and B octahedral volumes in both samples decrease linearly as pressure increases; with a larger compression of the larger A site. It is worth noting that the difference in polyhedral bulk modulus of the A site for the two samples does not appear to relate directly to the octahedral sizes, as the A site is more compressible in the Fe-rich sample

compared to the Mn-rich one. By far the most compressible direction in both the analysed samples is along *b*. The cations are in fact free to move along this direction, thus allowing the octahedral chains to slide over each other, and this effect is particularly evident in the manganocolumbite sample which shows a steep shortening of inter-chain AB distances along *b*.

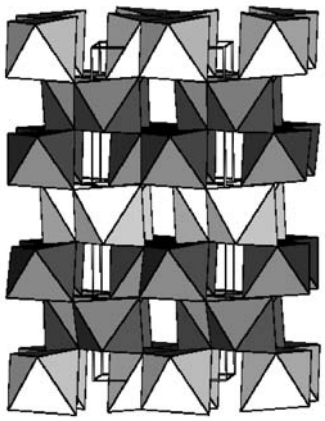

Fig. 3.3-8: The crystal structure of columbite viewed along [001]. B sites are indicated in a darker shade of grey.

h. *The elastic behaviour of leucite: An in situ single-crystal X-ray diffraction study (G.D. Gatta/Milano, in collaboration with T. Boffa Ballaran)*

Leucite, which has the ideal composition $K_{16}Al_{16}Si_{32}O_{96}$, is one of the most important feldspathoids. Feldspathoids are a class of (micro-porous) framework aluminosilicates present in a wide variety of geological environments of the Earth's crust: in alkali-rich igneous rocks, in metamorphic and metasomatic rocks, and in sedimentary rocks. The behaviour of this group of alkali-silicates has extensively been investigated under high- and low-temperature. On the other hand, because of experimental difficulties and structural complexity, the elastic behaviour and the pressure-induced evolution of natural/synthetic feldspathoids is scarcely known, giving rise to a complete lack of knowledge of *1)* the elastic properties of these materials, *2)* the behaviour of (micro-porous) tetrahedral frameworks at high-pressure and *3)* the pressure-induced change in the "weak interactions" of extra-framework cations and water molecules confined in a porous host.

Leucite is isotypic with analcime and its crystal structure is built on the combination of two "secondary buildings units" (SBU): 4 and 6 SBU (4 and 6-membered rings of tetrahedra). The framework topology of this group of minerals shows the maximum symmetry ($Ia\bar{3}d$). In leucite, the extra-framework content is represented only by K, which is located in the same site occupied by H_2O oxygens in the analcime structure (coordination number 12). At room temperature leucite is tetragonal (with space group $I4_1/a$ and a~13.07, c~13.75Å); whereas at $T > 630$ ºC leucite inverts to a cubic form (space group $Ia\bar{3}d$). For both high-T cubic and low-T tetragonal forms, no Si/Al-ordering in the tetrahedral framework was found. The leucite structure admits ionic substitution: compounds in the system $KAlSi_2O_6$-$RbAlSi_2O_6$-$CsAlSi_2O_6$ have been synthesised. However, the elastic behaviour and the P-induced structural evolution of leucite are unknown.

Elastic and structural behaviour of a natural tetragonal leucite from the volcanic Lazium district (Italy) was investigated at high pressure by *in situ* single-crystal X-ray diffraction with a diamond anvil cell at the Bayerisches Geoinstitut (BGI) and at the Earth Sciences Dept. of the University of Milan (ESD-MI). The evolution of the unit-cell parameters with *P* measured in this study is shown in Fig. 3.3-9.

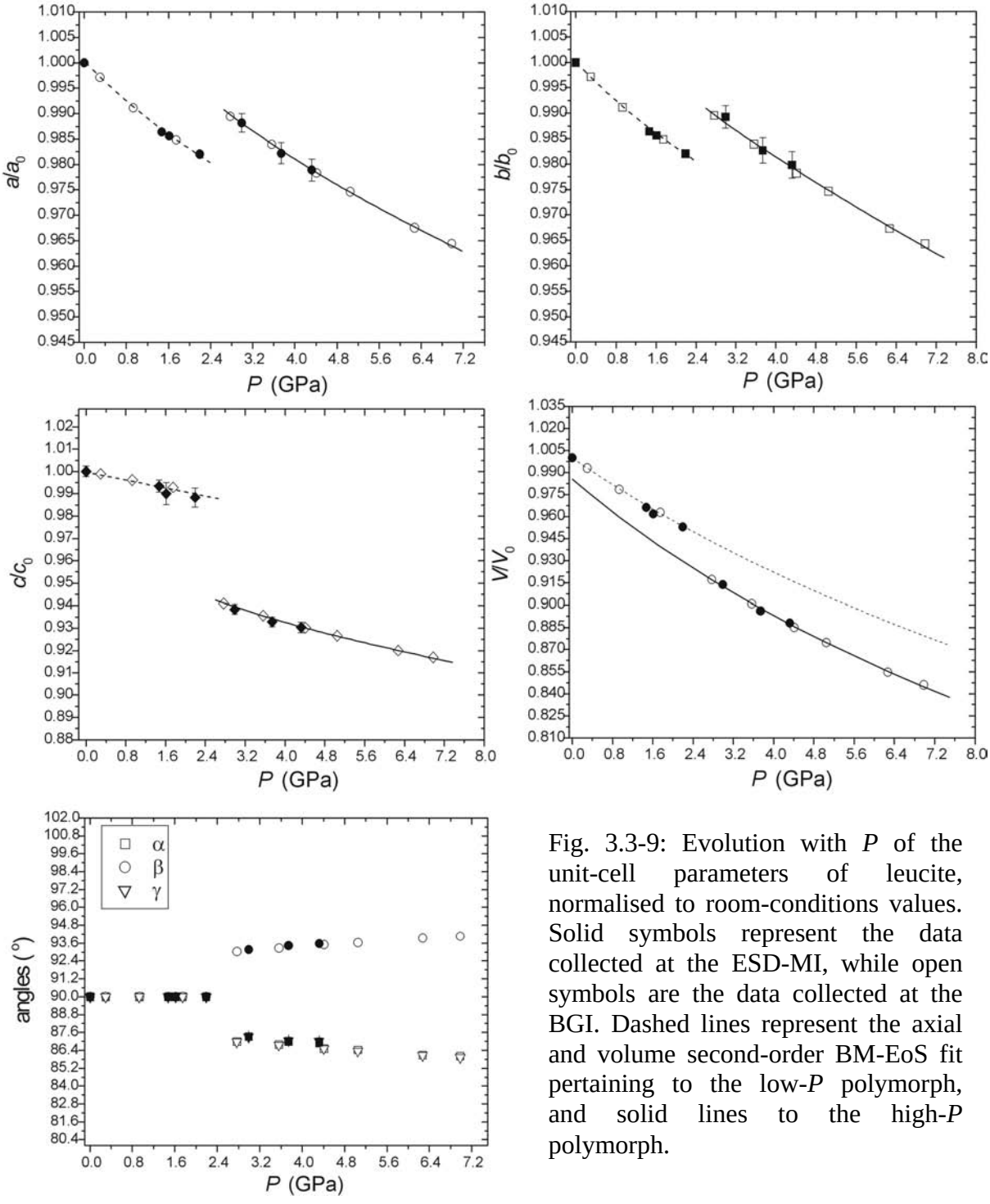

Fig. 3.3-9: Evolution with *P* of the unit-cell parameters of leucite, normalised to room-conditions values. Solid symbols represent the data collected at the ESD-MI, while open symbols are the data collected at the BGI. Dashed lines represent the axial and volume second-order BM-EoS fit pertaining to the low-*P* polymorph, and solid lines to the high-*P* polymorph.

A first-order phase transition is observed at P=2.4±0.2 GPa from tetragonal to triclinic symmetry. The transition pressure was bracketed by several measurements in compression and decompression. No further phase-transition has been observed at least up to 7 GPa. Fitting the volume data (normalised to room conditions values) collected at the BGI and at the ESD-MI of the tetragonal polymorph with a second-order Birch-Murnaghan Equation-of-State (BM-EoS), we obtain: K=41.9(6) GPa and K'= 4 (fixed). For the triclinic polymorph, a second-order BM-EoS gives: K= 33.5(7)GPa. The axial bulk moduli of the tetragonal polymorph, calculated with a linearised BM-EoS, are: $K(a)$= 34.5(5) GPa for the a-axis and $K(c)$ =78(1) GPa for the c-axis. For the triclinic polymorph, we obtain: $K(a)$ = 33.5(7) GPa, $K(b)$ = 34.9(7) GPa and $K(c)$ = 35.5(7) GPa. The elastic behaviour of the low-P polymorph appears to be drastically more anisotropic than that of the high-P polymorph. As for analcime, the relevant structural variations in response to the tetragonal → triclinic phase transition are expected to be due to tetrahedral tilting.

i. *Stability of hydrous ringwoodite in the $(Mg_1Fe_1)SiO_4$-H_2O system (G. Ganskow and F. Langenhorst/Jena, in collaboration with D.J. Frost)*

The nominally anhydrous $(Mg,Fe)_2SiO_4$ high-pressure polymorphs wadsleyite and ringwoodite can accommodate up to 2-3 wt.% H_2O; hence the transition zone of Earth has an enormous potential to store water. This finding is almost exclusively based on high-pressure experiments with Mg-rich mantle compositions relevant for the Earth's interior. Other planetary interiors such as the Martian mantle are, however, more enriched in iron. In the water-free $(Mg,Fe)_2SiO_4$ system, an increase in iron results, for example, in a decrease of the melting temperature and the destabilisation of wadsleyite. There is, however, little known about the influence of water on phase stabilities when iron is a major constituent in the $(Mg,Fe)_2SiO_4$ system.

We have therefore conducted a series of multianvil experiments in the $(Mg_1Fe_1)SiO_4$-H_2O system. Experiments cover a wide pressure range from 6 to 23 GPa at variable temperatures between 500 °C and 1150 °C. A powder starting material with a nominal Fo50 composition was prepared by mixing the following starting materials: 2 $Mg(OH)_2$ + Fe_2SiO_4 + SiO_2. Recovered samples were examined using electron microprobe (EPMA), analytical transmission electron microscopy (TEM), and Raman and FTIR spectroscopies.

Phase identification by Raman spectroscopy and TEM analysis reveal ringwoodite to be the dominant mineral phase under various experimental run conditions (15-18 GPa and 750 °C - 1150 °C). At temperatures up to 950 °C ringwoodite exists as single phase; whereas at 1150 °C a three-phase assemblage of co-existing stishovite, magnesiowüstite and ringwoodite is developed. In comparison to the dry $(Fe_1Mg_1)SiO_4$ system the phase boundary between single-phase ringwoodite and the three-phase assemblage is lowered by about 4 GPa (Fig. 3.3-10). Our first FTIR measurements show that single phase ringwoodite (15 GPa, 1150 °C)

with a nominal Fo50 composition incorporates 0.28 wt.% H_2O, which is an order of magnitude lower than the water content of endmember Mg_2SiO_4 ringwoodite. In order to identify the incorporation mechanism of H_2O into the ringwoodite structure we have measured Fe L_{23} electron energy loss spectra, revealing that iron is purely ferrous. It is thus likely that water is only accommodated by the common substitution mechanism which involves the replacement of Mg^{2+} or Fe^{2+} by $2H^+$.

Our first results suggest that the incorporation of water in nominally anhydrous ringwoodite is considerably reduced if Mg is significantly replaced by Fe. This means that the water storage capacity of the Martian transition zone may be lower than that of Earth. The addition of water to the system has also the effect of shifting the phase boundary between single phase ringwoodite and the three-phase assemblage rw + mw + sti to lower pressure. If the Martian mantle is not depleted in water, its mineralogical structure would thus be distinctly different than currently assumed.

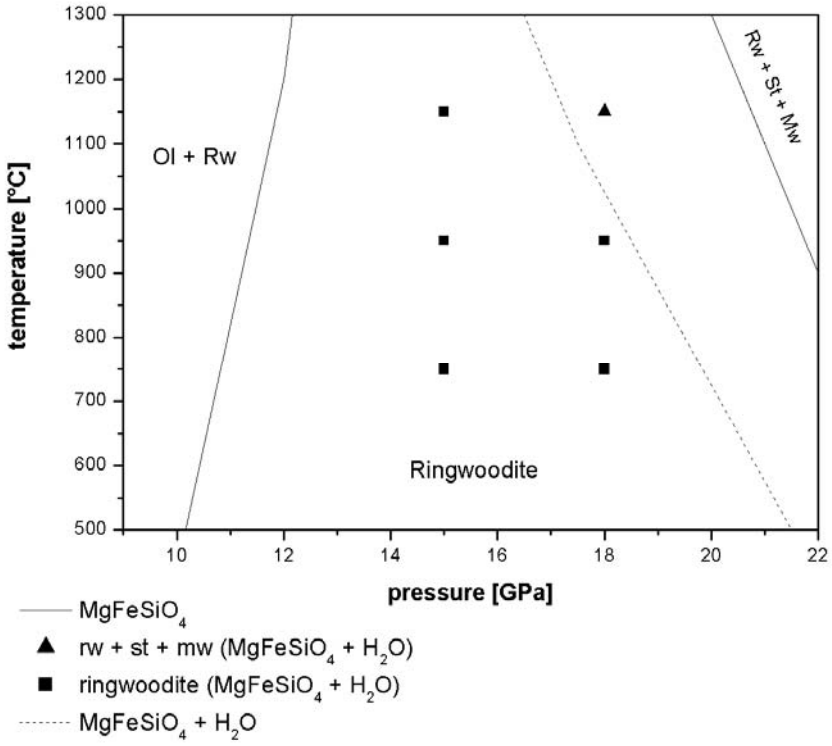

Fig. 3.3-10: Phase diagram for the $(Mg_1Fe_1)SiO_4$-H_2O system

j. *High-pressure behaviour of $FeAl_2O_4$ (K. Schollenbruch and A. Woodland/Frankfurt, in collaboration with D.J. Frost)*

At high pressures, many spinels are known to either transform to a denser structure with orthorhombic symmetry or break down into their constituent oxides. In the case of $MgAl_2O_4$, break down to MgO + Al_2O_3 is followed at still higher pressures (~ 26-28 GPa) by

reconstitution into an orthorhombic phase with the same stoichiometry as spinel. It has been proposed in the literature that hercynite ($FeAl_2O_4$) breaks down to wüstite and corundum at 12 GPa and 1000 °C, but otherwise very little is known about the high-pressure phase relations of this Fe-bearing end member.

Experiments were performed with two capsules, one containing hercynite along with 6 wt.% Fe metal, and another containing a stoichmetric mixture of wüstite and corundum. An 18mm edge length octahedral was employed with 11 mm edge length WC cube truncations. The samples were heated using a $LaCrO_3$ furnace for time durations of up to 5 hours. The results from both capsules in each experiment were consistent, such that each experiment was simultaneously reversed. The high-pressure stability limit of hercynite was constrained to lie in the range of 7-8 GPa at temperatures of 1000-1500 °C (Fig. 3.3-11). This boundary lies ~ 8 GPa lower than that for the breakdown of $MgAl_2O_4$ at similar temperatures and is consistent with the general tendency that phase transitions in Fe-bearing silicates and oxides occur at lower pressures than in the analogous Mg-bearing systems. At 8.5 GPa and 1720 °C melt appeared, due to melting of wüstite. Considering that hercynite has a high melting point (1740 °C at 1 bar), melting in the hercynite-bearing capsule implies that hercynite must have broken down to wüstite and corundum, and the wüstite subsequently melted.

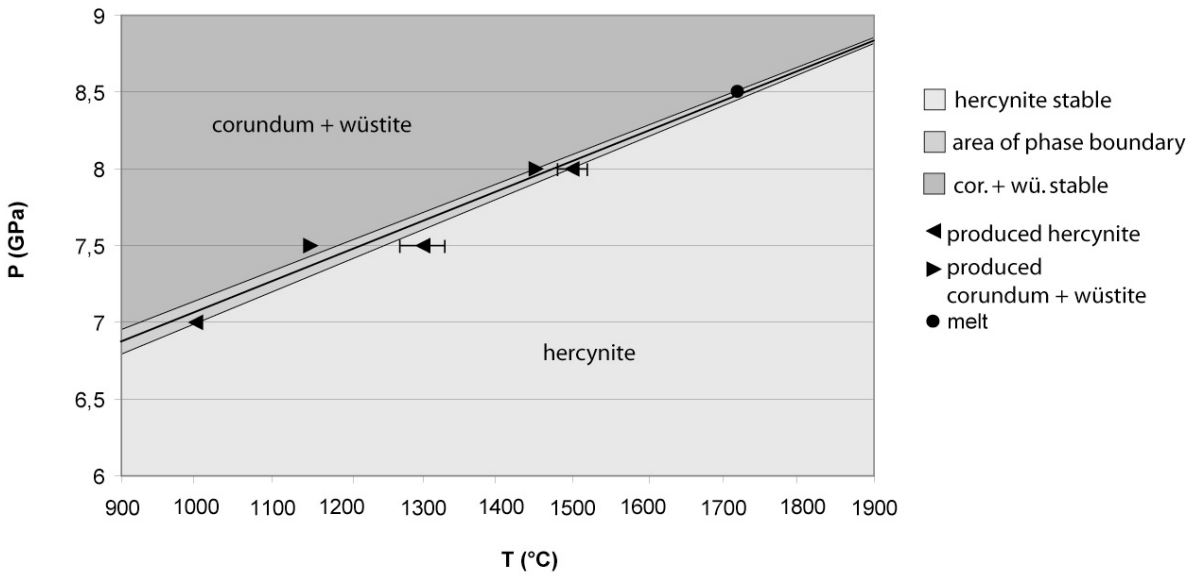

Fig. 3.3-11: The breakdown of hercynite ($FeAl_2O_4$) to wüstite (Fe_{1-x} O) and corundum (Al_2O_3) bracketed using reversed multianvil experiments.

Two further experiments were performed with hercynite at 16 GPa and 1400 °C and at 24 GPa and 1600 °C to test whether an orthorhombic phase becomes stable at higher pressures. In both cases only corundum and wüstite were found, indicating an important difference between the Fe-bearing and Mg-bearing systems. The bracketed breakdown reaction of hercynite will be used to extract and refine thermodynamic data for hercynite, wüstite and corundum.

k. *The effect of pressure on* $Fe^{3+}_{VIII}Al^{3+}_{VI}O_3$ *substitution in perovskite: Implications for Fe disproportionation in the lower mantle (A. Saikia, D.J. Frost, T. Boffa Ballaran and D.C. Rubie)*

Experimental observations have shown that even at the lowest plausible oxygen fugacity for the lower mantle, (Fe,Mg)(Al,Si)O_3 perovskite contains a significant Fe^{3+} content ($Fe^{3+}/\sum Fe > 0.5$). As the upper mantle has a very low $Fe^{3+}/\sum Fe$ ratio (< 0.03) it has been proposed that if the mantle convects as a single unit, Fe^{2+} in the lower mantle must disproportionate to create the required Fe^{3+} for perovskite and metallic Fe via the reaction,

$$\underset{\text{Perovskite}}{AlAlO_3} + \underset{\text{Mw}}{3FeO} = \underset{\text{Metal}}{Fe} + \underset{\text{Perovskite}}{2AlFeO_3}, \qquad (1)$$

where Mw is magnesiowüstite. Whether such a disproportionation reaction will occur at pressures throughout the lower mantle can be assessed by considering the likely volume change of equation (1). This can be determined by assessing the effect of $Al^{3+}_{VIII}Al^{3+}_{VI}O_3$ ($Al^{3+}_{VIII} + Al^{3+}_{VI} \leftrightarrow Mg^{2+}_{VIII} + Si^{4+}_{VI}$), $Fe^{3+}_{VIII}Al^{3+}_{VI}O_3$ ($Fe^{3+}_{VIII} + Al^{3+}_{VI} \leftrightarrow Mg^{2+}_{VIII} + Si^{4+}_{VI}$) and $Fe^{2+}_{VIII}Si^{4+}_{VI}O_3$ ($Fe^{2+}_{VIII} \leftrightarrow Mg^{2+}_{VIII}$) substitutions on the volume of $MgSiO_3$ perovskite. To examine this effect for $Fe^{3+}_{VIII}Al^{3+}_{VI}O_3$ substitution requires not only accurate volume determinations of perovskite samples, but also the characterisation of $Fe^{3+}/\Sigma Fe$ ratios.

In this study single crystals of (Fe,Mg)(Al,Si)O_3 perovskite with four different Fe and Al concentrations were synthesised using a multianvil press at 25 GPa and 1700-2000 °C. Precise volume determinations were carried out using single crystal X-ray diffraction. $Fe^{3+}/\Sigma Fe$ ratios were accurately determined using Mössbauer spectroscopy and electron energy loss spectroscopy. We have also determined the $Fe^{3+}/\Sigma Fe$ ratios in some other samples of previous workers by assuming that Al^{3+} is always charge balanced by Fe^{3+} and the remaining Fe will be Fe^{2+}.

Figure 3.3-12 shows the change in molar volume of magnesium silicate perovskite as a function of three possible substitution mechanisms. The data show that in comparison to $Al^{3+}_{VIII}Al^{3+}_{VI}O_3$ and $Fe^{2+}_{VIII}Si^{4+}_{VI}O_3$ substitutions, the $Fe^{3+}_{VIII}Al^{3+}_{VI}O_3$ substitution causes a larger increase in the molar volume of magnesium silicate perovskite. Almost all $Fe^{3+}_{VIII}Al^{3+}_{VI}O_3$ samples also have a $Fe^{2+}_{VIII}Si^{4+}_{VI}O_3$ component, as indicated by the numbers in parentheses which are the mol.% $Fe^{2+}_{VIII}Si^{4+}_{VI}O_3$ contents. The only sample reported with no $Fe^{2+}_{VIII}Si^{4+}_{VI}O_3$ is that of Nishio-Hamane *et al.* [Geophys. Res. Lett., 32:L16306, 2005]. If this point is used to define the trend of $Fe^{3+}_{VIII}Al^{3+}_{VI}O_3$ substitution, then it becomes apparent that the larger the $Fe^{2+}_{VIII}Si^{4+}_{VI}O_3$ content, the larger the molar volume. This is exemplified by the sample of Vanpeteghem *et al*. [Phys. Earth Planet. Int., 155, 96, 2006], which has the largest molar volume of a $Fe^{3+}_{VIII}Al^{3+}_{VI}O_3$-bearing perovskite and also the largest $Fe^{2+}_{VIII}Si^{4+}_{VI}O_3$ content. The substitution of $Fe^{2+}_{VIII}Si^{4+}_{VI}O_3$ into Al-free perovskite, therefore, has a much smaller effect on perovskite molar volume than when it substitutes into Al-bearing perovsktie. As perovskite

must contain Al in the lower mantle, the large effect on the molar volume should make Fe^{2+} substitution in perovskite unfavourable with increasing pressure.

Using these results the volume change of equilibrium (1) is calculated to be approximately -2 cm^3/mol. This implies that disproportionation of FeO should be favoured with increasing pressure and therefore is likely to take place throughout the perovskite region of the lower mantle. In addition, however, the large effect on the perovskite molar volume of $Fe^{2+}_{VIII}Si^{4+}_{VI}O_3$ substitution into (Fe,Mg)(Al,Si)O_3 perovskite should drive Fe^{2+} out of perovskite with increasing pressure and into magnesiowüstite. This should cause perovskite to decrease in total Fe content with pressure, but with an increase in the relative Fe^{3+} content. Some support of this can be found in the fact that while in this study it was not possible to synthesise pure Fe^{3+} bearing perovskite at 25 GPa, this was possible in the study of Nishio-Hamane *et al*. (2005) performed at approximately 50 GPa.

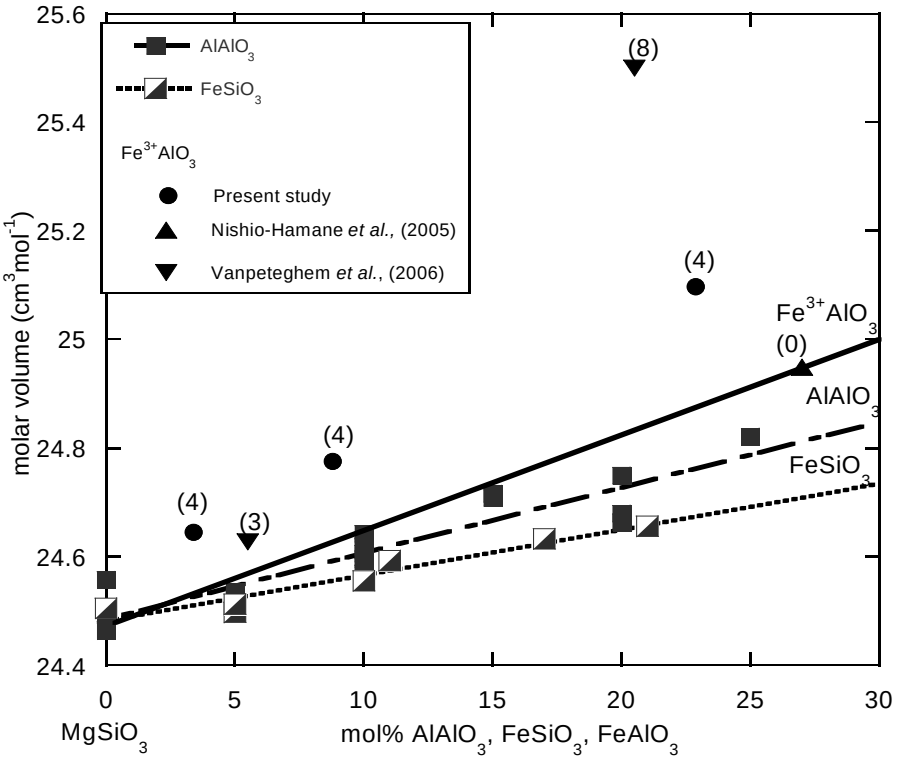

Fig. 3.3-12: Effect of $Fe^{2+}_{VIII}Si^{4+}_{VI}O_3$, $Al^{3+}_{VIII}Al^{3+}_{VI}O_3$ and $Fe^{3+}_{VIII}Al^{3+}_{VI}O_3$ substitutions on the molar volume of magnesium silicate perovskite. The figures in parentheses are the mol.% $Fe^{2+}_{VIII}Si^{4+}_{VI}O_3$ contents for $Fe^{3+}_{VIII}Al^{3+}_{VI}O_3$-bearing perovskites.

l. *TEM characterisation of (Fe,Al)-bearing Mg-perovskite in diamond anvil cell experiments (L. Armstrong and N. Miyajima, in collaboration with M. Walter/Bristol)*

Coupled Fe^{3+}, Al^{3+} substitution in Mg-perovskite (Mg-pv) has been postulated by previous studies to be so favourable that in the presence of (Mg,Al)-pv, Fe^{3+} will form by the

disproportionation reaction $3FeO = Fe_2O_3 + Fe$. This reaction would produce coexisting (Fe^{3+},Al)-rich perovskite and Fe metal in the lower mantle, along with other high pressure phases. If correct, literature models show that the reaction provides a mechanism for the 'self-oxidation' of the mantle during core formation, and may help to explain the siderophile element geochemistry of the mantle. Cation substitution in Mg-pv affects many properties of the lower mantle and is not yet fully documented, especially when involving Fe^{3+}.

We carried out a series of experiments in the laser heated diamond anvil cell (DAC) in the range 45-70 GPa and 1650-2500 K at the University of Bristol. We aimed to determine whether the disproportionation reaction took place on the basis of X-ray diffraction, phase relations and TEM analysis. We also made experiments along the joins $MgSiO_3$-Fe_2O_3 and -$FeAlO_3$ to bracket the solubility of the Fe_2O_3 component in Mg-pv, with and without aluminium. We determined the composition of Mg-pv grains using energy dispersive X-ray analysis on the TEM at Bayerisches Geoinstitut. When possible, electron energy loss spectroscopy was also performed and the $Fe^{3+}/\sum$ Fe ratio calculated. In experiments along the $MgSiO_3$-Fe_2O_3 join with up to ~ 40 mol.% Fe_2O_3, the Mg-pv sample contained less than 1 mol.% Fe_2O_3 and 4-12 mol.% $FeSiO_3$. This is in stark contrast to earlier results in the literature in which Mg-pv with 25 mol.% Fe_2O_3 was reported to be stable. It is also clear that oxygen fugacity was not imposed by the starting material as all iron was added as Fe^{3+}, but most of this was reduced during the experiments. Similar reduction was observed along the $MgSiO_3$-$FeAlO_3$ join, but in this case Mg-pv still contained a significant (20 mol.%) amount of $FeAlO_3$.

In experiments designed to test the Fe-disproportionation reaction at pressures of 40-60 GPa, mixtures of Mg-pv, ferropericlase, and stishovite were observed on the TEM. No Fe metal was associated with these regions, suggesting that disproportionation did not take place. However, we also observed 'ultra-reduced' areas devoid of oxides and silicates, which were mainly composed of diamond with smaller amounts of reduced phases such as Fe metal, Fe-Si-C phases, and amorphous carbon. This is consistent with previous reports in the literature of carbon transport in the DAC. The reduction taking place in some portions of the sample may indicate that the DAC is unsuitable for studying Fe-disproportionation at high pressures and temperatures, and suggests that Fe-bearing DAC experiments should be interpreted with caution.

m. *Determining the effect of pressure on the thermodynamic properties of the pyrope-grossular ($Mg_3Al_2Si_3O_{12}$-$Ca_3Al_2Si_3O_{12}$) solid solution (G.H. Gudfinnsson and D.J. Frost)*

Garnet is a major constituent of the Earth's upper mantle and transition zone and is stable into the topmost region of the lower mantle. Over this pressure range it undergoes a series of complex reactions with increasing pressure. The ability to constrain the conditions at which these reactions take place is important not only for determining the conditions at which some recovered mantle rocks equilibrated but also for interpreting the deeper structure of the mantle from seismic observations. The pyrope-grossular solid solution covers an important range of mantle garnet composition and many studies have examined thermodynamic relations for this

solid solution. Calorimetric and volumetric measurements along this join have revealed significant excess properties that result in large deviations from ideal mixing. One implication of this is that many models based on calorimetric data predict that a miscibility gap should form at temperatures and compositions quite compatible with the Earth's interior. Evidence for this immiscibility in garnets has also been reported from ultra-high pressure metamorphic rocks. Depending on the calorimetric data employed, however, a range of miscibility gaps can be calculated that extend over a variety of compositions and temperatures. One way of testing these models is to examine the pyrope-grossular solid solution at very high pressures where immiscibility, if it occurs, should be driven to the highest temperatures. Identifying a thermodynamic model for this solid solution that is valid to high pressures is, in addition, important for modelling garnet reactions in the transition zone and lower mantle, such as the reaction that forms $CaSiO_3$ perovskite at approximately 17 GPa.

In this study the stability of garnets along the pyrope-grossular join have been studied at 12 GPa and between 1200-1700 K using a multianvil apparatus. 65%Py-35%Gr was the principal starting composition as this falls in the middle of the predicted immiscibility field according to most models. The starting material was an oxide mixture of CaO, Al_2O_3 and SiO_2. In several experiments H_2O was added to speed up reaction rates. Experiments were performed for run durations of up to 96 hours. Quenched experiments were analyzed using the electron microprobe.

In all experiments performed garnets close to the starting composition were synthesized from the oxides. Figure 3.3-13 shows two miscibility gaps calculated using different thermodynamic models from the literature. The studies chosen are representative of the

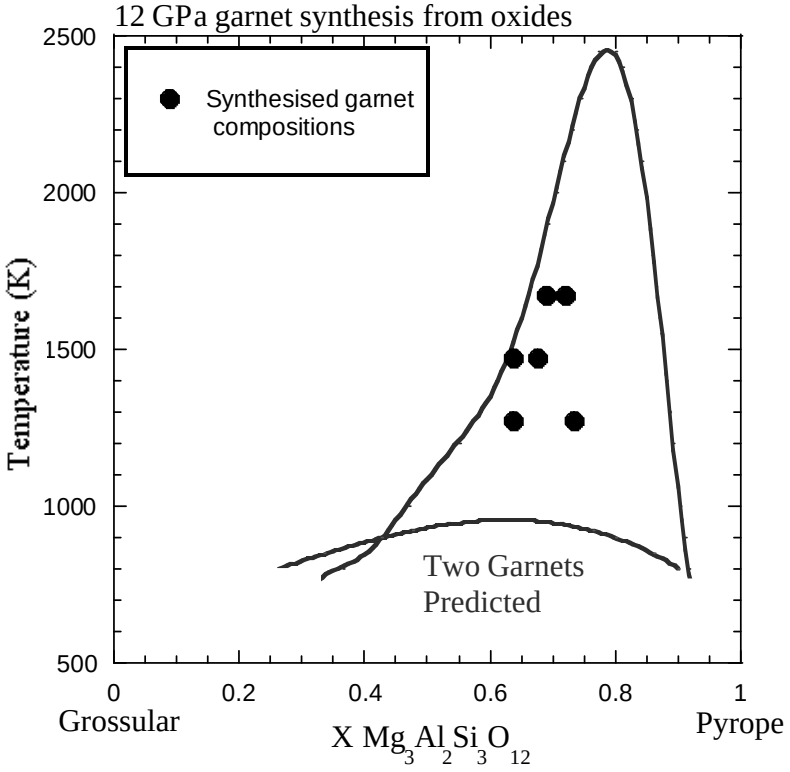

Fig. 3.3-13: Garnet compositions along the $Ca_3Al_2Si_3O_{12}$- $Mg_3Al_2Si_3O_{12}$ join synthesized from the oxides at 12 GPa as a function of temperature. Two regions of garnet immiscibility (where two garnets of differing composition are predicted to coexist) are shown for comparison, calculated from two thermodynamic studies from the literature. The model that predicts high temperature immiscibility is inconsistent with the experimental results.

highest and lowest extents of miscibility predicted in the literature. In addition final garnet compositions from the high-pressure experiments are plotted for comparison. When starting compositions are compared with final run compositions there is no evidence for immiscibility. Further experiments are underway at slightly higher pyrope concentrations and at 1100 K; however it can be seen that the existing data allow certain models to be excluded. Non-ideality along the pyrope-grossular join, therefore, appears to be smaller than predicted by some models.

n. *A calorimetric study of the $Mg_3(Mg,Si)Si_3O_{12}$(majorite)-$Mg_3Al_2Si_3O_{12}$(pyrope) garnet solid solution (A Saikia, D.J Frost and D.C. Rubie, in collaboration with M. Akaogi and H. Kojitani/Tokyo)*

Garnet is known to be a major constituent of the upper mantle, transition zone and the top region of the lower mantle. Over its stability range, spanning from 2-28 GPa, garnet compositions change significantly as a result of reactions between other phases of the mantle. At shallow upper mantle conditions, garnet is a solid solution with major element substitutions that are described by the formula $(Mg,Fe,Ca)_3Al_2Si_3O_{12}$. However, above approximately 4 GPa substitution of Mg, Fe and Si onto the octahedrally-coordinated Al site occurs, causing $MgSiO_3$ and $FeSiO_3$ pyroxene components to dissolve into the garnet structure as majorite components. Ordering of Mg and Si on the octahedral sites leads to a symmetry breaking transition from cubic to tetragonal for garnets with molar $Mg_4Si_4O_{12}$ contents of > 80 %. This substitution can be described by the join $Mg_3(Mg,Si)Si_3O_{12}$(majorite)-$Mg_3Al_2Si_3O_{12}$(pyrope). Thermodynamic parameters along this garnet solid solution are crucial for modelling the formation reactions of silicate perovskites. Moreover, slow kinetics of silicate reactions inhibits the attainment of equilibrium under feasible experimental conditions at lower temperatures. Consequently, the experimental results are generally extrapolated to lower temperatures using suitable thermodynamic models. Uncertainties in such models can be reduced considerably, if thermodynamic parameters used for such fits are independently determined as has been done in our study of the pyrope-majorite solid solution using the drop solution calorimetric technique.

Enthalpies of dissolution of garnet solid solutions in the system $Mg_3(Mg,Si)Si_3O_{12}$ (majorite)-$Mg_3Al_2Si_3O_{12}$(pyrope) were measured by lead borate ($2PbO.B_2O_3$) oxide drop solution calorimetry under controlled oxygen fugacity to assess the ideality of this solid solution and estimate the enthalpy of solution of the fictive cubic $Mg_4Si_4O_{12}$ garnet end member. Nine garnet samples along the majorite-pyrope join were synthesized using the large volume 5000 tonne multianvil press. The large sample volumes ensured that a number of calorimetric drop measurements could be performed on each sample. A twin calvet-type microcalorimeter, installed at Gakushuin University, Tokyo, was used for the calorimetric measurements. Sample pellets of 3 mg were dropped from room temperature into 5 g of $2PbO{\cdot}B_2O_3$ solvent

at 978 K inside the sample chamber of the calorimeter and allowed to dissolve. The recorded heat change, *i.e.*, the heat of dissolution, is equal to the heat content of the sample plus the enthalpy of solution at the temperature of the calorimeter.

The enthalpies of dissolution are plotted in Fig. 3.3-14. The data show a negative deviation from a straight line joining the two end members. This implies that the mixing properties of the solid solution deviate positively from ideality. Results show that starting from the pyrope end member, the enthalpies of dissolution decrease nonlinearly with increasing majorite content. A sharp break in the slope occurs for the enthalpies of dissolution between pyrope contents of 32-mol.% and 24-mol.%, which is close to the symmetry breaking cubic-tetragonal transition. Thermodynamic refinement of the data using a symmetric regular solution model for the garnet solid solutions enables the data to be extrapolated in composition through the cubic-tetragonal transition to obtain the properties of the fictive cubic $Mg_3(Mg,Si)Si_3O_{12}$(majorite) end member, which is required in thermodynamic calculations. A value -37 kJ/mol was obtained for the enthalpy of solution of the fictive cubic majorite garnet, which is significantly lower than the previous estimate of 5 kJ/mol (Fig. 3.3-15).

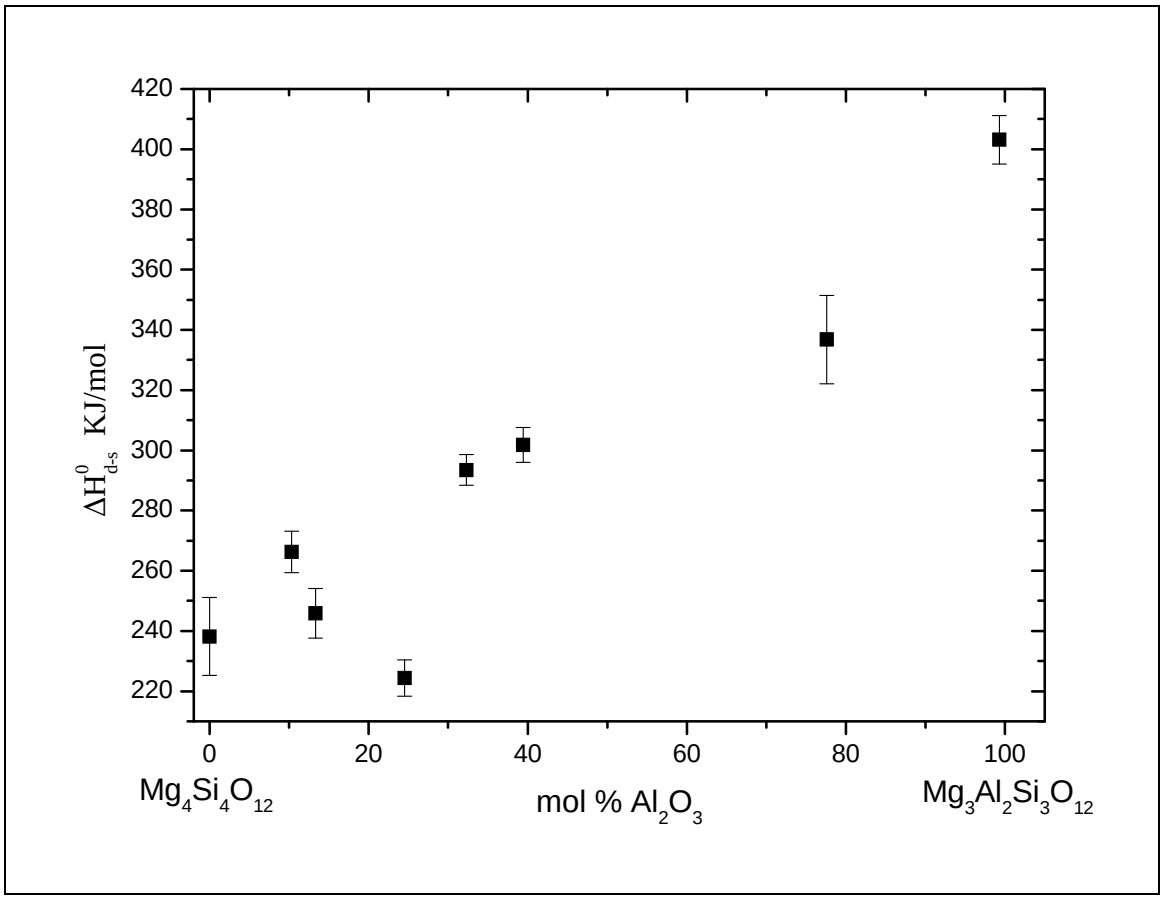

Fig. 3.3-14: Enthalpies of dissolution of $Mg_3(Mg,Si)Si_3O_{12}$-$Mg_3Al_2Si_3O_{12}$ garnets in $2PbO{\cdot}B_2O_3$ solvent at 978K.

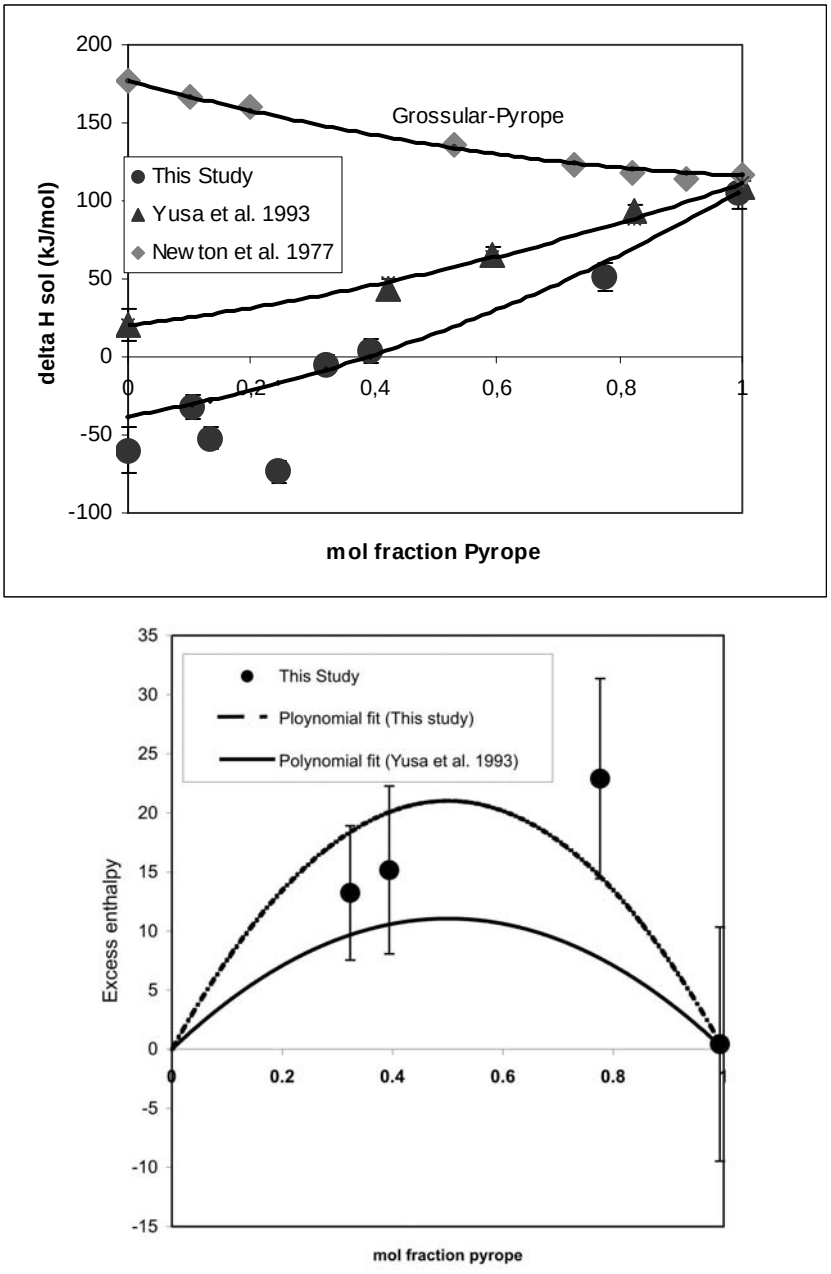

Fig. 3.3-15: Top: The ΔH^{sol} of $Mg_3(Mg,Si)Si_3O_{12}$-$Mg_3Al_2Si_3O_{12}$ garnets determined in this study compared with the results of Yusa *et al.* [J. Geophys. Res. 98, 6453, 1993] for the same solid solutions and results of Newton *et al.* [J. Geophys. Res. 85, 6973, 1977] for the $Ca_3Al_2Si_3O_{12}$-$Mg_3Al_2Si_3O_{12}$ (grossular-pyrope) solid solution. Bottom: Symmetric solution fits made to all data, excluding data with $X_{pyrope} < 0.3$ for this study.

o. *Thermodynamic aspects of methane hydrates, methane and ice VII at high pressure (A. Kurnosov, L.S. Dubrovinsky, in collaboration with M. Hanfland and W. Crichton/Grenoble)*

Methane clathrate hydrates are believed to play an important role in the outer solar system evolution, particularly for Titan and other moons of giant planets. Among clathrate hydrates

methane clathrates appears to have the most irregular behaviour. The probable reason is the high degree of complementarity between methane molecules and hydrogen bonded water frameworks. Formation of metastable phases impedes the understanding of the thermodynamics of methane hydrates.

Using synchrotron X-ray diffraction we studied the two-component three-phase system CH_4-H_2O. The goal was to obtain the molar volume of all solid phases in the system (clathrate hydrates, ice and solid methane) and to analyze ΔV (the difference of the clathrate phase molar volume and the corresponding molar volumes of the reagents ice and methane) of reaction of hydrate formation in the system. This analysis allows us to constrain the phase diagram of the system using the Clausius-Clapeyron equation $^{dP}/_{dT} = {}^{\Delta H}/_{T\Delta V}$.

The Clausius-Clapeyron relation is normally applicable to one-component systems to describe the slope of the coexistence curve of two phases. It can be also used for two-component systems with the assumption that the composition of the system is constant. In experiments performed in the DAC we can assume that the composition is fixed and apply the Clausius-Clapeyron equation for describing coexistence curves (monovariant lines) on the phase diagram. In the case of the CH_4-H_2O system the interesting monovariant line(s) is(are) the decomposition (melting) curve(s) of clathrate hydrate(s) hl_1l_2 where h is an appropriate hydrate phase (h_1, h_2 or h_3), and l_1 and l_2 are hydrate-forming substances (methane and water, respectively). In the high-pressure region all of the phases are solid.

According to the Clausius-Clapeyron equation in the form $^{dP}/_{dT} = {}^{\Delta H}/_{T\Delta V}$ the slope of the three-phase monovariant curve is dependent on ΔH and ΔV. Assuming ΔH to be positive for all clathrate hydrate phases in the methane-water system, only ΔV is responsible for the sign of the slope of the monovariant line. According to literature data the hydrate h_3 is stable up to a pressure of 50 GPa at room temperature. At the same time, clathrate hydrates of other gases are known to be unstable above pressures of a few GPa.

Using *in situ* synchrotron X-ray powder diffraction in DACs we studied the pressure dependence of unit cell parameters and molar volumes of clathrate hydrates in the methane-water system. Ice and solid methane were studied under the same experimental conditions to minimize the systematic errors. Two different beamlines were used for the same purpose. The present data support our idea that hydrate h_3 is most probably metastable starting from the pressure ~ 4 GPa. In Figure 3.3-16 we compare the volume of clathrate hydrate h_3 with the volume of the corresponding mole ratio of methane and ice. Despite of the very small volume difference, it can be seen that starting from ~ 2 GPa the volume of clathrate hydrate becomes lower than the volume of corresponding methane ice VII phases. With pressure increase this difference becomes higher. Assuming ΔH to be positive over the entire pressure range, the slope of the melting curve must become negative at pressures close to 2 GPa (although likely higher due to the different thermal expansion of related phases; however still in the range of a few GPa). The negative slope of the decomposition curve of clathrate hydrate implies the

unavoidable intersection of that curve with the melting curves of ice VII and methane. The intersection leads to the appearance of a quadruple point and the upper pressure boundary of thermodynamic stability of the hydrate.

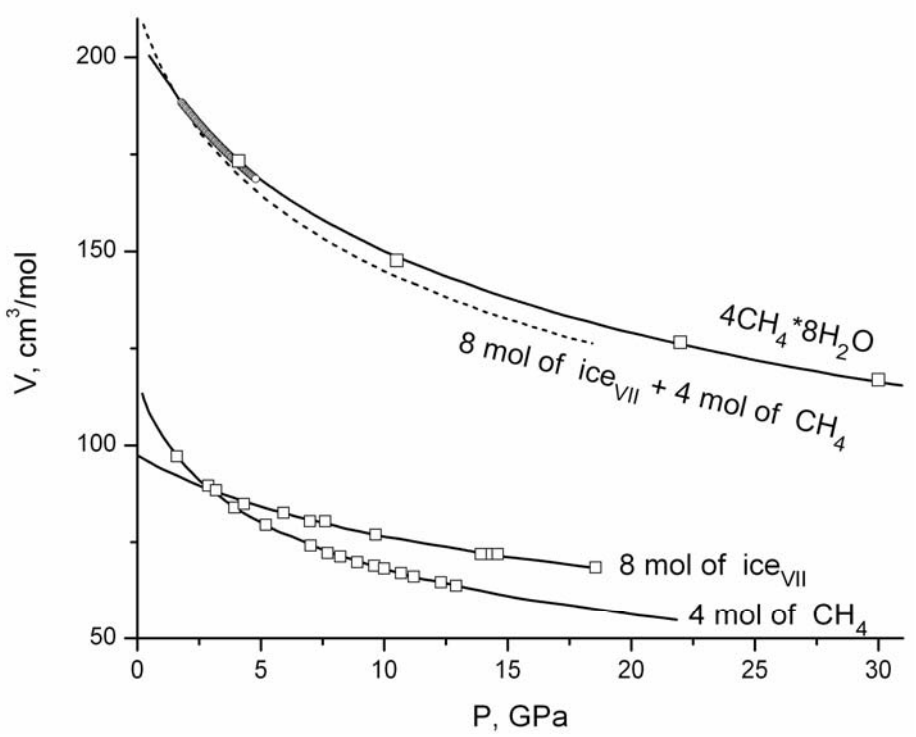

Fig. 3.3-16: Comparison of the molar volume of methane clathrate hydrate $CH_4 \cdot 2H_2O$ with the molar volumes of molar volumes of methane and ice VII. The dotted line is the molar volume of the corresponding methane and ice VII with clathrate hydrate stoichiometry.

3.4 Physical Properties of Minerals

The major aim of mineral physics is to constrain the behaviour of the Earth through a better understanding of the materials forming our planet. Geophysics is discovering the magnitude and location of radial and lateral changes in acoustic velocity, electrical conductivity, and magnetization within the Earth's mantle. These variations are inferred to reflect processes within the Earth and hence are tied to the origin of plate tectonics, earthquakes and volcanoes. However, without knowledge of the physical properties of the materials that make up the Earth's mantle and core at pressure and temperature conditions characteristic of these regions, we cannot interpret the geophysical and geochemical observations in terms of temperature, mass- or heat-flow, phase transformations, etc. Moreover, the diverse Earth's environment requires a continuous improvement of experimental sets up in order to reach extreme pressures and temperatures, and often minerals properties need to be investigated using both experimental and theoretical methods.

Water is an important factor in determining the mineral properties and phase relations. It is therefore not surprising that few studies of this section are dedicated to constrain the effect of water in hydrous or nominally anhydrous minerals. For example the incorporation of water in pyroxenes, which are after olivine the most abundant minerals of the Earth's upper mantle, may follow different mechanisms depending whether Al is present or not in the system and therefore will affect in different way their elastic properties. Any cation substitution, in the other end, may affect the physical properties of hydrous phases, which are potential hosts for H_2O within the cool regions of subducting slabs. Here we report a study on the physical properties of phase D, $MgSi_2O_6H_2$, containing both Al and Fe^{3+}. An *in situ* Raman study at high pressures and temperatures of gypsum reveals softening of hydroxyl stretching band and an associated unquenchable phase transition, as well as details of dehydration mechanism. These results help to constrain the structural and chemical changes in gypsum within the shallow crust which might control earthquake nucleation and aftershock triggering.

Measurements and analysis of elastic properties is a traditional subject of high-pressure mineral physics. Two studies are dedicated to such task and present new results obtained for wüstite and iron-nickel alloys. The anomalous elastic behaviour of wüstite has been known since decades and so far had no satisfactory explanations. Simultaneous inelastic X-ray scattering and single-crystal diffraction experiments at high pressure of $Fe_{0.94}O$ show a strong anelasticity behaviour in wüstite. This result suggests that most of minerals with internal degree of freedom (order-disorder phenomena, defects sub-structure, etc.) could also present anelastic behaviour at high pressure.

The investigation of magnetic properties of minerals at high pressure is a new and rapidly growing area. It requires a combination of sophisticated experimental and theoretical methods as demonstrated by several studies reported this year (magnetite, fayalite, cobalt, titanohematite). It is especially remarkable that the achieved theoretical level allows providing quantitative predictions of magnetic properties at high pressures.

a. *Effect of water on the compressibility of diopside (P. Gavrilenko, T. Boffa Ballaran and H. Keppler)*

The presence of hydroxyl in major mantle minerals causes defects in their structures and hence can significantly change their compressibility and seismic wave velocities. To detect water in the mantle from seismic observations we need to know the effect of water on elastic moduli of major mantle minerals. Previous work has shown that the bulk moduli of olivine, wadsleyite and ringwoodite decrease with water. However, little is know about the effect of water on the elastic properties of pyroxenes, which are after olivine the most important constituents of the upper mantle.

We performed high-pressure X-ray diffraction experiments on the effect of water on the equation of state of diopside. Two different BGI-designed diamond anvil cells (DAC) were used. The first DAC contained two pure diopside crystals, with different amount of water, 63 ppm H_2O and 1438 ppm H_2O. The second DAC contained one pure dry diopside and Al-bearing diopside with a high water concentration of 2510 ppm H_2O.

The single crystals were placed in the 300µm steel gasket hole together with ruby chips as an internal pressure standard and a 4:1 methanol:ethanol mixture as pressure medium. Unit cell parameters were collected on a four circle Huber diffractometer using the 8 positions centering technique. The unit cell volumes of four crystals for both experiments are reported as a function of pressure in Fig. 3.4-1. The *P-V* data were fitted with a third-order Birch-Murnaghan equation of state using the "EoS fit 52" software written by R.Angel. The obtained EoS parameters are listed in Table 3.4-1.

		EoS parameters:
DAC1	Crystal 1 (63 ppm H_2O)	K_0 = 107(1) K' = 6.3(4)
	Crystal 2 (1438 ppm H_2O)	K_0 = 108(1) K' = 6.3(4)
DAC2	Crystal 3 (Al-bearing diopside, 2510 ppm H_2O)	K_0 = 114(2) K' = 5.6(6)
	Crystal 4 (no water)	K_0 = 106(2) K' = 6.1(6)

Table 3.4-1

According to our data the compressibility of diopside decrease with increasing water content in the structure. This contrasts with previous work, which showed the compressibility of most other main mantle phases to increase with water. This could be explained by different OH incorporation mechanisms. In olivine, there are protonated vacancies on the Mg position ($2H^+ = Mg^{2+}$), which make it more compressible, but in diopside Al cations and protons substitute for Si in tetrahedral position ($Al^{3+} + H^+ = Si^{4+}$). This means that the dissolution of water in aluminous diopside actually does not create any vacancies, and accordingly, diopside gets stiffer in response to the coupled substitution of $Al^{3+} + H^+$ for Si^{4+}. Because of the contrasting effect of water on the equation of state of olivine and of pyroxenes in the upper mantle, detecting water from observations of seismic velocities alone is probably nearly impossible.

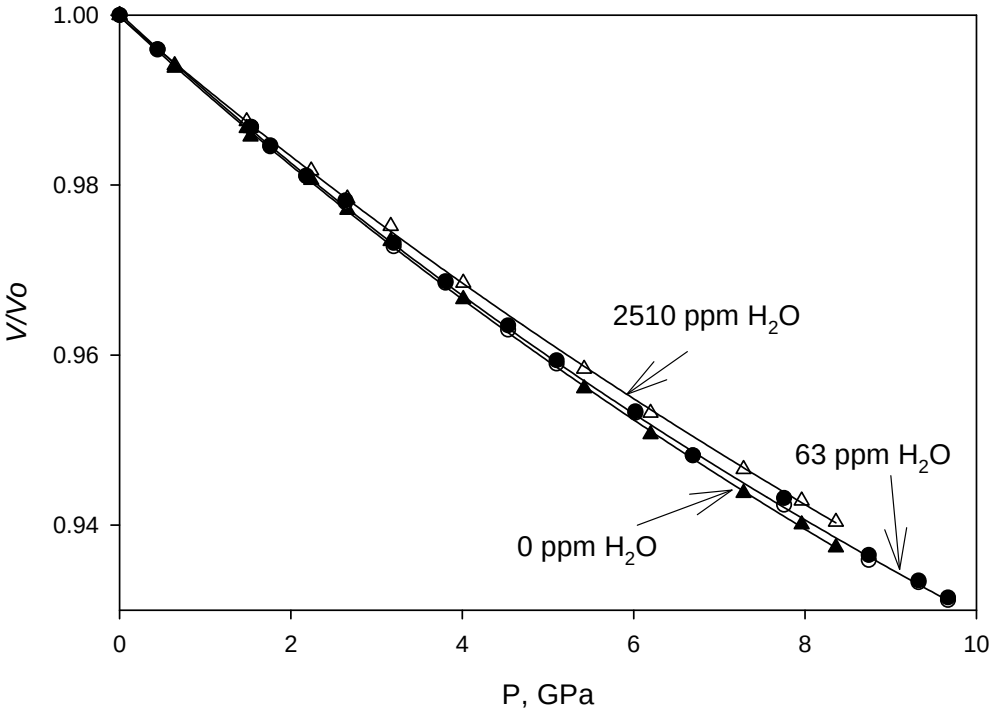

Fig. 3.4-1: Reduced unit cell volumes as a function of pressure for diopside samples with different water content. Empty and filled circles correspond to pure diopside crystals with 63 and 1438 ppm H_2O, respectively . Filled triangles – pure dry diopside; empty triangles – aluminous water-saturated diopside.

b. *A single-crystal compression study on iron-bearing hydrous Phase D (C. Holl, S.D. Jacobsen, K. Adams, C. Ebeling, and E. Martin/Evanston, in collaboration with D.J. Frost and C.A. McCammon)*

Dense hydrous magnesium silicate (DHMS) phases are potential hosts for H_2O within the cool regions of subducting slabs in the Earth's interior. In the past most studies on the stability of these phases have been performed in the MgO-SiO_2-H_2O system and the majority of reported physical property measurements have been performed on samples recovered from these experiments. In the Earth, however, DHMS phases may incorporate a range of additional elements that may not only influence the stability and H_2O contents of these phases but may also affect their physical properties

We are studying the crystal chemistry and physical properties of single-crystals of hydrous phase D containing aluminium (Al^{3+}) and ferric iron (Fe^{3+}) with approximate formula $MgSi_{1.5}Fe_{0.15}Al_{0.3}H_{2.5}O_6$. Phase D has the highest pressure stability of any DHMS phase yet identified and could be stable within slabs in the Earth's lower mantle. It possesses both a high density (ρ_0 = 3.35 g/cm^3) and a hydrogen-rich stoichiometry (16-18 wt.% H_2O). Phase D is stable to at least 30 GPa at 1100 °C. Furthermore, phase D has crystal chemical novelty because its structure features silicon in six-fold coordination with hydroxyl (OH).

Phase D was synthesized in the 1200-ton multianvil press at conditions of 1200 °C and 25 GPa from oxide starting materials in a Pt capsule. The starting composition was an oxide mixture of $Mg(OH)_2$, $Al(OH)_3$, Fe_2O_3 and SiO_2 in the stoichiometric proportion required to make Phase D with the general formula $(Mg,Fe)(Si,Al)_2O_6H_2$. Mössbauer spectroscopy indicated that the synthesized phase D contained 100 % ferric Fe. Recovered single crystals were prepared for X-ray diffraction studies using synchrotron and conventional sources to determine the structure, thermal expansivity, and compressibility. Compression data were obtained to 30 GPa using synchrotron X-ray diffraction in a helium pressure medium at the Advanced Photon Source, Argonne National Laboratory (Fig. 3.4-2). High-precision single-crystal techniques and the hydrostatic pressure medium were used to obtain an equation of

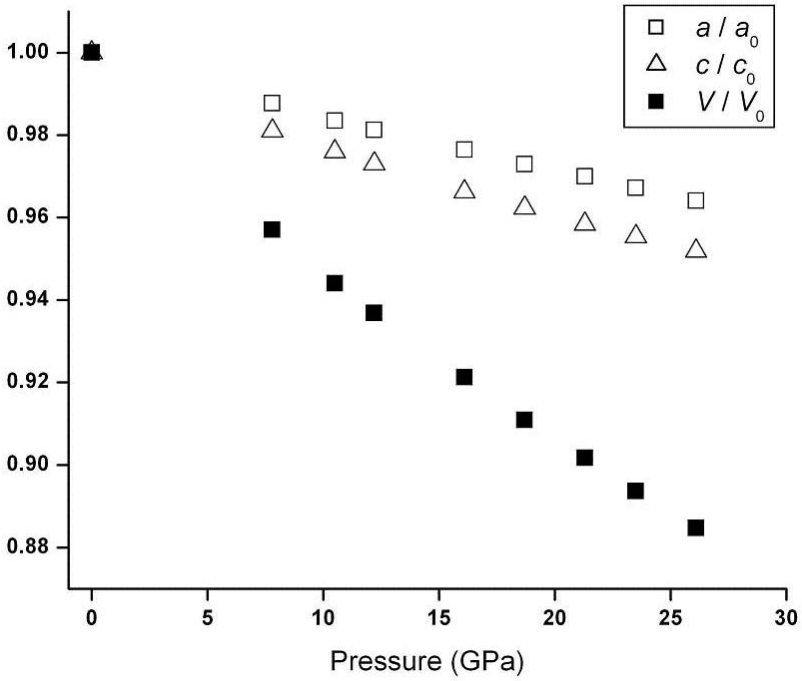

Fig. 3.4-2: Axial and volumetric strain versus pressure for phase D. Ambient pressure values were determined by SXD outside the diamond anvil cell with a conventional source.

state with third-order Birch-Murnaghan parameters V_0 = 85.85 (9) $Å^3$, K_0 = 171 (2) GPa, and K' = 4 (fixed). Ambient-pressure unit cell dimensions and intensity data were collected at low temperatures using a conventional X-ray source and a Bruker Apex II area detector at Northwestern University. Low-temperature structure refinements are underway and may help to refine the proton positions in the structure as well as determine thermal expansivity between 70 K and room temperature. Finally, In order to study the response of the strong, nearly symmetric hydrogen bond to pressure we used synchrotron-IR radiation to collect absorption spectra to 43 GPa at the National Synchrotron Light Source, Brookhaven National Laboratory (Fig. 3.4-3). The frequency of O—H stretching is not strongly dependent on

pressure, with dν/dP = 1.3 cm^{-1}/GPa and we observe no unusual broadening of the spectral absorption, which may have been indicative of hydrogen bond symmetrization. Further elasticity measurements with GHz-ultrasonic interferometery and Brillouin scattering will be performed in order to provide a complete picture of the elastic properties of this dense hydrous phase.

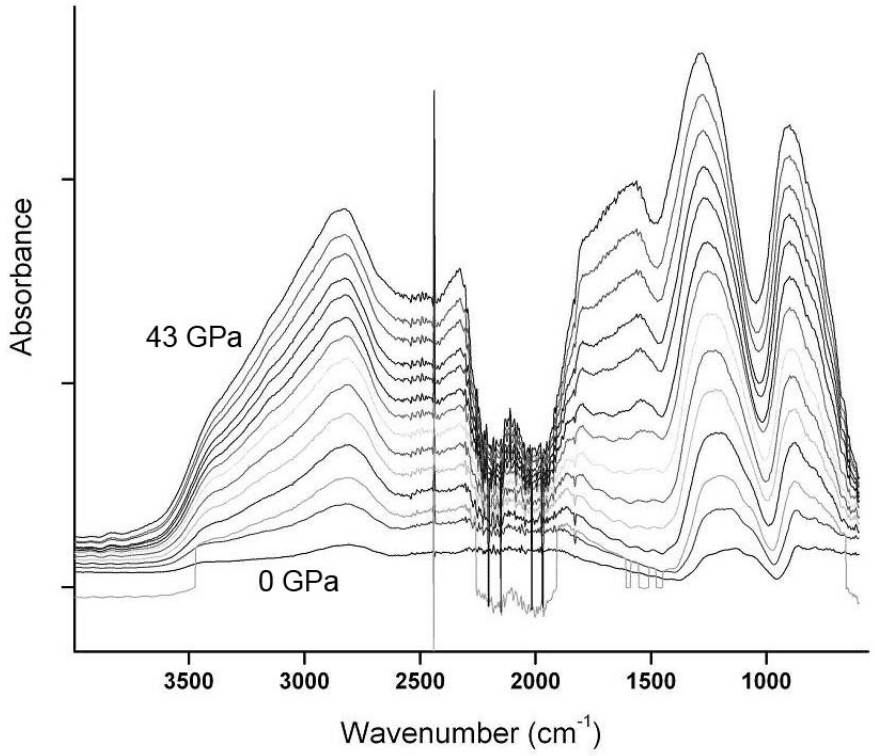

Fig. 3.4-3: Stacked infrared absorption spectra for phase D between room pressure and 43 GPa at approximately equal 3-4 GPa steps.

c. *In situ HP-HT Raman spectroscopy of gypsum (P. Comodi and S. Nazzareni/Perugia, in collaboration with L.S. Dubrovinsky)*

Gypsum ($CaSO_4$ $2H_2O$) is one of the most common sulphate mineral and is very important both in Earth and material sciences. In fact it is part of the evaporitic sequences where it seems to determine their rheological behaviour and it is largely employed in the concrete industries. Its geological importance lies in the hydration-dehydration reactions that have been considered fundamental on the generation of pore pressure within the shallow crust and in turn controlling earthquake nucleation and aftershock triggering.

The gypsum structure contains both molecular water and molecular-like sulphate groups bound ionically to calcium. Transition sequence gypsum-bassanite-anhydrite occurring at low temperature is not well know: several authors retain that the dehydration mechanism from gypsum to bassanite and to anhydrite is a sequential transformation, but other authors

indicated that the bassanite is formed from the rehydratation of anhydrite when the temperature is decreased from 390 K to 363 K.

Neutron diffraction and energy dispersive data showed that gypsum undergoes two phase transitions at 5 and 9 GPa and then converted to a disordered phase above 11 GPa. MicroRaman study under high pressure and low temperature showed a phase transition occurring at about 5 GPa, manifested with the coalesce of the OH- stretching bands, and the splitting of the ν_1 sulphate mode.

In order to study the *P* and *T* behaviour of gypsum and to understand the dehydration mechanism as well the temperature dependence of the high-pressure phase transformation, we carried out Raman spectroscopy experiments simultaneously at high pressure (up to 16 GPa) and high temperature (up to 223 °C) along different isotherms and isobars in electrically heated diamond anvil cell. Raman modes were collected in the low frequencies region, between 200 and 1200 cm^{-1} and in the high frequencies region between 3400 and 3700 cm^{-1}.

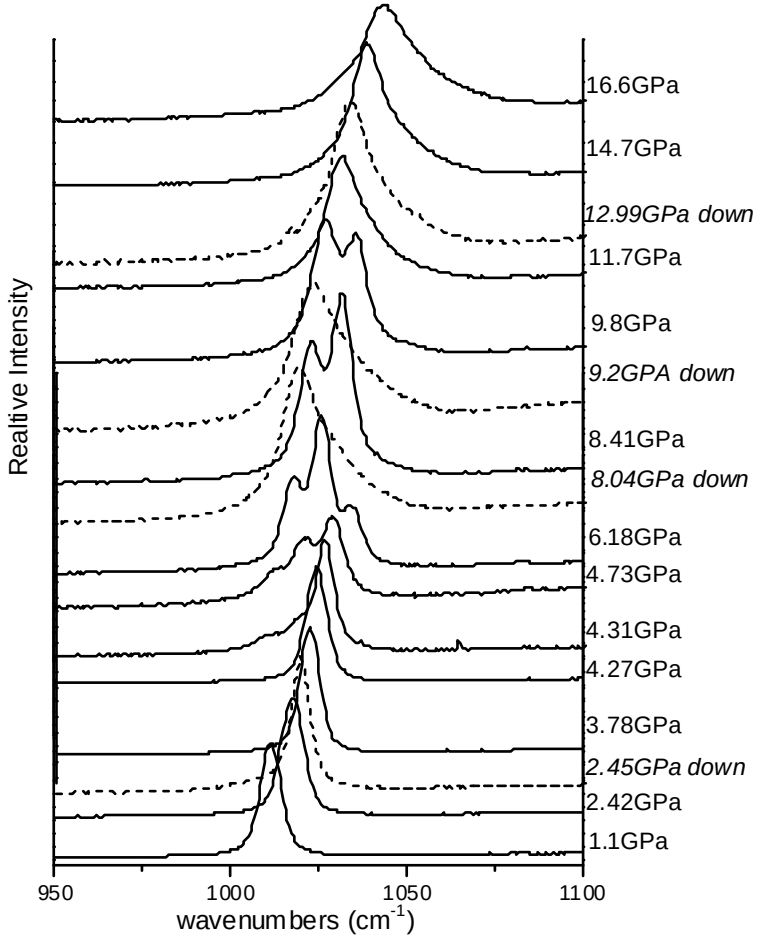

Fig. 3.4-4: Detail of the Raman spectra of gypsum up to 16 GPa at room temperature: behaviour of the ν_1 sulphate stretching mode during compression (continuous line) and decompression (dotted curves) experiments.

The pressure dependences of all low-frequency modes are positive and show a discontinuity at about 4 GPa, where the ν_1 sulphate stretching modes is split into three modes (Fig. 3.4-4). The split occurs at lower pressures with increasing temperature; for example at 109 °C the splitting is already observed at 3 GPa. In the high frequency region the stretching bands of the two hydroxyls show a negative dependence with pressure, however, the red shift of the shorter hydroxyl is larger than that of the longer one producing the coalesce of the two peaks at about 4.5 GPa. The modes disappear at about 16 GPa at room condition. The reappearance of the bands when pressure is decreased indicates that the phenomenon is not associated to dehydration. Also all low frequency modes, in particular the position of the sulphate mode, are relative to gypsum and not to bassanite or anhydrite. The process resulted reversible even if some hysteresis was observed. The disappearance of the OH modes may be related to the approaching of the symmetrization of H bond as observed for phase D and δAlO(OH). The value of O-O associated to the symmetrization is 2.4 Å, near to the value that might be extrapolated from the single-crystal X-ray diffraction data.

During heating along the 150 °C isotherm the Raman modes of bassanite occur at 1.53 GPa and along the 3.0 GPa isobar at 209 °C. The results indicate that the dehydration mechanism is sequential and has a positive slop with pressure (Fig. 3.4-5). Rehydration mechanism is observed when both the temperature and pressure are decreased.

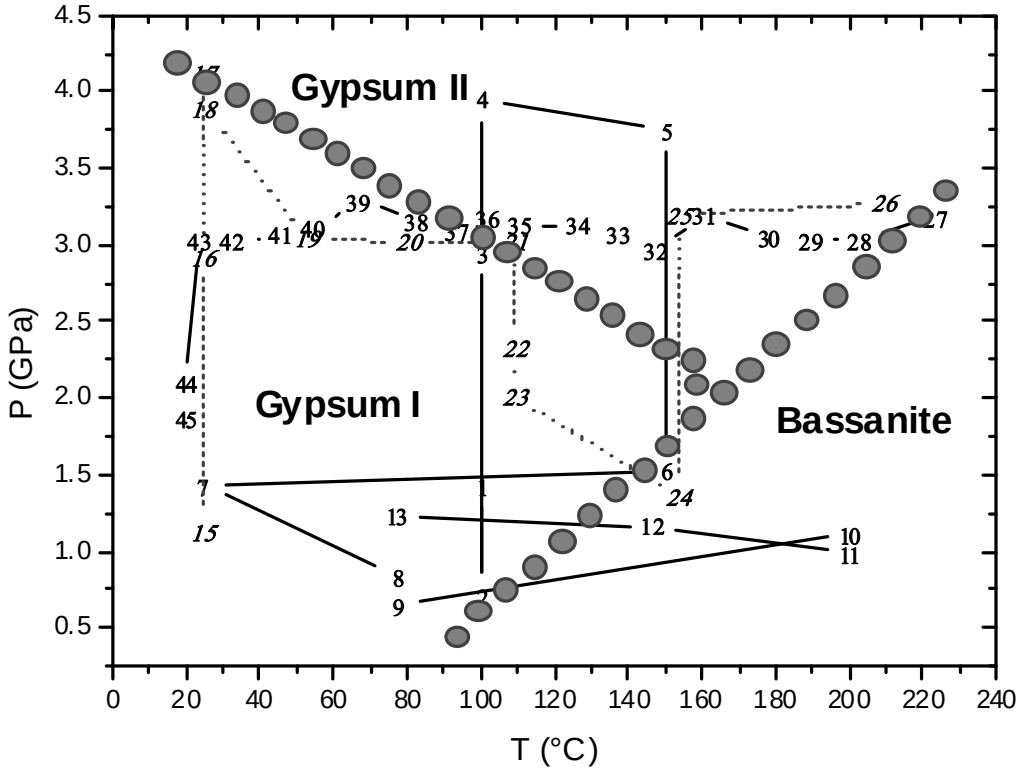

Fig. 3.4-5: *P-T* diagram of gypsum-bassanite. Experimental *P-T* paths (sequential numbers), gypsum I and gypsum II phase boundary and gypsum-bassanite dehydration boundary (dots) are reported.

d. *Elasticity of wüstite under high pressure from dynamic and static measurements (A.P. Kantor, I.Yu. Kantor and L.S. Dubrovinsky, in collaboration with M. Krisch and A. Bosak/ Grenoble)*

One of the most important goals of high-pressure mineralogy is the determination of the elastic constants. There are several experimental methods for doing this; one can determine the bulk modulus indirectly from pressure-volume relations (obtained from static or shock-wave compression), from acoustic waves velocities measurements (ultrasonic measurements), or from acoustic branches of the phonon dispersion curves (neutron and X-ray inelastic scattering). In case of an ideal perfectly elastic crystal elastic modulii determined using different techniques are identical. However, in case of anelastic behaviour the effective elastic modulii measured by different methods can be different. We performed simultaneous single-crystal X-ray diffraction measurements and inelastic X-ray scattering measurements on the nonstoichiometric $Fe_{0.94}O$, a material with a strong anelastic relaxation, at high pressures up to 18 GPa. Wüstite has long been of interest on account particularly of its very wide range of non-stoichiometry and its antiferromagnetic behaviour at certain conditions. The importance of magnesiowüstite $(Mg,Fe)_xO$ as a mineral phase in the Earth's lower mantle and indications of substantial oxygen solubility in the Earth's liquid outer core have focused attention on the high-pressure behaviour of wüstite.

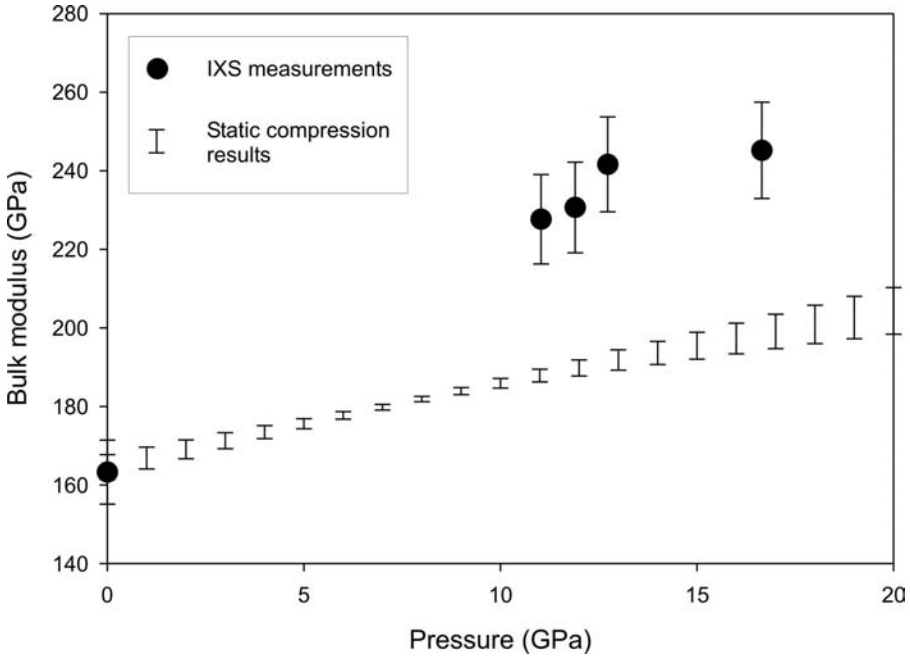

Fig. 3.4-6: Bulk moduli of $Fe_{0.94}O$ determined by means of X-ray diffraction and X-ray inelastic scattering as a function of pressure.

In the present study the effective adiabatic bulk modulus K_S was calculated for every dataset (at every pressure point) using the individual elastic constants. The bulk modulus was

calculated and converted into isothermal modulus K_T using the following equation $K_T = K_S(1+\alpha\gamma T)^{-1}$ (where α and γ are thermal expansion and Grüneisen parameter respectively). The values of the effective ambient conditions bulk modulus determined from IXS and compressibility measurements coincide within the experimental error (K_T = 162 ± 3 GPa). However, the *K'* values, *i.e.*, the variation of the bulk modulus with pressure (Fig. 3.4-6), obtained from the two measurements differ significantly (5.3 ± 0.2 for IXS data vs. 1.79 ± 0.9 for diffraction data). Such behaviour could be explained by a strong anelasticity effect in wüstite under high pressure.

e. *An in situ study of the structural properties of $Fe_{0.78}Ni_{0.22}$ alloys under high-pressure and high-temperature conditions (O. Narygina, I.Yu. Kantor and L.S. Dubrovinsky; V.B. Prakapenka/Chicago)*

According to geophysical data the Earth's core is mainly composed of Fe-Ni alloy with Ni concentration from 10 to 25 %. Therefore physical properties of iron and iron-nickel alloys at the core pressure-temperature conditions are of great importance for interpreting seismic data and for modeling the core composition and dynamics. Phase diagrams of $Fe_{1-x}Ni_x$ alloys are well investigated at low pressures: at ambient conditions iron-nickel alloys are stable in the magnetic body-centred cubic (*bcc*) phase, which under pressure transforms to the nonmagnetic hexagonal close packed (*hcp*) phase; at high temperatures iron-nickel alloys are stable in the face-centred cubic (*fcc*) phase, whose pressure-temperature stability area increases with increasing Ni concentration. Despite considerable effort of theoreticians and experimentalists, data about the temperature effect on the high-pressure behaviour of iron-nickel alloys are still lacking, especially for compositions richer than 20 % Ni.

We performed *in situ* angle-dispersive X-ray diffraction experiments on a $Fe_{0.78}Ni_{0.22}$ samples in a diamond anvil cell up to 42 GPa in the temperature range between 300 and 2600 K, using a double-side Nd:YLF laser heating system at APS (GSECARS, sector 13). LiF was used as pressure transmitting and thermal isolation medium and as internal pressure standard. Temperature was measured by means of multiwavelength spectroradiometry. The collected images were integrated using the Fit2D program, in order to obtain conventional diffraction patterns, and processed using the GSAS package. Lattice parameters of $Fe_{0.78}Ni_{0.22}$ alloy, obtained at room temperature, were fitted using the Birch-Murnagan equation of state and we got the following parameters: K_0 = 185 (7) GPa, V_0 = 6.83 (0.03) cm^3/mol at K'=4 (fixed) (Fig. 3.4-7). For comparison the compression curve of $Fe_{0.9}Ni_{0.1}$ *fcc*-phase is also presented.

Analysis of the high-temperature data reveals that in a certain pressure-temperature region (25-37 GPa 1500-2100 K) the *fcc*-phase reflections are doubled (Fig. 3.4-8b). For comparison on Fig. 3.4-8 diffraction pattern with single reflections of the *fcc*-phase lower (Fig. 3.4-8a) and higher (Fig. 3.4-8c) pressures and nearly the same temperature are presented. Thus the studied *PT*-region is separated into three parts: at pressures lower than 25 GPa and pressures larger than 37 GPa no anomalies in the *fcc*-phase behaviour are observed, whereas at

intermediate pressures the *fcc*-phase reflections are doubled. Lattice parameters of *fcc* iron nickel alloy at pressures lower than 25 GPa and higher than 37 GPa were fitted to the thermal Birch-Murnagan equation of state separately. Values of K_0 and V_0 were taken from room temperature fits and fixed. The results are presented in Table 3.4-2. Lattice parameters of *fcc* $Fe_{0.78}Ni_{0.22}$ at pressures 25-37 GPa and temperatures 1500-2100 K have not been fitted yet due to difficulties with the XRD-patterns interpretation.

	0-25 GPa, 300-2600 K	37-42 GPa, 300-2400 K
V_0, cm^3/mol	6.83 (fixed)	6.83 (fixed)
K_0, GPa	185.19 (fixed)	185.19 (fixed)
K'	4 (fixed)	4 (fixed)
α_0, 10^{-5} K^{-1}	5.05 (0.98)	4.78 (0.98)
α_1, 10^{-8} K^{-1}	3.97 (1.11)	3.77 (1.11)
dK/dT	-0.0694 (0.0009)	-0.0699 (0.0012)

Table 3.4-2: Thermoelastic parameters of *fcc* $Fe_{0.78}Ni_{0.22}$.

The origin of the observed doubling of the *fcc*-phase reflections is still not clear. It could be connected with changes in magnetic properties and (or) could be the sign of pressure-induced invar behaviour of iron-nickel alloy with 22 % of nickel. To understand the nature of this phenomenon we are conducting further high-pressure high-temperature investigations on Fe-Ni alloys with 10, 15 and 22 % of Ni combining Moessbauer spectroscopy, XRD, and chemical analyses by microprobe and SEM techniques.

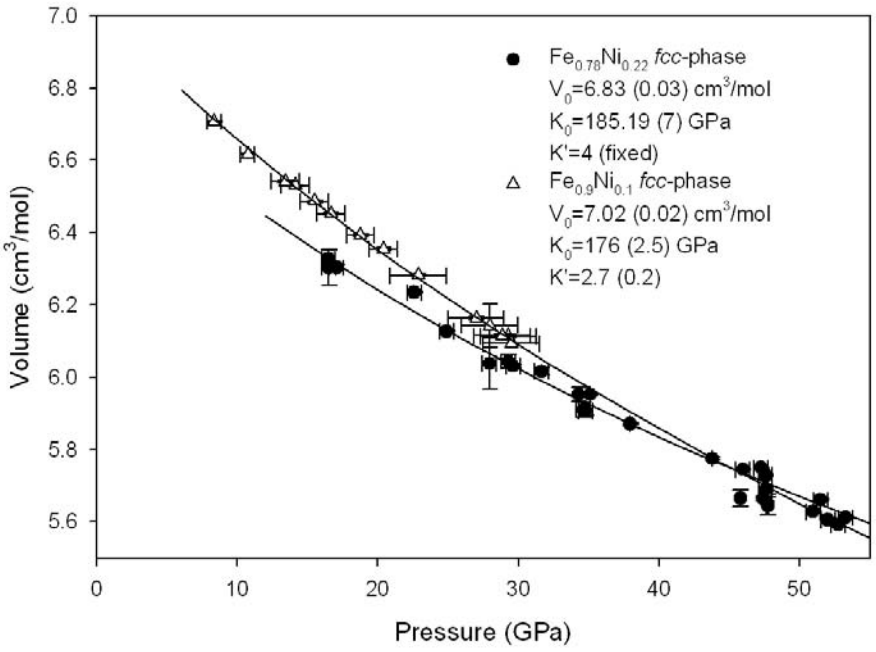

Fig. 3.4-7: Compression curves of *fcc*-phases of FeNi alloys with Ni concentration of 22 % (open triangles) and 10 % (filled circles); T=300 K.

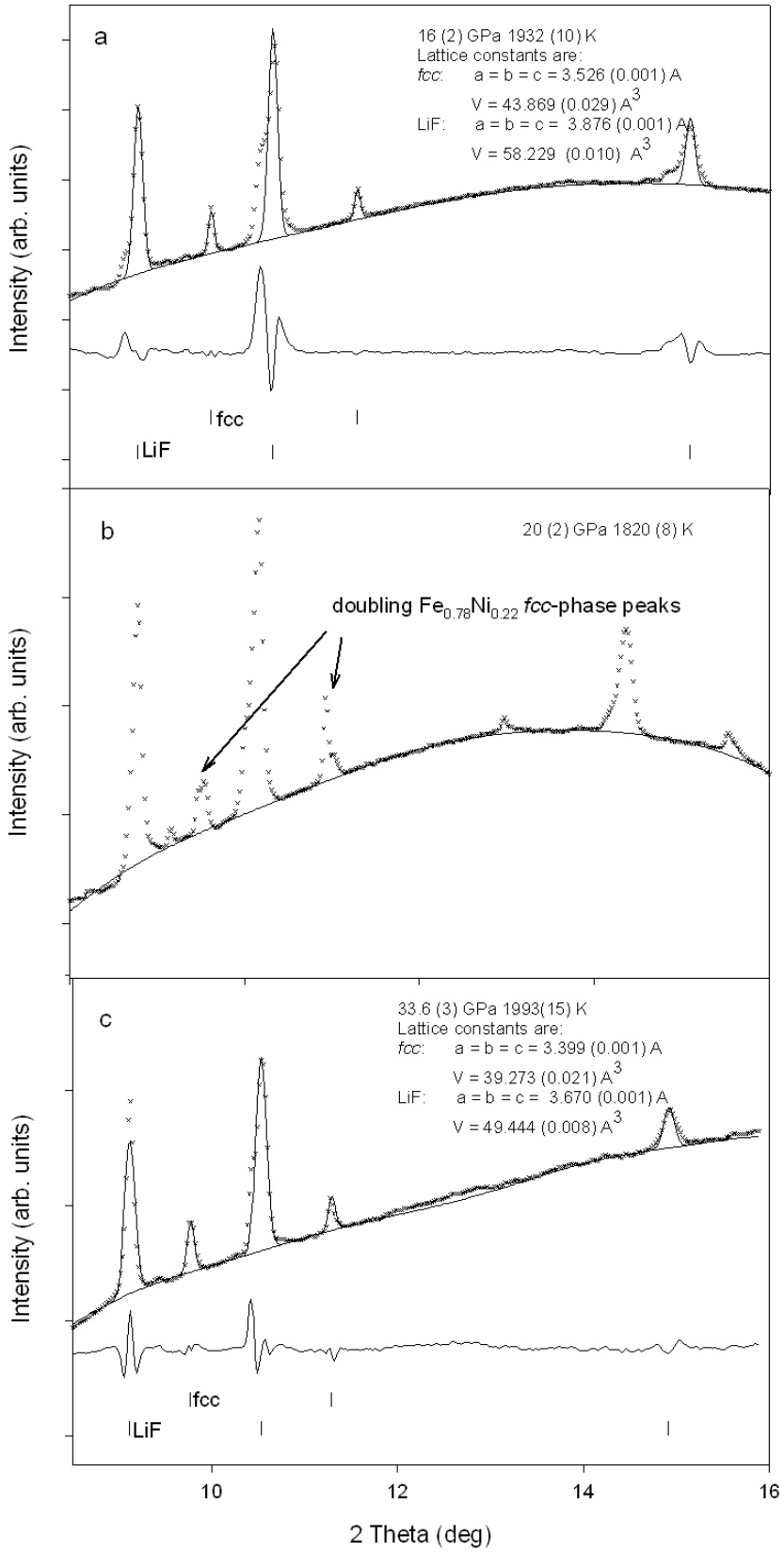

Fig. 3.4-8: Integrated X-ray diffraction patterns, collected from $Fe_{0.78}Ni_{0.22}$ alloy at a) 16(2) GPa and 1932(10) K; b) 20(2) GPa and 1820(8) K; and c) 33.6(3) GPa and 1993(15) K.

f. *The behaviour of magnetism in Fe_3O_4 magnetite under pressure (S. Klotz/Paris, G. Steinle-Neumann, Th. Strässle/Villingen, J. Philippe/Paris, Th. Hansen/Grenoble and M.J. Wenzel/ Berkeley*

Due to its fascinating electronic properties related to the Verwey transition magnetite has been extensively investigated under high pressure. Fe_3O_4 crystallizes at ambient conditions in the inverse spinel structure, *i.e.*, the tetrahedral (A) sites are occupied by Fe^{3+}, whereas Fe^{2+} and Fe^{3+} are randomly distributed on the octahedral B sites. As the magnetic moments on the A and B sites point in opposite directions magnetite is ferromagnetic, yielding a net magnetic moment of 4 μ_B per formula unit. The inverse spinel structure manifests itself in the fractional atomic z-position of the oxygen atom, u(O). For inverse spinel u=0.255, whereas one would expect u=0.260 for the normal spinel in which the A and B sites are occupied by Fe^{2+} and Fe^{3+}, respectively. A difference as small as ~ 2 % in u could be considered as irrelevant if it did not entail two important consequences: First, if the A sites were occupied by Fe^{2+} (normal spinel), the net magnetic moment would be $(5+5-4)\mu_B=6\mu_B$, *i.e.*, a 50 % increase in direct compared to inverse spinel Fe_3O_4. And second, in normal spinel the B sites are occupied by Fe^{3+} only, which means that charge ordering can no longer be evoked to explain the metal-insulator Verwey transition observed at high pressures and low temperatures. The pressure dependence of the u-parameter hence monitors the charge and magnetic state.

We have investigated the problem of magnetism in Fe_3O_4 in more detail, both experimentally as well as by first-principle calculations. We have applied the most direct experimental method to probe magnetism, *i.e.*, *in situ* high-pressure neutron scattering that also allows for a direct inversion of u(O) from the diffraction pattern. Data were collected at nine different P/T points between 0 and 8.1 GPa in the temperature range 130-300 K. Rietveld refinements were carried out using FullProf, refining a minimal set of variables, *i.e.*, the lattice parameter, the internal oxygen coordinate u, the magnitude of the magnetic moments on the A and B sites, as well as background and profile coefficients.

The experiments were complemented by first-principles computations using the state-of-the-art all electron linearized augmented planewave method (LAPW) as implemented in the Wien2k code. We perform computations for both the cubic structure and an orthorhombic structure (space group Imma) in which the B sites are split (B1 and B2) to allow for their non-equivalency as proposed at high pressure. We carry out computations for volumes of 0.925-1.025 V_0, with $\Delta V/V_0=0.025$, out of which three volumes fall within the experimental pressure range of this study. We relax internal parameters in both structures until forces are below 0.5 mRy/Bohr, and analyze results for the Imma structure in terms of the u parameter for O. Although in the Imma structures the O position is split in two sites, the relaxed structures can all be described in the cubic structure with one parameter u for the O.

Under pressure, both moments at the A and B site decrease slightly in magnitude (Fig. 3.4-9). There appears to be no temperature dependence, *i.e.*, the data points at 130 K fall within the error bars on the lines valid for high temperature. This might be expected since the Néel temperature at 1 bar is 851 K and at 8 GPa ~ 1015 K, *i.e.*, in both cases far above the

temperature of our measurements. Therefore, although m_A and m_B decrease under pressure, the data clearly rule out a change in the magnetic structure in the 0-9 GPa and 100-300 K range. The experimentally observed pressure-induced decrease of both moments is also confirmed by the computational results (Fig. 3.4-9). In addition, they indicate that the moments of the B1 and B2 sites (up and down triangles in Fig. 3.4-9) remain the same up to the highest pressure studied, and that the moments between the cubic and the orthorhombic setups are indistinguishable. The B site moments agree with the experiments, whereas the ones on the A site are slightly lower than found experimentally.

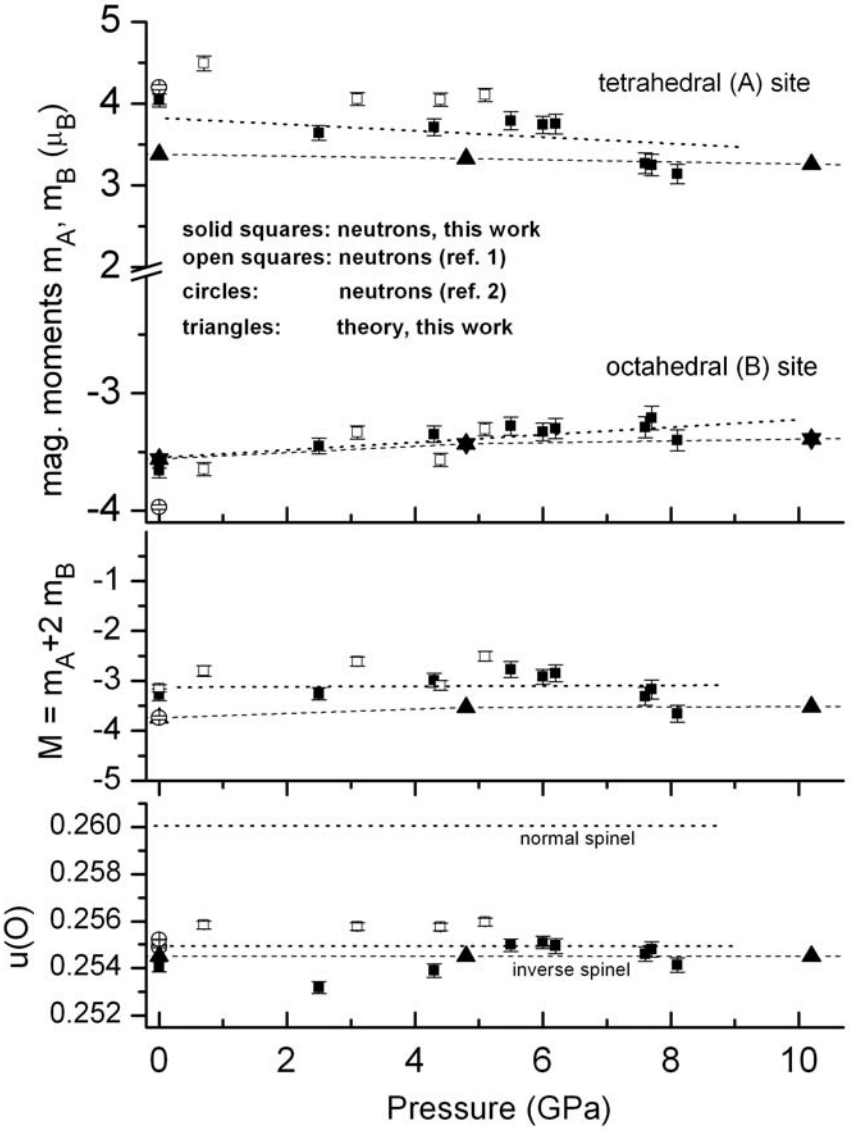

Fig. 3.4-9: Magnetic moments (upper), total moment M (middle) and fractional atomic coordinate of oxygen (lower) of Fe_3O_4. The dotted and dashed lines are guides to the eye for the experimental and theoretical data, respectively. Ambient pressure neutron data as well as previous neutron data to 5 GPa are given for comparison. Note that in the calculations the two magnetic moments on the B site (triangles up and down) in the Imma setting are identical.

The variation of the moments is fully consistent with the behaviour of u(O) as a function of pressure and temperature (Fig. 3.4-9), *i.e.*, u(O) remains close to the value for inverse spinel (u=0.255). In the computations there is a slight difference between u in the cubic (0.2541) and the orthorhombic cell (0.2546), but no changes as a function of pressure have been observed, *i.e.*, at all volumes the structural parameters yield a force smaller than the convergence criterion.

A pressure-induced charge transfer from $[Fe^{3+}]_A[Fe^{2.5+}Fe^{2.5+}]_B$ to $[Fe^{2+}]_A[Fe^{3+}Fe^{3+}]_B$ would, as mentioned above, *decrease* the magnetic moment of the A site but *increase* the magnitude of the one at the B site. What we find is, however, a decrease of *both* moments. Interestingly, although the individual moments decrease by as much as 20 %, the effect on the net moment, *i.e.*, $M=(m_A+2m_B)$, is very small because of partial cancellation linked to the ferrimagnetic structure. The straight forward conclusion of our work is a pressure-induced delocalization of the 3d electrons which entails a continuous quenching of the magnetic moments, as detected in our measurements. No transfer between the different sites in Fe_3O_4 is found up to at least 10 GPa, and u remains close to the value characteristic for the inverse spinel structure. This explains the weak pressure dependence of the magnetisation and rules out an inverse to direct spinel transition in Fe_3O_4. Charge ordering can therefore not be precluded to explain the Verwey transition under high pressure and low temperatures.

g. *Magneto-elastic effects in compressed cobalt (G. Steinle-Neumann)*

Characterizing elasticity of 3d transition metals under compression has been at the center of experimental development in high-pressure physics and geophysics over the past decade as cores of terrestrial planets are primarily composed of iron. As the study of elasticity on the high-pressure hexagonal close packed (hcp) phase of iron has proven challenging, a lot of effort has focused on cobalt, the metal adjacent to iron in the periodic table which crystallizes in the hcp phase at ambient pressure. In addition, the discovery of the high-pressure phase transition from the hcp to the fcc phase near 100 GPa raises a number of interesting question, *e.g.*, the role of magnetism and elasticity in phase stability.

Here we perform density functional theory based computations on the magneto-elastic properties of both close packed phases of cobalt, paying particular attention to the effect of magnetism on the elastic constants with the goal to elucidate the experimental findings. To this effect we compare results from spin-polarized computations to non-magnetic results, allowing for a direct assessment of the influence of spin on physical properties. We investigate the energetics of the close-packed phases of cobalt using the full-potential linearized augmented plane-wave method (LAPW) with the generalized gradient approximation (GGA) to the exhange-correlation potential. Elastic constants are inverted from the bulk modulus, the relative compressibility of the hexagonal axes (for hcp), and four (two) strains for the hcp (fcc) cell. Aggregate properties are computed from the single crystal elastic constants.

For both phases of cobalt we find a ferromagnetic phase with an initial magnetic moments near 1.65 μ_B that decreases slowly with compression due to delocalization effects (for V > 60 Bohr^3). At higher compression the magnetic moment is lost almost instantaneously from the fcc phase; for the hcp phase it more slowly vanishes, reaching zero at 50 Bohr^3 (Fig. 3.4-10). The initial slow decrease of magnetic moment is consistent with a slight increase in the Curie temperature of Co with pressure, but in conflict with X-ray magnetic circular dichroism results where a uniform decrease of magnetic moment with compression is reported. A critical re-assessment of high-pressure magnetism in cobalt, for example through neutron diffraction, is clearly advised.

In agreement with experiments and previous computations we find the hcp cobalt phase stable over the fcc phase for a large volume range, up to a compression of ~ 55 Bohr^3. Magnetism in the hcp phase vanishes in the structural phase transition region. The equation-of-state for magnetic hcp cobalt is in good agreement with experiments.

At ambient pressure (V=75 Bohr^3) the elastic constants for the magnetic hcp phase are in good agreement with ultrasonic experiments. The shear elastic moduli and c_{13} show the largest difference between magnetic and non-magnetic moduli: magnetic constants for c_{44} and c_{13} are larger than their non-magnetic counterparts, c_{66} is significantly smaller. For the magnetic hcp phase the elastic moduli start deviating from a monotonic increase above 65 GPa. The shear elastic constants show a significant softening to the extent that their values at 55 Bohr^3 are smaller then the ones at larger volumes. This elastic anomaly coincides with the loss of magnetism in the hcp phase (Fig. 3.4-10), and once magnetism has been lost completely in hcp cobalt the shear moduli coincide with their non-magnetic counterpart. The longitudinal elastic constants also show a softening in the same volume range. Aggregate acoustic velocities reflect the anomalies in the single crystal elastic constants (Fig. 3.4-11). For the magnetic and non-magnetic hcp phase the longitudinal acoustic (compressional) wave velocity (v_L) and the transverse acoustic (shear) wave velocity (v_T) are similar at low compression and depend linearly on density, following Birch's law (Fig. 3.4-11). For the non-magnetic velocities the linear dependence continues for the whole compression range while v_T for the magnetic phase shows a strong softening, decreasing over some compression range, before recovering the non-magnetic value at highest density. v_L for magnetic hcp shows a slight deviation from the linear dependence. The compression dependence of aggregate velocities agrees well with experiments to above 100 GPa, except for v_L at highest pressure where the ISLS experiments show a stronger softening (Fig. 3.4-11). The good agreement between the ISLS measurements and the computations for magnetic hcp cobalt also indicate that in the experiments cobalt remained in the hcp structure to the highest pressure. The strong magneto-elastic coupling in the shear elastic constants for hcp cobalt at high pressure computed here as well as the anomaly in v_T and v_L measured by ISLS and IXS shows that cobalt can be used as an analogue to hcp iron only with great caution.

In fcc cobalt there is also considerable difference between the magnetic and non-magnetic elastic constants: the magnetic constants have a lower value than the non-magnetic moduli. At volumes below the magnetic transition (55 Bohr^3) the elastic constants merge with the non-

magnetic values, and there is only a slight softening of c_{44} near the transition. As in the case of hcp cobalt the non-magnetic elastic moduli can readily be fit with an Eulerian finite strain expression. Magnetism is lost from the fcc phase at lower compression (Fig. 3.4-10) and the acoustic velocities for the magnetic phase change smoothly to the values of the non-magnetic phase (Fig. 3.4-11). Again, acoustic velocities for non-magnetic fcc cobalt follow Birch's law over the whole compression range (Fig. 3.4-11).

Across the phase transition between the hcp and the fcc phase considerable changes in the aggregate velocities are predicted: for v_T we predict an increase of more than 10 %; for v_L an increase on the range of 5-10 % can be expected. Such a change has not been observed to date in experiments as the relevant pressure range has not yet been reached for measurements of elastic properties.

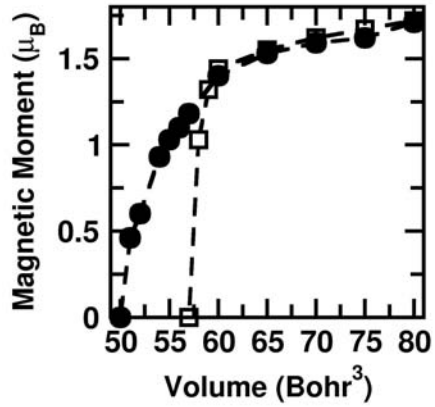

Fig. 3.4-10: Magnetic moment (lower panel) for the hcp (filled circles) and fcc phase (open squares) of cobalt. Dashed lines are drawn to guide the eye.

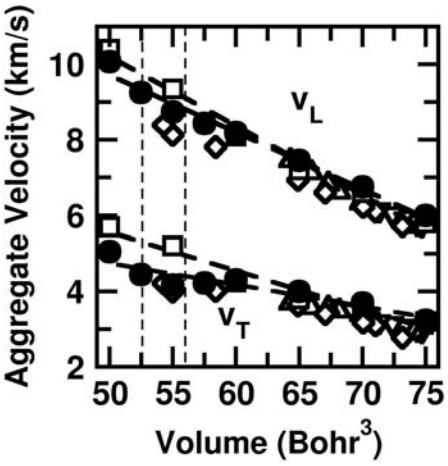

Fig. 3.4-11: Aggregate acoustic velocities for cobalt. Results for the hcp (filled circles) and fcc phase (open squares) are compared with experimental data from IXS (triangles up and triangles left) and ISLS (triangles down and diamonds).

h. *Magnetic structure of Fe_2SiO_4 fayalite from ab initio computations (Z. Tang and G. Steinle-Neumann)*

The olivine solid solution between Mg_2SiO_4 forsterite and Fe_2SiO_4 fayalite determines physical properties in the upper mantle, and the incorporation of Fe into the olivine structure can change physical properties considerable: variations in Fe content will have an effect on

phase transition pressure, the sharpness of the phase transition, and physical properties, that can cause lateral variations in mantle properties. In order to fully understand the variation of properties along the olivine-fayalite solid solution a good characterization of the end-members is of critical importance. While forsterite has been studied extensively at high pressure in both experiments and computations, information on Fe_2SiO_4 fayalite has been limited. This is true in particular for the magnetic structure of Fe_2SiO_4, even at ambient pressure. At cryogenic temperature below ~ 65 K Fe_2SiO_4 is reported to be non-collinear anti-ferromagnetic (afm), but neutron diffraction data can not distinguish between two possible magnetic configurations.

The olivine structure has two distinct Mg/Fe (M1 and M2) sites that connect the isolated SiO_4 tetrahedra, and crystallizes in an orthorhombic structure. In fayalite the magnetic structure has a lower symmetry, as the Fe atoms have different magnetic directions for the single sites: on the M2 site the Fe atoms order anti-ferromagnetically in a collinear way. On the M1 site Fe order in a non-collinear afm structure where the spins are canted away from the z-axis. The ambiguity in the magnetic structure stems from the relative arrangement of the afm lattices, resulting in two possible configurations (Fig. 3.4-12), one of which could be characterized as a ferromagnetic coupling sites 3 and 5 (afmI, Fig. 3.4-12, right), the other by afm coupling between these two sites (afmII, Fig. 3.4-12, left).

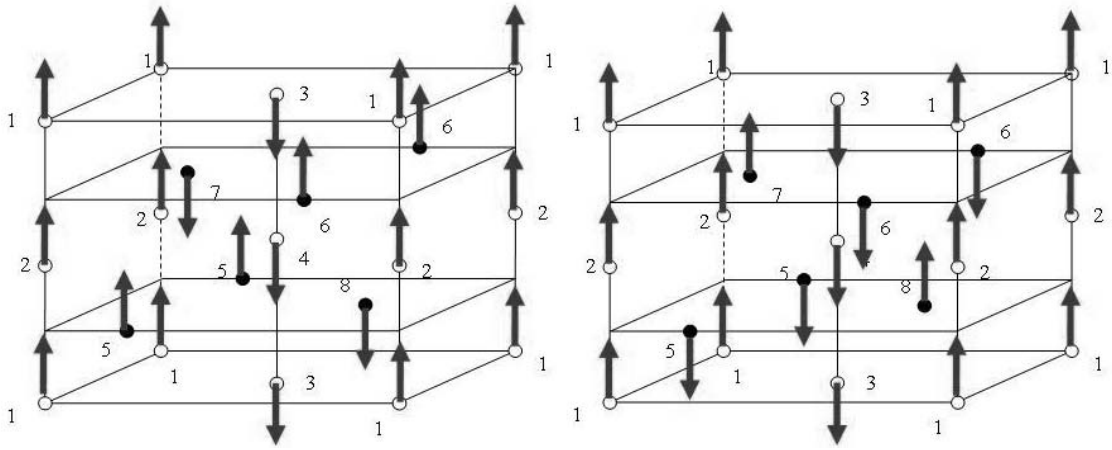

Fig. 3.4-12: Magnetic structure of the Fe ions in fayalite on the M1 (open symbols) and M2 sites (filled symbols).There is afm coupling between M1 sites (arrows), *i.e.*, site 1(2) and site 3(4), as well as between M2 sites (arrows), *i.e.*, site 5(6) and site 7(8) . Two possible couplings between the M1 and M2 sites are shown: on the right ferromagnetic coupling between site 3 and site 5(6) (afmI structure), on the left there is afm coupling between site 3 and 5(6) (afmII structure).

Here we investigate the energetics of two possible afm structures both at ambient pressure and under compression by means of full-potential first-principles computations, using the linearized augmented plane wave method (LAPW) as implemented in the Wien2k software package. At the moment we approximate the magnetic structures by collinear arrangements

(Fig. 3.4-12). We find that the afmI structure is stable compared to the afmII structure by 204 meV at ambient condition. Under compression the afmI structure remains the stable phase relative to afmII at least up to 20 GPa, and magnetic moments on the two sites decrease only slightly up to this pressure due to delocalization effects under compression.

i. *High-resolution X-ray diffraction study of synthetic hematite-ilmenite solid solutions for confirmation of phase composition and detection of impurities (S.A. McEnroe/Trondheim, T. Boffa Ballaran, P. Robinson/Trondheim, B.P. Burton/Gaithersburg)*

A program is in progress to elucidate the high- and low-temperature magnetic properties of synthetic metastable solid solutions in the system Fe_2O_3-$FeTiO_3$. This program has three aspects: 1) Studies of natural mineral intergrowths that create dramatic terrestrial magnetic anomalies and magnetic property information can be a key to their identification; 2) studies of low-temperature properties that may be essential to the magnetism of cold planetary bodies; and 3) studies of low-temperature properties as keys to growing synthetic intergrowths for technological applications (*e.g.*, spin valves).

High-resolution X-ray diffraction has been used for a detailed study of a group of samples that were synthesized by B. Burton under controlled-oxygen-fugacity conditions. X-ray diffraction work is a prerequisite for a precise study of the magnetic properties, because very small concentrations of impurity phases, or deviations from ideal stoichiometry, can strongly alter magnetic properties (see next contribution on synthetic titanohematite). Most recently these results were used to construct a magnetic phase diagram in the composition – temperature ranges $0.60 < XFeTiO_3 < 1.00$, and $0\ K < T < 470\ K$. Additional magnetic property measurements have been made on samples throughout the full composition range, $0.00 < XFeTiO_3 < 1.00$. Of particular interest, is the occurrence of a re-entrant spin-glass phase at low-T, apparently as a result of competition between interatomic magnetic interactions. In addition, several samples exhibit two-phase magnetic behaviour, demonstrating either: 1) the presence of magnetically ordered and disordered rhombohedral phases; or 2) magnetic phases of different structure that remain undetected, even in high-resolution diffraction studies.

j. *Cryptic intergrowth of magnetite-like phase in synthetic titanohematite (S.A. McEnroe/ Trondheim, N. Miyajima, P. Robinson/Trondheim, K. Fabian/Trondheim, B.P. Burton/ Gaithersburg, T. Boffa Ballaran)*

A synthetic sample with nominal composition $XFeTiO_3 = 0.40$ was annealed for 7 days at 887 °C in a matrix of sodium borate flux. The run product consists of crystals in a glass matrix. In reflected light, some grains show two or three areas of different reflectivity along very sharp contacts, possibly due to twinned crystal orientation. Optical observations indicated only one phase and no exsolution was evident. The X-ray diffraction pattern shows no line broadening

that would indicate significant variation in composition, nor evidence for other phases. Lattice parameters: a = 5.0557 Å, c = 13.8528 Å, V = 306.646 $Å^3$ indicate a composition $XFeTiO_3$ = 0.405, extremely close to the nominal composition. Magnetic hysteresis experiments from 300 to 10 K, showed two-phase behaviour and below 35 K an extreme increase in coercivity and a strong shift in remanence (M_{rs}). Exchange coupling across interfaces of two phases with different magnetic properties appears necessary to explain this behaviour.

Thus, magnetic experiments clearly indicated the presence of a second phase that was not detected by XRD, and that this second phase would only be resolvable with a transmission electron microscopy study. HRTEM (Fig. 3.4-13) demonstrated the presence of extremely fine lamellae parallel to (001) of the host rhombohedral phase, ~ 6-8 nm thick, or approximately 4-6 unit cells of the rhombohedral oxide host. Electron diffraction patterns of host areas with lamellae indicated the rhombohedral titanohematite coexists with a spinel-structured phase, together with a pattern of moiré effects. The parallel orientations of ***c**** of the hematite and 111* of the spinel-structure phase indicate that the prominent lamellar interfaces are on the (001) basal plane of the host and on the (111) octahedral plane of the lamellae, a well known interface in natural magnetite-ilmenite integrowths. This is a plane in the two structures common to the dioctahedral (2/3 octahedral) layers of ilmenite and the 3/4 octahedral layers of spinel. TEM-EDS measurements of Fe/Ti confirm the Ilm 40 composition of the host, but neither TEM-EDS, nor EELS measurements of Fe^{3+}/Fe total, have determined a chemical difference between host and lamellae. This opened the possibility that the spinel-structured lamellae are a titanomaghemite polymorph of the titanohematite (spinel structure with octahedral vacancies).

Additional high-field magnetic experiments were run between room temperature and 720 °C to determine the Curie/Néel temperatures of the two phases (Fig. 3.4-14). The magnetically dominant phase loses magnetization at 360 °C, corresponding closely to the expected Néel temperature of the Ilm 40 host. The magnetically subordinate phase loses magnetization at ~ 560 °C, which would correspond to the Curie temperature of a magnetite of composition ~ Usp 4 ($4\%Fe_2TiO_4$), or possibly titanomaghemite of composition ~ Ilm 14. This strong high-T magnetization, compared to the small amount of spinel-structured lamellae, is explained by its expected strong magnetization compared to single-phase titanohematite. Another contribution could come from lamellar magnetic moment at the two-phase interface. Exchange coupling across the interfaces of the lamellae stabilizes the magnetic moment, which otherwise would be superparamagnetic at room temperature, due to finite size effects.

This study aims to characterize all phases present, and to estimate the nature and role of interfaces in causing the very high observed coercivity and possibly the magnetic exchange bias. This constitutes an exciting example in which magnetic bulk-property measurements strongly indicate the presence of an exsolved phase that is only directly observable by HRTEM.

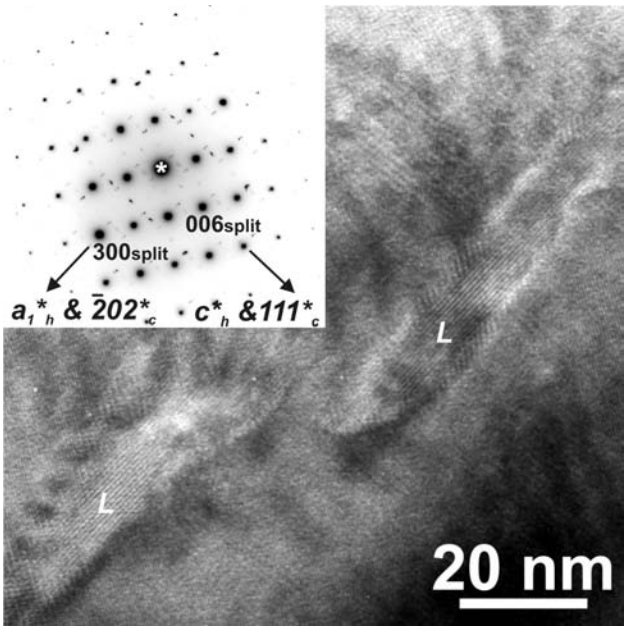

Fig. 3.4-13: HRTEM image of lamellae of a spinel-structured phase in a titanohematite host. The inset shows the selected area electron diffraction pattern, which is indexed with <010> hexagonal (host) and $<1\,\bar{2}\,1>$ cubic (lamellae, ***L***) zone axes.

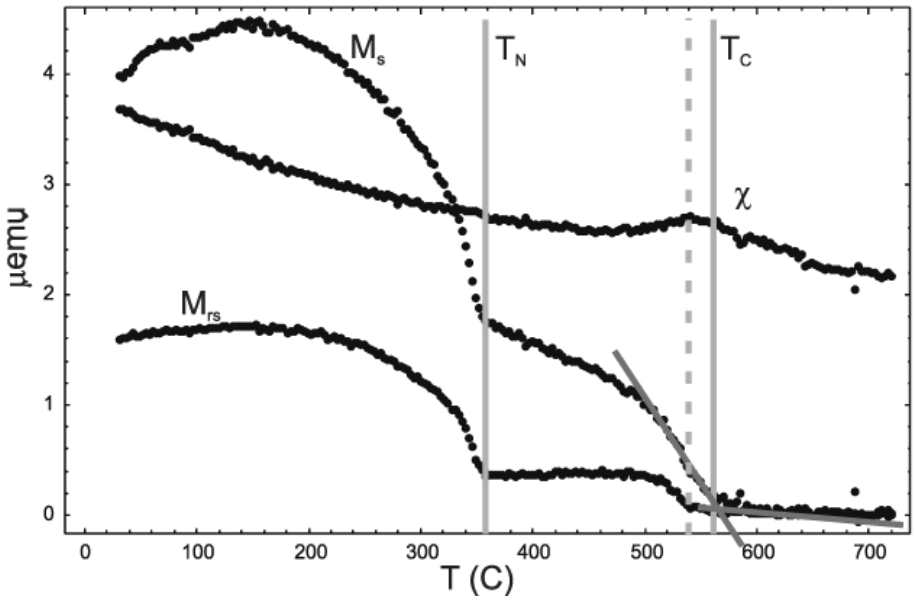

Fig. 3.4-14: Saturation magnetization M_s, saturation remanence M_{rs} and susceptibility χ (rel. units) for sample Ilm40-887 °C as a function of temperature (T). M_s shows two distinct phase transitions at T_N ~ 360C and T_C ~ 560 °C. Both transitions are associated with distinct remanence losses (M_{rs}) indicating that both phases carry remanence. The drop in M_{rs} related to the high-temperature phase transition occurs already at ~ 540 °C, due to remanence unblocking below T_C. This is consistent with the parallel peak in susceptibility (Hopkinson-peak) in this temperature region.

3.5 Fluids and their Interaction with Melts and Minerals

High-pressure fluids cannot be quenched to room temperature. Estimating mineral solubilities from conventional quench experiments is therefore rather difficult. Solubility data obtained by such methods often differ by several orders of magnitude. For a long time, it was believed that high field strength elements, such as titanium or zirconium are highly soluble in aqueous fluids at mantle pressures. Recent work, both at Bayerisches Geoinstitut and in other laboratories has shown that rutile (TiO_2) solubility in aqueous fluids is orders of magnitude lower than previously assumed. Here, we show first data on zircon solubility in aqueous fluids at up to 900 °C and 1.5 GPa, obtained by *in situ* observation of zircon dissolution in an externally-heated diamond cell. The data suggest that zircon solubility is even lower than rutile solubility. This implies that the depletion of high field strength elements see in arc magmas is probably simply a consequence of the inability of hydrous fluids to transport these elements into the zone of melting.

The strong smell of sulfur compounds is experienced by anyone approaching an active volcano. Sulfur compounds are indeed major constituents of volcanic gases and they are responsible for the global cooling observed after major explosive eruptions. However, surprisingly little is known about the behaviour of sulfur during an eruption. Although it is known that sulfur strongly partitions into an aqueous fluid, the dependence of the partition coefficients on melt composition, fluid composition and other parameters has never been thoroughly studied. A comprehensive study on sulfur partitioning between felsic melt and fluid reveals a complicated dependence of the partition coefficient on melt and fluid composition, with the observed dependence being different at oxidizing and reducing conditions.

While the high fluid/melt partition coefficients favor the injection of massive amounts of sulfur compounds into the stratosphere, adsorption on ash particles in eruption columns may reduce it. In fact, if the sulfur is relatively diluted in the fluid, almost all of it may be removed from the volcanic gases by adsorption. The experimental studies presented here therefore very much improve our capability to predict the environmental effect of volcanic eruptions. This effect has to be properly understood to correctly sort out natural and anthropogenic causes of climate change.

The last two contributions in this section look at water storage in nominally anhydrous minerals. The first one shows that water solubility in clinopyroxenes strongly increases with aluminium content. This means that omphacitic clinopyroxenes in eclogites may contribute significantly to the subduction of sea water in the global water cycle. The second study shows a dramatic effect of oxygen fugacity on water solubility in wadsleyite in equilibrium with C-H-O fluids. One important consequence of this study is that perhaps fluids may be stable in the transition zone even at rather low bulk water contents.

a. *Zircon solubility in aqueous fluids at high pressures and temperatures (D. Bernini, A. Audétat, D. Dolejš and H. Keppler)*

The depletion of high field strength elements (HFSE) is the most characteristic geochemical feature of subduction zone magmas. Various models have been proposed to explain the low abundance of these elements in arc magmas. Many of them relate the depletion to the presence of accessory minerals in the subducted slab, while others attribute it to the intrinsically low solubility of high field strength elements in aqueous fluids, which trigger melting in subduction zones. There are however, hardly any data on the solubility of these elements in aqueous fluids at typical mantle pressures and the few available data are often contradicting and differ by several orders of magnitude.

In this study, we have started to systematically study the solubility of zircon in aqueous fluids at high pressures and temperatures, using a hydrothermal diamond anvil cell of the Bassett type. This method allows the direct visual observation of dissolution and precipitation and therefore eliminates a major source of error in traditional experiments using quench techniques. Moreover, the very low temperature gradients in the cell allow measurements of high precision.

For our experiments we have used rhenium gaskets with a bore of 500 μm in diameter and 150 ± 25 μm height after indentation. The sample chamber was loaded with a piece of natural quartz crystal, a fragment (~ $3 \cdot 10^6$ μm^3) of natural zircon from Sri Lanka, plus ~ 38 μm^3 of ultrapure water. The cell followed nearly isochoric paths with 50-72 °C/kbar during heating (Fig. 3.5-1). By the addition of quartz, silica activity was buffered during the experiment.

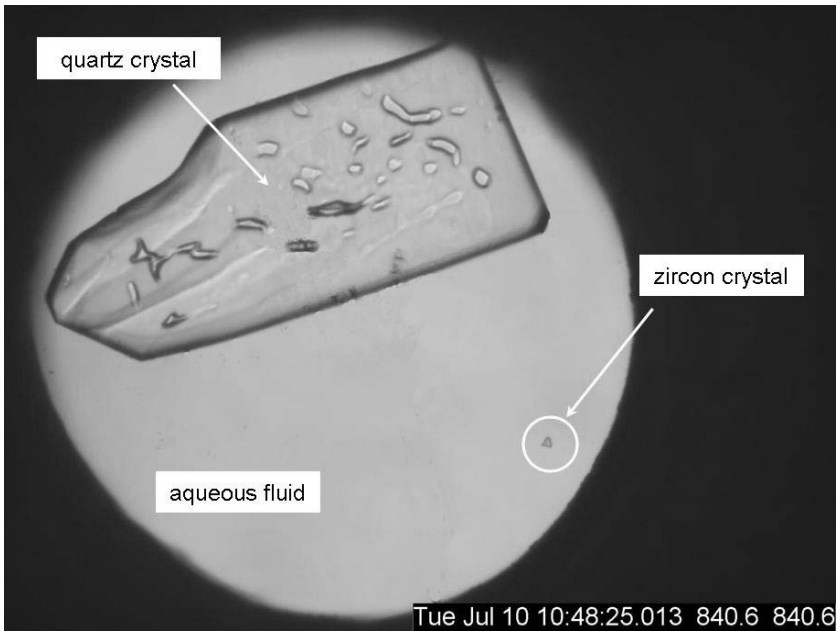

Fig. 3.5-1: A zircon solubility experiment at quartz saturation in an externally heated diamond cell.

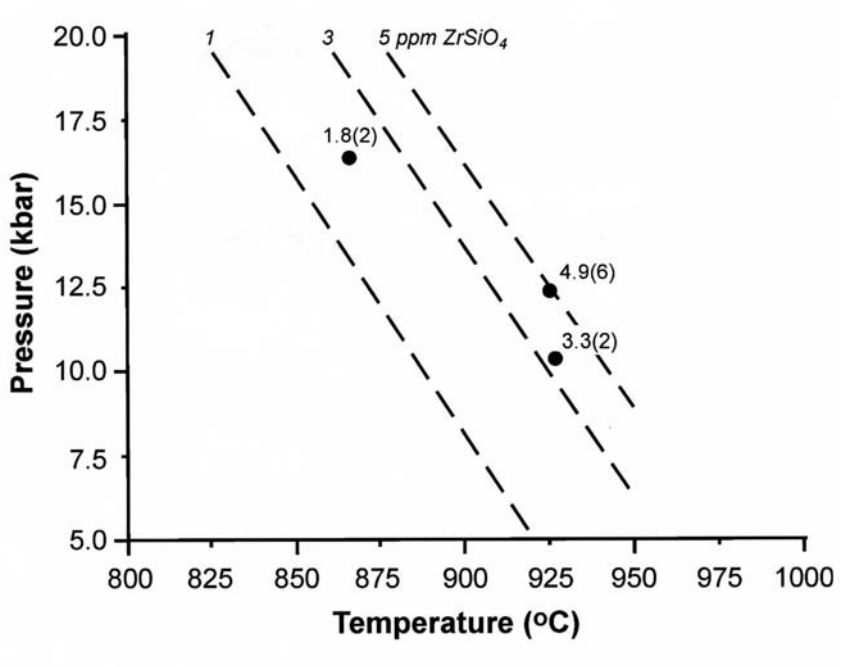

Fig. 3.5-2: First experimental results on zircon solubility in water in equilibrium with quartz.

Our measurements demonstrate that the solubility of zircon in aqueous fluid in equilibrium with quartz at 860-930 °C and 10-16 kbar is extremely low (< 3 ppm Zr). It increases both with increasing temperature and with increasing pressure (Fig. 3.5-2). Equilibrium constants for the dissolution reaction

$ZrSiO_4$ (s) = ZrO_2 (aq) + SiO_2 (s)

vary from $10^{-5.01}$ to $10^{-4.57}$ (in molality units) at 860-930 °C and 10-16 kbar.

Small amounts of quartz are often found in eclogites of the subducted slab. Our data are therefore directly applicable to zircon mobility in this environment. In the mantle wedge, silica activity is buffered by the equilibrium between olivine and orthopyroxene. Due to the lower silica activity, zircon solubility should increase. However, based on our data, we would expect the solubility of zircon still to be very low. We therefore tentatively conclude that zirconium, just as titanium, is intrinsically immobile in aqueous fluids under mantle conditions. The depletion of HFSE elements in arc magmas is therefore probably a direct consequence of element fractionation during fluid transport into the zone of melting.

b. *The partitioning of sulfur between aqueous fluids and granitic melts (B. Binder/Tübingen and H. Keppler)*

Sulfur compounds are important constituents of volcanic gases. Variations in sulfur emission and H_2S/SO_2 ratio can be easily measured by spectroscopic remote sensing techniques and provide a tool for forecasting volcanic eruptions. At the same time, sulfur strongly affects the

behaviour of metals in magmatic-hydrothermal systems and the formation of hydrothermal ore deposits. Understanding the partitioning of sulfur between silicate melts and aqueous fluids is therefore crucial both for the monitoring of active volcanoes and for modeling the formation of hydrothermal ore deposits.

We studied the partitioning of sulfur between haplogranitic melts and aqueous fluids at 750-850 °C, 1-3 kbars and the oxygen fugacity of the Ni-NiO or Re-ReO_2 buffer. Experiments were carried out in gold capsules in externally heated cold seal bombs with run durations of several weeks. The sulfur content in the quenched glasses was measured by electron microprobe and the sulfur content in the fluid was calculated by mass balance.

Oxygen fugacity is the main control of sulfur partitioning. At 850 °C and 2 kbar, $D^{fluid/melt}$ of sulfur is 323 ± 14 for Ni-NiO buffer conditions, but 74 ± 5 for the conditions of the Re-ReO_2 buffer, in reasonable agreement with previous work. CO_2 up to a molar fraction of 0.2 has no detectable effect of the partition coefficient. The effect of NaCl on sulfur partitioning depends on the redox conditions. With the Re-ReO_2 buffer, NaCl has no effect on the partition coefficient up to a molar fraction of 0.3 in the fluid. On the other hand, under reducing conditions, NaCl strongly reduces the partition coefficient from 323 without NaCl to 84 ±12 for a NaCl molar fraction of 0.3 in the fluid (Fig. 3.5-3). This is probably due to a reduction of water activity, which reduces the solvation of H_2S in the fluid.

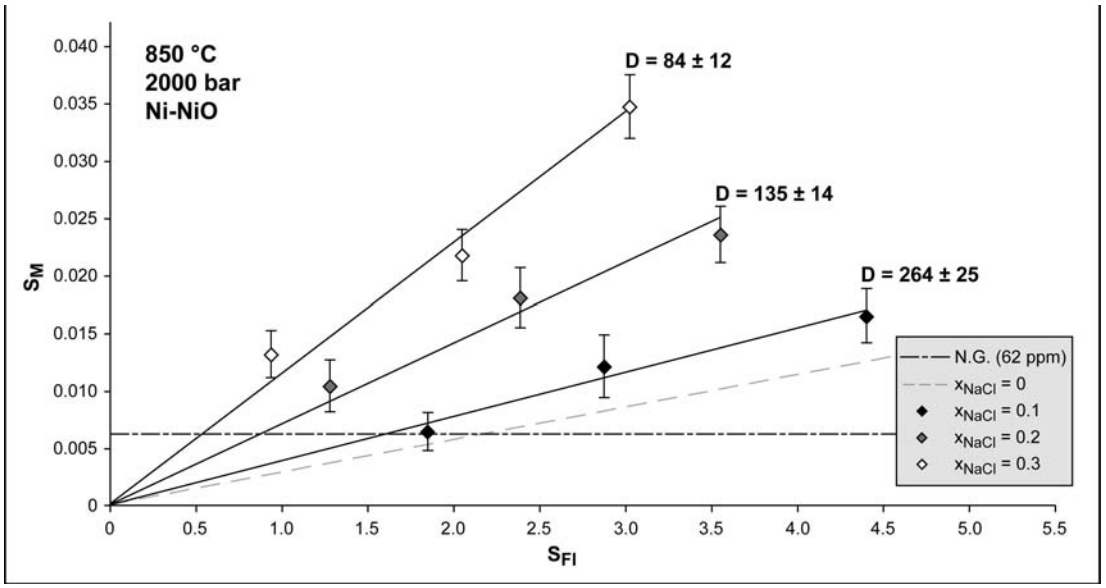

Fig. 3.5-3: The effect of NaCl on the fluid/melt partitioning of sulfur in the system haplogranite-H_2O-NaCl. Sulfur concentrations in melt (S_m) and fluid (S_{Fl}) in wt.%.

The effect of the alkali/aluminium ratio in the silicate melt on sulfur partitioning is also different for different redox conditions. Under reducing conditions, the fluid/melt partition

coefficient of sulfur decreases with increasing alkali content (Fig. 3.5-4). This may be related to the stabilization of NaSH in the melt. On the other hand, under oxidizing conditions, the partition coefficient has a pronounced minimum near a molar ratio of (Na + K) / Al = 1 in the silicate melt (Fig. 3.5-5). This may imply that the sulfate ion, which is the dominant sulfur species in the melt at Re-ReO_2 buffer conditions, preferentially mixes with a polymerized silicate melt.

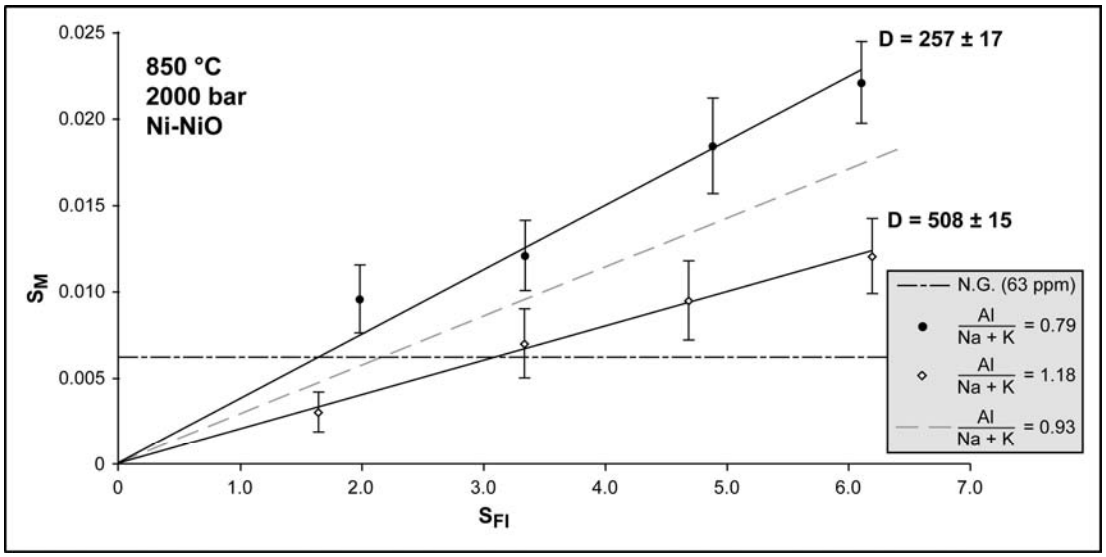

Fig. 3.5-4: Influence of melt composition on the partitioning of sulfur between aqueous fluid and haplogranitic melt under reducing conditions. Sulfur concentrations in melt (S_m) and fluid (S_{Fl}) in wt.%.

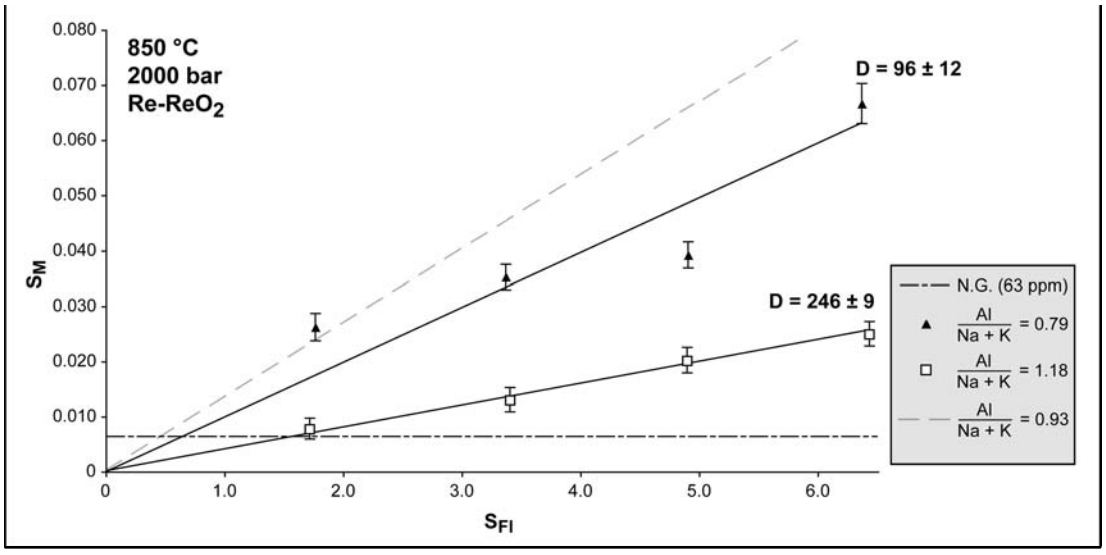

Fig. 3.5-5: Influence of melt composition on the partitioning of sulfur between aqueous fluid and haplogranitic melt under oxidizing conditions. Sulfur concentrations in melt (S_m) and fluid (S_{Fl}) in wt.%.

c. *A model for predicting the adsorption of SO_2 on volcanic ashes (D. Schmauß-Schreiner and H. Keppler)*

Adsorption on volcanic ashes may remove a considerable fraction of SO_2 from the eruption column of a volcano. Since SO_2 is mostly responsible for the global cooling following major volcanic eruption, a quantification of this effect is essential for predicting the effect of explosive volcanism on climate.

We have systematically studied the adsorption of SO_2 on glasses of andesitic, dacitic and rhyolitic composition at variable temperatures ranging from -80 °C to 150 °C and at pressures ranging from a few mbar to 1 bar. For each glass composition, adsorption can be described by a generalized Freundlich model

$$\ln c = A\,(1/T) + B\ln P + C$$

(with c = surface concentration of adsorbed SO_2 in mg/m^2, T in K and P in mbar). For dacite glas, the relevant parameters are A = 3139, B = 0.29 and C = -9.32. Figure 3.5-6 compares predicted and measured surface concentrations for SO_2 on dacite glass.

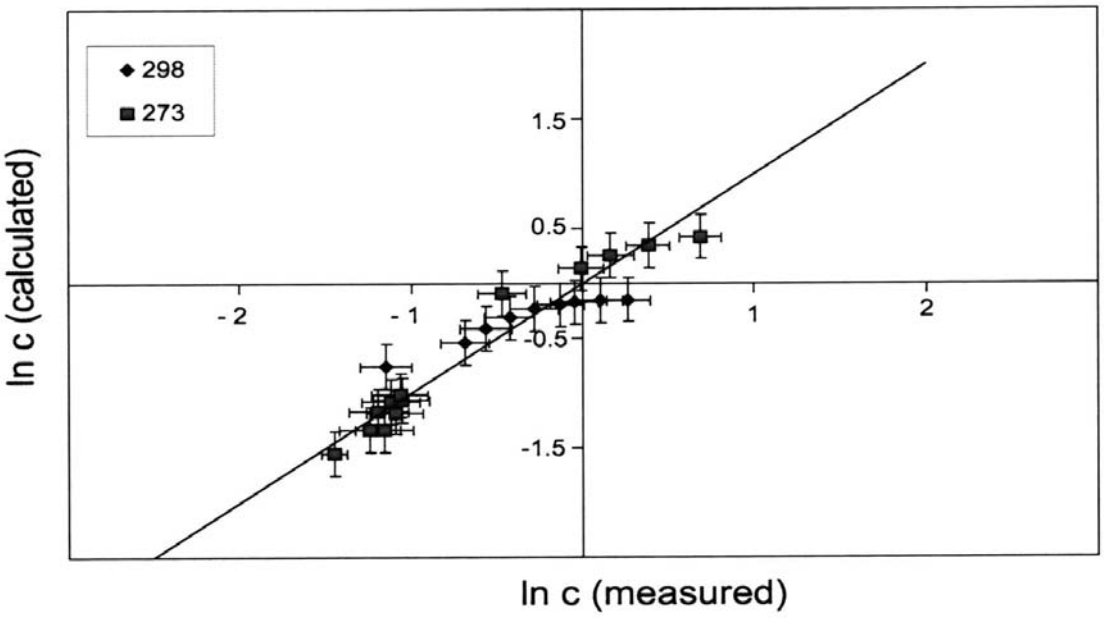

Fig. 3.5-6: Regression model for the adsorption of SO_2 on dacite glass. Shown are data for 273 K and 298 K covering a range of pressures from a few mbar to 1 bar.

For all glasses studied, the parameter B is always around 0.3, *i.e.*, adsorption is approximately proportional to $P^{0.3}$, where P is the partial pressure of SO_2. This means that the fraction of SO_2 adsorbed on the ash surface is particularly high if the SO_2 is strongly diluted in the volcanic plume by other gases such as H_2O. Indeed, it can be shown that at low SO_2 concentrations in the volcanic gas, most of the SO_2 may be adsorbed on the ash surface and may therefore be

removed from the plume. The magnitude of this effect decreases with increasing initial SO_2 concentration.

d. *Water solubility in diopside (P. Gavrilenko and H. Keppler)*

Clinopyroxene is only a minor constituent of the upper mantle. However, natural clinopyroxenes form mantle xenoliths contain more water than other nominally anhydrous minerals. Moreover, omphacitic clinopyroxenes may transport water deeper into the mantle after the breakdown of hydrous minerals in subducted slabs. Therefore, aluminous clinopyroxenes may actually play an important role in recycling water back into the mantle. In this study, we looked at water solubility in both pure diopside and in diopside containing variable proportions of aluminium.

Water-saturated pure and Al-containing diopside was synthesized in an end-loaded piston-cylinder apparatus at 1.5-3.5 GPa and 800-1100 °C. The starting material was a mixture of high-purity $Mg(OH)_2$, $Ca(OH)_2$, $Al(OH)_3$ and SiO_2 with excess water. The compositions of the starting materials for Al-bearing diopside are along the join diopside ($CaMgSi_2O_6$) – Ca-Tschermak's component ($CaAl_2SiO_6$) with different ratios of these two end members. The water concentration in diopside was determined from polarized infrared measurements on double-polished single crystals. Water contents were calculated by integrating the absorption bands and using published extinction coefficients for water in diopside.

For all experiments with pure diopside, water contents were relatively small, in the order of several hundreds ppm H_2O. However, two different types of infrared spectra were observed for pure diopside. The first type shows one band at high wavenumbers (3650 cm^{-1}) while the second type shows bands at lower wavenumbers (3480-3280 cm^{-1}) (Fig. 3.5-7). The differences in the spectra point towards substitution mechanisms involving different vacancies, which in turn could be the result of different oxide activities in the starting material. Therefore, a separate series of experiments was carried out with starting materials with excess or deficiency of MgO or SiO_2. These experiments yielded diopside with different absorption spectra. Starting materials with low silica activity yielded type I bands, which are therefore likely to be related to Si vacancies. Type II bands form at high silica activity and may therefore be related to Mg or Ca vacancies.

All infrared spectra of the Al-containing diopside show one main absorption band at 3650 cm^1 (Fig. 3.5-8). It means that only one type of substitution mechanism takes place. The water solubility strongly increases with the presence of Al up to 2500 ppm H_2O. Figure 3.5-9 shows the dependence of water solubility on Al content for two different conditions. Preliminary results on temperature dependence of water solubility in Al-bearing diopside show that water solubility decreases with increasing temperature.

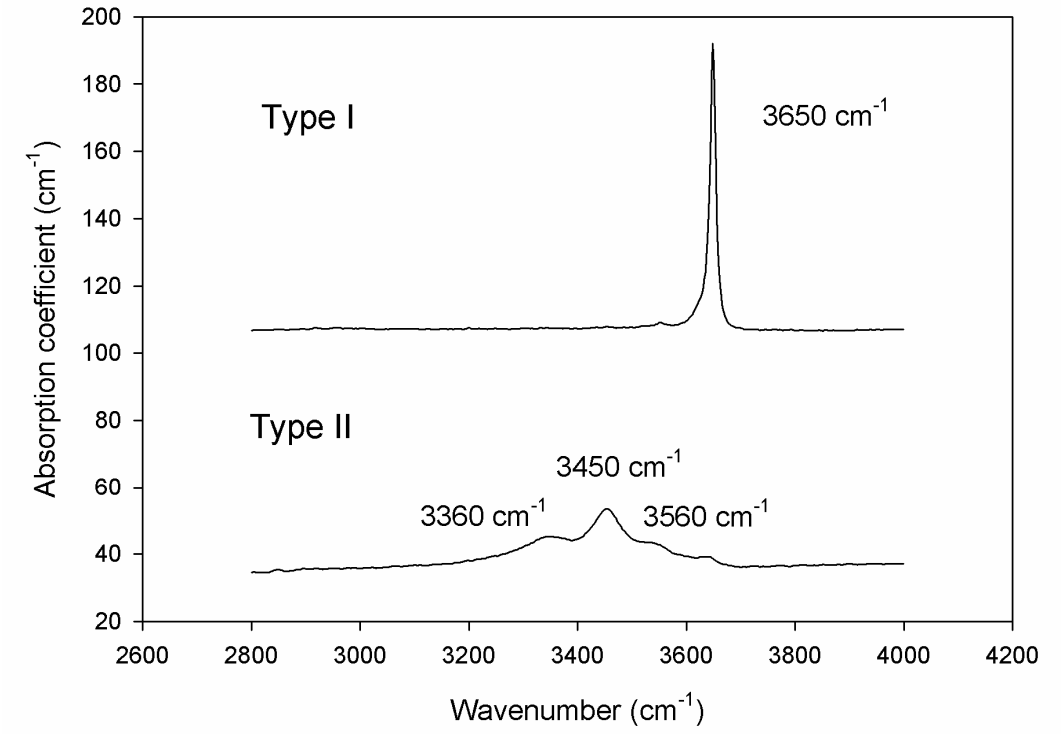

Fig. 3.5-7: Different types of spectra observed from IR measurements of pure diopside crystals.

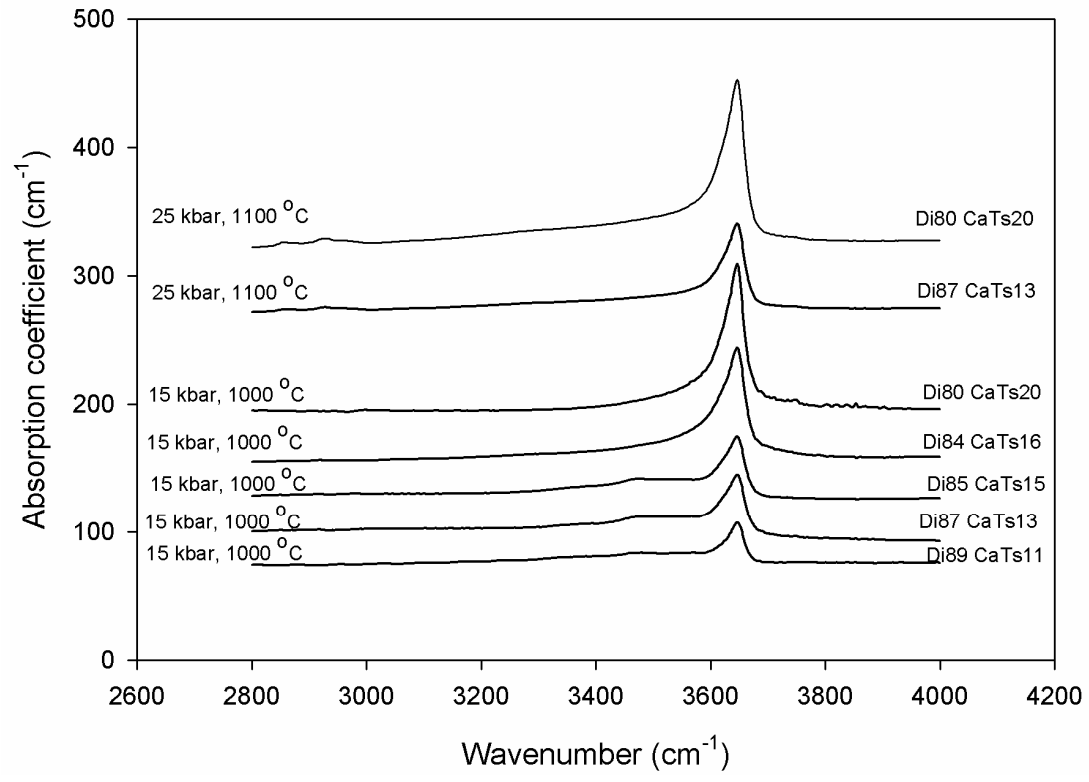

Fig. 3.5-8: Unpolarized FTIR spectra for Al-bearing diopside of different composition.

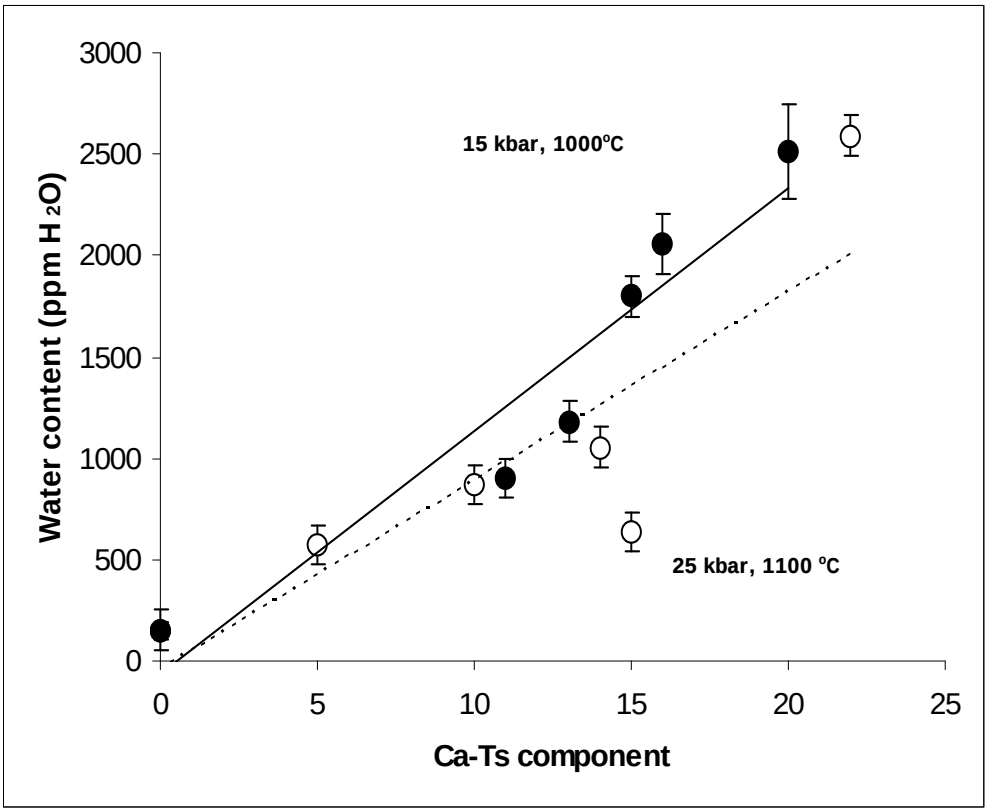

Fig. 3.5-9: Correlation between water solubility and Al content in diopside, expressed as mol.% calcium Tschermak component. Empty circles correspond to experimental conditions of 25 kbar, 1100 °C, filled circles represent experiments at 15 kbar, 1000 °C.

e. *The hydroxyl content of high-pressure minerals coexisting with CH_4-rich fluids (D.J. Frost)*

The high solubility of water in nominally anhydrous minerals such as olivine and wadsleyite is often used to argue that these phases may be the major hosts for water in the deep upper mantle and transition zone. Following this reasoning, the formation of a free water-rich fluid or melt phase in the deep mantle would require significant quantities of water to be present in order to saturate the nominally anhydrous minerals. Analyses of out-gassing fluids and fluid inclusions in mantle rocks infer that volatiles in Earth's interior are, in general, more accurately described by the system C-O-H (or even C-O-S-H), where the activity of H_2O becomes a function of the oxygen fugacity. The oxygen fugacities in the lower regions of the upper mantle and in the transition zone are likely to be quite low and at least 4 log units below the fayalite-magnetite-quartz (FMQ) oxygen buffer. Calculations based on the equations of state of the individual gas species indicate that at these conditions a C-O-H fluid will be CH_4-rich (Fig. 3.5-10). The lower activity of water in the fluid should lower the equilibrium water content of coexisting nominally anhydrous minerals such as wadsleyite making a free fluid phase a viable possibility even at relatively low volatile concentrations.

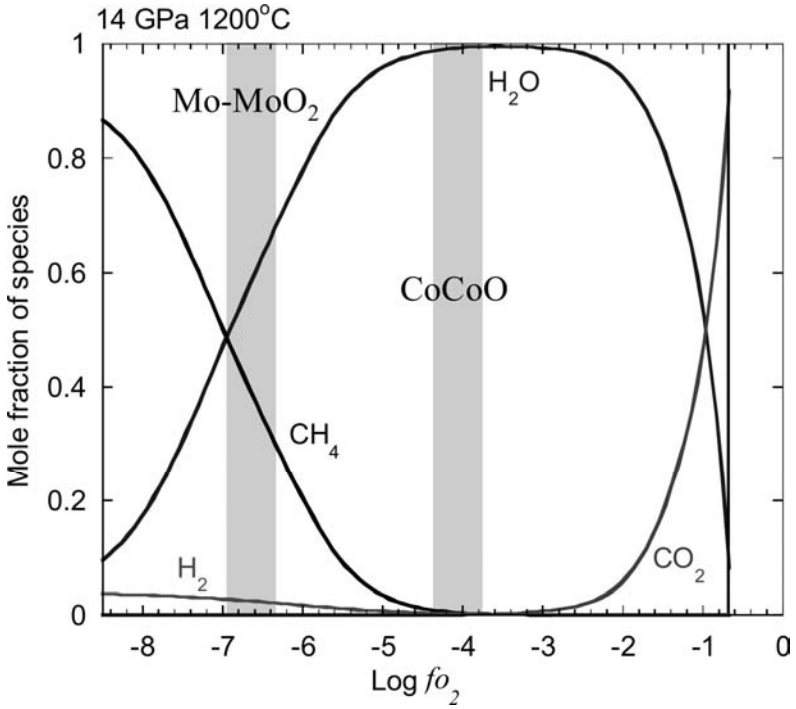

Fig. 3.5-10: Speciation of a C-O-H fluid in equilibrium with diamond at 14 GPa and 1200 °C calculated using equation of state data from the literature. The vertical shaded bands indicate the oxygen fugacities of the $Mo+O_2=MoO_2$ and $2Co+O_2=2CoO$ oxygen buffers.

In this study, experiments have been performed to examine the solubility of water in the minerals olivine and wadsleyite in equilibrium with a C-O-H fluid at oxygen fugacities compatible with the base of the upper mantle and transition zone. The experiments use a standard double capsule technique with an outer capsule containing a redox buffer (Mo-MoO_2 or Co-CoO) plus H_2O and an inner Pt capsule containing San Carlos olivine or garnet compositions in a graphite liner. Samples were equilibrated between 10 and 15 GPa in the 5000 tonne multianvil press at 1200 and 1400 °C. Recovered samples were made into thin sections and analyzed using FTIR spectroscopy and scanning electron microscopy.

When an outer Co-CoO buffer is employed the fluid phase in the inner capsule should be composed almost entirely of H_2O (Fig. 3.5-10). Unpolarised FTIR measurements indicate that olivine samples equilibrated with this fluid at 1200 °C contain the equivalent of approximately 3500 ppm water. This water content is in good agreement with those measured for olivine samples from water-saturated experiments performed in the absence of graphite at similar conditions. This result indicates that the composition of the fluid phase was likely at or close to the water maxima, as shown in Fig. 3.5-10, where H_2O is the major volatile species. In addition to H_2O the fluid also contained a significant dissolved silicate component, which crystallized into a fine mat of loose crystals on quenching. The water concentration of wadsleyite equilibrated at the same oxygen fugacity was too high to measure using FTIR, but similar experiments from the literature performed in the presence of water and analyzed using an ion probe indicate that wadsleyite contains the equivalent of 2.5 wt.% H_2O at these conditions.

For experiments buffered with Mo-MoO_2 the oxygen fugacity in the inner capsule is close to the iron-wüstite oxygen buffer which is compatible with the likely conditions throughout most of the transition zone. At these oxygen fugacities and at 1200 °C the C-O-H fluid should

be a 1:1 mixture of H_2O and CH_4. Wadsleyite recovered from these experiments contains 1700 ppm H_2O (*i.e.*, 0.17 wt.%) compared with 2.5 wt.% at H_2O saturation. The presence of CH_4 therefore dramatically decreases the equilibrium H_2O content of wadsleyite. There is no evidence of quenched silicate material in these experiments implying that CH_4 also suppresses silicate solubility in the fluid phase. Wadsleyite synthesized using the same Mo-MoO_2 buffer but at 1400 °C has a slightly higher H_2O content of 5000 ppm.

An increase in the H_2O content of wadsleyite with temperature in C-O-H experiments is opposite to the behaviour in observed in H_2O saturated experiments, where the solubility decreases strongly with temperature. One explanation for this is that the fluid/melt phase in H_2O saturated experiments contains an increasing dissolved silicate content with increasing temperature, which decreases the activity of H_2O in the fluid and lowers the equilibrium OH^- content of wadsleyite. In the C-O-H system, however, at fixed oxygen fugacity calculations show that the activity of CH_4 decreases with increasing temperature and the H_2O activity therefore increases. As the solubility of silicate in the fluid is still suppressed by the presence of CH_4, the equilibrium water content of wadsleyite increases with temperature. As shown in Fig. 3.5-11, it is possible that at temperatures above 1400 °C the H_2O content of wadsleyite is higher under reducing conditions than at water saturation. Such an effect would have important implications for the storage of water in the transition zone.

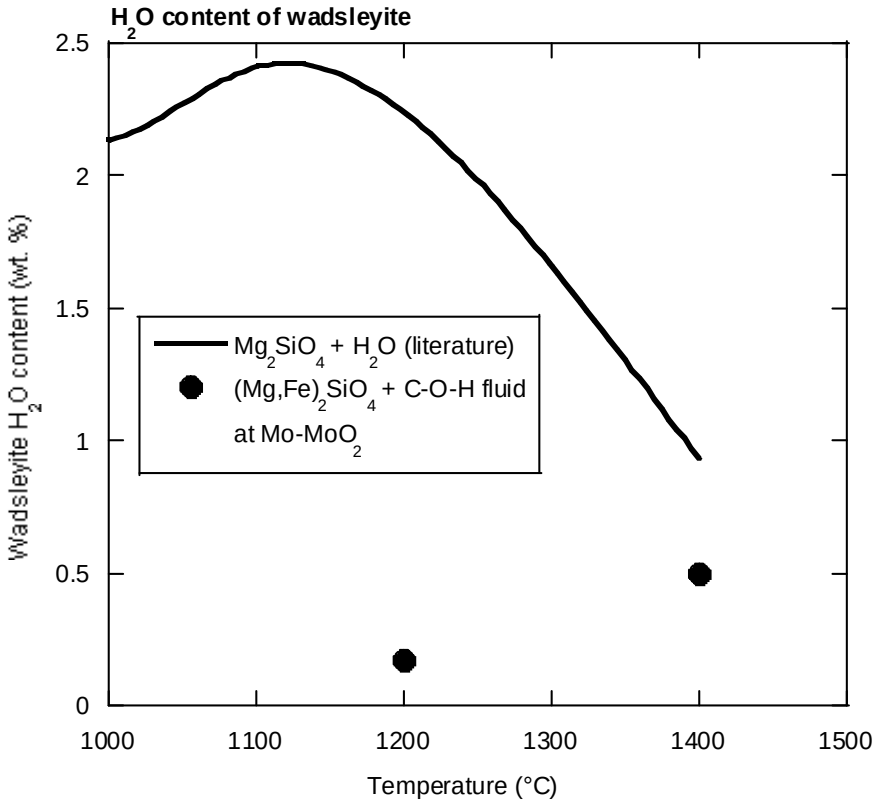

Fig 3.5-11: Water contents of wadsleyite equilibrated with a reduced C-O-H fluid, produced by buffering with Mo-MoO_2 in a double capsule experiment (closed symbols). For comparison, wadsleyite water contents are also shown from samples equilibrated with an excess H_2O fluid phase at similar conditions (solid line).

3.6 Physics and Chemistry of Melts and Magmas

The production of magma (molten or partially molten rock) occurs in the Earth's interior as a consequence of melting reactions that occur as the consequence of changes in pressure-temperature conditions and/or by fluxing with volatiles. The subsequent migration of magma and its crystallization results in chemical differentiation, a process that has been occurring throughout the entire history of the Earth. During the early accretional stage of Earth history, it is likely that a large part of the Earth was melted due to the huge amount of energy that was delivered by impacting bodies. The resulting formation of a deep magma ocean greatly facilitated the efficient differentiation of the Earth into a metallic core and silicate mantle. The subsequent crystallisation of the magma ocean may have resulted in further differentiation and possibly mantle stratification, depending on the dynamics of convection and crystal settling. The first contribution in this section describes the results of computational research on the structural and transport properties of Mg_2SiO_4 liquid (a simple analogue of silicate liquid in a magma ocean) that are important for understanding the dynamics and thermal evolution of magma oceans. The second contribution presents the results of a preliminary experimental investigation of the solvus between Fe-rich and FeO-rich liquids in the Fe-FeO system at high pressure. This system is important for evaluating the oxygen content of the Earth's core. In order to extrapolate results to the extreme pressures and temperatures of the core, a thermodynamic model must be developed for which precise determinations of the solvus are required.

The third contribution concerns the origin of diamonds in the Earth's mantle. Based on an experimental study performed at BGI, it is shown that diamonds from Brazil that contain mineral inclusions must have crystallised from a CO_2-rich melt that originated by the partial melting of carbonated eclogite (a high-pressure metamorphic rock that orginates by subduction of oceanic crust.

Throughout Earth history, the occurrence of volcanism has played a major role in the cycling of volatiles between the Earth's interior and the surface. In particular, magma transports significant quantities of volatiles to the surface and affects the chemistry of the atmosphere and, therefore, climate. In addition, the volatile content of magma determines whether or not volcanic eruptions are explosive in nature. For such reasons, research into the solubility and speciation of volatiles in silicate liquid is important: the two studies presented here are concerned with carbon dioxide and chlorine respectively.

The final contribution in this section presents the preliminary results of a novel *in situ* method for studying the crystallisation behaviour and kinetics in a basaltic glass using a moissanite anvil cell. The aim is to perform such experiments on silicate liquids at higher temperatures and thus derive data that can be used to interpret the textures of volcanic rocks in terms of cooling histories.

a. *Properties of Mg_2SiO_4 liquid under high pressure from molecular dynamics (O. Adjaoud and G. Steinle-Neumann, in collaboration with S. Jahn/Potsdam)*

Melting is a ubiquitous process in planetary interiors and one of the dominant mechanisms for heat transport and chemical differentiation in planets. Knowledge of the properties of silicate liquids is thus essential for understanding a wide range of geophysical phenomena related to the deep Earth and its origin and evolution. As a major mineralogical component of the Earth's upper mantle, forsterite is of considerable importance in controlling its rheological and thermal structure. Mg_2SiO_4 liquid can also be considered as an analogue for the silicate liquid of deep magma oceans that are considered to have existed on terrestrial planets during their early accretional history.

Experimental determinations of structural and dynamical properties of silicate melts at high pressure and temperature are currently difficult. Therefore, computational methods are useful to supplement experimental data in addressing structural and transport properties of silicate melts at high pressure and temperature.

In the present study, we have used large-scale molecular dynamics computer simulations at temperature T=2800 K and pressure up to P=24 GPa to investigate the structure and transport properties of Mg_2SiO_4 liquid. The interactions between the atoms are modeled by an aspherical ion model (AIM). The AIM accounts for polarization and deformation of the ions up to quadrupolar level. The present potential was found to be transferable up to pressures and temperatures conditions of the Earth's lower mantle in solid phases and its accuracy is comparable to results obtained from electronic structure calculations for a range of mineral phases.

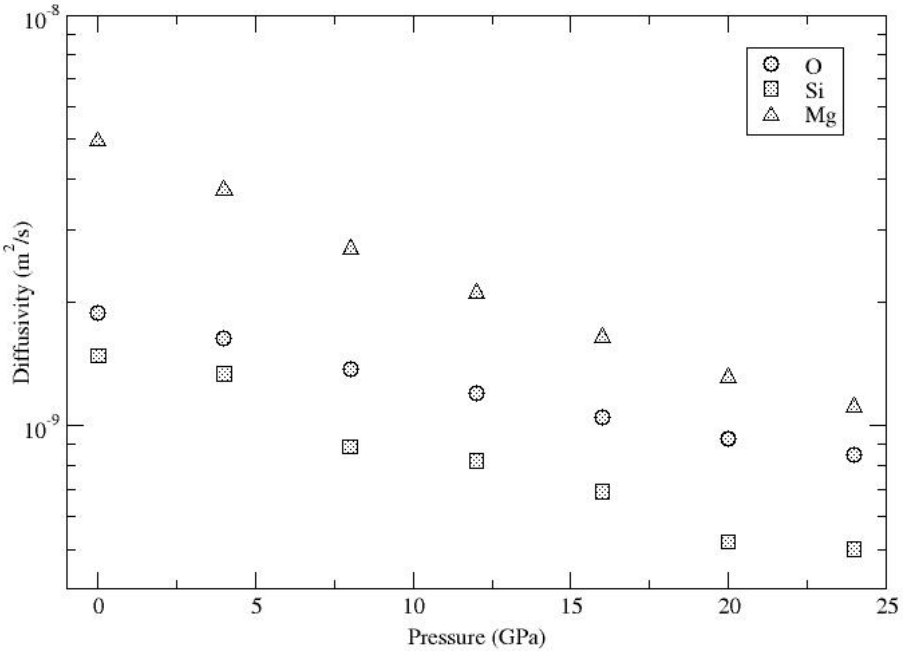

Fig. 3.6-1: Diffusivity as function of pressure of liquid Mg_2SiO_4 at 2800 K.

Molecular dynamics simulations were performed using a cubic simulation box with 2016 ions (288 formula units) and time steps of 1 fs. The system is equilibrated by an isotropic barostat coupled to the thermostat for 50 ps (NPT ensemble) before the production run of 150 ps in NVT is performed. We find that the coordination of Mg and Si as well as the degree of polymerization increase with pressure and there is considerable distortion of MgO_N polyhedra. There is also a large redistribution of the T-O-T (T = Si,Mg) bond angles with pressure. The equation of state of the simulated melt is consistent with experimental data and previous simulations. As we have long run durations for the simulation we were also able to compute reliably self-diffusion coefficients as function of pressure (Fig. 3.6-1). We find that self-diffusion coefficients decrease with pressure for all species and that diffusion coefficient for the network modifier (Mg) is faster than for the network formers (Si, O).

b. *Preliminary in situ determination of the solvus in the Fe-FeO system at 2-5 GPa up to 2800 K (Y. Asahara/Hyogo, D.J. Frost, D.C. Rubie and A. Saikia; H. Terasaki and E. Ohtani/ Sendai, K. Funakoshi/Hyogo, T. Mastuzaki/Misasa)*

The solvus in the Fe-FeO system at 1bar and how it varies with pressure are important for understanding the process of core-mantle differentiation in the Earth and the oxygen content of the Earth's metallic core. However, it is very difficult to determine the solvus using conventional experimental methods because oxygen diffuses very rapidly in liquid metal during quenching at low pressures and high temperatures. *In situ* observations present a possible way to determine the solvus at relatively low pressures, below 10 GPa. Therefore, we have conducted *in situ* solvus determination experiments using the synchrotron X-ray radiography technique at the SPring-8 synchrotron radiation facility in Japan.

We performed experiments using a Kawai-type multianvil press (SPEED1500) combined with an X-ray radiography system at the SPring8 beamline BL04B1. The range of experimental pressure and temperature conditions was 2-5 GPa and 1000-2800 K. We used layered Fe and FeO pellets as the starting material. The bulk composition of starting material was controlled by varying the volume ratio of these two components in the pellets. We used single crystal MgO and h-BN as sample containers. Both of these materials are characterized by high X-ray transparency and stability at high temperatures. Chemical analysis of the recovered samples was conducted with an electron microprobe.

The use of MgO capsules was not successful because they were not mechanically stable and failed to confine the liquid sample. In contrast, when using a BN capsule the Fe-FeO liquids were well confined and we could image the sample inside the capsule up to 2800 K. Representative radiographic images are shown in Fig 3.6-2. During the experiments, we increased the temperature for several bulk compositions until 2 immiscible liquids transformed to a single liquid. To examine quench textures and to check for possible contamination, we also quenched two samples, with bulk Fe:FeO values of 3:2 and 1:4, after

reaching 2173 K. The *in situ* radiography images did not change significantly during quenching in either experiment irrespective of composition. Using a constant composition, we observed the solvus temperature decreasing with increasing pressure.

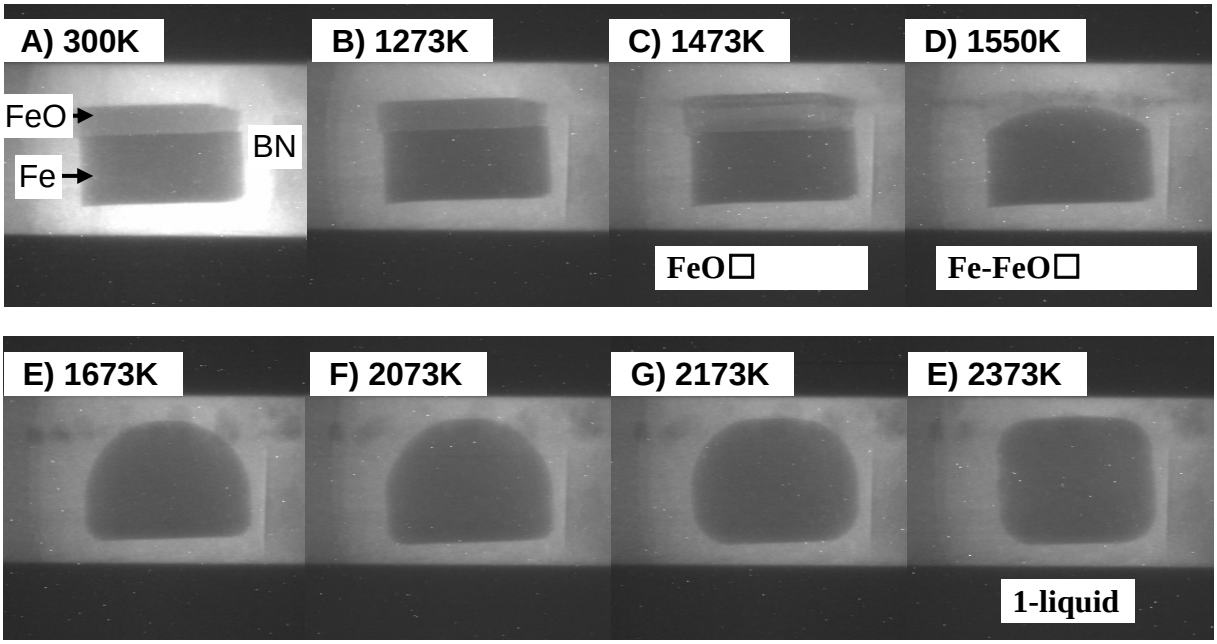

Fig 3.6-2: X-ray radiographic images from a representative *in situ* experiment at 2.7 GPa using a BN capsule

Although the *in situ* experiments appeared to have been successful, a significant problem was identified when checking the quenched samples using the electron microprobe. Both the Fe and FeO quenched liquids were contaminated by reaction with the BN sample capsule and MgO components in the pressure cell. Therefore, in future experiments, the capsule material needs to be modified in order to avoid this problem.

c. *Melting of carbonated, Ti-bearing peridotite and eclogite at 20 GPa: Implications for the formation of $Ca(Ti,Si)O_3$ inclusions in diamond (L. Armstrong/Bristol, S. Keshav and G. Gudfinnsson, in collaboration with M. Walter/Bristol)*

Composite inclusions of coexisting $CaSiO_3$ and $CaTiO_3$ are rare, but have previously been reported in diamonds from Juina, Brazil. They are interpreted as exsolution products of a high-pressure $Ca(Ti,Si)O_3$ perovskite stable in the transition zone of the Earth's mantle based on $CaTiO_3$-$CaSiO_3$ phase relations. Diamond inclusions with 'perovskite' stoichiometry are commonly interpreted as entrapped fragments of solid mantle from the transition zone or lower mantle. In peridotitic or eclogitic bulk compositions, Ca-perovskite is saturated in the

$MgSiO_3$ component because it coexists with majorite or Mg-perovskite. Experimental phase relations have shown that $CaTiO_3$-$CaSiO_3$ perovskite solid solutions at high pressures can dissolve large amounts of $MgSiO_3$, and that this solubility increases with $CaTiO_3$ content. The Juina inclusions are estimated to contain 50-65 mol.% $CaTiO_3$, and yet are remarkably low in $MgSiO_3$ at less than 0.2 mol.%. This makes a subsolidus origin for the inclusions unlikely.

Melts rich in CO_2 have been proposed previously as parental melts from which both diamonds and their mineral inclusions could crystallize at high pressures. Accordingly, multianvil experiments were performed at BGI to study the melting phase relations of model carbonated peridotite (CMS-Ti-CO_2) and eclogite (CMAS-Ti-CO_2) at 20 GPa. In model peridotite at 1525˚C, we located the univariant curve along which the assemblage Ca-perovskite + ringwoodite + magnesite + majorite + melt is produced. Ca-perovskite contains 28 wt.% $CaTiO_3$ and coexists with a Ca and CO_2-rich melt (Ca/Ca+Mg = 0.77). In model eclogite, an even more Ti-rich Ca-perovskite is produced (48 wt.% $CaTiO_3$) in equilibrium with a similar melt (Ca/Ca+Mg of 0.71), majorite, and magnesite (Fig. 3.6-3). In both cases, the $MgSiO_3$ component is virtually absent in the liquidus Ca(Ti,Si)-perovskite phase. The Ti-rich diamond inclusion compositions are well matched by perovskite crystallized from melt produced from a model eclogite source. We suggest that Juina diamonds and CaTi-perovskite crystallized syngenetically from a melt derived from carbonated eclogite in the transition zone.

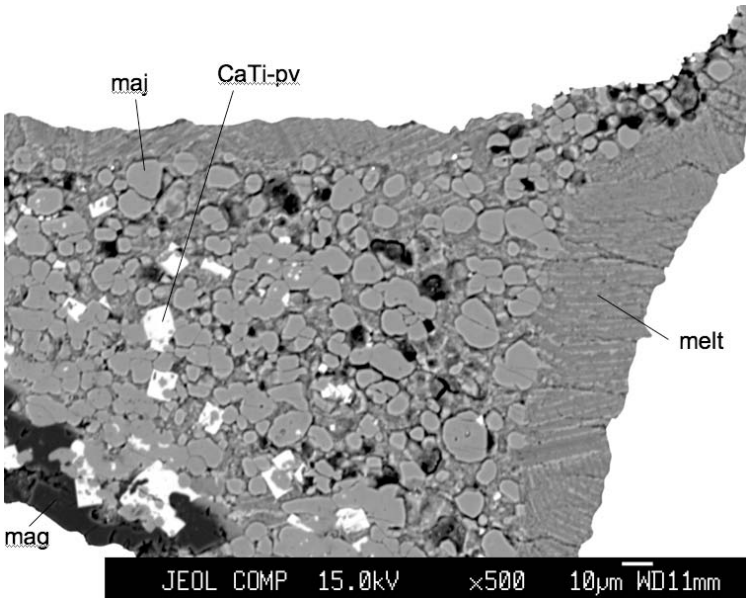

Fig. 3.6-3: Backscattered electron image of model carbonated eclogite quenched from 20 GPa and 1475˚C. Calcic CO_2-rich melt did not quench to a glass. Abbreviations are:- melt: quenched melt; maj: majorite; CaTi-pv: $Ca(Ti,Si)O_3$ perovskite; mag: magnesite.

d. *The speciation of carbon dioxide in silicate melts from in situ infrared measurements (A. Konschak and H. Keppler)*

Although important for understanding the volatile contents of magmas, the speciation of CO_2 in silicate melts has never been measured directly. Here, we present the first direct measurements of CO_2 speciation at temperatures above 1000 °C and pressures up to 5 GPa in various silicate melt compositions with silica contents ranging from 54 to 70 wt.%, thus

covering the entire NBO/T range of most natural magmas. We used three silicate melt compositions corresponding to natural melts with dacite, phonolite and alkali-basalt (shoshonite) compositions and also investigated one synthetic alkali silicate melt composition because of its low melting point.

We measured CO_2 speciation in silicate melts *in situ* by infrared absorption spectroscopy in an externally heated diamond anvil cell with thin type IIa diamonds to minimize absorption due to the anvils. In order to overcome strong thermal black body radiation of the hot sample, we used an intense infrared beam from the ANKA synchrotron source in Karlsruhe and focused it on a spot with 40 µm diameter.

In the spectra of the synthetic alkali silicate glass and the corresponding melt (NBO/T=1) only the peak of carbonate is seen up to the highest temperatures of 1000 °C. Molecular CO_2 cannot be detected. Therefore we conclude that in the alkali silicate glass, all CO_2 is dissolved in the form of carbonate groups. However, the integral intensity of the carbonate peak decreases with increasing temperature, indicating a decrease of the extinction coefficient of carbonate.

Both CO_2 species - molecular CO_2 and carbonate - are present in the glass with dacite composition (NBO/T=0.1). On the other hand, the spectra of the corresponding dacite melt shows a strong peak of molecular CO_2 at 1000 °C, while the carbonate peak has nearly disappeared, suggesting that molecular CO_2 is the dominant species in dacite melt at high temperature. Also in phonolite melt composition (NBO/T=0.2) both CO_2 species are present in the glass. Both the molecular CO_2 and carbonate peaks decrease with increasing temperatures up to 700 °C. However above 700 °C the molecular CO_2 peak increases up to the maximum temperature of 1000 °C while the carbonate peak decreases further (Fig. 3.6-4).

Carbonate is the only CO_2 species in basaltic melt of shoshonite composition (NBO/T =0.4) in contrast to dacite and phonolite glasses. Even at temperatures of 1050 °C no molecular CO_2 was observed and the carbonate peak remained as the only CO_2 species feature.

The quantitative evaluation of speciation was complicated by the fact that the extinction coefficients of both molecular CO_2 and of carbonate were found to significantly decrease with temperature in all melt compositions. This decrease is related to changes in the population of the vibrational states of CO_2 and carbonate with temperature. At room temperature, nearly all of the CO_2 molecules and all of the carbonate groups are in their vibrational ground states. At elevated temperatures, some of the low frequency vibrational states become significantly populated, and the population of the ground states decreases. Since the measured infrared absorption corresponds to the transition between the ground state and higher excited states, the reduced population of the ground state reduces the probability of the transition and therefore also the extinction coefficient. Accordingly, we calculated the population of all states in the CO_2 molecules and carbonate groups according to the Boltzmann distribution and we asumed that the extinction coefficient decreases with temperature in proportion to the population of the ground state. With this assumption, we calculated concentrations of

molecular CO_2 and carbonate as a function of temperature in all melt compositions. From these data, we determined the equilibrium constants for the speciation reaction $CO_{2(molecular)} + O^{2-} = CO_3^{2-}$ and derived reaction enthalpies ΔH.

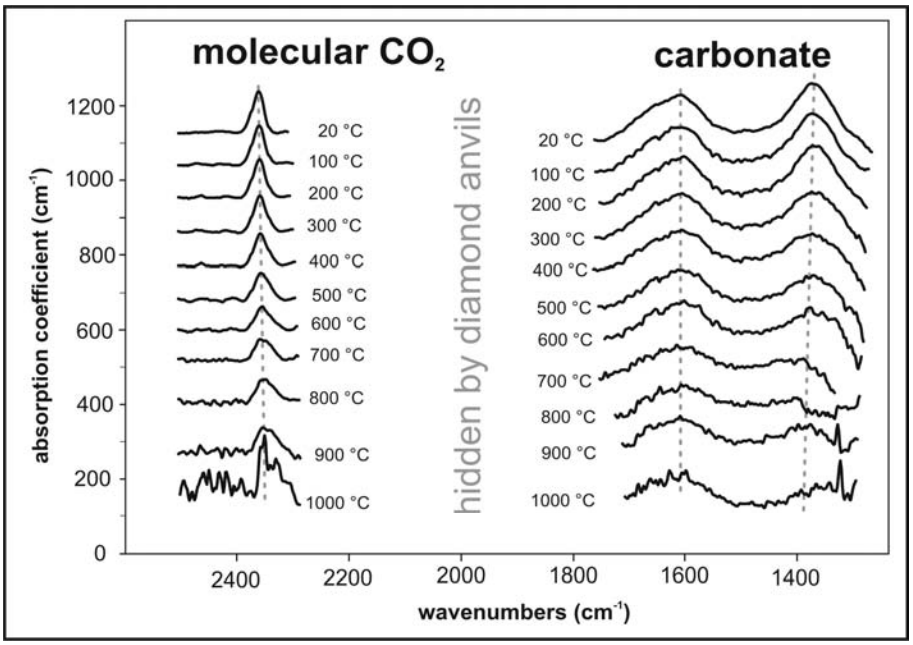

Fig. 3.6-4: *In situ* infrared spectra of CO_2 species in phonolite melt composition up to 1000 °C and 5 GPa.

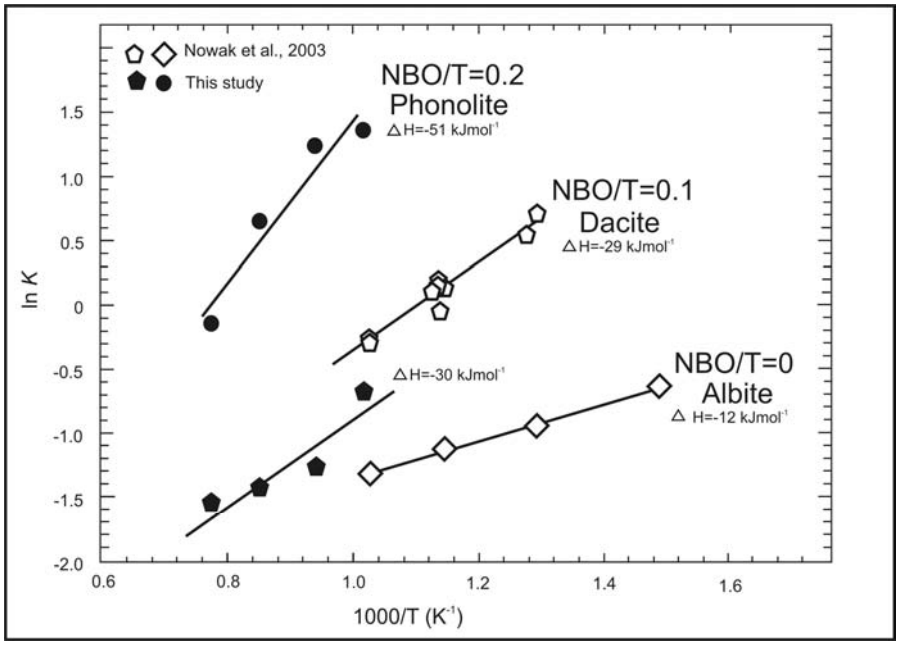

Fig. 3.6-5: Temperature dependence of the equilibrium constants K of the reaction $CO_{2(molecular)} + O^{2-} = CO_3^{2-}$ obtained for different compositions from *in situ* measurements (this study, filled symbols) and from previous annealing experiments (open symbols) suggesting a compositional dependence of the reaction enthalpy.

From our data, we can show that CO_2 dissolves in depolymerized silicate melts such as basalts exclusively as carbonate even at temperatures higher than 1000 °C; this contrasts with previous predictions based on annealing experiments. In dacitic and phonolite melt, the molecular CO_2 to carbonate ratio increases at high temperatures and the equilibrium between CO_2 and carbonate is strongly temperature-dependent, with the enthalpy ΔH for the reaction $CO_{2(molecular)} + O^{2-} = CO_3^{2-}$ of about -30 kJ/mol for dacite and -50 kJ/mol for phonolite composition, suggesting a strong dependence of ΔH on melt composition, as expressed by NBO/T.

Our data show that the increase of CO_2 solubility with melt depolymerization is a direct consequence of the stabilization of carbonate in the melt. The measured equilibrium constants between carbonate and molecular CO_2 in the melt are therefore key parameters in any general model of CO_2 solubility that is applicable for a wide range of melt compositions. Such models are essential for predicting magmatic degassing and mechanisms of volcanic eruptions.

e. *Chlorine solubility in polymerized aluminosilicate melts (V. Stagno and D. Dolejš)*

Chlorine is the most important halogen in aqueous fluids ranging from sea water in subduction zones to fluids in magmatic, porphyry and epithermal environments along convergent plate boundaries. In order to characterize the geochemical cycle of chlorine, the pressure and temperature dependence of chlorine solubility in silicate melts must be understood. Previous experimental studies using hydrous chlorine-bearing melts have yielded inconsistent results because the chlorine solubility is significantly affected by activity-composition relationships in the saturating vapor, brine or supercritical fluid. As a consequence, primary effects of pressure, temperature or melt composition have remained unresolved.

In this study, we have experimentally determined chlorine solubility in five anhydrous aluminosilicate melts at 1100-1600 °C and up to 20 kbar. These temperatures lie above the silicate liquidus of all melt compositions studied whereas the pressure range was chosen to accurately capture the pressure dependence of solubility. The starting compositions were: albite (AB-1), albite-quartz eutectic, $Ab_{59}Qz_{41}$ ($NaAlSi_6O_{14}$, AQ-1) and its peralkaline and peraluminous derivatives with nominal alumina saturation index, ASI = 0.6 (AQ-4), 0.8 (AQ-2) and 1.2 (AQ-3), respectively. All starting glasses were doped with 5 wt.% NaCl as a chlorine source. Experiments were performed in quenching furnaces (1100-1575 °C and 1 atm) and piston cylinder apparatus (1400 °C and 5-20 kbar). All runs were saturated with molten NaCl, forming an immiscible phase. Random checks of final H_2O concentrations in the quenched liquid were conducted by FTIR spectroscopy and have revealed less than 0.4 wt.% H_2O.

In all studied melts, the chlorine solubility appears to be independent of temperature but increases significantly with pressure (Fig. 3.6-6). The absence of temperature dependence implies that the dissolution of NaCl into the silicate network is entropic and is not associated

with a change in enthalpy. This situation is compatible with NaCl remaining completely associated (no interaction with the silicate network) and being passively incorporated as a molecular species in the melt network. For all melt compositions, the chlorine solubility increases by 0.044-0.062 wt.% Cl/kbar, leading to an increase by a factor of 3-4 over a 20-kbar pressure range. The pressure dependence is described by the volume of dissolution, $\Delta_r V$, and the isothermal compressibility of NaCl, β, in the silicate melt as follows:

NaCl (molten salt) = NaCl (solute)

$$0 = \Delta_r S + \int_1^P \Delta_r V dP / RT + \ln x$$

where

$$\Delta_r V = \Delta_r V_1 \cdot e^{-\beta(P-1)}$$

Experimental solubilities for individual melt compositions yield $\Delta_r V$ = -2.82 to -1.77 J mol^{-1} bar^{-1} and β = (8.3 to 13.5)·10^{-5} bar^{-1}. These data imply a volume decrease by 45-75 % when compared to pure molten salt at 1400 °C and 10 kbar.

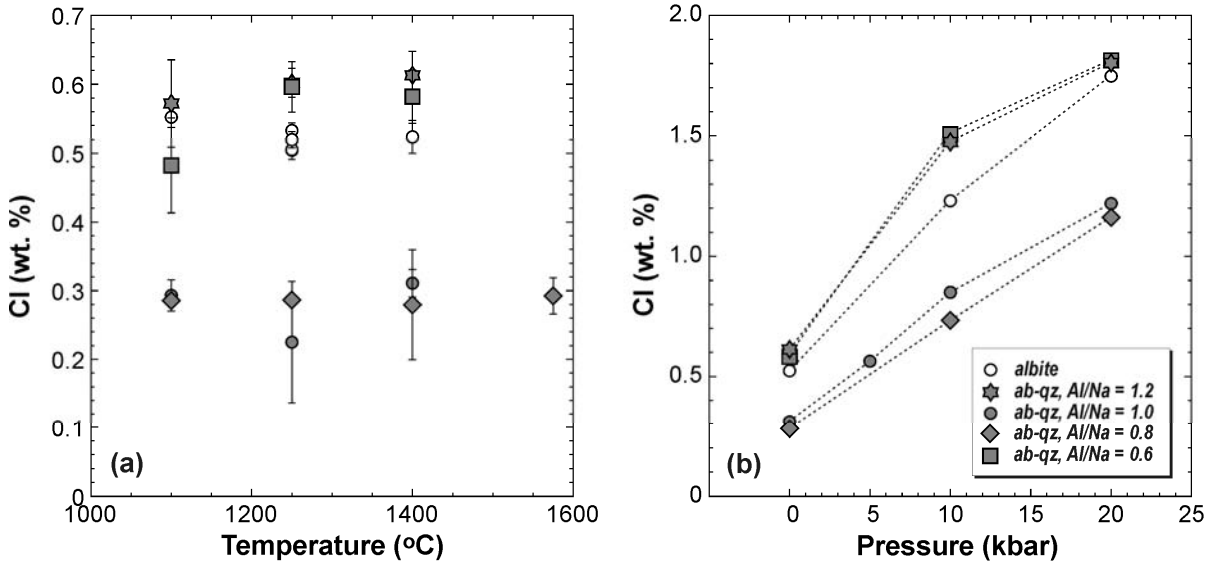

Fig. 3.6-6: Chlorine solubility in sodium aluminosilicate melts: (a) temperature dependence at 1 atm; (b) pressure dependence at 1400 °C.

The effect of melt composition on the chlorine solubility was studied along two joins: $NaAlO_2$-SiO_2 binary and peralkaline $NaAlSi_6O_{14}$ – peraluminous $NaAlSi_6O_{14}$ binary (Fig. 3.6-7). At 1400 °C the chlorine solubility in the $NaAlO_2$-SiO_2 system increases with the aluminate concentration. The magnitude of the solubility increase increases with pressure as follows: 2.5 mole Cl/mole $^{[T]}$Al at 1 atm, 4.2 mole Cl/mole $^{[T]}$Al at 10 kbar and 5.7 mole

Cl/mole $^{[T]}$Al at 20 kbar, where [T] indicates tetrahedral coordination. In the absence of temperature dependence of chlorine solubility, this effect cannot be related to configurational mixing of Cl^- and $[AlSi_3O_8]^-$ units at the sodium sites in the melt. In contrast, the pressure dependence suggests that chloride species compete for free volume in the silicate tetrahedral framework.

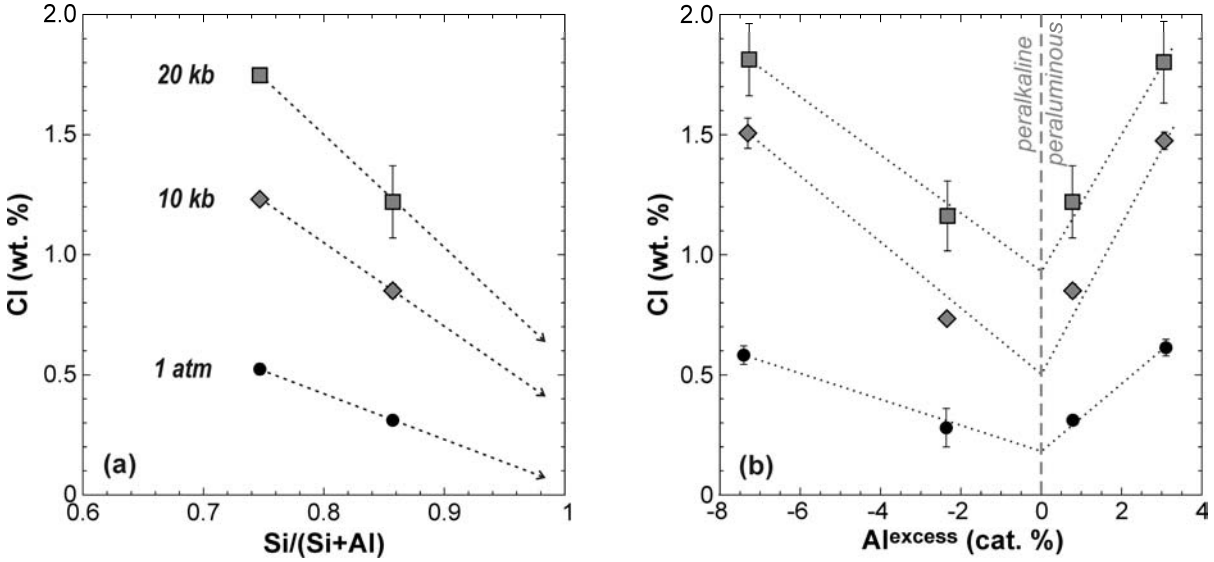

Fig. 3.6-7: Variations of chlorine solubility in sodium aluminosilicate melts at 1400 °C: (a) Chlorine solubility vs. Al/(Al+Si) in the $NaAlO_2$-SiO_2 system; (b) Chlorine solubility vs. Al^{excess} in the $NaAlSi_6O_{14}$-Na_2O-Al_2O_3 system.

In the $NaAlSi_6O_{14}$-Na_2O-Al_2O_3 system with NaCl, the chlorine solubility exhibits a minimum near the subaluminous composition where molar Al/(Na-Cl) ~ 1 (Fig. 3.6-7b). It increases in both peralkaline and peraluminous melts. In the peralkaline compositional space, the chlorine solubility increases by 0.07 and 0.16-0.18 mole Cl/mole $^{[M]}$Na at 1 atm and 10-20 kbar, respectively, whereas in the peraluminous space, it increases by 0.22 and 0.46-0.51 mole Cl/mole $^{[M]}$Al, at the same conditions, respectively, where [M] indicates a network modifier. It is noteworthy that magnitudes of solubility increases differ by a factor of 2.8-2.9 in peraluminous and peralkaline compositions, which is comparable to a charge ratio of Al/Na = 3. Hence the whole dataset can be interpreted by a simple quasi-ternary system, SiO_2-$NaAlO_2$-MO, whereby the charge equivalence is treated by converting the composition variables to anion units. In the thermodynamic model, we expand the entropy and volume contributions to become functions of composition as follows:

$$\Delta_r S = x_{SiO_2} \cdot \Delta_r S_{SiO_2} + x_{NaAlO_2} \cdot \Delta_r S_{NaAlO_2} + x_{MO} \cdot \Delta_r S_{MO}$$

$$\Delta_r V = x_{SiO_2} \cdot \Delta_r V_{SiO_2} + x_{NaAlO_2} \cdot \Delta_r V_{NaAlO_2} + x_{MO} \cdot \Delta_r V_{MO}$$

Individual parameters have been calibrated for the temperature range of 1100-1600 °C and the pressure range of 0.001-20 kbar (Table 3.6-1) and allow calculation of chlorine solubility in peralkaline to peraluminous sodium aluminosilicate melts.

anion units	SiO_2	$NaAlO_2$	MO
$\Delta_r S_i$ (J mol^{-1} K^{-1})	7.085	1.109	-33.469
$\Delta_r V_i$ (J mol^{-1} bar^{-1})	-2.692	-0.462	13.063
β (bar^{-1})		$1.23 \cdot 10^{-4}$	

Table 3.6-1: Thermodynamic model parameters for the SiO_2-Na_2O-Al_2O_3-NaCl system

In summary, the chlorine solubility in sodium aluminosilicate melts exhibits strong pressure as well as concentration dependences. For all melt compositions, chlorine solubility increases by 0.044-0.062 wt.% Cl/kbar. This leads to chlorine solubilities of 1.7 and 1.2 wt.% Cl in albitic and $NaAlSi_6O_{14}$ melts at 20 kbar, respectively. The chlorine solubility increases both with the progressive substitution of aluminium in the silicate network and the concentration of network modifiers. Changing the alumina saturation index from unity (subaluminous) to 0.6 or 1.2 have comparable effects; it leads to a solubility increase by a factor of 2-3 at 1 atm and by a factor of 1.5 at 20 kbar. These experimental results have the following geological applications: (1) chlorine solubility strongly decreases with decreasing pressure, which increases chloride activity and promotes halide saturation during magma ascent, and (2) variations in the alumina saturation index during magma differentiation have a substantial effect on chlorine solubility. The activity of chlorides, partitioning coefficient of chlorine, $D^{fl/melt}$, and the fluid salinity are predicted to increase towards subaluminous melts.

f. *Observation of crystallization processes in basaltic glass by in situ heating experiments with the moissanite anvil cell (F. Schiavi, N.P. Walte and H. Keppler)*

Many experimental studies of time-dependent geological processes occurring at high temperature, such as melt crystallization, have been carried out to investigate the formation of magmatic textures. However, in conventional experimental setups the experimental runs have to be quenched to investigate intermediate stages of crystallization and texture formation. *In situ* experimental investigation of these ongoing processes, directly and continuously observed through the optical microscope, may help us to better understand the evolution of crystallizing magmatic bodies and the texture of igneous rocks. For this purpose, a new experimental technique using heated moissanite windows is being developed that enables small thin section-like samples to be heated and to be simultaneously observed *in situ* with an optical microscope.

We aim to examine and interpret the textural development of basaltic glass undergoing heating and cooling processes, in order to unravel the kinetics of nucleation and growth of mineral phases in basaltic melts and provide direct textural evidence of variations in crystal shape, crystal size, and degree of crystallinity as a function of growth rate, nucleation rate and melt composition. These parameters in turn are controlled by time, temperature, diffusion of chemical components, reactions at the crystal-melt interface, degree of undercooling of the system and latent heats of fusion and crystallization.

In our preliminary research work we have performed heating experiments on chips (volume ≤ 0.4 mm^3, maximum diameter of 2 mm and 100 µm in thickness) of basaltic glass with shoshonitic composition up to a temperature of 1200 °C. During the experiments the minimum temperature required for the nucleation of plagioclase crystals varied from 700 °C to 900 °C. Plagioclase crystal growth was monitored at constant temperature (900 °C) for a ~ 10 h time-span (Fig. 3.6-8). The beginning of crystallization was characterized by the formation of plagioclase clusters (Fig. 3.6-8a) that grow until the complete sample consists of a dense intergrowth of elongated crystals (Fig. 3.6-8d). The growth rate has been estimated to lie between 10^{-6} and 10^{-7} cm/s based on the time intervals and the length changes of individual plagioclase crystals observed in successive images of a time-lapse movie that was taken during the experiment. Notably, the intersertal texture showed by the sample after a period of ~ 2 h at 900 °C (Fig. 3.6-8d) closely resembles the texture of natural basaltic rocks.

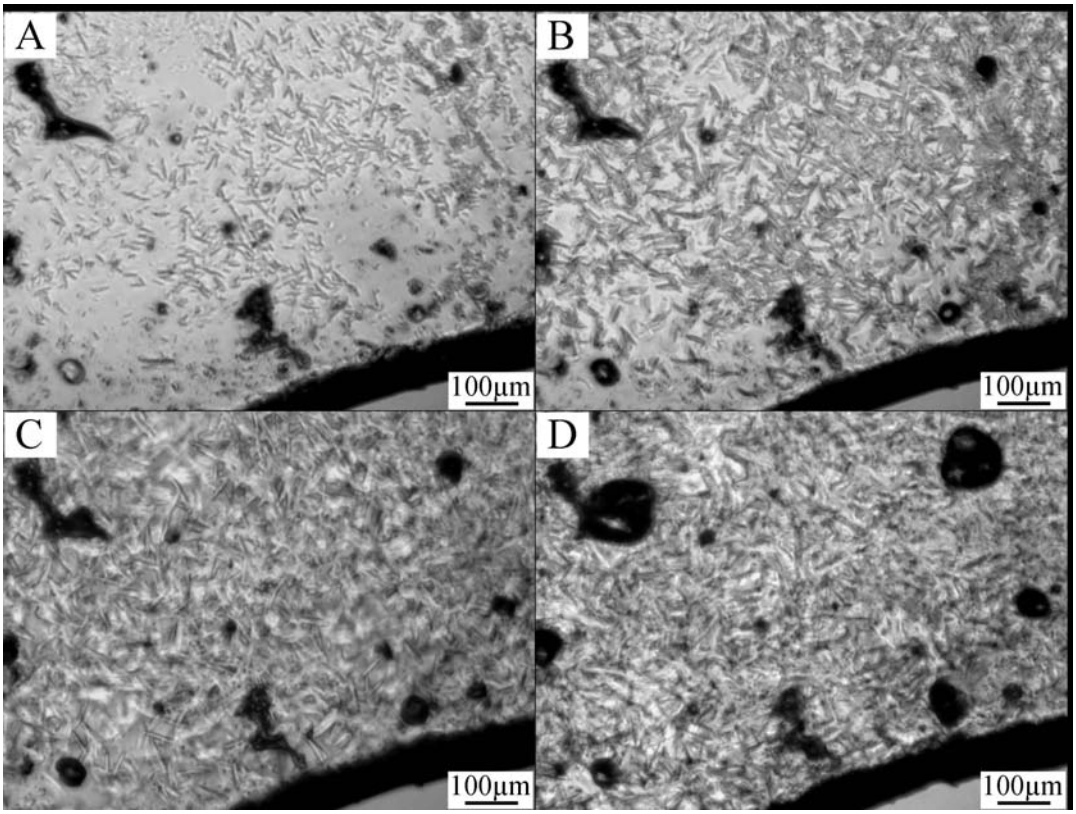

Fig. 3.6-8: Four steps of a time-lapse movie (A: t=0 min; B: t=40 min; C: t=80 min; D: t=150 min) showing the crystallization of plagioclase from a natural basaltic glass during a heating experiment at 900 °C.

In the initial stage of growth, plagioclase laths were characterized by dominant acicular shapes and subordinate prismatic habits; the longest single crystals measured about 200 µm. We observed that a longer heat treatment (> 3 h) of the sample at 900 °C and a further increase of the temperature up to 1200 °C, reached with heating rates of 1 or 2 °C/min, caused some changes in the sample texture: (i) most of the plagioclase crystals acquired prismatic shapes because of the increase of the width/length ratio with time; (ii) agglomeration occurred and contributed to crystal growth, suggesting the occurrence of Ostwald ripening; (iii) an increasing amount of dark-colored melt progressively filled the spaces between plagioclase crystals.

Our preliminary results suggest that heat treatment of a basaltic glass even below the solidus at 700-900 °C can produce apparently magmatic textures that resemble those of volcanic rocks. Subsequent work with the moissanite cell aims to increase and stabilize experimental temperatures above the basalt liquidus (> 1200 °C) so that texture development in magmatic rocks during solidification and melting can be better understood.

3.7 Rheology

The interior of the Earth is governed by dynamic processes which find their most prominent expression in phenomena like earthquakes or volcanic eruptions as well as the movement of lithospheric plates or the formation of mountain chains. The deformation behaviour of Earth materials is determined by their rheology, that is, their response to mechanical stresses. The rheology of minerals and rocks are described by flow laws which relate the applied stress to the deformation rate. Flow laws can be determined in mechanical tests in the laboratory, but the number of variables is rather large. Besides external parameters such as temperature, pressure, and fugacity/activity of various chemical components also intrinsic materials properties such as crystalline defects and crystallographic preferred orientations (texture) have to be taken into account. In addition, plastic deformation of a material will also change its physical properties and especially their orientational dependence (anisotropy). Anisotropic behaviour of the Earth's interior can be detected in geophysical measurements and then interpreted with the help of results from experimental rock deformation.

Deformation experiments at BGI have been focussed around the D-DIA multianvil press which allows to perform deformation in axial compression or direct shear at GPa pressures and high temperatures. The deformation behaviour of high pressure minerals such as coesite, aragonite or ringwoodite which is practically unknown up to now, can be explored with this type of apparatus. Preliminary results indicate that dislocation creep is the preferred deformation mode under experimental conditions and that therefore anisotropic rock fabrics are to be expected in these minerals of the upper mantle and transition zone. Minerals of the lower mantle and the core-mantle boundary region are not stable at the pressures of the D-DIA press and one has to resort to analogue materials. In the case of the phase transition from perovskite to post-perovskite, deformation experiments of the analogue material $CaIrO_3$ indicate that the phase transformation under deviatoric stress will produce a different pattern of anisotropy than pure deformation of the perovskite or post-perovskite phase. This may explain the variation of anisotropy observed near the CMB in seismic measurements.

The rheology of eclogite is critical for the behaviour of subducting slabs as well as for the formation of high pressure terranes which are found in mountain belts around the world. The strength of eclogite is largely governed by the mechanical behaviour of omphacite which is still poorly understood. Deformation experiments of omphacite in the D-DIA show that all the deformation mechanisms (slip systems etc.) observed in natural omphacites can also be reproduced experimentally. Diamond is likely the most important mineral in high pressure research. However, very little is known about its plastic deformation behaviour at elevated temperatures. Preliminary experiments at 4 to 6 GPa and 1800 °C in the D-DIA press show that plastic deformation processes such as activation of slip systems as well as pressure solution and precipitation can be induced in diamond at these high temperatures.

a. *Transition textures in $CaIrO_3$: Reconciling experiments with seismic evidence in the core-mantle region (N. Walte, F. Heidelbach and D.J. Frost)*

The existence and the seismic properties of the D" layer have been explained by a phase transition from (Mg,Fe)SiO_3 perovskite (pv) to a post-perovskite phase (ppv) that occurs at a pressure of approximately 125-130 GPa above the core-mantle boundary. One imporatnt observation in the D" layer is a shear wave splitting that usually results in fast horizontally polarized S-waves and slower vertically polarized S-waves ($V_{SV}<V_{SH}$). Because of the anisotropic ppv crystal structure it was suggested that the shear wave splitting could be explained by a lattice preferred orientation (LPO) induced by deformation. Experimental deformation studies with $MgSiO_3$ and $MgGeO_3$ ppv in a diamond anvil cell (DAC) indicated (100) and (110) slip planes. Modelling of the seismic anisotropy resulting from this LPO yielded fast vertically polarized shear waves ($V_{SV}>V_{SH}$), incompatible with present seismic observations in the D" layer. On the other hand, controlled deformation experiments with the analogue substance $CaIrO_3$ resulted in a dominant (010)[100] slip system, which produces a good agreement with the shear wave splitting in the D" layer. One major difference between the two sets of experiments is that the samples in the DAC deformation experiments all transformed to ppv during deformation. To reconcile results of seismic measurements and $CaIrO_3$ deformation studies with $MgSiO_3$/$MgGeO_3$ DAC deformation experiments, we performed $CaIrO_3$ analogue experiments that simulate the conditions of the DAC experiments by crossing the perovskite-post-perovskite phase boundary during axial shortening. All experiments started in the pv field at 1450 °C and 1 GPa; the pv-ppv stability field boundary was crossed by lowering the temperature to 1200 °C (Fig. 3.7-1).

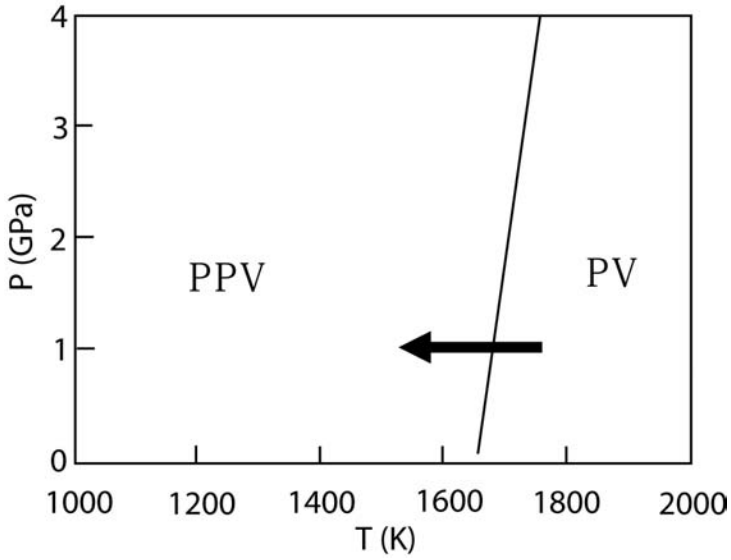

Fig. 3.7-1: $CaIrO_3$ phase diagram; experiments start in the perovskite (PV) field, temperature is lowered during deformation and the sample enters the post-perovskite (PPV) field as shown by the black arrow.

The resulting samples consist of a mixture of ppv and metastable pv. Relict pv crystals do not display a discernible texture, which suggests that they are either deformed by grain boundary sliding assisted diffusional creep or that several active slip systems prevent the formation of a

strong LPO. In the experiments that were deformed in the ppv field for less than 4h, EBSD measurements either show no discernable LPO or resulted in a LPO with an alignment of (100) and (110) poles approximately perpendicular to the compression direction (Fig. 3.7-2). Experiments that were deformed in the ppv field for longer than ca. 4 h show an oblique alignment of (100)/(110) and of (010) with regard to the direction of greatest compression (Fig. 3.7-2). Experiments that were deformed in the ppv field at the beginning result in an alignment of (010) poles parallel to the compression direction, which confirms previous deformation experiments. Our results indicate that a pv-ppv phase transition during deformation produces a different LPO than deformation in the ppv stability field. This difference cannot be explained by texture inheritance from the overgrowth of pv since the pv does not aquire a LPO by deformation, the transition texture of ppv must therefore be produced by the non-hydrostatic stress or strain during ppv growth.

We therefore interpret the LPO in the shorter experiments as a transformation texture that forms during the pv-ppv phase transition, which is slowly rotated by subsequent deformation in the ppv field. Thus, we are able to distinguish between deformation- and transformation-induced LPO in our ppv analogue and we predict that extended deformation of $MgSiO_3$ in the ppv field should eventually produce a LPO with the b-axis parallel to the shortening direction.

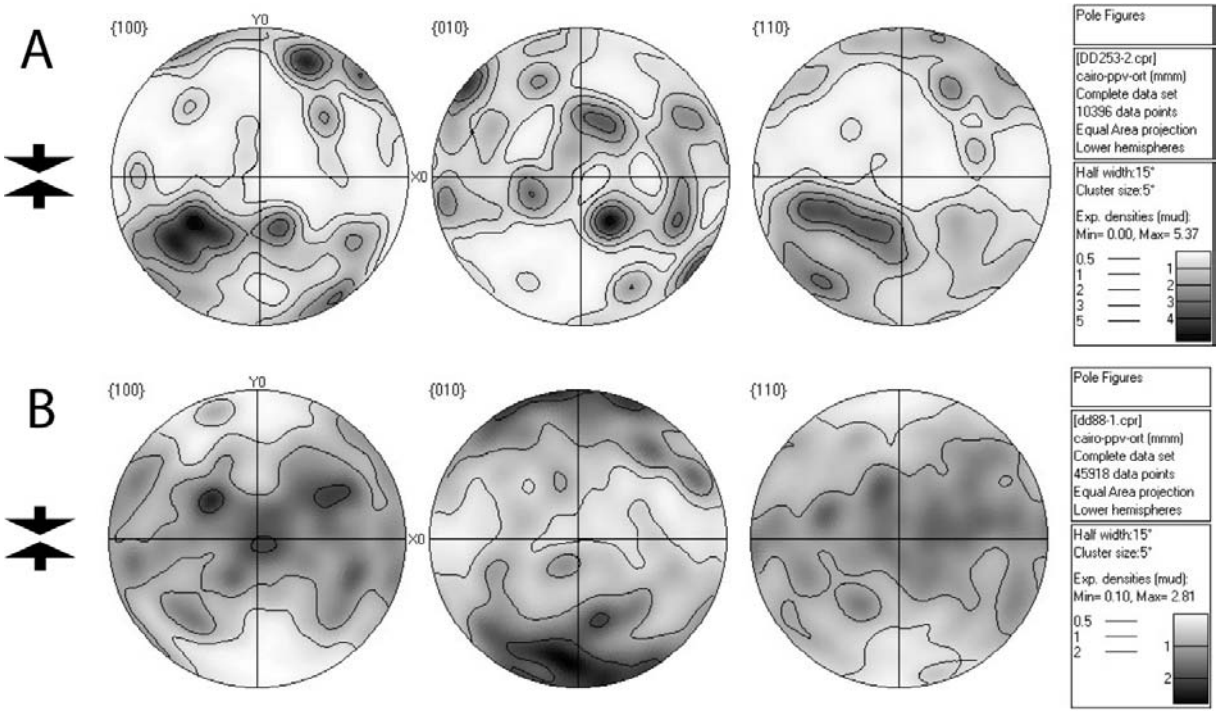

Fig. 3.7-2: Pole figures of deformation experiments with a pv-ppv phase transition (a) and experiments that deformed in the ppv field (b) of $CaIrO_3$. (a) shows an orientation of the a-axis roughly parallel to the compression axis and a girdle of the b-axis roughly parallel to the shear plane. This is interpreted as a transformation texture. (b) displays a typical deformation texture with the b-axis oriented parallel to the axis of greatest compression.

In the D” layer both texture types of ppv may occur: the transformation-type LPO in regions where material descends from the pv stability field, and the deformation-type LPO where horizontal shear flow is dominant. These regions will also have different seismic anisotropy signatures and could be distinguished seismologically.

b. *Determination of Burgers vector in perovskite and post perovskite in $CaIrO_3$ (N. Miyajima, N. Walte, F. Heidelbach and D. J. Frost)*

Knowledge of the deformation mechanisms of materials at high pressures and high temperatures are indispensable for understanding the rheology of the Earth’s mantle. However, in order to constrain the mechanisms, the deformation microstructure needs to be investigated in well-controlled deformation experiments up to the relevant pressure (*P*) and temperature (*T*) conditions. On the assumption that the deformation is controlled by dislocation glide under the extreme *P-T* conditions of the Earth, the determination of the Burgers vector is the first approach in clarifying the relation between macroscopic strains and microscopic deformation textures.

The thickness-fringe contour method for the complete determination of the character of a dislocation Burgers vector has been performed in deformed perovskite and post-perovskite with $CaIrO_3$ composition at 1-3 GPa and 1473-1723 K. The temperatures of those deformation experiments correspond to homologous temperatures (T/T_m) of 0.8-0.9. The samples were directly deformed by axial flattening with a total shortening of the sample of 40-70 % and strain rates of the order 10^{-5} to 10^{-4} sec^{-1}. The Burgers vectors have been unambiguously determined by selecting several main zone axes and determining the number of terminating thickness fringes at the exit of a dislocation in weak-beam dark field TEM images.

The perovskite phase shows {110} polysynthetic twins and curved dislocations with Burgers vectors of [100], [010], [001] and straight [110] screw dislocations on the (001) and {110} plane (Fig. 3.7-3a). Parallel arrays of the dislocations also form subgrain-boundary textures. On the other hand, the post perovskite phase shows a much higher density of [100] curved screw and pure edge dislocations (***edge*** and ***screw***, respectively), in addition to [001] dislocations, on the (010) slip plane (Fig. 3.7-3b). The result in the post-perovskite phase is consistent with the crystallographic preferred orientation of the ***b***-axis aligned to the direction of a uniaxial compression and the ***a***-axis to a shear direction in pure shear and simple shear experiments, previously determined with the EBSD technique. The differences in dislocation microstructures could reflect strongly on dominant deformation mechanisms of dislocation glide for the post perovskite and climb-accommodated dislocation creep with potential multi-easy slip systems for the perovskite at the high homologous temperatures.

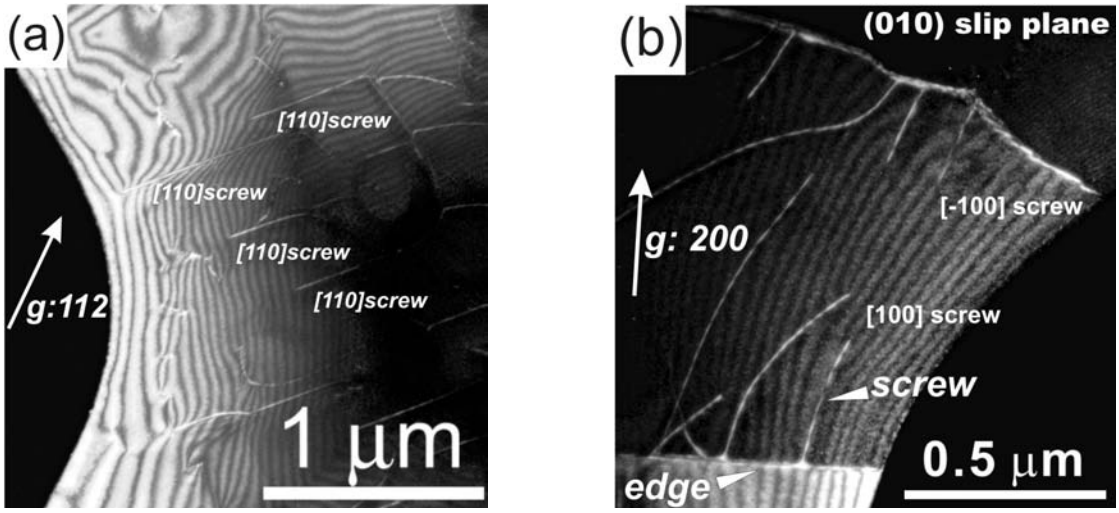

Fig. 3.7-3: Weak beam dark field TEM micrographs showing dislocation microstructures of (a) perovskite, $\boldsymbol{g} = 112$ and (b) post perovskite, $\boldsymbol{g} = 200$ in $CaIrO_3$. The deformed perovskite phase displays straight long <110> screw dislocations. The deformed post perovskite displays curved [100] screw dislocations and pure edge dislocations on the (010) plane.

c. *Deformation of Fe-rich ringwoodite at high pressure and temperature in the D-DIA (S. Hunt and D. Dobson/London, in collaboration with N. Walte and D.J. Frost)*

Ringwoodite (γ–$MgSiO_4$), one of the high-pressure polymorphs of olivine, is the dominant phase in the lower part of the transition zone with up to 60 volume percent abundance between 510 and 660 km. Its high phase proportion is likely to result in ringwoodite dominating the rheology of the lower part of the transition zone.

To date there have been no high-temperature studies of ringwoodite deformation. We have undertaken an investigation of the systematics of deformation in Fe-rich ringwoodite as a first step and are currently studying the effect of iron on the deformation properties under controlled strain rates.

We have developed a new cell for the D-DIA at the BGI that can achieve pressures in excess of 7 GPa, which is sufficient pressure for Fayalite (Fe_2SiO_4) to have the ringwoodite structure. The advantage of using the D-DIA offline is that the cell is not constrained to using X-ray transparent materials and so more efficient pressure generation can be achieved by judicious use of materials. The more usual boron epoxy has been replaced by pyrophyllite baked to 1000 °C, which is more efficient at generating pressure.

So far, experiments have been performed on γ-$FeSiO_4$ at 1000 and 1200 °C in both pure and simple shear geometries. The pressure efficiency is such that experiments should be able to be performed at least some way across the forsterite-fayalite join while still in the ringwoodite

structured field. Analysis of the deformation structures in the ringwoodite is ongoing but initial results show that only weak textures are developed in pure shear assemblies.

d. *Deformation of diamond under mantle conditions (D. Howell, D. Dobson and A. Jones/ London, in collaboration with D.J. Frost and N. Walte)*

Natural diamonds show many properties and textures that are yet to be reproduced during diamond synthesis experiments. Most notably brown colouration and cross-hatched birefringence patterns referred to as 'tatami'. Recent study of brown colouration has focused on the removal of the colour by HPHT annealing to create gem quality diamond. Experimental investigations into plastic deformation of diamond have predominantly been performed from a material science perspective, using indentation techniques often in vacuum conditions. The aim of this study is to use the deformation DIA (D-DIA) to take strain free diamonds to mantle pressure and temperature conditions and to then introduce a uniaxial strain. Observation of the resultant textures will hopefully shed light on the origin of these phenomena in natural diamonds.

The experimental plan involved using two different diamond types; type Ib diamonds which are yellow due to their unaggregated nitrogen (and are deemed as geologically young), and type II diamond which are colourless and relatively nitrogen free (most naturally occurring brown diamonds are of type II). To guarantee the samples started off strain free, synthetic diamond cubes were used, all with a known crystallographic orientation. Two experiments were carried out using each of the diamond types to test the hydrostatic nature of the D-DIA apparatus. The differential rams were not used during these tests so that any strain introduced during compression and decompression could be observed. The next two tests were carried out at *c.*4 GPa, *c.*1800 °C and with a strain rate of 3×10^{-5} s^{-1}. This strain rate was then repeated with two more samples at 1800 °C but at 6 GPa. A final test was carried out on a type II sample at 6 GPa, 1800 °C and a strain rate of 6×10^{-5} s^{-1}.

Optical analysis was carried out on the samples both before and after the experiments, namely InfraRed analysis of the nitrogen aggregation state and MetriPol birefringence analysis. SEM images were taken after the experiments to observe any small scale textural features as well. The results of the two 'hydrostatic' tests indicated that no colouration change occurred; only decompression fracturing was observed. Some birefringence was introduced as well, both related to the fractures and independent of them. The other experiments showed clear colour alteration, introduction of more intense birefringence patterns, evidence of nitrogen aggregation, and textural evidence of deformation. Figure 3.7-4 (left) shows evidence of diamond overgrowth on two sides of the diamond cube (yet to be confirmed with X-ray and Raman analysis). Figure 3.7-4 (middle) shows a clear change to the physical shape of the original cube. Figure 3.7-4 (right) shows an image taken under crossed-polars with birefringence related to both fractures and slip planes running through the sample.

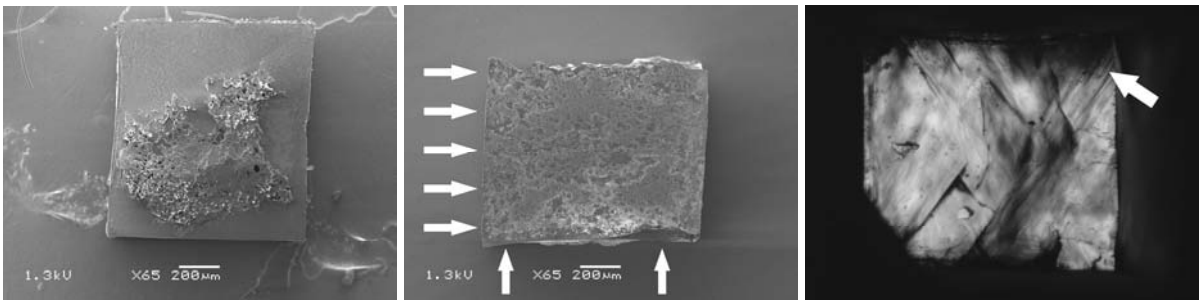

Fig. 3.7-4: left: SEM image showing possible overgrowth of diamond; middle: SEM image showing clear deformation to what once was a cube, plastic features are arrowed. The fracture on the top surface probably occurred during decompression; right: cross-polarized image showing fractures and slip planes. The slip planes are associated with plastic strain as evidence from macroscopic deformation of the original cube surface (arrowed)

e. *Deformation and lattice preferred orientation of coesite with the deformation-DIA (N. Walte, P. Cordier/Lille and F. Heidelbach)*

Coesite, the high-pressure SiO_2 polymorph that occurs at a pressure between ca. 2-9 GPa, controls the rheology of felsic rocks that are subducted to ultrahigh-pressure (UHP) metamorphic conditions. Thus, coesite, along with olivine and omphacite, is an important phase for understanding subduction and and deformation in the upper mantle. While several experimental studies have been conducted to derive the slip systems and flow laws for olivine and omphacite only few studies have dealt with coesite and the slip systems and lattice preferred orientation of deformed coesite are not agreed on, yet. A better understanding of coesite deformation will help to better understand subduction of felsic material and unravel the tectonic processes that lead to apparently undisturbed UHP granites that were subducted to depths of > 100 km and exhumed to the surface.

H_2O bearing SiO_2 glass and dried amorphous SiO_2 powder was used as starting materials for the experiments. A ca. 200 µm thick slice of silica glass or a layer of silica powder was placed between pistons that were cut at an angle of 45° to allow simple shear deformation. The starting materials were pressurized to 3.5 GPa and heated to 900 °C in the D-DIA and statically annealed for 4 hours to synthesize coesite prior to deformation. The strain rate of the experiments varied between 10^{-4}-10^{-3} s^{-1} and the bulk shear strain γ remained below 1.

After static annealing the glass samples display an intergrowth of elongated lath-shaped coesite crystals with a length of approximately 50 µm; deformed samples show subgrain boundaries and dynamic recrystallization of the coesite crystals (Fig. 3.7-4). The silica powder samples consist of a fine grained matrix of equigranular coesite grains with a diameter up to ca. 5 µm that display a weak crystal shape foliation after deformation (Fig. 3.7-5).

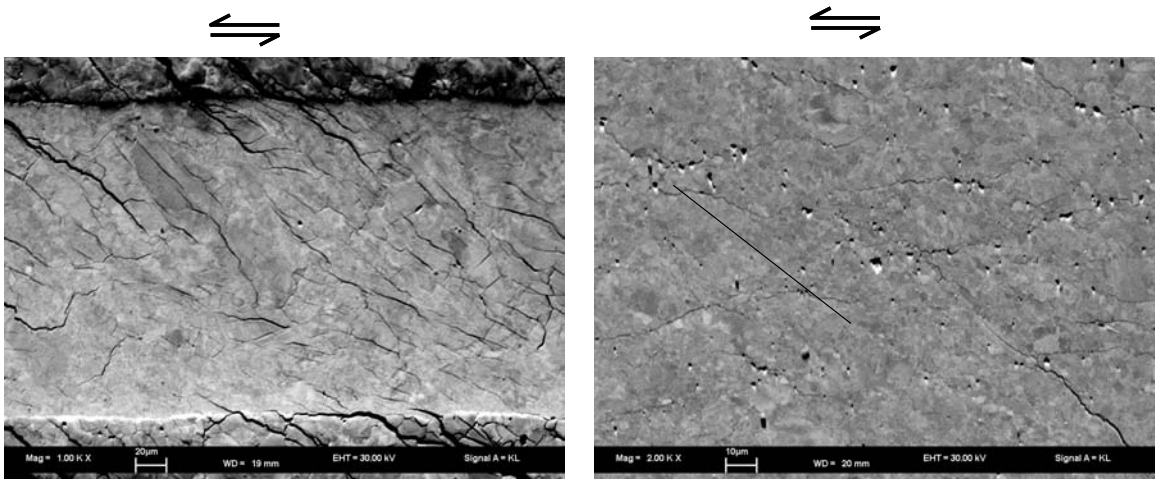

Fig. 3.7-5: SEM orientation contrast images of coesite deformation microstructures; (left) Hydrous SiO_2 glass starting material and (right) SiO_2 powder starting material. The black line marks the grain shape foliation.

Both silica glass and silica powder samples display a lattice preferred orientation after deformation with an orientation of the poles of {010} planes perpendicular to the shear direction and girdles of the poles of {100} planes approximately parallel to the shear direction (Fig. 3.7-6). One LPO shows a weak orientation of the <101> direction parallel to the shear direction although this has to be confirmed by future experiments. We interpret these textures as resulting from a dominant (010) slip plane at the experimental conditions. This slip plane differs from the (110) slip plane that was inferred from TEM analysis of undeformed coesite grains but confirms earlier predictions from deformation experiments in a Griggs-type apparatus. Future experiments will aim to deform coesite samples to a higher finite strain (γ>1) to possibly constrain the dominant Burgers vector in addition to the {010} slip plane and compare the macroscopic EBSD results to ongoing TEM analysis of the samples.

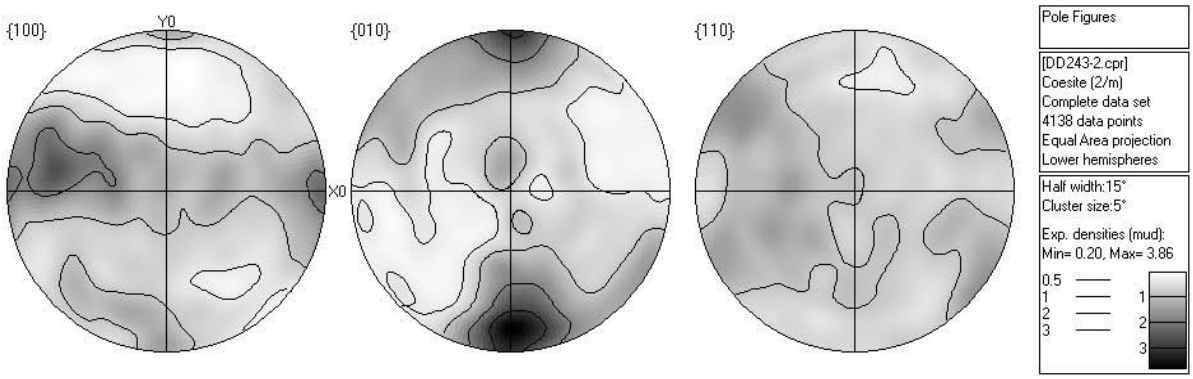

Fig. 3.7-6: Pole figures of a coesite deformation experiment at 3.5 GPa and 900 °C with a strain rate of 10^{-4} s^{-1} using SiO_2 powder as starting material.

f. *Plastic deformation of aragonite (F. Heidelbach and N. Walte)*

Aragonite ($CaCO_3$) is the orthorhombic high-pressure modification of trigonal calcite and is formed in carbonaceous sedimentary sequences that undergo deep subduction. Structurally similar to calcite it is likely one of the weaker components in the subducting slab and thus accommodating large strains during the subduction process. Little is known about the deformation microstructures and textures of aragonite. The aragonite-calcite transformation is a reconstructive phase transition such that aragonite is rarely preserved in exhumed subducted terranes. However, aragonite deformation fabrics may be still inherited in the calcite microstructures in exhumed material.

In this study we investigate the deformation fabrics of aragonite and how they may still be detectable after the back-transformation to calcite. Therefore we deformed aggregates of aragonite plastically at 3 GPa and 800 °C in the D-Dia multianvil press in order to produce deformation fabrics that may be similar to those in natural aragonite mylonites. We performed experiments in different deformation geometries (axial compression, simple shear) and analyzed the fabrics with SEM-EBSD. The starting material was produced by pressurizing (3 GPa) and heating (800 °C) Carrara marble for up to five days in Piston cylinder press. The long run duration were needed to produce a sufficiently large grain size (10 µm) in the starting material (Fig. 3.7-7).

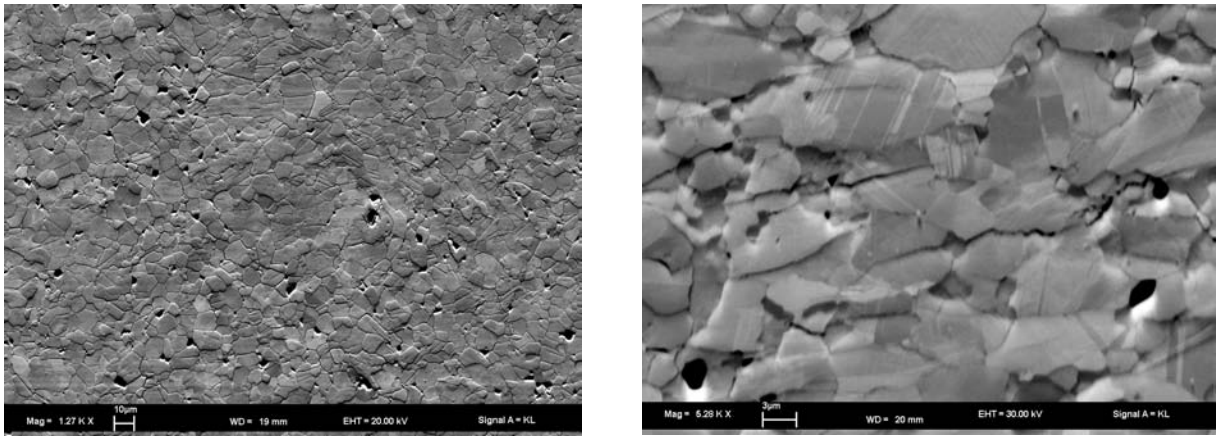

Fig. 3.7-7: SEM-orientation contrast image of polycrystalline aragonite starting material (left) and a sample DD259 deformed in axial compression (right).

The deformation experiments were carried with strain rates of 10^{-4} sec^{-1} (axial compression) and 10^{-5} sec^{-1} (simple shear) and reached strains of 30 % (axial compression) and $\gamma \sim 2$ (in simple shear) sufficient to produce a characteristic fabric. The resulting samples showed grain shape preferred orientation indicative of dislocation creep and abundant (011) twinning (Fig. 3.7-7). Crystallographic preferred orientations display an alignment of (100), (001) and (101) in the compression plane/shear plane (Fig. 3.7-8) making them likely to be intracrystalline

slip planes. The (100) plane, which shows the strongest alignment corresponds structurally to the basal plane of calcite. The [010] direction is aligned perpendicular to the compression direction and parallel to the shear direction respectively indicating that **b** (as shortest lattice repeat) may serve as a Burgers vector in intracrystalline slip.

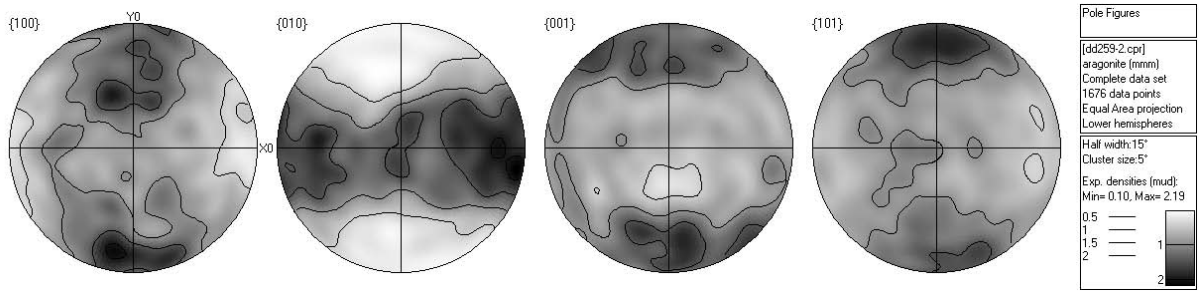

Fig. 3.7-8: Pole figures for sample DD259, deformed in axial compression to about 30 % strain.

The preliminary results of this study show that aragonite deforms by dislocation creep at 3 GPa and 800 °C giving rise to a crystallographic and shape preferred orientation. In further experiments we will explore how these fabrics may be preserved during the static or dynamic retrograde aragonite-calcite transition and compare them with naturally occurring calcite fabrics from subduction zones.

g. *Experimental deformation of ordered omphacite (W.F. Müller/Darmstadt, N. Walte, N. Miyajima, D. Frost and R. Klemd/Würzburg)*

The rheological properties of the eclogites are dominated by the mechanical behaviour of omphacite. Therefore, the plastic behaviour of omphacite is most important for the geodynamic processes of subduction and exhumation of oceanic and continental crust. Omphacite, a clinopyroxene with the ideal composition $Na_{0.5}Ca_{0.5}Mg_{0.5}Al_{0.5}Si_2O_6$, can occur in an ordered structure with the space group *P*2/*n* and a disordered structure with the space group *C*2/*c*. At temperatures above about 800 °C, omphacite is disordered with respect to its cations; at temperatures below about 800 °C the cations Mg and Al convergently order on the M1 positions of the structure.

Most eclogites found in the crust contain ordered omphacites with the space group *P*2/*n*. In natural *P*2/*n*-omphacites antiphase domains, exsolution lamellae, chain multiplicity faults parallel to (010), deformation twin lamellae on (100), non-crystallographic faults, free dislocations, small-angle grain boundaries, and recrystallised grains can occur. With exception of the antiphase domains and exsolution lamellae, all microstructures are due to deformation, and recovery and recrystallisation as consequence of deformation. However, the

nature and concentration of deformation features can be quite different in omphacites from different geological areas. This shows that the omphacites react differently to different thermo-mechanical histories of their rocks.

In order to see whether it is possible to reproduce the deformation microstructures of *P*2/*n*-omphacites and eventually to attribute their specific microstructures to the deformation conditions of the eclogite in its geological environment, deformation experiments on natural *P*2/*n*-omphacite under conditions of high-pressure metamorphism have been started. Eight experiments were meanwhile conducted using a deformation-DIA (D-DIA) high-pressure apparatus at strain rates from ca. 10^{-4} s^{-1} to 10^{-6} s^{-1}, temperatures between 500 °C and 800 °C, and at a confining pressure of mostly 2 GPa. The specimens were subsequently studied by TEM-methods.

The starting materials were a fibroblastic omphacite sample from Tianshan and omphacite grains from the coarse-grained eclogite of Weissenstein, Münchberger Gneiss Massif. Both omphacites are well-ordered, with the space group *P*2/*n*, and display antiphase domain boundaries. TEM-investigations of the experimentally deformed specimens revealed deformation twin lamellae on (100) and (001), traces of failed twin attempts on (100), dislocations, faults parallel to (010) and {110} and non-crystallographic faults. These crystal defects were not observed in all specimens, but a correlation between the deformation effects and the experimental conditions is not yet apparent.

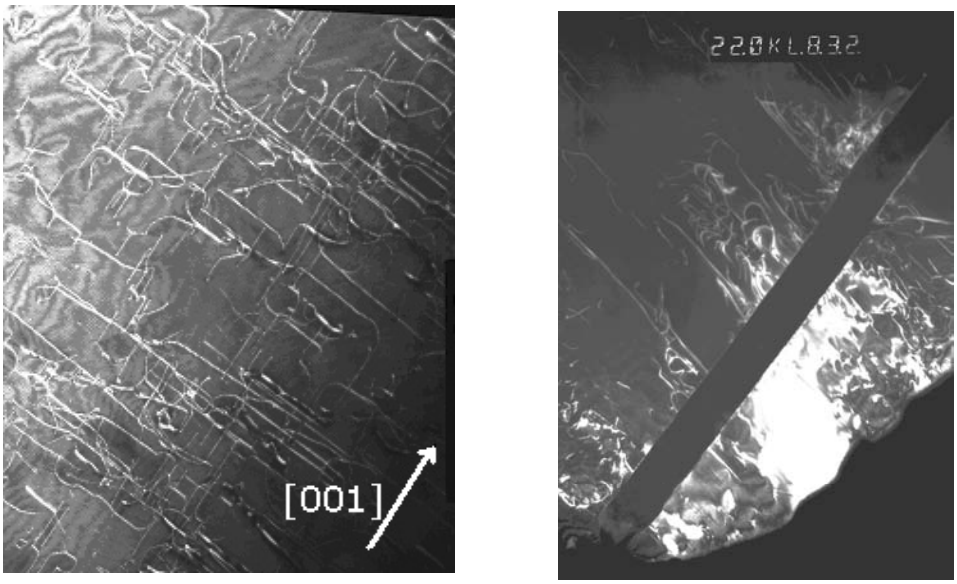

Fig. 3.7-9: left: Dislocations with the Burgers vector **b** = [001] in Weissenstein omphacite. The orientation of the crystal is close to [100]. The weak beam dark field image was taken with the reflection **g** = 002. Most dislocation lines are parallel to [001] – screw dislocations –and/or parallel to [010] – edge dislocations. The short length of the micrograph corresponds to 3.4 µm; right: Deformation twin lamella on (001) in omphacite from Weissenstein. The dark field image was taken with a matrix reflection. The short length of the micrograph corresponds to 2.8 µm.

Deformation twin lamellae on (100) were found in all specimens, often as polysynthetic twins. Their widths varied between a few nm and about 0.5 µm. Generally, the specimens with the Tianshan omphacite contain a higher density of twin lamellae. Rarely, defects parallel to (100) were seen which apparently consist of numerous dislocations lined up parallel to (100). They are interpreted as twin attempt or pre-stage of twin lamellae. Perfect and/or partial dislocations were seen in all specimens, too. The analysed dislocations had the Burgers vector **b** = [001], which are the dislocations most frequently mentioned in literature. Edge and screw components were observed in a crystal with an orientation near [100] (Fig. 3.7-9 left) thus proving the slip plane (100).

Deformation twins on (001) are rare and occur mostly as single lamellae (Fig. 3.7-9 right). They are broader than the average (100) twin lamellae. Deformation twins on (001) have not been reported before from omphacites nor from other clinopyroxenes with primitive Bravais lattice. Deformation twin lamellae on (001) are known from shock-deformed diopside and augite in meteorites and have been produced by shock experiments. However, surprisingly they did not occur in shock-deformed pigeonite (space-group $P2_1/c$).

Faults parallel to (010) between dislocations have been observed in two specimens, with a high density of faults in one of them. The dark field images of the faults are in agreement with their interpretation as chain multiplicity faults which are frequently observed in omphacites from the Tauern Window. Faults parallel to {110} stretched between dislocations with a displacement vector **R** close to 1/2[110] were occasionally found. Planar faults parallel to (110) have been seen so far only in one single omphacite from the ultrahigh-pressure metamorphic rocks from Lago di Cignana. Non-crystallographic faults – in addition to antiphase domain boundaries – with a displacement vector **R** close to 1/2[110] have also been found. Similar faults, however sub-parallel to (100), have been recently discovered in omphacite from the Eclogite Zone of the Tauern Window.

In conclusion: Most of the experimentally produced crystal defects are also found in naturally deformed omphacites. The experiments show that there are sufficient mechanisms for deformation of *P*2/*n*-omphacite at lower temperatures, which can compensate for the loss of perfect dislocations with the Burgers vector 1/2<110> which are only available in *C*2/*c*-omphacite.

3.8 Metamorphism

Metamorphism is a process of solid-state transformation that rock masses undergo under changing physical conditions *e.g.*, as they are brought into greater depths in subduction zones or buried in the roots of newly forming mountain chains. The rocks react to changing pressure and temperature conditions by the formation of new phases during solid-state recrystallization of the mineral assemblage, thereby attaining a new thermodynamic equilibrium. After exhumation, metamorphic rocks can be investigated to gain insight into the physical and chemical processes that act in the deep, inaccessible parts of the Earth.

In subduction zones and during continental collision, sometimes low-density slivers of continental crust are dragged deep into the mantle by the downgoing slap, before they disconnect and rise back near the surface of the Earth. The resulting ultra-high-pressure metamorphism is the subject of the first contribution. The authors investigated diamond-bearing metapelites from northern Greece that have reached a depth exceeding 220 km at peak metamorphic conditions. By applying different geobarometers and geothermometers the authors were able to trace part of the pressure-temperature path that these rocks have undergone in the upper mantle.

In the second contribution the magnetic properties of Norwegian granulites were investigated. These rocks produce regional geomagnetic anomalies, which are mainly caused by nano-scale exolution lamellae of heamatite in ilmenite or vice versa that produces a strong and stable remanent magnetization. For this contribution a large crystal of titanohematite was analysed in detail by SEM, TEM, and electron microprobe techniques to investigate the interplay between exsolution lamellae of different compositions and their magnetic properties.

In addition to the variables pressure and temperature, the oxygen fugacity can have an important role in determining metamorphic reactions in rocks. In the third contribution the interplay between mineral equilibria, Fe^{2+}/Fe^{3+} ratios in minerals and devolatilization reactions was investigated with the aim to predict the redox state of eclogitic assemblages in slap subduction environments. The author shows that the oxygen fugacity in the subducting slap is significantly higher than in the surrounding garnet peridotite of the upper mantle.

While regional metamorphism on Earth often takes place over millions of years, in the final contribution a shock-metamorphosed meteorite is investigated, during which metamorphic reactions occur within seconds. These meteorites preserve high-pressure phase transitions that are not accessible in the Earth. By careful chemical and textural mapping the authors reinterpret the textural development in their sample and show that previous time constrains for similar reactions may have been too long.

a. *Transmission electron microscopic and spectroscopic study of diamondiferous ultrahigh-pressure (UHP) rocks from northern Greece (D. Kostopoulos and A. Godelitsas/Athens; N. Miyajima and F. Heidelbach)*

The Rhodope Massif in northern Greece is a newly established ultrahigh-pressure metamorphic (UHPM) province in the world. We have documented the presence of microdiamonds included in zircon and garnet from metapelites and subsequently argued that these rocks had once been transported to depths exceeding 220 km, well into the upper mantle. We have already carried out a detailed laser μ-Raman study as well as a TOF-SIMS investigation of zoned diamondiferous zircons indicating Y-enriched detrital cores and Y-depleted, diamond-bearing overgrowth rims. Such findings are in excellent agreement with recent experimental work suggesting preferential partitioning of Y into garnet in the presence of zircon at temperatures exceeding 1070 °C at high pressures. By contrast, Li shows the reverse distribution pattern being depleted in the detrital core and enriched in the rim domain. This suggests breakdown of phengite during H_2O-undersaturated melting of the pelitic protolith at P-T conditions of the order of 7 GPa / 1100 °C and further implies significant recycling of Li at subduction depths well in excess of 200 km.

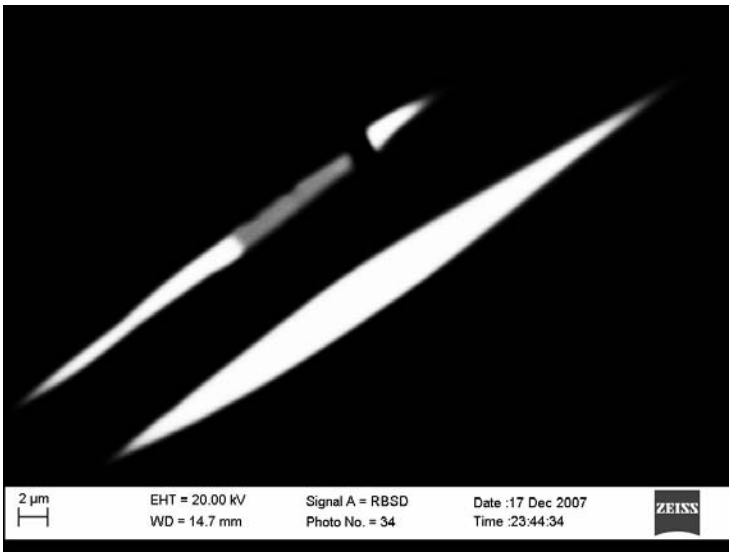

Fig. 3.8-1: SEM-BSE image of a composite exsolution lamellae of monazite (bright) and iron sulphide (gray) in apatite.

Our research at BGI involved the measurement of the titanium content of quartz inclusions in diamondiferous garnets from UHP metapelites and the application of the newly calibrated Ti-in-Qtz thermometer. Statistically significant temperature peaks occur at 530, 590, 650, 710 and 770 °C. Interestingly, however, temperatures between 815 and 1250 °C were also calculated that are in accord with the highest temperature estimates for these rocks at pressures of 8 GPa.

Moreover, detailed electron microscopic investigation of apatite porphyroblasts revealed the presence of exsolved micro-/nano-crystals of monazite and pyrrhotite. Although monazite exsolutions in apatite are known from UHP rocks from Dabie-Shan (China), iron sulphide exsolutions have not been reported before from such rocks and are only known from apatite phenocrysts in volcanic rocks. Taken collectively, the above data strongly support the interpretation that the Rhodope UHPM rocks in fact represent melts of mainly pelitic protoliths at approximately 8 GPa / 1200 °C.

Finally, preliminary HRTEM-EELS results on diamondiferous zircons indicated the presence of fibrous graphite in nanoscale tentatively correlated with an unresolved μ-Raman peak at 1329 cm^{-1}.

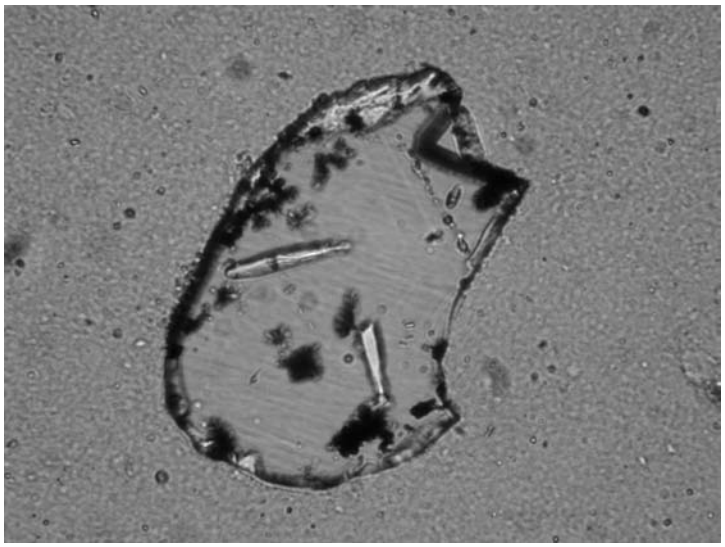

Fig. 3.8-2: Photomicrograph of diamondiferous zircon extracted from a Rhodope UHP metapelite prior to Ar-ion milling and HRTEM-EELS examination

The results of the project will help to elucidate the immediate environment of diamond formation during deep subduction of continental crust and the recycling of carbon, lithium and hydrogen in the geosphere.

b. *Geikielite and coupled spinel-rutile exsolution from coarse-grained titanohematite found in Mesoproterozoic granulite-facies rocks, south Norway (P. Robinson/Trondheim, F. Langenhorst/Jena, S. McEnroe and K. Fabian/Trondheim, M.J. Jercinovic/Massachusetts and T. Boffa Ballaran)*

Areas of extensive negative magnetic anomalies in the Modum District of the Sveconorwegian metamorphic belt, south Norway, have been under investigation. The anomalies appear to be caused by a variety of rocks containing minerals capable of carrying a

strong and stable remanent magnetization, most notably ilmenite with hematite exsolution lamellae and hematite with ilmenite exsolution lamellae. Important rocks in the district include gabbros variously recrystallized and invaded by hydrous and chlorine metasomatism, metamorphosed hydrothermally altered felsic volcanic rocks, and unusual calcareous highly oxidized metamorphosed sedimentary rocks, commonly rich in chlorine-bearing scapolite, that could be metamorphosed evaporitic sediments. Commonly in this work, magnetic properties are studied at room temperature, at high temperature, and at very low temperature, as an aid to phase identification, usually before detailed microscopic, electron microprobe, XRD and TEM studies. In one altered volcanic rock, titanohematite showed a special property of magnetic exchange bias at temperatures below 57 K, the Néel temperature of ilmenite, which was proved by TEM to be present in lamellae only 1 nm thick (McEnroe *et al.* Nature Nanotechnology 2007).

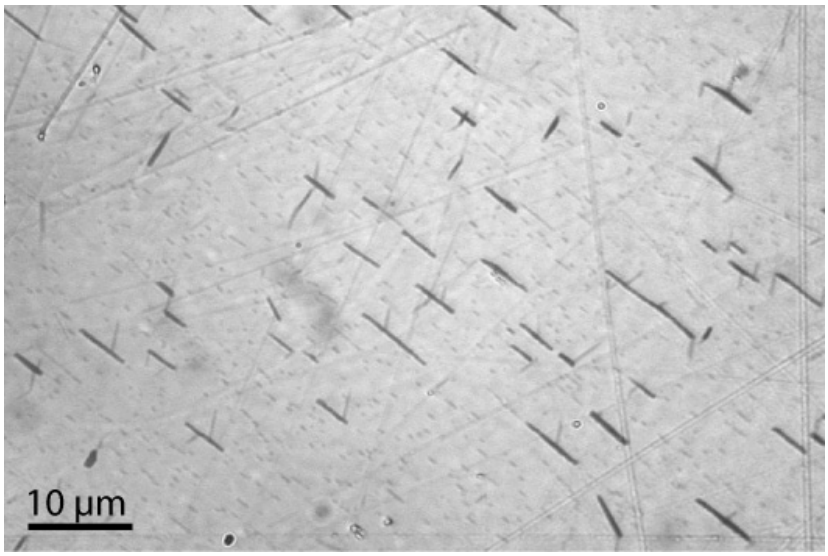

Fig. 3.8-3: Reflected-light photomicrograph, with scale, of Modum 24 titanohematite. Darkest lamellae are magnesian spinel oriented parallel to (0001) of the host. Attached to these, commonly at angles of ~ 60° are rods of rutile (gray). Most of the fine lamellae (gray) parallel to (0001) of the host are ferroan geikielite. These are much less abundant in proximity to the spinel-rutile intergrowths, indicating prior depletion of Mg and Ti in these areas.

In one area of oxidized metamorphosed sedimentary rocks we found a metamorphic vein containing a crystal of titanohematite ~ 3 cm in diameter, proving more useful for studies of mineral magnetism than separations of dispersed small grains in the host rock. Initial reflected-light and SEM observations, and EMP analyses showed that the titanohematite (8 % $R^{2+}TiO_3$ of which 2 % $MgTiO_3$) contains three types of exsolution lamellae (Fig. 3.8-3): spinel plates on (0001) of the host; rutile rods and irregular patches, probably along edges of rhombohedral faces of the host and nearly always forming as satellites of spinel lamellae; and very fine lamellae (0.1-0.3 µm thick) also parallel to (0001) of the host. These last were too

small for definitive EMP analyses, but showed enrichment in MgO and TiO_2. The lack of Al_2O_3 indicates that spinel cannot account for MgO enrichment. Thus, it is likely that overlap analyses represent a mixture of titanohematite and a geikielite-rich solid solution (Fig. 3.8-4a, 34 % $R^{2+}TiO_3$ of which 29 % $MgTiO_3$). The overlap analyses were used to project a possible geikielite composition at ~ 90 % $MgTiO_3$, however, our experience with overlap analyses in the rhombohedral oxides indicates that they are notoriously unreliable, particularly with MgO, calling for study using TEM-EDS. X-ray powder diffraction gave lattice parameters a = 5.0393 (1), c = 13.7687 (3), V = 302.81 (1) for the hematite host, only weak reflections (not refined) indicating presence of rutile and geikielite. Hematite parameters compare with a = 5.034, c = 13.750, V = 301.758 for end-member hematite, and indicate a composition ~ Ilm 9-10 from working curves, depending on estimated effect of minor Mg substitution.

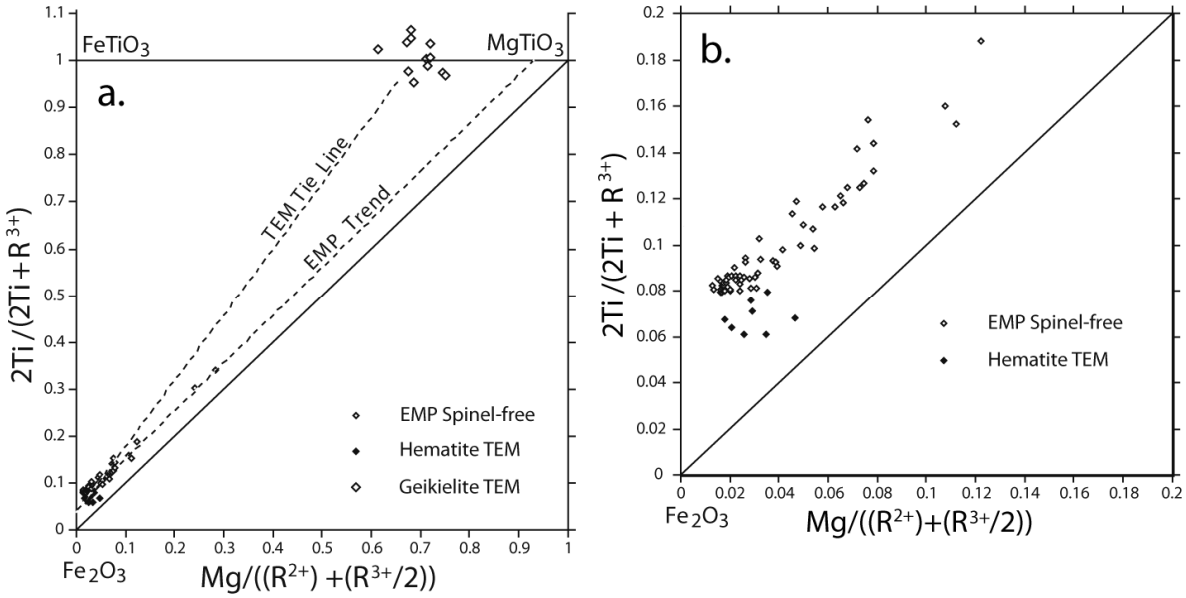

Fig. 3.8-4: a) Hematite and geikielite compositions, determined by EMP and TEM analyses, plotted in the right triangle Fe_2O_3-$FeTiO_3$-$MgTiO_3$. b) Detail showing compositions in the hematite-rich region.

The spinel plates and rutile rods and patches were coarse enough locally for EMP analyses and appeared to have formed earlier than the fine geikielite-rich lamellae. The best spinel analyses showed high MgO, Al_2O_3, moderate Fe total, and only trace amounts of Zn, Cr, V, and Ti, and calculated to about 96 % $MgAl_2O_4$ and 3 % $FeFe_2O_4$ with a ratio Mg/ total R^{2+} = 0.98. How could such a magnesian and aluminous mineral with a dearth of R^{4+} ions exsolve from a Ti-bearing rhombohedral solid solution? The answer appears to lie in coupled exsolution of R^{4+}-rich rutile (Fig. 3.8-3). The best two out of only four EMP analyses showed 80-81 % TiO_2, 15-16 % total Fe, 1.77 % V_2O_3 (corrected for Ti peak overlap), 0.2 % MgO, and only trace Al, Cr, Mn, Nb, Ta, and Zn. The combined spinel and rutile components appear to have been in solution in the high-temperature titanohematite mainly as corundum,

V_2O_3 and geikielite substitutions, and, upon phase separation, depleted the hematite in nearly all corundum component, and lowered the geikielite component of the remaining rhombohedral oxide. Later TEM-EDX analyses of fine rutile rods were not able to reproduce the high V_2O_3 of the coarsest rutile patches, but spinel analyses were in good agreement.

TEM-EDX analyses were made of the titanohematite host and of geikielite lamellae (Fig. 3.8-4a), which can never be as precise as EMP analyses of pure phases. The hematite averages 6 % $R^{2+}TiO_3$, of which 2 % $MgTiO_3$ (Fig. 3.8-4b), and the geikielite averages 100 % $R^{2+}TiO_3$, of which 70 % $MgTiO_3$ (Fig. 3.8-4a), thus much poorer in geikielite component than the projected composition. The correct $MgTiO_3$ component in hematite and in geikielite is of considerable importance because, unlike Fe^{2+} and Fe^{3+}, Mg^{2+} is not a paramagnetic ion. It cannot contribute to the magnetic moment of the host mineral, but its presence can break up the magnetic linkages between Fe atoms, lowering Néel temperatures, and possibly leading to unsual magnetic properties at low T. For this sample we have determined a Néel T of 878K for the hematite host and a Néel T of 34K for the geikielite lamellae, with possible spin-glass behaviour below 13 K, where the corresponding temperatures for pure Fe_2O_3 and pure $FeTiO_3$ are 953 K and 57 K respectively. The initial study reported here opens the door to a systematic study of the magnetic properties of synthetic samples in the systems $FeTiO_3$-$MgTiO_3$ and Fe_2O_3-$MgTiO_3$.

c. *Redox state of the subducting slab: Thermodynamic constraints (D. Dolejš)*

Oxybarometry of natural peridotite xenoliths and shifts in phase equilibria, which include incorporation of ferric iron in silicate phases, suggest a progressively decreasing oxygen fugacity of the upper mantle. In contrast, metasomatized mantle xenoliths and those from arc settings record relatively oxidizing conditions. In order to understand origins of the high oxidation state in the mantle, we have to evaluate: (1) changes in the redox state of the slab during subduction, (2) changes in redox state due to the release of H_2- and CH_4-bearing fluids, and (3) effect of pressure on mineral-fluid equilibria involving elements of multiple valence.

In this contribution, we examine relationships between mineral equilibria, Fe^{2+}/Fe^{3+} effects and devolatilization reactions during slab subduction with the aim to predict the redox state of final eclogitic assemblage. Previous models of slab metamorphism and dehydration ignored effects of oxygen fugacity on mineral-fluid equilibria in the subducting slab. Ferric iron is incorporated by Al-Fe exchange in hydrous and anhydrous aluminosilicates (*e.g.*, epidote, alkali amphiboles, alkali pyroxenes, garnet) and its presence is expected to affect the locations of individual mineral reactions and the onset of dehydration and decarbonation.

Phase equilibrium calculations were conducted in the SiO_2-TiO_2-Al_2O_3-FeO-MgO-CaO-Na_2O-K_2O-H_2O-CO_2-O_2 system by Gibbs energy minimization. This composition space allows one to simultaneously (1) incorporate Fe-Ti oxides, (2) vary oxidation state of iron, (3)

test for saturation with Fe and C, and (4) treat C-H-O fluids. Thermodynamic data for mineral end-members and their solutions were based on the Holland-Powell equations of state. The pressure-volume-temperature relationships of fluid species were calculated from the Belonoshko-Saxena equation of state, supplemented by van Laar volume-dependent mixing rules. Consideration of excess properties of the fluid phase has lead to slightly positive deviations from ideal mixing. As a consequence, H_2 and CH_4 proportions in the fluid during slab dehydration decrease slightly, contributing to a very minor decrease in oxygen fugacity, $f(O_2)$, of the subducting slab. Thermodynamic calculations were performed by using a three-layer slab model, consisting of global oceanic subducting sediment (GLOSS), oceanic basalt supercomposite (OBSC) and serpentinized harzburgite (SHB). In all calculations we have used a linear geotherm of 16 °C/kbar, which is intermediate between warm and cold geotherms of the Japanese subduction system.

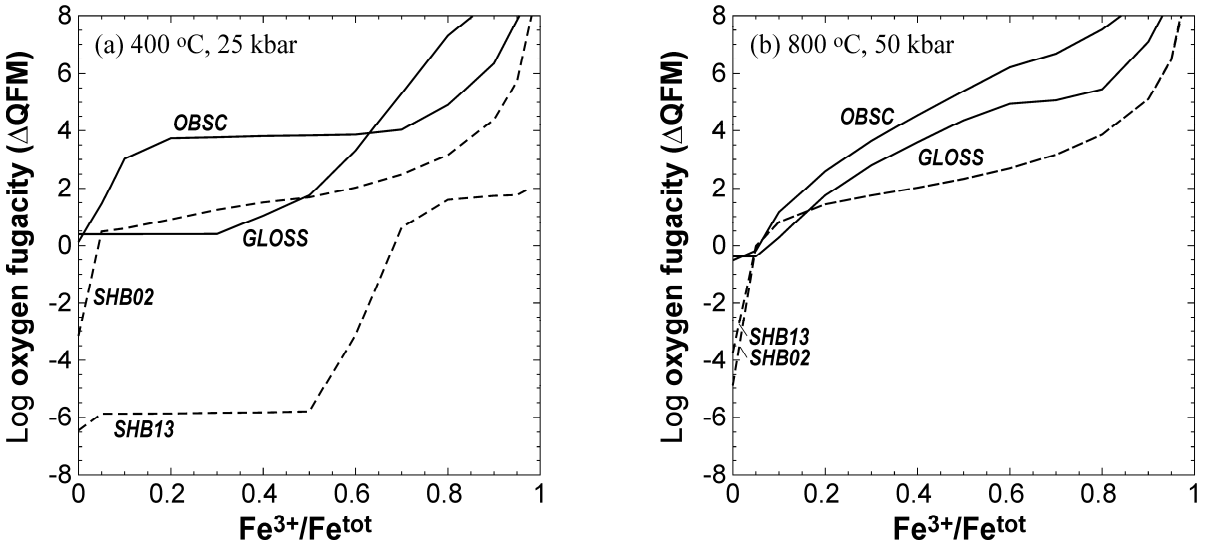

Fig. 3.8-5: Relationships between whole-rock Fe^{3+}/Fe^{tot} ratio and oxygen fugacity, defined by equilibrium mineral (+fluid) assemblage at 400 °C, 25 kbar (a) and 800 °C, 50 kbar (b). Numerical abbreviations indicate 2 and 13 wt.% H_2O in the serpentinized harzburgite.

For all rock types, the relationship between oxygen fugacity and the whole-rock Fe^{3+}/Fe^{tot} ratio is monotonous but non-linear (Fig. 3.8-5). Oxygen fugacity remains buffered over certain ranges of the Fe^{3+}/Fe^{tot} ratio (generally less than 0.5) in dependence on the whole-rock composition and the amount of H_2O. In carbonate-bearing protoliths, the lower limit of oxygen fugacity is defined by the graphite/carbonate equilibrium (ΔQFM ~ 0-1), whereas in serpentinized ultramafics it corresponds to iron/ferrous silicate equilibrium. None of the lithotypes has a unique upper limit of oxygen fugacity; with increasing Fe^{3+}/Fe^{tot} ratio, mineral assemblage progressively changes: ilmenite – magnetite – hematite, ferrous silicates to andraditic garnet and acmitic clinopyroxene, eventually leading to the saturation with an

O_2-bearing aqueous-carbonic fluid. The initial oxidation and redox states of the subducting lithologies were estimated by comparing equilibrium assemblages with natural low-grade assemblages in sea-floor and forearc settings. For sediments, we use Fe^{3+}/Fe^{tot} ratio = 0.4, which is bracketed by graphite occurrence (0.3) and acmite or hematite stability (0.7-0.8). The initial low-grade assemblage includes quartz, celadonite, lawsonite, jadeite, rutile and carbonates. Oceanic basalts develop characteristic blueschist assemblage of chlorite, epidote, glaucophane, tremolite and lawsonite with accessory talc, phengite, garnet and dolomite-ankerite solid solution at Fe^{3+}/Fe^{tot} = 0.2-0.5; we choose the Fe^{3+}/Fe^{tot} ratio = 0.3, which corresponds to ilmenite stability. Mineral assemblages of serpentinized peridotites have high variance and depend on the whole-rock Al_2O_3 and H_2O contents rather than the oxidation state. Fertile lherzolites with high calcium and aluminium abundances hydrate to chlorite-tremolite assemblages, which are more oxidizing and stable to higher temperatures than serpentine-dominated derivatives of Ca- and Al-poor harzburgites. For olivine and orthopyroxene-bearing assemblages altered to chlorite, antigorite, pargasite and brucite, the modal amount of magnetite (6-7 %, chosen to match natural samples) gives the most reliable estimate of the initial whole-rock Fe^{3+}/Fe^{tot} ratio (0.5).

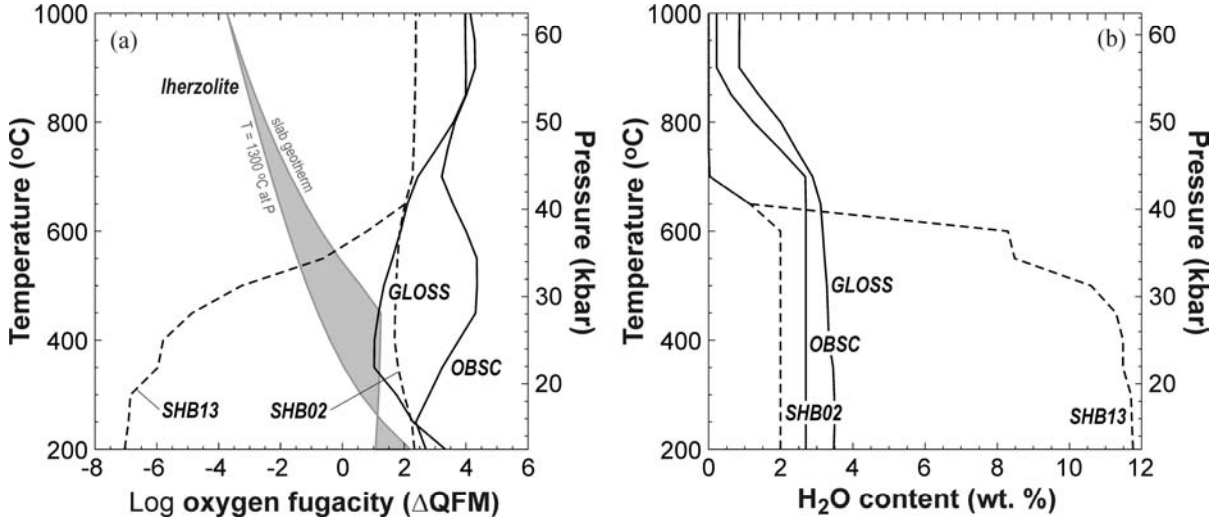

Fig. 3.8-6: Variations in the oxygen fugacity (a) and H_2O content (b) during progressive slab metamorphism and devolatilization. The redox state of lherzolite, buffered by olivine, orthopyroxene and garnet/spinel (Mg/(Mg+Fe) = 0.9, Fe^{3+}/Fe^{tot} = 0.02) and calculated with the same thermodynamic dataset, is shown for reference.

Changes in the oxygen fugacity during progressive metamorphism, dehydration and decarbonation are illustrated in Fig. 3.8-6. The initial redox states of sediments and oceanic basalts are 2 to 3.5 units above the QFM buffer and are related to tremolite, lawsonite and epidote equilibrium. At medium grade, the redox states of GLOSS and OBSC differ by as much as 3 log units, which is dictated by the stability of almandine-rich garnet in metabasalts.

Above 800 °C and 50 kbar, the redox states of metasediments and metabasalts converge to ΔQFM ~ 4 as both rock types contain the same mineral assemblage consisting of acmitic jadeite, grossular-andraditic garnet, celadonite, kyanite, coesite with accessory rutile and Mg-rich carbonate. The oxygen fugacity is controlled by the equilibrium ferroceladonite + kyanite + jadeite + O_2 = muscovite + acmite and it can be estimated from phengite and garnet mineral compositions.

Progressive dehydration and the redox state of serpentinized peridotites have been studied for two extreme cases of hydration (2 and 13 wt.% H_2O in the rock). The weakly serpentinized harzburgite has the oxygen fugacity of ΔQFM = 2.0-2.5, which remains constant throughout the subduction progress (Fig. 3.8-6a). This is related to the enstatite, forsterite and magnetite/hematite buffer where small quantities of clinochlore, pargasite and antigorite cannot affect the Mg/(Mg+Fe) ratio of anhydrous silicates. In contrast, completely serpentinized harzburgite defines extremely reducing conditions at the onset of subduction (ΔQFM = -6 to -7), which is controlled by the antigorite, chlorite and magnetite/hematite buffer, and the inability of antigorite to incorporate any significant amounts of Fe^{2+}. The redox state of serpentinite increases dramatically to ΔQFM + 2 between 400-650 °C as antigorite dehydrates to enstatite and forsterite. Above 700 °C and 45 kbar, harzburgites contain ferrian pyrope, whose amount is dictated by the whole rock Al_2O_3 content. They remain significantly more oxidized than garnet lherzolites (by more than 5 log units). This is explained by distinct amounts of garnet (related to whole-rock Al_2O_3 content), which can affect the balance of Fe^{2+} and Fe^{3+} to a lesser extent only, inhibiting a decrease in the oxygen fugacity with pressure of garnet harzburgites.

The effect of fluid exsolution on the redox state of the residual slab has been investigated by open and close devolatilization models. During open devolatilization, the C-H-O fluid leaves the system instantaneously (here in 50 °C steps) whereas in the closed system approach it is retained in the rock and allowed to achieve the global equilibrium. In all cases, open and closed simulations give virtually identical results and return a negligibly small shift in the oxygen fugacity (less than 0.2 log units). Such a large efficiency of rock buffering is related to very small fluid/rock ratios (< 0.1).

The dominant aqueous species are H_2O and CO_2 in metasediments and metabasalts, and H_2O and H_2 in serpentinites. In the former case, the CO_2 concentrations slowly increase with temperature and pressure, reaching 1-8 mol.% CO_2 above 800 °C and 50 kbar. More than 80 % of the solid carbonates are preserved in the slab up to these conditions. The serpentinite fluids contain up to 0.04 mol.% H_2 below 450 °C and 30 kbar, which is sufficiently close to iron metal saturation, but become pure H_2O during antigorite breakdown. In Figure 3.8-6b we show that several major changes in the redox state overlap with main dehydration reactions. The above models demonstrate that the change in the redox state cannot be explained by the removal of reduced or oxidized species in the aqueous fluid phase but it is solely dependent on the Al-Fe^{3+} partitioning during dehydration reactions.

Comparative effects of the initial whole-rock oxidation state on the oxygen fugacity and the onset of dehydration reactions are illustrated in Fig. 3.8-7. More oxidized protoliths record systematically higher oxygen fugacities except near 400-500 °C where they converge along the ilmenite, hematite and rutile buffer (Fig. 3.8-7a). Subsequently, hematite becomes unstable in favor of acmitic pyroxene and andraditic garnet. These phases control the location of lawsonite breakdown and can cause a shift by as much as 150 °C or 9 kbar for the most significant dehydration reaction of the upper slab portion (Fig. 3.8-7b).

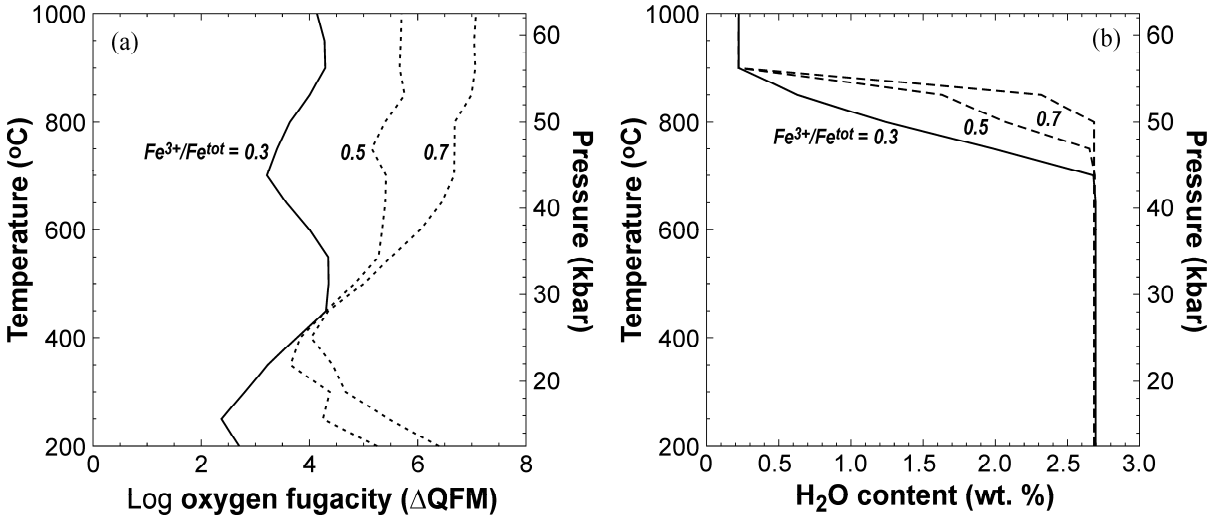

Fig. 3.8-7: Effects of variable oxidation and hydration on the redox state during metamorphism of oceanic basalts (OBSC): (a) increasing the whole-rock Fe^{3+}/Fe^{tot} ratio extends the applicability to hematite-bearing ophicarbonates; (b) increasing the degree of initial hydration leads to changes in the redox state due to the shifts in lawsonite-pyroxene-garnet equilibria.

In summary, phase equilibrium calculations of progressive metamorphism and devolatilization of three main slab lithologies demonstrate that: (1) the initial redox state of oceanic sediments, sea floor basalts and harzburgites with incipient serpentinization is ΔQFM ~ 2-3; completely serpentinized harzburgites are strongly reducing at ΔQFM = -7; (2) aqueous fluids released during slab devolatilization are dominated by H_2O, with lesser amounts of CO_2 above 800 °C and 50 kbar; concentrations of H_2 become only significant in low-temperature serpentinite fluids. Comparative calculations of episodic devolatilization *vs.* retainment of pore fluids show no significant effect on the slab redox state; (3) the location of major dehydration reaction, the lawsonite breakdown, is sensitive to the whole-rock Fe^{3+}/Fe^{tot} ratio; a change of Fe^{3+}/Fe^{tot} by 0.4 units shifts the onset of dehydration by ~ 150 °C (or 9 kbar); (4) changes in the redox state during metamorphism are driven by Fe-Mg and Fe^{3+}-Al substitutions in silicates and reflect the formation of iron oxides during medium grades and their breakdown at eclogite facies where acmitic pyroxene and andraditic garnet become stable. Upon complete devolatilization, the oxidation state of metasediments and metabasalts is close to ΔQFM = 4 whereas that of harzburgites is ΔQFM = 2. The oxygen fugacity of the

subducting slab does not decrease with pressure and it is 6-8 orders of magnitude higher than that of garnet-bearing peridotites.

d. *Evidence for fractional crystallization of Mg-rich wadsleyite and Fe-rich ringwoodite in selectively melted olivine phenocrysts in chondrules entrained in shock-melt veins in an L6 chondrite: An SEM, Raman and TEM study (A. El Goresy, L.S. Dubrovinsky; M. Miyahara and E. Ohtani/Sendai; T. Ferroir and P. Gillet/Lyon; A. Simionovici/Grenoble)*

Many shocked chondritic meteorites contain mm-sized shock-melt veins produced during natural impact events on their parental asteroids. The veins are interpreted to have formed through friction along shock-induced fractures or concentration of shear in glide bands as a result of a deviatoric component. The veins contain an inventory of high-pressure polymorphs of the major chondritic minerals formed either by direct isochemical solid-state phase transitions or crystallization from the chondritic melt at high pressures and temperatures. The shock-induced high-pressure phases in the melt veins may mimic phase transformation processes active in planetary interiors. The olivine-ringwoodite inversion in these veins was extensively investigated due to its relevance to mechanisms in Earth's transition zone and the lower mantle. Many ringwoodite grains in shock-melt veins are polycrystalline and have identical chemical compositions with their parental olivine. It is generally accepted that these polycrystalline ringwoodites were formed by direct solid-state incoherent mechanism. Wadsleyite of similar composition of the coexisting ringwoodite encountered in melt veins in Peace River chondrite was interpreted to have formed by solid-state back transformation from ringwoodite upon decompression.

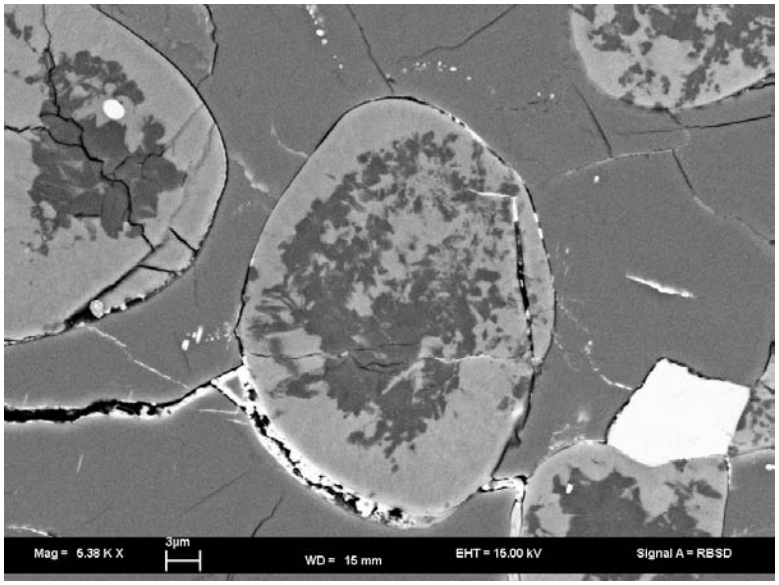

Fig. 3.8-8: SEM-BSE photograph of a former porphyritic olivine in a chondrule entrained in a shock-melt vein in the Peace River meteorite. The former olivine depicts a concentric arrangement of the high-pressure polymorphs wadsleyite (in the core) and ringwoodite shell.

Large olivine grains intersected by chemically zoned thick ringwoodite bands (called lamellae) of different chemical compositions than the parental olivines were also encountered in shock melt veins in the Sixiangkou L6 chondrite. The ringwoodite bands were interpreted to have formed by diffusion controlled intracrystalline solid-state nucleation and growth along shock induced fractures. Solid-state mechanisms were frequently considered despite the diversity of the olivine ringwoodite textural relations and compositions. This assumption resulted in contrasting and unrealistically long time scales between several tens of seconds and 500 seconds for the duration of the high-pressure regime.

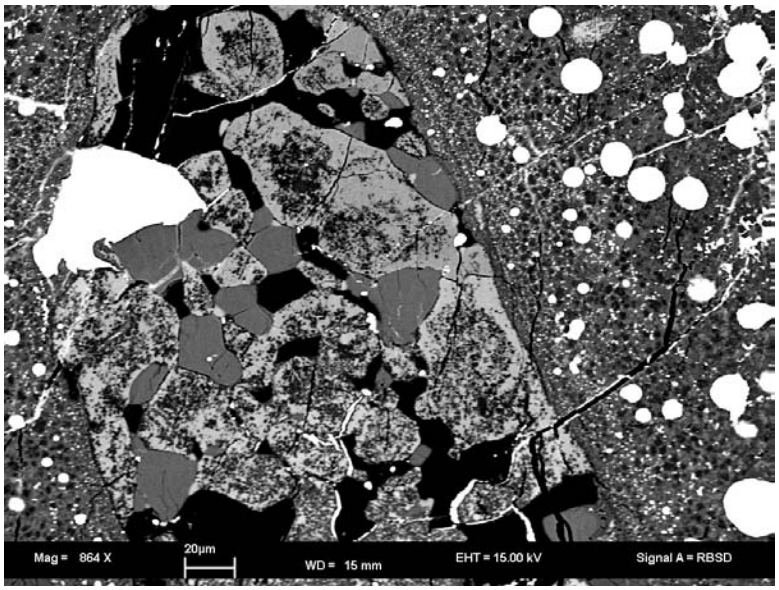

Fig. 3.8-9: A squeezed and flattened former olivine porphyritic chondrule from the same meteorite also depicting the concentric arrangements of wadsleyite (dark grey) and ringwoodite (gray rim).

The Peace River L6 chondrite is one of the few shocked L6 chondrites that contain both high-pressure polymorphs of olivine, ringwoodite and wadsleyite in its shock-melt veins. Porphyritic olivine chondrules entrained in melt veins in this chondrite are squeezed and flattened unambiguously demonstrating intense plastic deformation and possible partial melting. The former olivines consist of intergrowths of ringwoodite bands around wadsleyite cores. Evolution of this setting through selective olivine melting and fractional crystallization of the olivine melt under high pressure opens a new venue to realistically scrutinize the formational mechanism and ultimately clarify the discrepancies emerged from the solid-state mechanism leading to unrealistic time scales obtained in the last few years. The dominant texture consists of concentric Fe-rich ringwoodite (Fa_{28-38}) bands encompassing Mg-rich wadsleyite (Fa_{6-10}) cores of the individual former olivines (Fig. 3.8-8). The wadsleyite-ringwoodite interface is sharp with a compositional gap of at least 18-mol.% fayalite. No evidence for diffusion between the high-pressure polymorphs was found and the chemical change at the interface is sharp. The composition of the ringwoodite bands shift spatially from

Fa_{29} at the wadsleyite contact to Fa_{35} at the contact to the clinopyroxene chondrule matrix. TEM studies were conducted on FIB slice cuts across the ringwoodite-wadsleyite contact in a squeezed olivine chondrule in the same melt vein (Fig. 3.8-9).

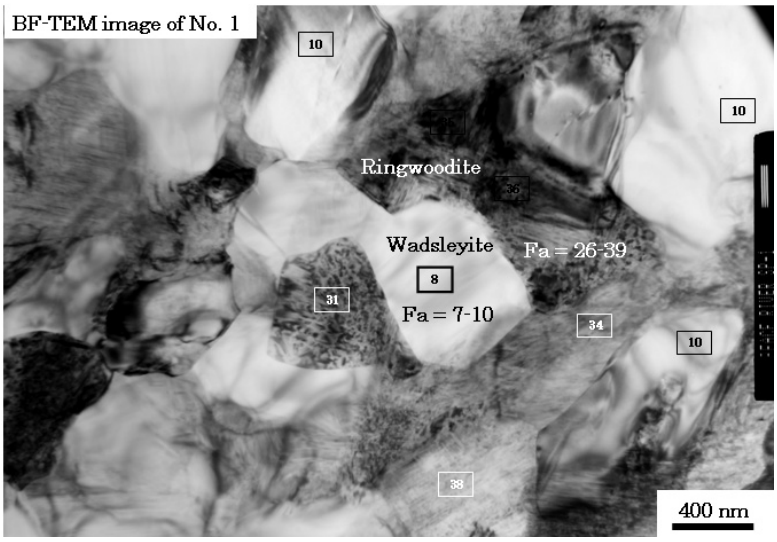

Fig. 3.8-10: A TEM photograph of an FIB cut (Fig. 3.8-9) depicting the intergrowth and compositions (Fa-content) of wadsleyite and ringwoodite crystallites.

The encountered assemblage consists of equi-granular ringwoodite and wadsleyite crystallites with a texture feigning a granoblastic intergrowth (Fig. 3.8-10). Ringwoodite crystallites depict abundant stacking faults along (110) and many dislocations (dislocation density: ρ = 3.30-13.76 x10^{10} cm^{-2}). In comparison, wadsleyite crystallites seem to be barren of stacking faults suggesting lack of shear. The dislocation density in wadsleyite is: ρ = 0.30-1.10 x10^{10} cm^{-2}. Ringwoodite compositions vary between Fa_{31} and Fa_{38}. In comparison, the wadsleyite composition is quite narrow: $Fa_{07\text{-}10}$. No zoning profiles were encountered in ringwoodite or wadsleyite crystallites at their interfaces. Texture of the wadsleyite cores and ringwoodite bands (Fig. 3.8-8) and the contrasting compositions of the wadsleyite and ringwoodite crystallites are not reminiscent of solid-state transformation. Concentric arrangements of both dense phases and the zoning behaviour of ringwoodite away from the wadsleyite interface are strongly suggestive of fractional crystallization from individual olivine melts commencing with a Mg-rich wadsleyite followed by Fe-rich ringwoodite from an olivine melt that is continuously depleted in Mg due to progressive wadsleyite followed by ringwoodite crystallization at 17-20 GPa and below 2400 °C. None of the findings presented here were recognized in the many published articles in the recent years thus leading to unrealistically long time scale calculations.

3.9 Materials Science

Experimental research at Bayerisches Geoinstitut is closely tied to developments in materials science, not only through the quest for materials stable at high pressure and temperature, but also from the unique pressure and temperature conditions which BGI offers for materials synthesis. Such research at BGI has traditionally focused on diamond-based materials and ceramics with grain sizes in the nanometre range. In the following chapter eight projects are presented where these experimental capabilities are exploited in the synthesis and characterisation of materials with superior properties for various applications. Boron-doped diamond is used to investigate the carbon isotope effect on superconductivity, and the isotope effect also provides the possibility to use ^{13}C diamond for pressure calibration in the diamond anvil cell. Production of nanomaterials under high pressure may lead to partial amorphisation, which can be enhanced by cycles of compression and decompression to increase the bulk modulus. Better homogenisation of nanometre-sized ceramic compounds can be achieved through sintering under gigapascal pressures in the multianvil press. High pressure also induces a ferromagnetic to antiferromagnetic transition in manganite perovskites, and a first-order transformation resulting in a ferromagnetic moment in ferrite spinels. It is well known that substitution of nitrogen into zirconia creates oxygen vacancies that stabilise the industrially useful high temperature modification, but less is known about the potentially interesting effects of pressure. The high pressure modifications of various hydrides (alanites and borohydrides) are interesting materials for hydrogen storage, which continues to motivate studies of their structure and properties.

a. *Large carbon-isotope shift of T_c in boron-doped diamond (N.A. Dubrovinskaia/Heidelberg; L.S. Dubrovinsky; T.P. Papageorgiou and J. Wosnitza/Dresden-Rossendorf; A. Bosak and M. Krisch/Grenoble; H.F. Braun/Bayreuth)*

One of the basic ingredients for the development of BCS theory based on a phonon-mediated coupling mechanism was the observation of the isotope effect. A shift of the superconducting transition temperature, T_c, with changing isotope mass, M, can be regarded as clear evidence for superconductivity caused by electron-phonon interaction. In the simplest picture, $T_c \propto 1/\sqrt{M}$ is expected. Soon after the report of superconducting boron-doped diamond (BDD), extensive theoretical investigations led to the conclusion that superconductivity is most likely caused by electron-phonon coupling. Some experimental results, including inelastic X-ray scattering from BDD grown by chemical vapour deposition, support theoretical models suggesting a phonon-mediated pairing mechanism via coupling of optical-phonon modes to Fermi surfaces around the zone centre. In this context data of the isotope effect on T_c are of fundamental importance in order to test the theoretical predictions and to probe to which extent phonons mediate superconductivity. Here we investigate experimentally the carbon-isotope effect for BDD.

Cylindrical samples were obtained by direct reaction of graphite or amorphous carbon with an appropriate amount of boron carbide, and subjected to high P,T using the 5000-tonne

multianvil press at BGI (P =20 GPa, T = 2700 K). We also synthesised two BDD samples from ^{13}C under the same P,T conditions. Equal doping levels between samples was confirmed by X-ray diffraction (^{12}C and ^{13}C BDD gave identical lattice parameters of a = 3.5724(4) Å) and electrical transport measurements (^{12}C and ^{13}C BDD gave identical slopes of the Hall signal: Fig. 3.9-1, inset). Further evidence for the equal boron concentration in both samples was obtained from Raman data, which are sensitive to the interaction of the dopant atoms with the electronic continuum. The Raman spectrum of ^{13}C BDD looks similar to that of ^{12}C BDD, but is slightly shifted towards lower frequencies (Fig. 3.9-2). If the Raman shift of ^{13}C BDD (solid curve in Fig. 3.9-2a) is scaled according to the relation $M_{12}\omega_{12}^2 = M_{13}\omega_{13}^2$, the scaled ^{13}C BDD spectrum (dotted curve in Fig. 3.9-2a) reproduces exactly the Raman-shift position of the ^{12}C BDD spectrum, as expected for a purely isotope-mass induced difference in the Raman spectra.

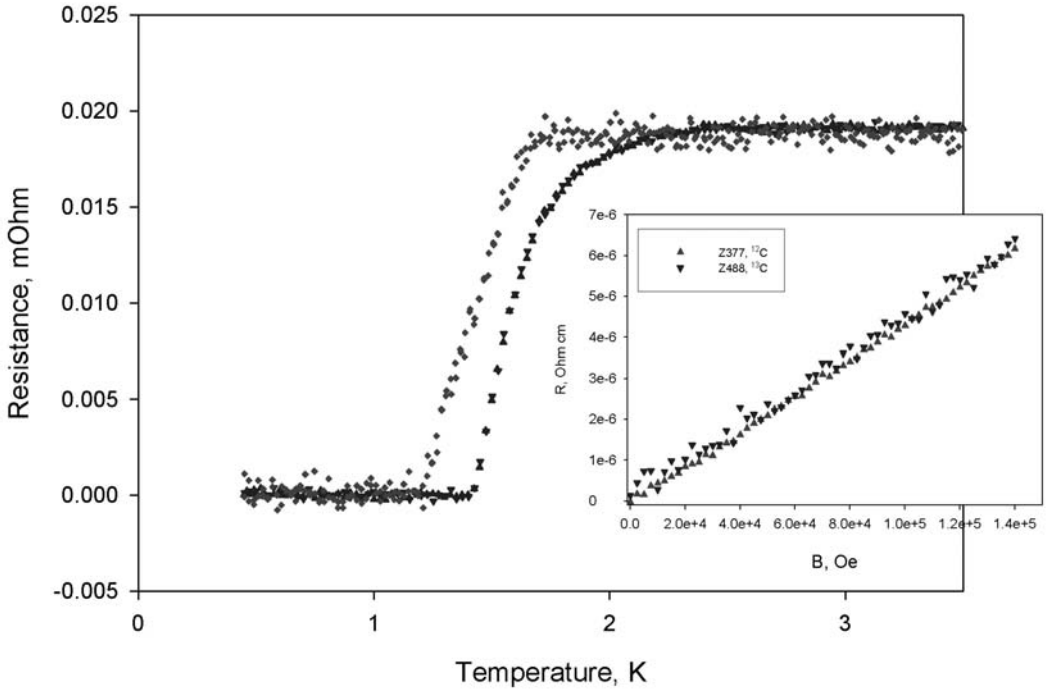

Fig. 3.9-1: Temperature dependence of the resistance for both BDD samples. The superconducting transition of the sample containing ^{12}C is higher by about 0.2 K than for the ^{13}C sample. The inset shows the Hall resistivity of the two samples revealing the equal charge-carrier concentration.

For phonon-mediated superconductivity in BDD the replacement of ^{12}C in BDD by ^{13}C with 8 % higher mass should cause a decrease in T_c according to

$$T_{c13} = T_{c12}\left(\frac{M_{12}}{M_{13}}\right)^{\alpha}, \qquad (1)$$

where M_{12} and M_{13} are the masses of the isotopes, and T_{c12} and T_{c13} the corresponding transition temperatures. For a number of metals, the isotope exponent is found to be close to α = 1/2, *i.e.*, in accordance with the expectation from the simplest BCS picture. For many other

superconductors, deviations from α = 1/2 (in most cases α < 1/2) have been observed and explained by more complex theoretical treatments taking into account the phonon spectrum, the Coulomb repulsion, and details of the electron-phonon coupling. For BDD, the T_c shift expected from Eq. (1) with α = 1/2 would be below 0.1 K based on the zero resistance T_c of 1.4 K for ^{12}C BDD. We used electrical-resistance and specific-heat measurements to determine T_c for our samples. From the resistance data (Fig. 3.9-1) a clear shift in T_c was observed. For ^{12}C BDD, some inhomogeneities led to a much higher T_c onset at about 2.3 K than was found for ^{13}C BDD (at about 1.7 K). Zero resistance was reached at 1.4 K and 1.2 K, respectively. Altogether a zero resistance T_c shift of about 0.2 K is inferred from the resistance data, *i.e.*, two times larger than expected. This shift is much larger than any variation in T_c observed for different ^{12}C or ^{13}C samples; however, resistive measurements might reflect the properties of a small volume fraction of the sample.

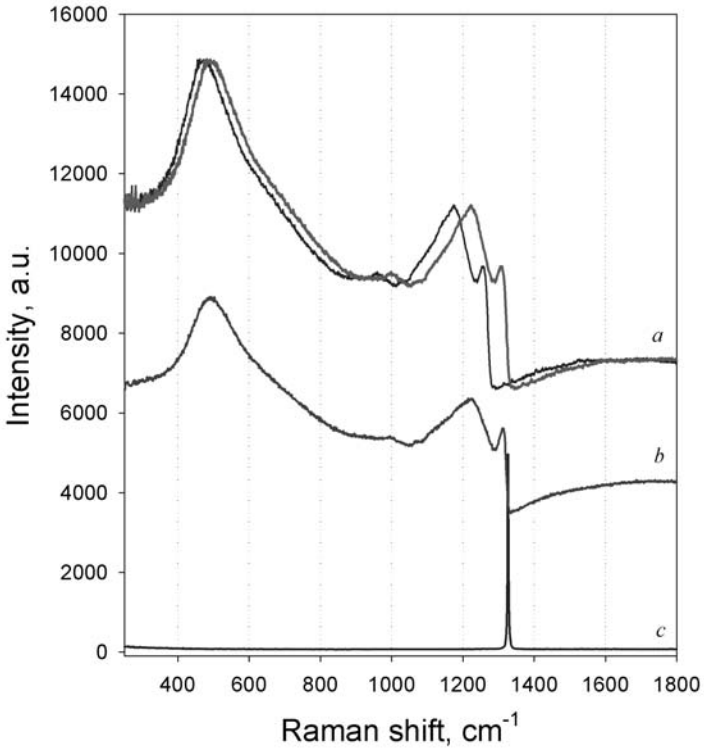

Fig. 3.9-2: Raman spectra of BDDs containing ^{13}C (a) and ^{12}C (b) isotopes in comparison with that of pure synthetic diamond (c). The spectrum of ^{13}C BDD is shifted to higher wave numbers according to the relationship $M_{12}\omega_{12}^2 = M_{13}\omega_{13}^2$ [right curve in (a)] and resembles that of ^{12}C BDD (b).

A more reliable method to determine T_c is specific heat measurements. We obtained the temperature dependence of the electronic part of the specific heat, C_e divided by T (Fig. 3.9-3) by subtracting the phonon contribution, $C_{\mathrm{ph}} = (12\pi^4 R/5)/\Theta_D^3$, from the total specific heat (R is the gas constant and Θ_D is the Debye temperature, which for diamond is high – on the order of 2000 K). Consequently, C_{ph} is very small for the temperature range shown, only about 4 % of

the total heat capacity at 5 K, and could not be determined directly from the specific-heat data. We therefore used an independent method to find Θ_D for our samples, *i.e.*, inelastic X-ray scattering. Using this data, the energy-dependent phonon density of states was determined and we obtained Θ_D = 2040 K for ^{12}C and Θ_D = 1960 K for ^{13}C BDD. From the dominant linear specific-heat contribution we found an electronic Sommerfeld coefficient of $\gamma \sim 0.15$ mJ/mol K^2 for both materials, which is in reasonable agreement with earlier reports for ^{12}C BDD. For both samples, clear anomalies in the specific heat, *i.e.*, bulk superconductivity, can be resolved (Fig. 3.9-3). These anomalies are, however, broadened due to the inhomogeneous polycrystalline nature of the samples and, possibly, due to fluctuations. When approximating the transitions by mean-field-like jumps at T_c we obtained T_{c12} = 1.90(1) K and T_{c13} = 1.70(1) K. Here, we used the usual entropy-conserving constructions. From these we obtained $\Delta C/\gamma T_c$ = 0.27 and 0.31 for the ^{12}C and ^{13}C samples, respectively. This is 19 % and 22 % of the BCS weak-coupling value 1.43, which indicates that only parts of the samples became superconducting. Nevertheless, our specific-heat data prove a clear isotope effect with a T_c shift of 0.2 K in agreement with the resistance data.

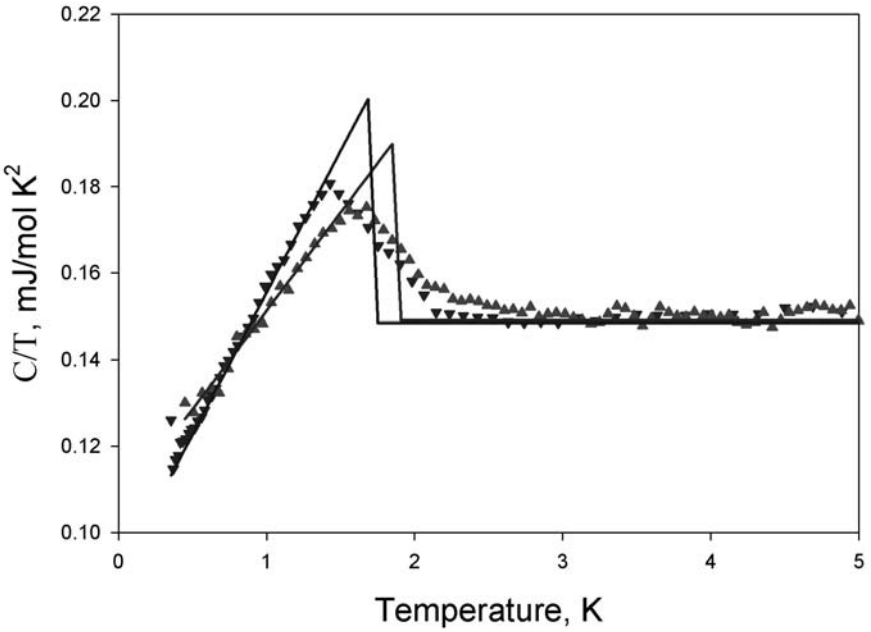

Fig. 3.9-3: Temperature dependence of the electronic part of the specific heat divided by temperature, C_e/T, for both samples. The phonon contribution was subtracted using the Debye temperature extracted from inelastic X-ray scattering data. The solid lines are entropy-conserving constructions revealing T_{c12} = 1.9 K and T_{c13} = 1.7 K.

b. *Pressure dependence of the A_{2g} Raman mode of ^{13}C diamond (E.Yu. Zarechnaya and L.S. Dubrovinsky)*

Raman spectroscopy is generally a simple technique and straightforward to interpret for detailed structural and phase studies. Analysis of the frequencies, line widths, and shapes of

the zone centre vibrational modes provides information on changes in the structure and bonding at high pressure and temperature. However, accurate determination of the conditions at which the measurements are made is difficult. One such problem is the choice of the pressure scale calibrant material in order that it has the required sharpness of peaks, chemical stability, hardness and reproducibility. Diamond is a hard and optically transparent material, but the direct measurement of pressure from the diamond anvils is impossible due to the broad first-order phonon spectrum arising from the inhomogeneous stress distributions. Thus, the diamond anvil cell (DAC) is a poor candidate as a pressure standard. Simultaneously using a diamond chip as a pressure calibrant in the DAC is experimentally difficult to implement. This is due to difficulties in resolving a useful signal, scattering from the anvils and the low intensity of the signal as compared to ruby. It may only be useful in the very high pressure region. A more responsive material could prove to be ^{13}C diamond, because the corresponding peak can be easily observed in Raman spectra at 1280 cm^{-1} (at ambient pressure and temperature). To investigate the potential of ^{13}C diamond as a pressure calibrant, we carried out a study of the pressure dependence of its Raman spectra.

We synthesised ^{13}C diamond using the Sumitomo 1200-tone multianvil press at a pressure of 14 GPa and a temperature of ~ 2600 °C. A mixture of ^{13}C and Pt powders was used as a starting material and loaded into a Pt capsule. We used the classic 14/8 cell assembly, composed of truncated WC cubes, MgO octahedron and cylindrical $LaCrO_3$ furnace. We investigated the high-pressure behaviour of the synthesized material using the DAC. The sample was clamped between two diamond anvil culets with diameters of 300 μm. A rhenium metal gasket was indented to a thickness of ~ 50 μm and a hole with 120 μm diameter was drilled in the centre. A small isometric piece of ^{13}C diamond (about 10 μm in diameter) was loaded together with a ruby ball and chip of Sm:YAG crystal (each ~5 μm in diameter) to serve as pressure markers. Ne was loaded at 1.4 kbar for use as a pressure transmitting medium. Raman scattering experiments were carried out using the LabRam spectrometer with a resolution of 2 cm^{-1}. The 632.8 nm line from a 100 mW He-Ne laser was used for excitation.

Figure 3.9-4 shows examples of the Raman spectra and demonstrates the displacement of the position of the A_{2g} Raman mode of ^{13}C diamond to higher wavelengths with increasing pressure. At 16.7 GPa the peak from ^{13}C diamond merges with the signal from the diamond anvils. The Raman shift as a function of pressure is shown in Fig. 3.9-5. The presented data were normalised to the zero-pressure frequencies of A_{2g} ^{13}C (1280 cm^{-1}) and ^{12}C (~ 1332 cm^{-1}) diamonds, respectively. The calibration of ^{13}C diamond made by Sm:YAG shows a steeper slope of 3.25 cm^{-1}/GPa with a linear fit compared to the ruby scale (2.81 cm^{-1}/GPa), which likely reflects a discrepancy between the Sm:YAG and ruby scales. The pressure behaviour of the Raman shift of the A_{2g} mode of ^{13}C diamond is in good agreement with the dependence reported in the literature (Fig. 3.9-5.). Further investigation is required to determine the simultaneous temperature and pressure influence on the A_{2g} Raman peak of ^{13}C diamond for its use as a calibrant material.

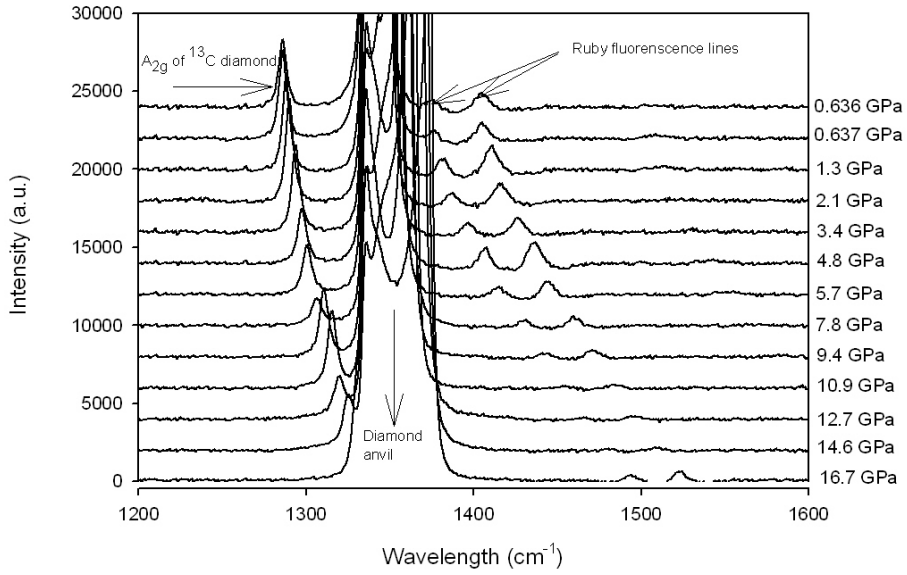

Fig. 3.9-4: The Raman spectra of ^{13}C diamond under pressure in the 1200-1600 cm^{-1} wavelength region.

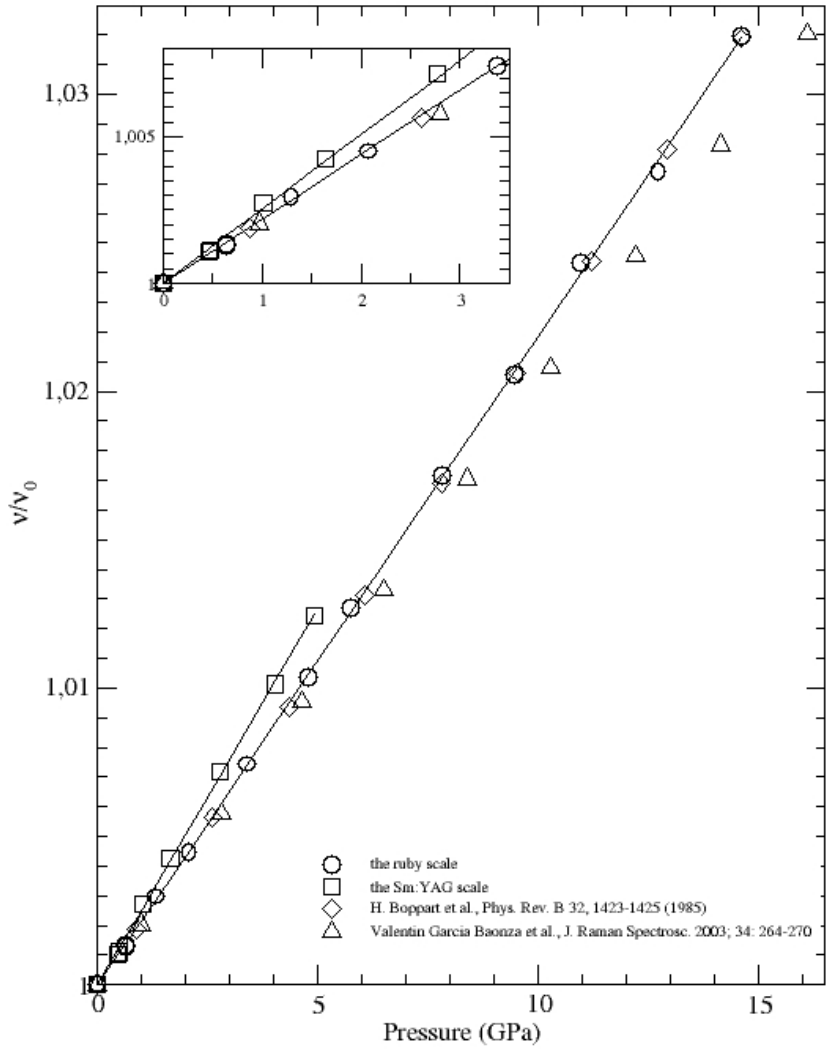

Fig. 3.9-5: Pressure dependence of the first-order phonon Raman peaks of ^{13}C and ^{12}C diamonds according to different pressure scales normalised to the corresponding zero-pressure ν_0. Symbols are as follows (pressure transmitting medium in parentheses): circles - ^{13}C with ruby (Ne); squares - ^{13}C with Sm:YAG (Ne); diamonds - ^{12}C with ruby (H_2); triangles - ^{12}C with Sm:YAG (methanol-ethanol).

c. *Stiffening of Zr-doped nanoanatase upon cycles of compression and decompression (E. Holbig and L.S. Dubrovinsky; R. Wirth/Potsdam, V.B. Prakapenka/Chicago and V. Swamy/Clayton)*

In a previous study, we observed Zr-doped anatase $Ti_{0.9}Zr_{0.1}O_2$ to have an increased bulk modulus compared to its microscale and undoped counterparts (see BGI Annual Report 2006). In order to study the compression behaviour of the material in more detail, we performed a diamond anvil cell experiment with cycles of compression and decompression on Zr-doped anatase $Ti_{0.9}Zr_{0.1}O_2$, mixed with the pressure medium LiF. *In situ* XRD patterns were collected in order to gain information about the structural parameters. Figure 3.9-6 shows the refined pressure-volume data of the sample, fitted to a second order Birch-Murnaghan equation of state with K_0' fixed to 4. The bulk modulus of the material during the first compression was determined to be K_0 = 211(7) GPa, then upon decompression K_0 decreased to 199(3) GPa, and then increased upon the second compression to 249 (9) GPa. It follows that the precompressed sample is stiffer than the uncompressed sample. The figure also shows the data of a previous experiment performed on the same material upon the second compression, exhibiting K_0 = 266(6) GPa.

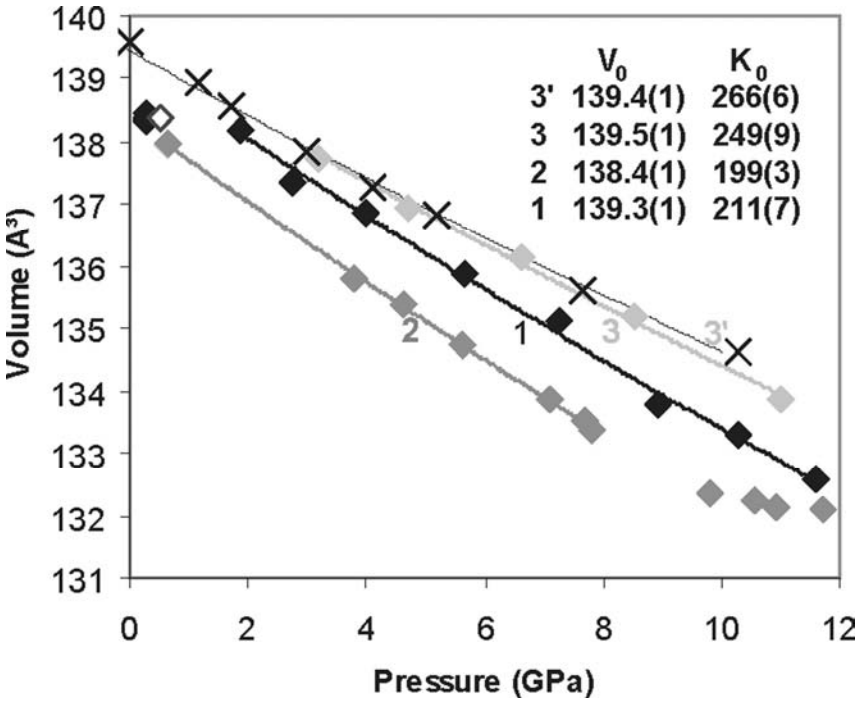

Fig. 3.9-6: Results of a DAC experiment on nanocrystalline $Zr_{0.1}Ti_{0.9}O_2$ with cycles of compression and decompression. Experimental room temperature pressure-volume data are shown, and the curves are fits to a second order Birch-Murnaghan EoS with K_0' = 4. Data are from the experiment on an originally uncompressed sample (diamonds) and the experiment on a precompresed sample (crosses). The sequence of experiments was as follows: first compression (labelled *1*); first decompression (labelled *2*), second compression (labelled *3*), second decompression (open diamond). The symbols labelled *3'* are from the experiment on precompressed material.

Figure 3.9-7 shows high-resolution TEM images of the starting material as well as of the quenched sample after a second experiment with analogous cycles of compression and decompression, performed on anatase $Ti_{0.9}Zr_{0.1}O_2$ without the use of a pressure medium. The crystallite sizes are 12(±3) nm for both samples and therefore remain more or less constant during the experiment. The crystallites of the quenched sample show spherical crystal shape and are defect-free.

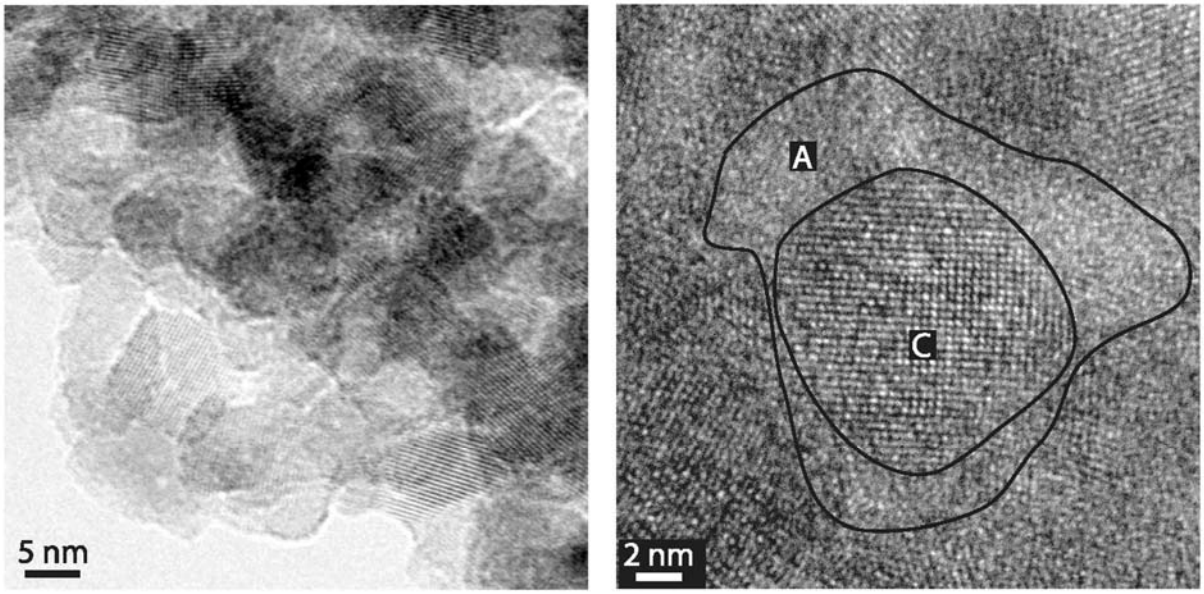

Fig. 3.9-7: HRTEM images of the nanoscale anatase $Ti_{0.9}Zr_{0.1}O_2$ sample before (left) and recovered after the experiment (right). *A* indicates the area of a suggested amorphous rim, and *C* indicates a crystalline area.

There are several lines of evidence suggesting that the crystallites are surrounded by amorphous rims and that amorphisation takes place gradually upon compression. Pressure-induced amorphisation was observed before for anatase with a crystallite size < 10 nm; whereas coarser samples undergo transformations to crystalline high-pressure polymorphs. Partial amorphisation was suggested earlier from experiments, but could not be detected by the *in situ* XRD analysis, because the broad amorphous features would be hidden in the background signal – a phenomenon that also applies for this study. Partial amorphisation was theoretically predicted for nanoscale anatase from molecular dynamics computations. At 25 GPa, the simulations suggest the appearance of disorder in the surface-shell region (about 30-40 % of the atoms), surrounding a more rigid crystalline core, which also contains some defects. In our study, the TEM analysis of the material after compression shows in fact features that can be assigned as rims of amorphous material with a thickness of several nanometres (Fig. 3.9-7, right), confirming the suggested appearance of partial amorphisation. However, the TEM image shows a foil of the sample in which several crystallites overlap and the features seen could be the consequence of the overlap. To avoid overlap of crystallites, TEM foils with a thickness of 10-15 nm would be necessary.

The above evidence leads us to conclude that the nanoscale anatase $Ti_{0.9}Zr_{0.1}O_2$ undergoes partial pressure-induced amorphisation, which leads to stiffening of the material. Upon compression, amorphous rims start to envelope the crystallites and amorphisation takes place gradually. We can use the phenomenon of amorphisation to explain the compression behaviour of the sample as follows. Part of the compression energy is used for the formation of amorphous crystallite rims, and the rims seem to shield the anatase particles against pressure change and most probably deform and exhibit strain while they are assimilating the compression energy. The anatase nanocrystallites therefore undergo less pressure change than the LiF particles. The partial amorphisation is accompanied by stiffening of the material, making it an interesting phenomenon for materials research with the goal of creating new abrasive materials.

d. *High-pressure hot pressing of nanostructured composite materials (I. Zalite/Riga, in collaboration with D.J. Frost)*

Successful fabrication of nanostructured materials from ceramic powders with the traditional compacting methods (sintering, hot pressing, etc.) is complicated due to the high chemical activity of nanopowders and the tendency for agglomeration, which can result in rapid grain growth during sintering. These problems may be partially solved through the use of high-pressure (> 3 GPa) hot pressing, which may act to destroy agglomerates and limit their formation by allowing a reduced sintering time and temperature, thus ensuring the formation of a fine structure.

No.	Sample	Phases and composition	SSA, m^2/g	d_{50}, nm
1	Si_3N_4 – SiC	18 wt.% Si_3N_4; 74 wt.% SiC; 8 wt.% Cfree	35	60
2	Si_3N_4 – SiC	20 wt.% Si_3N_4; 80 wt.% SiC; 0 wt.% Cfree	40	50
3	Si_3N_4 – TiN	30wt.% Si_3N_4 – 70wt.% TiN	140	15
4	TiCN	$TiC_{0,4}N_{0,6}$	40	30
5	WC	WC_{1-x}; (W_2C; C)	49	10
6	Al_2O_3	Al_2O_3	50	40

Table 3.9-1: Characteristics of the investigated powders

In this study plasma-produced nanopowders of different refractory compounds were investigated (Fig. 3.9-8). This fabrication process involves the rapid evaporation of raw components in a high frequency nitrogen or air plasma (at the average mass temperature of 5000-6000 K) followed by rapid freezing of the reaction products. The investigated powder compositions are reported in Table 3.9-1.

These materials were hot pressed in a multianvil apparatus at pressures of 8 GPa and sintering temperatures of 1400-1500 °C. A Re foil capsule was employed to encapsulate the compacted starting powders. Temperatures were raised at an approximate rate of 100 °C/min and samples were annealed at the highest temperature for between 5 and 10 minutes. Although samples await further transmission electron microscopy analysis, initial observations indicate that the grain size in all recovered samples was similar to that of the starting powders and grain growth was not significant during high-pressure hot pressing (Fig. 3.9-9).

Phase analysis by X-ray powder diffraction confirmed that in most cases the samples contained the same phases that form during conventional hot pressing at lower pressures. However in carbide-containing samples which contain free amorphous carbon, diamond could be identified in the recovered samples, which is noteworthy given that annealing was performed at relatively low temperatures and for quite short time durations. The samples await micro-hardness tests; however initial results indicate that nano-TiCN-C (diamond), Si_3N_4-SiC-C (diamond), and WC-Co-C (diamond) may be promising hard composite materials.

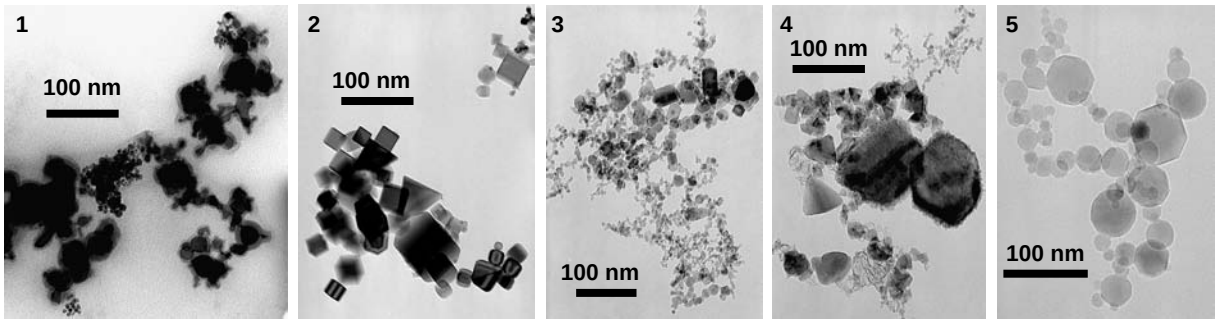

Fig. 3.9-8: TEM micrographs of the tungsten carbide (1), titanium carbonitride (2), silicon nitride-titanium nitride (3), silicon nitride-silicon carbide (4) and alumina (5) starting nanopowders.

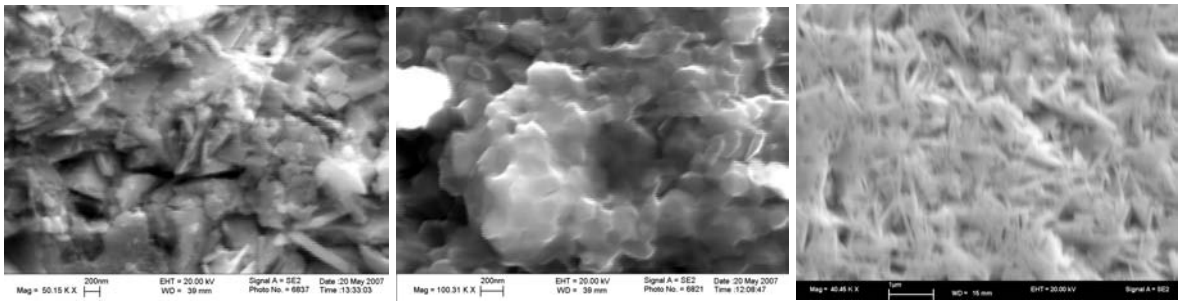

Fig. 3.9-9: Electron micrographs of the ceramics fracture surface of samples 2 (left), 4 (middle) and 5 (right).

e. *Pressure-induced compression anisotropy and antiferromagnetism in $Pr_{0.52}Sr_{0.48}MnO_3$ (D.P. Kozlenko and B.N. Savenko/Dubna, L.S. Dubrovinsky, Z. Jirák/Prague)*

Perovskite manganites $R_{1-x}A_xMnO_3$ (*R* - rare earth, *A* - alkaline earth elements) exhibit a rich variety of fascinating physical phenomena extensively studied during the previous years – colossal magnetoresistance, charge and orbital ordering, and mesoscopic phase separation. A complicated balance of ferromagnetic (FM) double exchange mediated by charge carriers of e_g nature and antiferromagnetic (AFM) superexchange interactions between localised magnetic moments of t_{2g} nature, coupled to lattice distortion effects and orbital degrees of freedom, lead to especially complex phase diagrams of compounds with $x \sim 0.5$. While manganites with x slightly less than 0.5 commonly exhibit a FM metallic ground state, in systems with $x \geq 0.5$ the ground state becomes antiferromagnetic with properties depending substantially on the distortion of the Mn^{3+}-O^{2-}-Mn^{4+} network. In $La_{0.5}Sr_{0.5}MnO_3$ and $Pr_{0.5}Sr_{0.5}MnO_3$ compounds with a larger $\langle r_A \rangle$, the metallic conductivity and layered A-type AFM ground state with $d(x^2\text{-}z^2)$ e_g orbital order occur at ambient pressure. In $Nd_{0.5}Ca_{0.5}MnO_3$, $Pr_{0.5}Ca_{0.5}MnO_3$, $La_{0.5}Ca_{0.5}MnO_3$ and $Nd_{0.5}Sr_{0.5}MnO_3$ with smaller $\langle r_A \rangle$, a charge-ordered insulating ground state with $d(3x^2\text{-}r^2)/d(3z^2\text{-}r^2)$ e_g orbital order occurs.

Important insight into the formation of the magnetic phase diagram of manganites near the 0.5 composition can be made by investigation of the high-pressure effects on compounds with a FM metallic ground state. For this purpose, we have investigated the crystal and magnetic structure of $Pr_{0.52}Sr_{0.48}MnO_3$ manganite by X-ray and neutron diffraction at pressures up to 31 and 4 GPa, respectively.

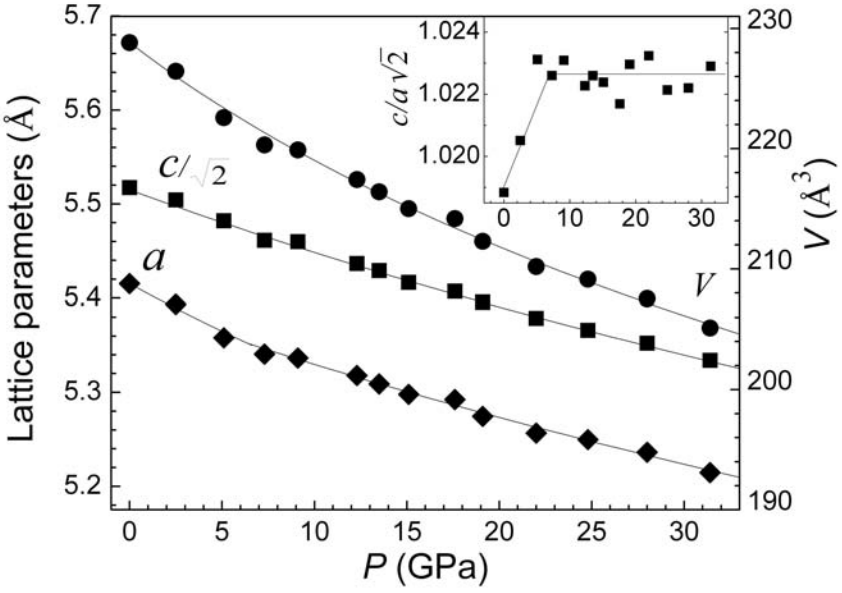

Fig. 3.9-10: Lattice parameters, their ratio (inset) and unit cell volume of $Pr_{0.52}Sr_{0.48}MnO_3$ as a function of pressure.

The tetragonal crystal structure of *I4/mcm* symmetry remains stable in the investigated pressure range up to 31 GPa, as found from X-ray diffraction. At intermediate pressures up to

6 GPa the anisotropic compression of the unit cell with the most compressible *a*-axis is observed, as seen by the increase of the $c/a\sqrt{2}$ lattice parameter ratio (Fig. 3.9-10). At higher pressures, the $c/a\sqrt{2}$ value becomes nearly independent of pressure, implying equal compressibilities of the *a* and *c* lattice parameters. The bulk modulus value B_0 = 235(5) GPa was calculated from fitting the volume compressibility data with the Birch-Murnaghan equation of state and fixed B' = 4 and V_0 = 205.1(3) Å^3.

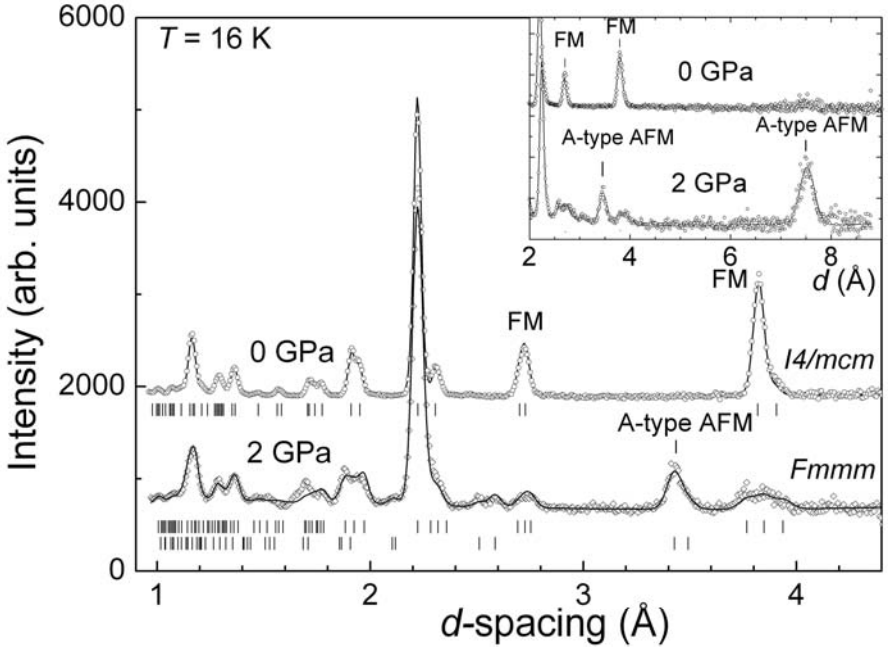

Fig. 3.9-11: Neutron diffraction patterns of $Pr_{0.52}Sr_{0.48}MnO_3$ measured at P = 0 and 2 GPa, T = 16 K at scattering angles 2θ = 90° and 45.5° (inset) and processed by the Rietveld method. The experimental points and calculated profiles are shown. Ticks represent the calculated positions of the nuclear peaks of the *I4/mcm* tetragonal phase (upper row) and positions of the nuclear (middle row) and magnetic (lower row) peaks of the *Fmmm* orthorhombic A-type AFM phase.

Neutron diffraction patterns of $Pr_{0.52}Sr_{0.48}MnO_3$ measured by the time-of-flight method at selected pressures and temperatures are shown in Fig. 3.9-11. At ambient pressure on cooling at $T < T_c$ = 270 K an additional intensity is observed in two sets of nuclear peaks, (110)/(002) and (200)/(112) of the tetragonal *I4/mcm* structure, which are characteristic of the FM phase. The manganese magnetic moments are oriented along the tetragonal *c*-axis and their value is μ_z=3.6(1) μ_B. At P = 2 GPa on cooling below $T_N \approx$ 250 K, some splitting of diffraction peaks in *d*-spacing regions 1.8-2 Å and 3.7-3.95 Å are evident (Fig. 3.9-11). In addition, new magnetic lines at d = 7.53 and 3.44 Å appear, indicating an onset of the new AFM state. No ferromagnetic contribution to diffraction patterns is found at high pressures. The data analysis shows that observed modifications of diffraction patterns correspond to the pressure-induced

onset of the A-type AFM state, which is accompanied by the structural phase transformation from the tetragonal crystal structure of *I4/mcm* symmetry to the orthorhombic structure of *Fmmm* symmetry. At ambient pressure the similar A-type AFM state is found in $Pr_{1-x}Sr_xMnO_3$ manganites with $0.5 < x < 0.6$.

f. *High-pressure study of zinc and magnesium ferrite spinels (G.Kh. Rozenberg and E. Greenberg/Tel Aviv, in collaboration with A. Kurnosov and L.S. Dubrovinsky)*

The present investigation stems from our recent extensive high-pressure magnetic (Mössbauer effect) studies in normal and inverse zinc and magnesium ferrite spinels AFe_2O_4 (*A*=Zn, Mg). These studies to 80 GPa revealed for both materials a pressure-induced first-order phase transition in the pressure range 25-35 GPa manifested by dramatic changes of the hyperfine interaction parameters. In the high-pressure phase *two Fe sites with different hyperfine interaction parameters* were observed, which is not entirely consistent with the $CaMn_2O_4$-(CML) or $CaTi_2O_4$-like (CTL) structures suggested by recent X-ray diffraction results reported in the literature. A strong magnetic relaxation effect was observed around the magnetic ordering temperature which decreased with increasing pressure, implying a ferromagnetic coupling in the high-pressure (HP) phase. Upon releasing the pressure the HP phase is metastable, but below 20 GPa only one type of Fe site in the crystal structure is observed. The discrepancies with recent X-ray results motivated the present studies of both materials. Our objectives were to carry out thorough XRD and Raman spectroscopy studies with data analysis in order to clarify the structure of the HP polymorph for both ferrite spinels.

We studied the pressure evolution of the vibrational properties of the AFe_2O_4 (*A*=Zn, Mg) spinels by Raman spectroscopy at 300 K. The Raman spectra were measured using a LabRaman system spectrometer equipped with a microscope and charge-coupled device detector. An Ar laser operating at 632 nm wavelength and power of ~ 30 mW was used for excitation. The samples were loaded into the opposing-plates diamond anvil cell into a cavity of 100 μm in diameter and 30-40 μm thickness drilled in Re gaskets. To improve hydrostatic conditions and hence the data quality, Ne was used as a pressure medium. High-pressure Raman studies were performed up to 60 GPa, and spectra were collected over the range 150-1300 cm^{-1}. Two slots of measurements including compression and decompression cycles were performed. A few X-ray diffraction experiments were performed under pressure and after releasing pressure to ambient conditions.

Raman studies revealed a significant pressure evolution of the Raman spectra (Fig. 3.9-12). The modes shift towards higher energy and broaden with increasing pressure. In the pressure range 24-32 GPa and 35-44 GPa for Zn and Mg ferrite spinels, respectively, a significant evolution of the Raman spectrum was observed. These observations are in good agreement with present XRD studies which revealed structural phase transitions within almost the same

pressure ranges. These transitions are not reversible down to ambient pressure. Analysis of the structural data for $ZnFe_2O_4$ allows us to definitively distinguish between the CTL and CML structures proposed by previous researchers for $ZnFe_2O_4$ and to choose the former one. The revelation in Mössbauer studies of the presence of two different Fe sites in the HP phase can be rationalised on the grounds that in the selected CTL structure, Zn occupies one of the octahedral sites and therefore one of the Fe ions is eightfold coordinated. After decreasing pressure to ~ 20 GPa, Zn and Fe cations change their positions. In the case of $MgFe_2O_4$ none of the above considered structures (CTL, CML or $CaFe_2O_4$-like) match the observed XRD patterns well, and therefore further careful studies are necessary.

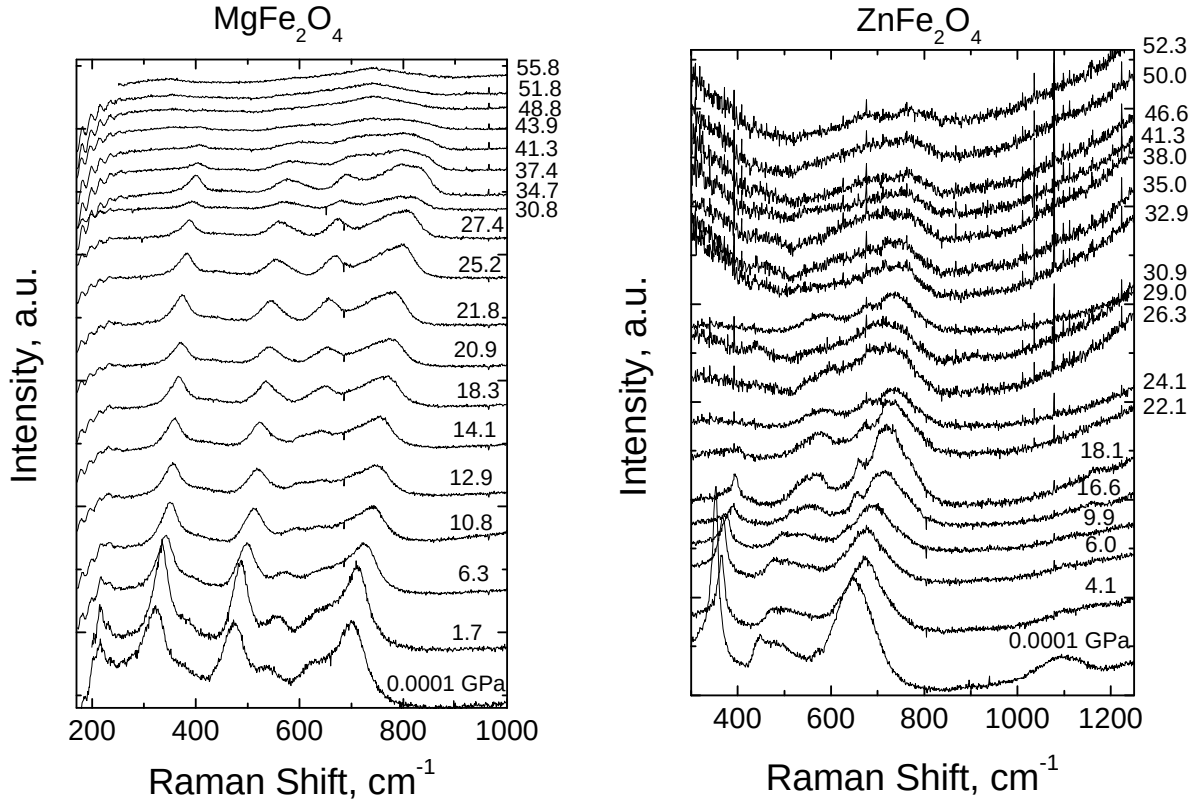

Fig. 3.9-12: Raman spectra of spinels $MgFe_2O_4$ (left) and $ZnFe_2O_4$ (right) recorded as a function of pressure (values in GPa).

g. *High-pressure high-temperature behaviour of nitrogen-doped zirconia (T. Locherer and H. Fuess/Darmstadt, in collaboration with D.J. Frost)*

The substitution of nitrogen into the ZrO_2 sublattice creates oxygen vacancies that stabilise the high-temperature modification of ZrO_2, which has a number of practical applications. In this study the stability of nitrogen-doped zirconia/zirconium oxonitride $Zr_7O_{11}N_2$ has been examined at pressures up to 20 GPa and temperatures up to 2000 °C using a multianvil press. $Zr_7O_{11}N_2$ powder was used as a starting material and encapsulated in Zr foil. Experiments

were performed between 3 and 20 GPa at 750-2000 °C. Recovered samples were sliced into disks using a diamond wire saw and examined using X-ray powder diffraction.

Above ~ 7.5 GPa $Zr_7O_{11}N_2$ was found to decompose into a 48:52 mixture of ZrN and monoclinic zirconia as shown in Fig. 3.9-13. Although monoclinic ZrO_2 was identified in the analysed run products, at the conditions of the experiment ZrO_2 assumes the non-quenchable ZrO_2 tetragonal structure (*t*-ZrO_2). Thermodynamic calculations that take into account the fact that the high-pressure product at 7.5 GPa and temperatures above 600 °C contains the unquenchable *t*-ZrO_2 modification are in excellent agreement with our experimentally determined breakdown curve. Figure 3.9-13 shows the comparison between the thermodynamically and determined breakdown curves and the experimental run products. *In situ* studies of the high-pressure and temperature behaviour of ZrO_2 are therefore very important for understanding the behaviour in this system.

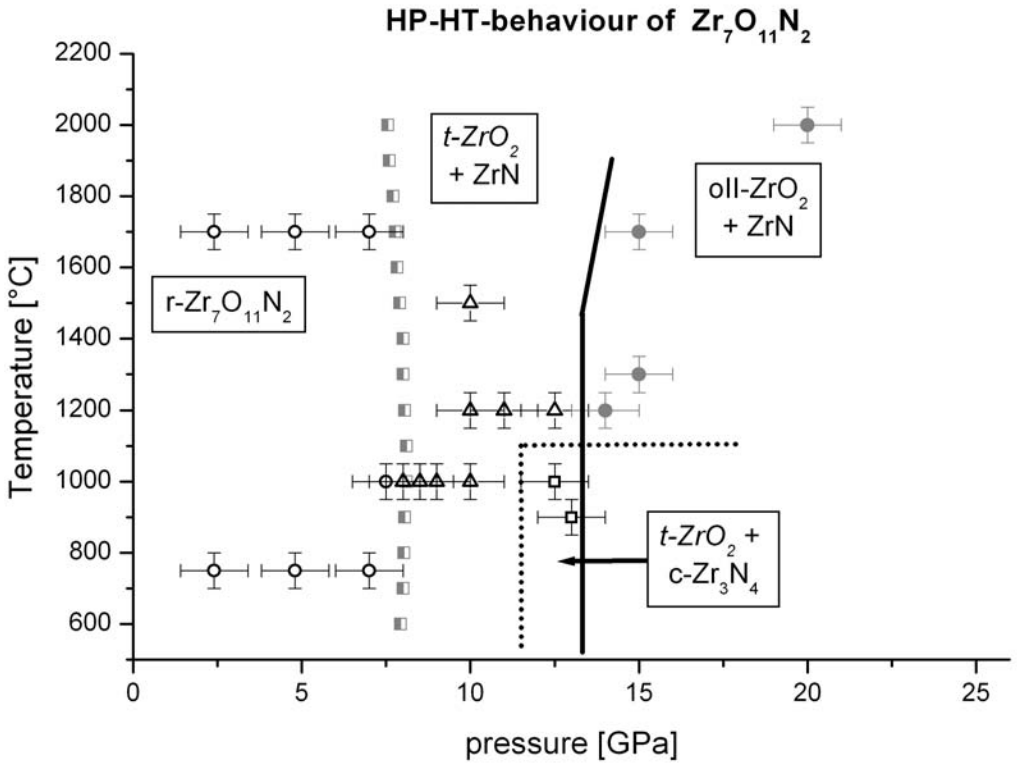

Fig. 3.9-13: The experimental and thermodynamically calculated stability of $Zr_7O_{11}N_2$ between 3 and 20 GPa. The known phase boundaries of ZrO_2 are shown for comparison. Non quenchable phases are denoted in italics. Open circles signify the zirconium oxonitride with rhombohedral symmetry. Open triangles mark the conditions where the quenched composite consisted of monoclinic zirconia and zirconium mononitride. Open squares represent cubic Zr_3N_4 and monoclinic zirconia. Full circles signify the experiments which yielded cotunite-type zirconia and zirconium mononitride. The thermodynamically calculated decomposition conditions are marked with half-full squares.

At pressures above 12 GPa and temperatures below 1100 °C the formation of Zr_3N_4 with the thorium phosphide structure was observed. In this pressure range a certain amount of $ZrO_{0.27}$, a suboxide with trigonal symmetry (*P*3*c*1), was found in addition to ZrO_2. In samples produced above 1200 °C, neither Zr_3N_4 nor $ZrO_{0.27}$ was observed. At pressures above 14 GPa cotunite-type ZrO_2 with orthorhombic symmetry and nine-fold coordinated zirconium were formed. The fact that no oxy-nitride compounds were formed at pressures above 7.5 GPa and up to 20 GPa most likely results from the preferential formation of ZrO_2 as a result of numerous phase transformations producing denser ZrO_2 structures.

h. *High-pressure phase transitions in alkali metal borohydrides (A.V. Talyzin and B. Sundqvist/Umeå, in collaboration with L.S. Dubrovinsky)*

Complex hydrides (alanates and borohydrides) are interesting materials due to their possible applications for hydrogen storage. Many of the recent activities in high-pressure studies of these materials have been stimulated by theoretical studies which predict a large volume collapse for high-pressure modifications of $LiAlH_4$ and $NaAlH_4$. Experimental studies showed that phase transitions do occur in these materials at high-pressure conditions, although not exactly into the predicted structures. Similar studies have recently been initiated also for borohydrides. Two high-pressure phase transitions were observed experimentally for $NaBH_4$ using Raman spectroscopy and diamond anvil cell (DAC) methods and thermal conductivity measurements. Subsequent experiments using Raman spectroscopy and XRD were performed with $LiBH_4$, which among all borohydrides has the maximum hydrogen storage capacity. XRD experiments were also performed on KBH_4 and $NaAlH_4$.

Both the Raman spectrum and the crystal structure of $LiBH_4$ at ambient conditions are well known. It is usually described to be composed of tetrahedral $(BH4)^-$ anions and Li^+ cations. Borohydrides with a *fcc* lattice structure ($NaBH_4$, KBH_4, $RbBH_4$, $CsBH_4$) are known to undergo phase transitions into more ordered phases at low temperatures and ambient pressure. However, the crystal structure of $LiBH_4$ is different from that of the above compounds and no phase transition has been observed at low temperatures at atmospheric pressure. A phase transition from ambient pressure $LiBH_4$ into an almost 6 % denser high-pressure phase was observed almost forty years ago to occur at around 0.6 GPa at 298K and 0.84 GPa at 341 K, but the structure of the high-pressure phase was not solved and the Raman spectra were not recorded. Recently the structural stability of $LiBH_4$ was studied theoretically by several groups. One group predicted a phase transition into a monoclinic high-pressure phase with space group *Cc* to occur at ~ 3 GPa. Another theoretical prediction was recently made of a proposed phase transition into the tetragonal β-KBH_4 structure at 6.2 GPa. The high temperature hexagonal phase of $LiBH_4$ was predicted to be stable at pressures below 6.2 GPa and assumed to be the high-pressure phase previously found. A third study suggested that $LiBH_4$ should transform first into a $P2_1/c$ phase at 1 GPa, and then into the *Cc* structure near 2.2 GPa.

In order to verify these theoretical predictions we performed a set of experiments using the DAC. Raman spectra were recorded at Umeå University and XRD patterns were collected at pressures up to ~ 9 GPa at room temperature using facilities at BGI. The phase transition from ambient pressure α-$LiBH_4$ to high pressure β-$LiBH_4$ was observed by Raman spectroscopy and X-ray diffraction to occur between 0.8 and 1.1 GPa. The phase transition is reversible and pristine α-$LiBH_4$ was observed upon decompression (see Fig. 3.9-14).

While the XRD patterns recorded at BGI allowed us to detect phase transitions in $LiBH_4$, KBH_4 and $NaAlH_4$, they exhibited an insufficient number of reflections for structural identification of the high-pressure phases. It should be taken into account that borohydrides and alanates consist of some of the lightest elements in the periodic table and X-ray scattering from these materials is relatively weak. New experiments with synchrotron radiation were performed during 2007 in order to determine the structure of high-pressure phase of $LiBH_4$, KBH_4 and $NaAlH_4$, and these data are currently being analysed.

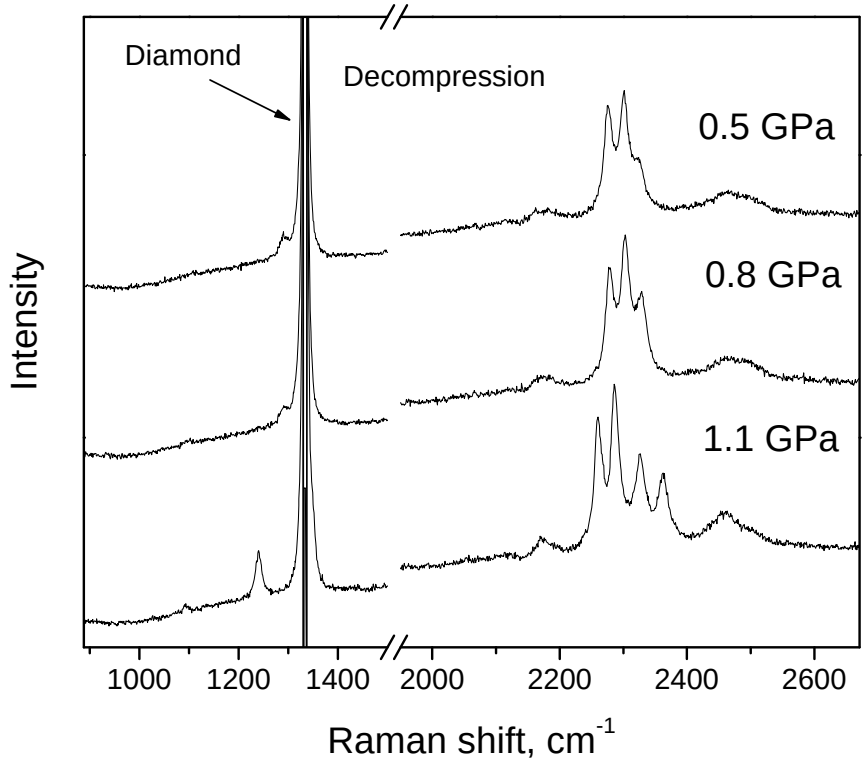

Fig. 3.9-14: Raman spectra of $LiBH_4$ in the region of the phase transition recorded during decompression.

3.10 Methodological Developments

The development of new experimental and analytical techniques paves the way for major breakthroughs in science and technology. The Bayerisches Geoinstitut has a long tradition in competing in this discipline, with many of its innovations having been adopted by labs worldwide.

In the last year, new developments were made in the determination of stress in multi-anvil experiments, in the determination of iron oxidation state of ferropericlase, in the preparation and loading of diamond anvil cells, and in the welding of sample capsules. In the first contribution a new method for determining stress in multianvil experiments is presented that makes use of the piezoelectric property of $GaPO_4$. The second contribution deals with the calibration of the flank method for determining iron oxidation state in ferropericlase, with the aim that it later can be applied to microscopic inclusions in diamonds. The third and fourth contribution focus on the preparation of gaskets and loading of diamond anvil cells for ultrahigh-pressure experiments. Finally, a new technique is presented that allows welding of large amounts of fluid into noble metal capsules without changing the cylindrical shape of the capsules.

a. *The use of $GaPO_4$ as a piezoelectric transducer for stress determinations in high-pressure deformation experiments (S. Shekhar/Kharagpur, in collaboration with N. Walte, S. Linhardt, S. Feulner and D.J. Frost)*

Characterizing the rheological properties of minerals requires the ability to measure the sample strain induced by a known applied deviatoric stress. In multianvil systems, such as the deformation DIA apparatus, samples can be deformed by advancing 2 of 6 anvils independently, such that the entire cubic ceramic pressure medium is deformed. If hard parts are placed inside the pressure medium a significant proportion of the strain can be proportioned into a mineral sample. While the strain rate is generally proportional to the advancement of the outer anvils, the magnitude of the deviatoric stress cannot be determined from a knowledge of the applied force because a large proportion of the force is absorbed by the gaskets surrounding the pressure medium. At a synchrotron facility where *in situ* X-ray diffraction measurements can be made, broadening of powder diffraction lines can be used to constrain the deviatoric stress acting upon a sample. However, such facilities can be visited only a few times in a year, while a single deformation experiment can take many days. A method of in house *in situ* stress measurement would therefore be very useful.

The use of a piezoelectric crystal that produces an electrical potential in response to an applied mechanical stress would be a promising possibility if a suitable crystal can be found that exhibits a piezoelectric effect at high pressures and temperatures. Gallium orthophosphate ($GaPO_4$) is a structural analogue of quartz which displays a larger

piezoelectric effect than quartz. It does not undergo a phase transformation at high temperatures and thus displays the piezoelectric effect up to 970 °C at room pressure. In this study the piezoelectric charge produced by a single crystal of $GaPO_4$ has been measured at high pressures and under high deviatoric stresses.

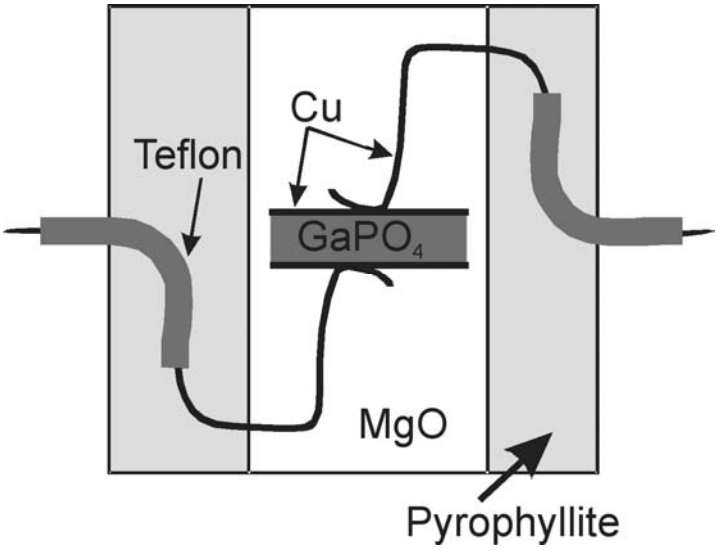

Fig. 3.10-1: High-pressure deformation DIA assembly for piezoelectric measurements of a $GaPO_4$ single crystal. The assembly is made of a pyrophyllite cube of 8mm edge length with a cylindrical hole drilled in it for the insertion of the 0.5 mm thick $GaPO_4$ crystal and MgO spacers.

A single crystal of $GaPO_4$ was kindly provided by Piezocryst Advanced Sensorics GmbH of Graz, Austria. A core of the crystal 1.5mm in diameter and 0.5 mm long was extracted for loading in longitudinal mode. The crystal was placed at the center of an MgO cylinder inside a pyrophyllite DIA cube assembly of 8mm edge length. Disks of Cu were in contact with each of the crystals surfaces with Cu wires leading out of the assembly. Teflon insulator sleeves are required to prevent contact between the Cu wires and the WC anvils.

As the crystal is deformed, electrical charge builds up on the two crystal faces. The resulting low-level current is measured using an integrator amplifier where the current charges an integrator capacitor and the time duration is measured for the charge across the capacitor to reach 10 volts. From a measurement of the charging time the average current produced over this period can be determined. As shown in Fig. 3.10-2, after quasi-hydrostatic compression to 1 GPa at room temperature (*i.e.*, advancement of all 6 anvils simultaneously) an initial high current was measured, which dropped off only after several hours at constant load. It has been well recognized that multianvil assemblies produce deviatoric stresses even under quasi-hydrostatic loading as a result of anisotropic elastic properties of the ceramic assembly components. The measurements show that these stresses relax after approximately 5 hours.

After 17 hours the samples was deformed by advancing 2 of the 6 anvils independently, such that the initially cubic sample assembly was shortened by 17 μm. This caused a clear and measurable increase in the current produced by the crystal. The next phase of the project will be to test the crystal at simultaneous high pressure and temperature. The goal will be to use the crystal as a stress transducer in the colder regions of the assembly, where it will be in mechanical contact with a mineral sample in the hot spot via hard pistons. It should be possible to calibrate the high pressure piezoelectric response in terms of applied stress using *in situ* X-ray diffraction or a lower pressure deformation apparatus where applied stresses can be accurately measured such as a Paterson apparatus.

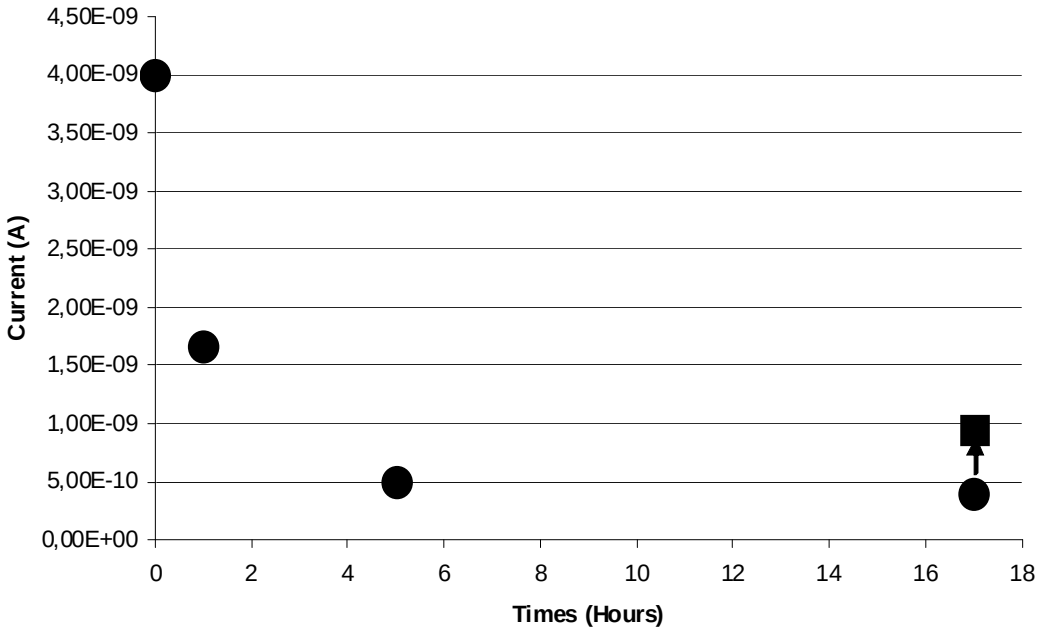

Fig. 3.10-2: Measurements of the piezoelectric current produced by a $GaPO_4$ crystal as a function of time after initial compression to approximately 1 GPa at room temperature. After initial quasi-hydrostatic compression the current drops with time, most likely as a result of relaxation of deviatoric stresses within the high-pressure assembly (solid circles). After a base line current was achieved, the sample was deformed by 17 μm, which caused a measurable increase in the piezoelectric current (filled square).

b. *Iron oxidation state in (Mg,Fe)O: Calibration of the flank method (EMPA) as a new technique for diamond inclusion studies (M. Longo and C.A. McCammon)*

The lower mantle, which represents more than half the Earth by volume, is constituted predominantly of $(Mg,Fe)(Si,Al)O_3$ perovskite and ferropericlase (Mg,Fe)O. Studying these phases is therefore critical to determining redox conditions and their consequences for mantle properties and dynamics. Studies have shown that the Fe^{3+} concentration in $(Mg,Fe)(Si,Al)O_3$ perovskite is essentially insensitive to oxygen fugacity; hence our attention is turned to

(Mg,Fe)O. Our goal is to calibrate the "flank method", which is based on the chemical shift between the two peaks Lβ and Lα observed in the X-ray emission spectra of transition metals when a change in oxidation state occurs. The Lβ/Lα ratio is related therefore to the $Fe^{3+}/\Sigma Fe$ ratio, and in order to measure the Fe^{3+} content directly by electron microprobe, a calibration is needed for each mineral structure. Up to now a calibration of the flank method is available only for garnets, so we plan to calibrate the flank method using synthetic (Mg,Fe)O, and then apply the method to determine $Fe^{3+}/\Sigma Fe$ in ferropericlase inclusions from lower mantle diamonds.

A set of (Mg,Fe)O crystals over a wide range of composition (x_{Fe} = 2 to 60 at.%) and $Fe^{3+}/\Sigma Fe$ (1 to 12 %) were synthesized at 11-15 GPa and 1800-2000 °C in a multianvil apparatus. (Mg,Fe)O polycrystalline powders, after being reduced in a gas mixing furnace at 1300 °C under controlled oxygen fugacity, were loaded into Re capsules of 1.6 mm and 2.4 mm length and compressed up to 15 GPa in a 10/5 pressure assembly. Subsequently the crystals were analyzed using the flank method by electron microprobe at 15kV and 80nA. Mössbauer spectroscopy was used to determine $Fe^{3+}/\Sigma Fe$. A linear relationship between ΣFe and Lβ/Lα measurements was observed, with a variation of the Lβ/Lα ratio from 0.70 to 1.2 counts per second (cps). A positive correlation can also be observed for Lβ/Lα ratios as a function Fe^{2+}, which is slightly non-linear (Fig. 3.10-3b). Flank method measurements were also made directly on polycrystalline (Mg,Fe)O powders, and although data show an increase in Lβ/Lα as a function of Fe^{2+} following the same trend as the multianvil run products, the poor quality of the surface analyzed leads to less accurate data which cannot be included in the data set.

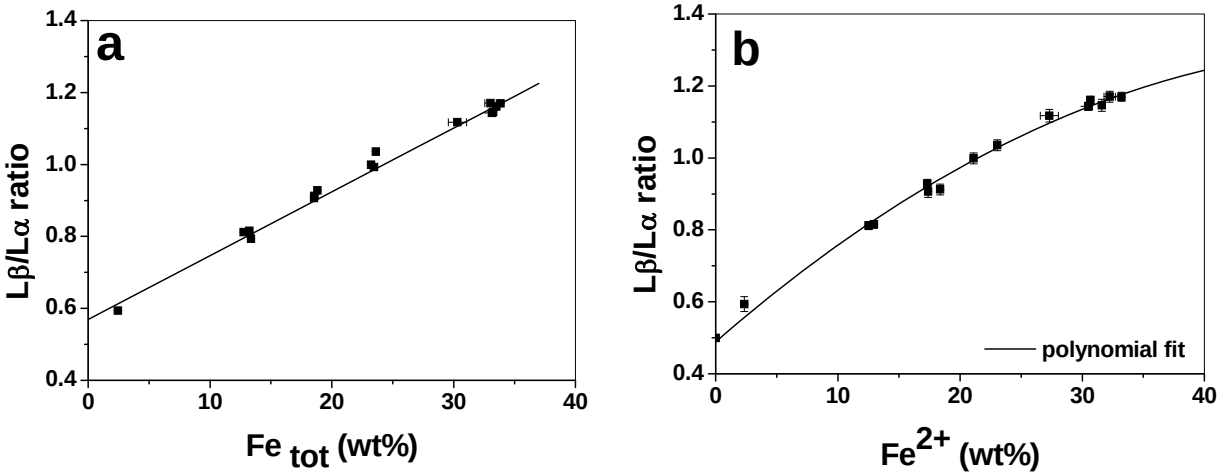

Fig. 3.10-3: Ferropericlase Lβ/Lα ratios as a function of ΣFe (a) and Fe^{2+} (b).

The Lβ/Lα ratio is therefore mainly affected by a self absorption effect due to bulk ΣFe and Fe^{2+}, as it was already demonstrated for garnets. The dependence can be described by the following relation:

$$Fe^{2+} = A + B(L\beta/L\alpha) + C\Sigma Fe + D\Sigma Fe \times (L\beta/L\alpha)$$

where A, B, C and D are empirical coefficients. This will enable us to quantify the $Fe^{3+}/\Sigma Fe$.

The reproducibility of flank method measurements was verified by monitoring Lβ/Lα ratios during several microprobe sessions. Data comparison has shown that data collected from different days are slightly different, but fall within the experimental error (Fig. 3.10-4). Flank method measurements show an accuracy of 1σ which is comparable to Mössbauer data with the advantage of a spatial resolution limit of about 10 μm. For that reason the flank method may be a promising technique for determining $Fe^{3+}/\Sigma Fe$ in natural ferropericlase from diamond inclusions.

Future work will focus on synthesis of further samples to cover the entire range of chemical composition from 0.2 to 60 at.%. This will help to understand the behaviour of the trend line, and fitting procedures will be used to find the best data regression line for Fe^{2+} as a function of ΣFe and Lβ/Lα ratio, in preparation to applying the calibration to natural samples.

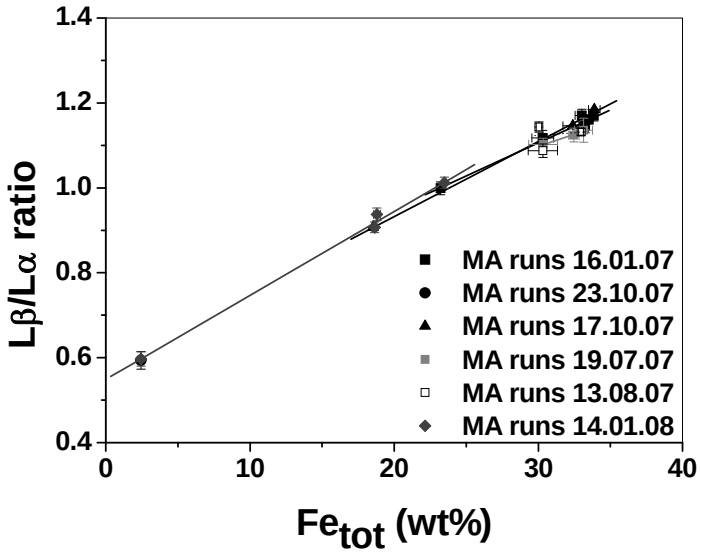

Fig. 3.10-4: Reproducibility of the flank method on multianvil run products: data comparison between different measuring days shows no significant change in slope.

c. *A flexible gas-loading system suitable for many types of diamond anvil cells (A. Kurnosov, I.Yu. Kantor, S. Linhardt, L.S. Dubrovinsky and T. Boffa Ballaran)*

The generation of ultra high pressures in diamonc anvil cells (DAC) is usually accompanied with the problem of reaching a homogeneous stress distribution within the sample chamber. The DAC is an opposite anvil device, and as a result the stress along the loading directions is always larger than the stresses in the gasket plane. To maintain hydrostatic or quasi-hydrostatic conditions in the DAC, pressure-transmitting media are normally employed. The

best pressure-transmitting media are light noble gases He and Ne. They are highly inert, stable over a wide pressure range, and have a relatively high solidification pressure. In addition, light inert gases have a low X-ray absorption and give a low background; therefore they are particularly suitable for X-ray diffraction measurements in DACs. However, the use of gases (especially helium and neon) as pressure-transmitting media requires special loading techniques. We built a very flexible gas loading system that is easy to operate, is suitable for many types of DAC (including gas-membrane DAC) without the use of special holders, and at the same time allows a fine control on the force applied to the diamonds by the use of an *in situ* force indicator.

The system can employ gas pressures up to 2 kbar, therefore special care was taken with regard to safety aspects. The pressure vessel has been manufactured by specialized company (SITEC-Sieber Engineering AG, Switzerland) and was certified by a test laboratory (TÜV SÜD Industrie Service GmbH, Freiburg, Germany). We also use an additional safety system composed of a shielding steel wall.

The internal diameter of the pressure vessel is 52 mm, and its length is 102 mm. Therefore, the system is suitable for any opposing-plate, piston-cylinder, or gas-membrane cells with a size fitting into these dimensions. The loading of gas-membrane DAC as well as of piston-cylinder part of Mao-Bell cells is possible without any modification of the devices if they are equipped with clamping screws.

Four electrical outlets have been introduced in the apparatus in order to connect the force-sensor mounted on the pushing end of the piston with an outer high-resolution force-indicator. The force sensor produced by Lorenz Messtechnik GmbH (Germany) has a maximum loading capacity of 2000 N (sensors with other force ranges are also available and could be more suitable for other types of DACs). The sensor works at gas pressures up to at least 2 kbar and allows controlling the loading force applied to the diamonds with a precision of 1 N resolution. This provides a high loading success rate (close to 100 %) and a safe mode of diamonds usage.

Once the system is assembled and selected gas is pumped in one can rotate the levers to move the piston towards the cell until the force sensor touches the cell and the indicator starts to show the force applied to the cell. Then the optimal force of 500-600 N (~ 90 deg. of the spindle rotation) can be fine adjusted. The piston (P) slightly squeezes the diamonds into the gasket, sealing the gas inside the pressure chamber of the DAC. After that, pressure can be vented from the vessel and the lid (L) removed to provide access to the screws of the cell. After tightening the screws, the DAC can be taken out of the vessel. During the tightening of the screws the gasket and sample chamber can be observed with any optical or ruby fluorescence system in order to control the response of the gasket to the tightening procedure or to measure directly the pressure in the DAC. We used a Logitech web camera as optical system, equipped with a focusing lens with x5 magnification and 15 mm focusing distance. The camera is connected to a laptop and we can observe the full-screen image of the sample chamber with acceptable resolution to estimate the reduction of the sample chamber volume.

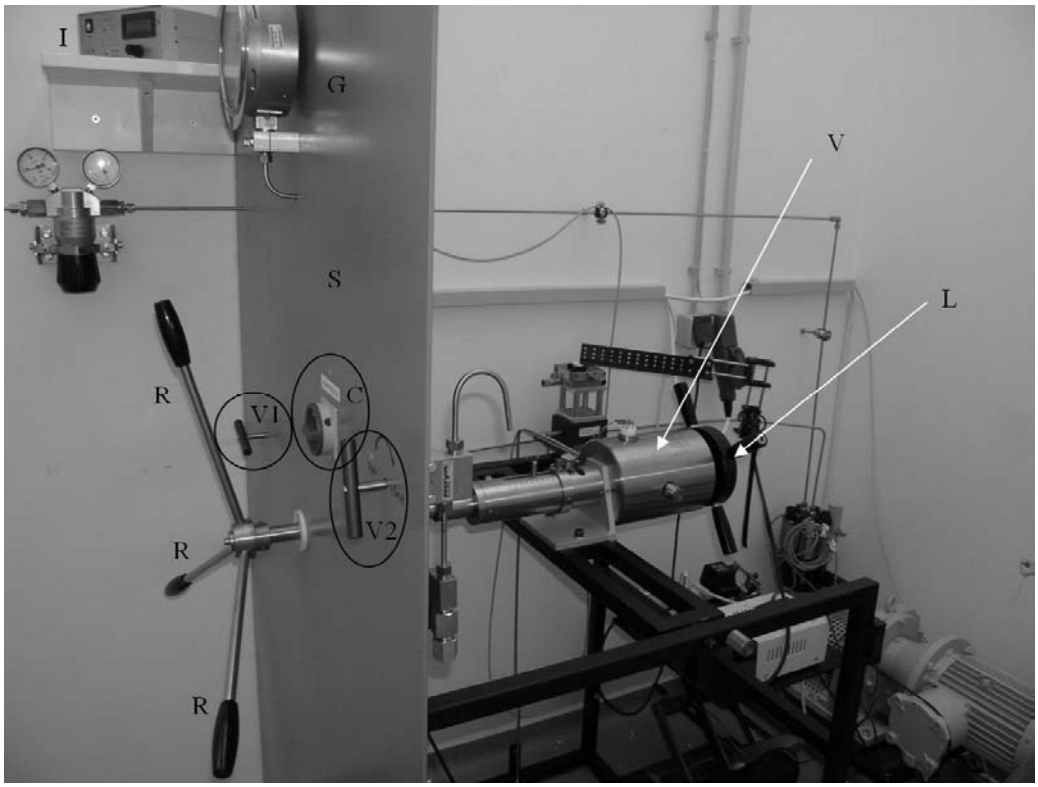

Fig. 3.10-5: General view of the gas-loading system. The management of the loading procedure can be done by one operator behind the safety sheet (S). Valve 1 (V1) provides the gas access to the vessel. Valve 2 (V2) releases the gas from the system. Switch (C) turns on the compressor to start the pumping procedure. The levers (R) are used for moving the piston. V – pressure vessel, L – front lid. G – pressure-gauge indicating the pressure in the vessel V.

d. *Gasket preparation for ultrahigh-pressure experiments (O. Narygina, A. Audétat and L.S. Dubrovinsky)*

In order to perform diamond anvil cell (DAC) experiments under megabar pressures diamond anvils with culet size of 150-120 μm or less are required, which causes additional difficulties in the DAC preparation procedure. The most difficult part is the gasket preparation: indentation and drilling of the hole for the sample. The size of the hole should be large enough to host a reasonable amount of sample, but at the same time it should be small enough to reach ultrahigh pressures. The latter requires holes of less than 100 μm in diameter, which are almost impossible to drill precisely by the electroerosion technique.

To obtain small, precisely drilled holes in the case of small size culet diamond anvils we therefore decided to use the laser ablation technique. Centered holes measuring 40-90 μm were drilled in pre-indented rhenium gaskets using the Geolas M 193nm ArF Excimer Laser system (Coherent / Lambda Physik) at BGI. This laser system features special homogenization optics to produce a perfectly flat-top energy distribution across the laser

beam. Pit sizes can be varied from 5 µm to 200 µm. For drilling the gaskets we operated the laser at 80 mJ and a frequency of 10 Hz, with a laser pulse duration of 15 ns. With these settings about 0.1 µm material is ablated per pulse. Figure 3.10-6 shows an example of a cell with a laser drilled hole. Using the laser ablation technique for gasket preparation dramatically increases the success rate in reaching ultrahigh pressures.

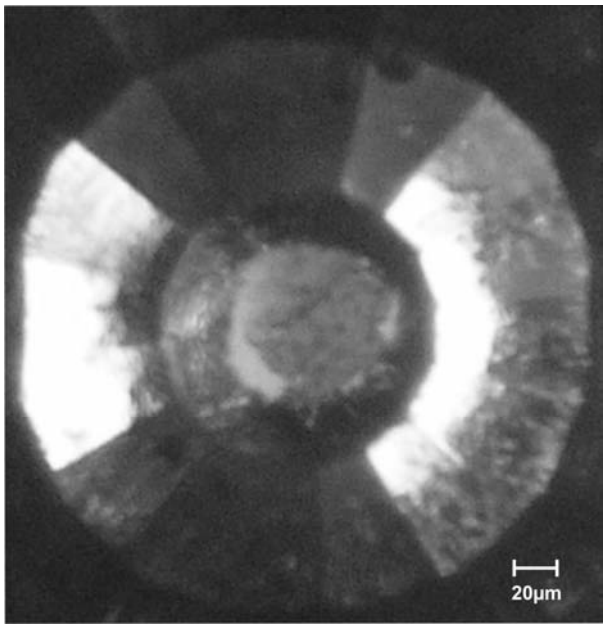

Fig. 3.10-6: Photo image of DAC with laser drilled hole. Diamond anvils culet size is 120 µm, the hole size is 90µm. The picture was taken at 82 GPa.

e. *A new method for welding large amounts of fluid into noble metal capsules (A. Audétat and E. Bali)*

Most people who have performed piston-cylinder experiments with volatile-bearing samples know that the welding of the noble metal capsules is not a trivial task, particularly if none of the volatiles should be lost during this process. Numerous techniques are being used to facilitate this task, ranging from cooling the capsules with icy water or liquid nitrogen, welding the capsules in a vice, or producing seals in the cold state. However, most of these approaches are left with some disadvantage. Cooling with water or liquid nitrogen works in practice only for samples in which the volume occupied by fluid is small relative to the entire capsule volume, because the heat generated by welding needs to dissipate before it reaches the fluid-bearing part of the capsule. Welding the capsule in a vice is an easy method to prevent fluid loss, but it deforms the capsule in such a way that it needs to be bent back into a round shape, which carries the risk of capsule failure and results in a rather complex capsule geometry. The latter is a disadvantage in piston-cylinder experiments because any space that

is not completely filled up leads to deformation of the heater assembly. Cold sealing techniques require relatively large amounts of metal and commonly are associated with significant loss of fluid, although it is difficult to say whether this loss occurred during pressurization or at some later stage in the experiments.

Here we would like to present a relatively fast, easy method that allows large amounts of fluid to be welded into noble metal capsules using a minimum amount of metal, and keeping the capsule in its original geometry. In this method a preliminary seal is produced in a two-piece die (Fig. 3.10-7) by squeezing the capsule wall around an inserted disc of noble metal, followed by final sealing by arc welding. The process is shown schematically in Fig. 3.10-8 and will be discussed with regard to 5.0 mm O.D., 4.4 mm I.D. capsules. In a first step (a), a small ledge is produced inside the capsule by squeezing the capsule wall around the end of a 4.35 mm diameter steel rod inserted 3.2 mm into the capsule. This ledge does not need to be wide – 0.025 mm is already enough. In a second step (b) the starting material and fluid is filled into the capsule. There are two options at this stage. If the aim is to load as much fluid as possible (but not a specific amount), then the capsule is filled completely, as shown in Fig. 3.10-8. The solid disc of noble metal is then pushed through the liquid until it hits the ledge produced in the first step. The capsule is then immediately brought back into the die and squeezed (d), this time higher up than in the first step, and using a die diameter of 4.8 mm instead of 4.9 mm. This provides a seal that is tight enough to prevent loss of fluid during subsequent welding of the upper lid. The last two steps require only 10-20 seconds, during which only very little fluid can evaporate. Solute concentrations thus remain unchanged.

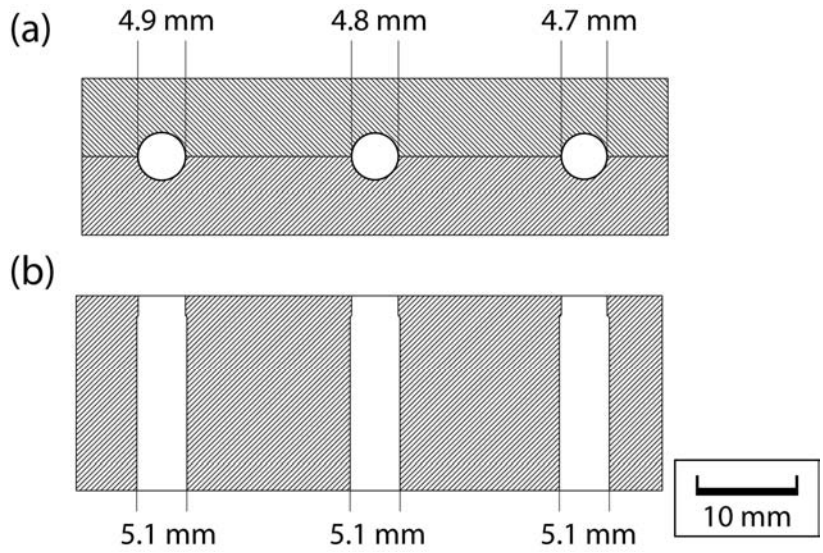

Fig. 3.10-7: Drawing of the hardened steel die used for welding 5.0 mm O.D. 4.4 mm I.D. capsules. (a) top view of the two pieces of the die. (b) side view of one of the pieces. Note the narrowing of the bore diameter in the uppermost 2 mm of the die.

Residual fluid above the disc is flushed away with distilled water, the water is cleaned off, and the capsule is kept in the vice until the upper parts of the capsule are completely dry. Finally, the upper lid of the capsule is welded on by standard arc welding using a carbon or tungsten rod. The fact that no hissing, sudden bursts, or difficult-to-close holes are observed demonstrates that no fluid from below the noble metal disc is evaporating during this process. The result is a cylindrical capsule that is almost completely filled with fluid, except for a small volume of air between the disc and the upper lid. A disadvantage of this option is that the amount of fluid trapped inside the capsule cannot be determined precisely beforehand. It can, however, be determined precisely afterwards. If a pre-determined amount of fluid needs to be sealed in, then the capsule can be filled only partly, and be processed as in the first variant. However, in this case a relatively large gap ($\geq$ 2 mm) has to be left between the fluid and the disc because otherwise fluid is drawn upward by surface tension and capillary forces to above the noble metal disc before the seal can be made.

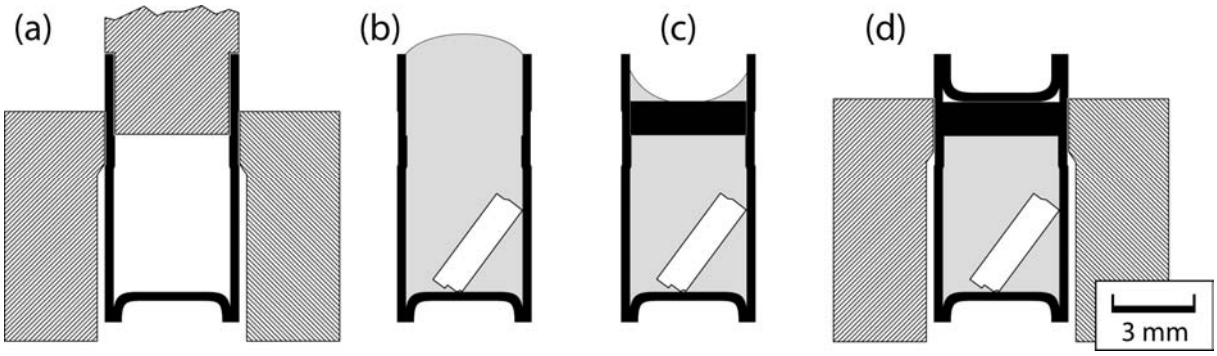

Fig. 3.10-8: Drawing of the four main steps involved in the capsule filling process, as seen in cross section through the top part of the die. (a) generation of a small ledge inside the capsule by squeezing the capsule wall (black) around the end of an inserted steel rod. (b) view after filling the capsule with a piece of solid starting material (white) and liquid (gray). (c) view after pushing in the noble metal disc. (d) generation of a preliminary seal by squeezing the capsule wall around the inserted noble metal disc. The upper lid can be welded on by standard arc welding after excess fluid has been flushed away with distilled water and the top part of the capsule has completely dried.

The first variant of the method has been used successfully to weld aqueous fluids containing 0.3 wt.% dissolved chlorides into $Pt_{95}Rh_{05}$ capsules of two different sizes: (1) 5.0 mm O.D., 4.4 mm I.D. and 10 mm length, and (2) 3.7 mm O.D., 3.2 mm I.D, and 8 mm length. The noble metal discs were pressed from scrap $Pt_{95}Rh_{05}$ sheet left after punching out the lids, using a die of hardened steel with an inner diameter of 4.35 mm. Typical amounts of loaded fluid were 30µg for the larger capsules, and 15-25 µg for the smaller capsules, depending on the amount of other added starting materials. Thirty capsules of the smaller size were used in piston-cylinder experiments at 1.0 - 3.5 GPa and 700 - 1150 °C that lasted from one to three days. The experiments were conducted in pure salt assemblies, such that the capsules could be

retrieved without any excess material attached to them. The amount of fluid lost during the experiments could, therefore, be determined with high precision by weighing the capsules before and after the run. In 40 % of the runs less than 1 % of the fluid was lost, in 10 % of the runs between 1 and 5 %, in 15 % of the runs between 5 and 10 %, and in the remaining 35 % of the runs more than 10 %. In one experiment a 5.0 mm O.D., 4.4 mm I.D. $Pt_{95}Rh_{05}$ capsule was filled up completely with a 20 % ammonia solution and subsequently brought to 250 °C and 2.5 GPa without failure. The new method can be used for a large number of applications in which volatile-bearing substances need to be welded into noble metal capsules, and in which short, cylindrical capsules need to be obtained.

4. International Graduate School
"Structure, Reactivity and Properties of Oxide Materials"

The interdisciplinary Graduate School is funded by the Free State of Bavaria and it encompasses three cooperating institutes: Bayerisches Geoinstitut (BGI), Institute of Inorganic Chemistry I (LAC), both in Bayreuth, and the Fraunhofer Institute for Silicate Research (ISC) in Würzburg. These institutes provide their experimental and analytical facilities, complement-tary expertise in basic and applied material research, and commitment to capitalize on syner-gies as well as international contacts to other leading research institutes all over the world.

The Graduate School is chaired by Prof. David Rubie, Ph.D. (BGI) and it includes eight other faculty members and one coordinator. Enrollment in 2007 was ten doctoral students on a full-time basis at all three institutes (BGI, LAC, ISC) and, in addition, nine doctoral students have associate status in the school which provides them with full access to all educational activities. Research projects include element partitioning between silicate materials and core-forming alloys at high pressures, thermodynamics of mantle phases, hydroxyl defects in minerals, synthesis of new layer silicates and mesoporous oxide substances as well as experimental and computer simulations of solid and liquid matter.

In May 2007, all graduate students presented their research results and the graduate program was evaluated by a scientific committee, chaired by Prof. U. Bismayer (Hamburg). The evaluation was very successful and we are grateful to the Bavarian Ministry for Sciences, Research and Arts for granting an extension for the time period of 2009 to 2012.

During 2007, four students have graduated:

Jun Liu (M.Sc. 2003, Peking) on 23.07.2007	(Na,K)-alumosilicate-hollandite: Structure, crystal chemistry and high pressure behavior Supervisors: PD Dr. L. Dubrovinsky, Dr. T. Boffa Ballaran
Maria Iuga (ISC Würzburg) (Dipl.-Mat.-Wiss., Erlangen) on 25.07.2007	Structure-property relations in ceramics simulated by finite element methods and molecular dynamics. Supervisor: Dr. Friedrich Raether
Innokenty Kantor (MA 2003, Moscow) on 18.08.2007	Structure and electronic properties of (Mg,Fe)O and FeO under high pressure and temperature Supervisors: PD Dr. L. Dubrovinsky, Dr. C. McCammon
Deborah Schmauß-Schreiner (Dipl.-Geophys. 2001, Bochum) on 27.09.2007	Adsorption of SO_2 on volcanic ashes Supervisor: Prof. H. Keppler

Three students (*Ashima Saikia, Ute Mann, Eva Holbig*) have submitted their theses at the end of 2007.

Three new associate students were accepted to the doctoral program in 2007:

Diego Bernini (M.Sc. 2006, Pavia) since 07.05.2007	Behavior of trace elements and halogens in subduction-zone mineral-fluid systems Supervisors: Prof. H. Keppler, Dr. D. Dolejš, Dr. A. Audétat
Evgeniya Zarechnaya (M.Sc. 2004, Moscow) since 01.08.2007	Synthesis and *in situ* characterization of boron-doped suberhard nanodiamond materials Supervisor: PD Dr. L. Dubrovinsky
Vincenzo Stagno (M.Sc. 2006, Palermo) since 01.10.2007	Study of natural diamond inclusions. Redox conditions and phase relations in natural and synthetic carbonatitic and kimberlitic systems Supervisor: Dr. D. Frost

Descriptions of the all student research projects are listed in Chapter 3 of this yearbook. Students gave presentations at several major international meetings in 2007: 8th Silicate Melt Workshop, La Petite Pierre (Strasbourg, France), 10th International Conference and Exhibition of the European Ceramic Society (Berlin), Study of Matter at Extreme Conditions (Miami Beach, USA), Frontiers in Mineral Sciences (Cambridge, U.K.), PETRA III Workshop: Nuclear Resonant and Inelastic X-Ray Scattering (Hamburg, Germany), 7th High Pressure Mineral Physics Seminar (Matsushima, Japan), annual Fall Meeting of the American Geophysical Union (San Francisco, USA), 17th Goldschmidt Conference (Cologne, Germany), 38th Lunar and Planetary Science Conference (Houston, USA), EuroMinSci Conference (La Colle-sur-Loup, France), and the European Geosciences Union General Assembly (Vienna, Austria). The list of presentations and publications may be found in Chapter 5.

As part of program requirements, all students undergo an intensive training program, in addition to their research project, that encompasses lectures, short courses, research colloquium, doctoral seminar, seminars by invited leading experts and weekend seminars on soft skills such as scientific writing, ethics and team work. Invited speakers from overseas and Europe gave 15 lectures during the last year and presented novel experimental techniques and current research results.

The following weekend seminars were held in 2007:

27.-28. 01.2007	2nd Joint Student Meeting on Geo- & Material Sciences KTB-GeoZentrum, Windischeschenbach Graduate schools *Oxides* (Univ. Bayreuth, ISC Würzburg) and *Advanced Materials and Processes (MAP)* (Univ. Erlangen)
04.-05.06.2007	Poster planning and design and presentation skills, Bayreuth
13.-14.10.2007	Soft Skills Seminar, Obertrubach

Three students (M. Iuga, U. Mann, and A. Saikia) and the speaker of the graduate school, Prof. D. Rubie, participated in the Graduation Ceremony of the Elite Network of Bavaria with the State Minister Dr. T. Goppel in Augsburg on November 17, 2007. Ms Saikia had been invited to present her research results in a short lecture.

Soft skills training, Obertrubach:
Students with the instructor

ENB 2007 Graduation Ceremony:
State Minister Dr. T. Goppel, M. Iuga,
U. Mann, A. Saikia (from left)

Members of the graduate school organized two short courses in the last year:
Diamond anvil cell techniques (24.-26.04.2007, L. Dubrovinsky, BGI) and a geodynamic modeling graduate short course in the Marie Curie Research Training Network "c2c" (04-15.06.2007, G. Steinle-Neumann, BGI). This short course was lead by Ondřej Čadek (Charles University, Prague), Susanne Buiter (Geological Survey of Norway, Trondheim), James Connolly (ETH Zurich) and consisted of theoretical presentations on solution of conservation equations and relevant computer algorithms. The course was accompanied by hands-on computer exercise using facilities of the University of Bayreuth.

In fulfillment of the program requirements, five graduate students carried out their research stays at international institutes:

Ashima Saikia	30.10.2006 -15.01.2007	Gakushin University/Spring 8, Tokyo, Japan; *Calorimetric studies of high pressure phases*
Ute Mann	07.03.-01.05.2007	California Institute of Technology, Pasadena, USA; *Spectroscopic methods – investigation of sub-µm mineral inclusions*
	01.05.-20.05.2007	University of New Mexico, Albuquerque, USA; *Platin group element analysis in silicate phases by SIMS*
Polina Gavrilenko	31.03.-03.07.2007	Virginia Polytechnic Institute and State University, Blacksburg, USA; *High pressure crystallography*
Ram Sai Yelamanchili	05.10.-28.12.2007	Department of Material Science and Engineering, Cornell University Ithaca/N.Y., USA *Synthesis of mesoporous Keggin-heteropolyoxometalates using evaporation induced self assembly*
Alexander Baumgartner	17.10.-15.12.2007	Binghamton University, Binghamton/N.Y., USA *Investigation of synthetic ferrous tainiolite as possible lithium battery cathode material*

Students and members of the graduate program received five international recognitions for their research excellence; these awards are listed in Section 7.2.

Detailed information on the Graduate School "Structure, Reactivity and Properties of Oxide Materials" can be found at http://www.uni-bayreuth.de/elitenetzwerk/oxides.

5. Publications, Conference Presentations, Seminars

5.1 Publications (published)

Supplement to **2006** (papers published at the end of 2006):

BERGESE, P.; ALESSANDRI, I.; BONTEMPI, E.; DEPERO, L.E.; ARONNE, A.; FANELLI, E.; PERNICE, P.; BOFFA BALLARAN, T.; MIYAJIMA, N.; SIGAEV, V.N. (2006): Phase transformations in bulk nanostructured potassium niobiosilicate glasses. Journal of Physical Chemistry B 110, 25740-25745

2007

Refereed international journals

ALÉON, J.; EL GORESY, A.; ZINNER, E. (2007): Oxygen isotope heterogeneities in the earliest protosolar gas recorded in a meteoritic calcium-aluminum-rich inclusion. Earth and Planetary Science Letters 263, 114-127

ALLWARDT, J.R.; STEBBINS, J.F.; TERASAKI, H.; DU, L.S.; FROST, D.J.; WITHERS, A.C.; HIRSCHMANN, M.M.; SUZUKI, A.; OHTANI, E. (2007): Effect of structural transitions on properties of high-pressure silicate melts: Al-27 NMR, glass densities, and melt viscosities. American Mineralogist 92 (7), 1093-1104

ASAHARA, Y.; FROST, D.J.; RUBIE, D.C. (2007): Partitioning of FeO between magnesiowüstite and liquid iron at high pressures and temperatures: Implications for the composition of the Earth's outer core. Earth and Planetary Science Letters 257, 435-449

BENNA, P.; NESTOLA, F.; BOFFA BALLARAN, T.; BALIC-ZUNIC, T.; LUNDEGAARD, L.F.; BRUNO, E. (2007): The high-pressure structural configurations of $Ca_{0.2}Sr_{0.8}Al_2Si_2O_8$ feldspar: The $I\bar{1}$ - $I2/c$ and $I2/c$ -$P2_1/c$ phase transitions. American Mineralogist 92, 1190-1199

BLAESS, U.W.; LANGENHORST, F.; FROST, D. J.; SEIFERT, F. (2007): Oxygen deficient perovskites in the system $CaSiO_3$-$CaAlO_{2.5}$ and implications for the Earth's interior. Physics and Chemistry of Minerals 34 (6), 363-376

BOFFA BALLARAN, T.; TRØNNES, R.G.; FROST, D.J. (2007): Equation of state of $CaIrO_3$ perovskite and post-perovskite phases. American Mineralogist 92, 1760-1763

BROMILEY, F.A.; BOFFA BALLARAN, T.; LANGENHORST, F.; SEIFERT, F. (2007): Order and miscibility in the otavite – magnesite solid solution. American Mineralogist 92, 829-836

BROMILEY, F.A.; BOFFA BALLARAN, T.; ZHANG, M. (2007): An infrared investigation of the otavite – magnesite solid solution. American Mineralogist 92, 837-845

CARACAS, R. (2007): Raman spectra and lattice dynamics of cubic gauche nitrogen. Journal of Chemical Physics 127, 144510

CARACAS, R.; COHEN, R.E. (2007): Effect of chemistry on the physical properties of perovskite and post-perovskite. Geophysical Monograph Series 174, 115-128

CARACAS, R.; COHEN, R.E. (2007): Prediction of polar ordered oxynitride perovskites. Applied Physics Letters 91, 092902

CARACAS, R.; HEMLEY, R.J. (2007): New structures of dense nitrogen: Pathways to the polymeric phase. Chemical Physics Letters 442, 65-70

COMODI, P.; CERA, F.; NAZZARENI, S.; DUBROVINSKY, L.S. (2007): Raman spectroscopy of 10-Å phase at simultaneously HP-HT. European Journal of Mineralogy 19-5, 623-629

CORGNE, A.; KESHAV, S.; FEI, Y.; MCDONOUGH, W.F. (2007): How much potassium is in the Earth's core? New insights from new partitioning experiments. Earth and Planetary Science Letters 256, 567-576

DOLEJŠ, D.; BAKER, D.R. (2007): Liquidus equilibria in the system K_2O-Na_2O-Al_2O_3-SiO_2-F_2O_{-1}-H_2O to 100 MPa: I. Silicate-fluoride liquid immiscibility in anhydrous systems. Journal of Petrology 48, 785-806

DOLEJŠ, D.; BAKER, D.R. (2007): Liquidus equilibria in the system K_2O-Na_2O-Al_2O_3-SiO_2-F_2O_{-1}-H_2O to 100 MPa: II. Differentiation paths of fluorosilicic magmas in hydrous systems. Journal of Petrology 48, 807-828

DUBROVINSKAIA, N.A.; SOLOZHENKO, V.L.; MIYAJIMA, N.; DMITRIEV, V.; KURAKEVYCH, O.; DUBROVINSKY L.S. (2007): Superhard nanocomposite of dense polymorphs of boron nitride: Noncarbon material has reached diamond hardness. Applied Physics Letters 90, 101912

DUBROVINSKY, L.S.; DUBROVINSKAIA, N.A.; NARYGINA, O.; KANTOR, I.Yu.; KUZNETZOV, A.; PRAKAPENKA, V.B.; VITOS, L.; JOHANSSON, B.; MIKHAYLUSHKIN, A.S.; SIMAK, S.I.; ABRIKOSOV, I.A. (2007): Body-centered cubic iron-nickel alloy in Earth's core. Science 316, 1880-1883

DUBROVINSKY, L.S.; DUBROVINSKAIA, N.A.; CRICHTON, W.A.; MIKHAYLUSHKIN, A.S.; SIMAK, S.I.; ABRIKOSOV, I.A.; DE ALMEIDA, J.S.; AHUJA, R.; LUO, W.; JOHANSSON, B. (2007): Noblest of all metals is structurally unstable at high pressure. Physical Review Letters 98, 045503

DUC-TIN, Q.; AUDÉTAT, A.; KEPPLER, H. (2007): Solubility of tin in (Cl,F)-bearing aqueous fluids at 700 °C, 140 MPa: a LA-ICP-MS study of synthetic fluid inclusions. Geochimica et Cosmochimica Acta 71, 3323-3335

DZWILEWSKI, A.; TALYZIN, A.; BROMILEY, G.; DUB, S.; DUBROVINSKY, L.S. (2007): Characterization of phases synthesized close to the boundary of C_{60} collapse at high temperature high pressure conditions. Diamond & Related Materials 16, 1550-1556

EECKHOUT, S.G.; BOLFAN-CASANOVA, N.; MCCAMMON, C.A.; KLEMME, S.; AMIGUET, E. (2007): XANES study of the oxidation state of Cr in lower mantle phases: Periclase and magnesium silicate perovskite. American Mineralogist 92, 966-972

FROST, D.J.; DOLEJŠ, D. (2007): Experimental determination of the effect of H_2O on the 410-km seismic discontinuity. Earth and Planetary Science Letters 256 (1-2), 182-195

GATTA, G.D.; KANTOR, I.Yu.; BOFFA BALLARAN, T.; DUBROVINSKY, L.S.; MCCAMMON, C.A. (2007): Effect of non-hydrostatic conditions on the elastic behaviour of magnetite: An *in situ* single-crystal X-ray diffraction study. Physics and Chemistry of Minerals 34, 627-635

GILLET, Ph.; EL GORESY, A.; BECK, P.; CHEN, M. (2007): High-pressure mineral assemblages in shocked meteorites and shocked terrestrial rocks: Mechanisms of phase transformations and constraints to pressure and temperature histories. Geological Society of America Special Paper 421, 57-81

HOLZAPFEL, C.; CHAKRABORTY, S.; RUBIE, D.C.; FROST, D.J. (2007): Effect of pressure on Fe-Mg, Ni and Mn diffusion in $(Fe_xMg_{1-x})SiO_4$ olivine. Physics of the Earth and Planetary Interiors 162, 186-198

IUGA, M.; STEINLE-NEUMANN, G.; MEINHARDT, J. (2007): *Ab initio* simulation of elastic constants for some ceramic materials. European Physics Journal B 58, 127-133

KANTOR, A.P.; KANTOR, I.Yu.; KURNOSOV, A.V.; KUZNETSOV, A.Yu.; DUBROVINSKAIA, N.A.; KRISCH, M.; BOSSAK, A.A.; DMITRIEV, V.P.; URUSOV, V.S.; DUBROVINSKY, L.S. (2007): Sound wave velocities of fcc Fe-Ni alloy at high pressure and temperature by mean of inelastic X-ray scattering. Physics of the Earth and Planetary Interiors 164 (1-2), 83-89

KANTOR, I.Yu.; DUBROVINSKY, L.S.; MCCAMMON, C.A. (2007): Reply to "Comments on 'Spin crossover in (Mg,Fe)O: A Mössbauer effect study with an alternative interpretation of X-ray emission spectroscopy data'". Physical Review B 75, 177103

KANTOR, I.Yu.; DUBROVINSKY, L.S.; MCCAMMON, C.A.; DUBROVINSKAIA, N.A.; GONCHARENKO, I.; KANTOR, A.P.; KUZNETSOV, A.; CRICHTON, W. (2007): FeO and MnO high-pressure phase diagrams: relations between structural and magnetic properties. Phase Transitions 80, 1151-1163

KANTOR, I.Yu.; KANTOR, A.P.; DUBROVINSKY, L.S.; MCCAMMON, C.A. (2007): High-pressure phase transformations in the system FeO-MgO. – In: OHTANI, E. (Ed.): Advances in High-Pressure Mineralogy, GSA Special Paper 421, Geological Society of America, Boulder, USA, 47-56

KEPPLER, H.; KANTOR, I.Yu.; DUBROVINSKY, L.S. (2007): Optical absorption spectra of ferropericlase to 84 GPa. American Mineralogist 92, 433-436

KESHAV, S.; SEN, G.; PRESNALL, D.C. (2007): Garnet-bearing xenoliths from Salt Lake Crater, Oahu, Hawaii: High-pressure fractional crystallization in the oceanic mantle. Journal of Petrology 48, 1681-1724

KOMABAYASHI, T.; HIROSE, K.; SATA, N.; OHISHI, Y.; DUBROVINSKY, L.S. (2007): Phase transition in $CaSiO_3$ perovskite. Earth and Planetary Science Letters 260, 564-569

KONRAD-SCHMOLKE, M.; O'BRIEN, P.J.; HEIDELBACH, F. (2007): Compositional re-equilibration of garnet: the importance of sub-grain boundaries. European Journal of Mineralogy 19, 431-438

KOZLENKO, D.P.; GOLOSOVA, N.O.; JIRAK, Z.; DUBROVINSKY, L.S.; SAVENKO, B.N.; TUCKER, M.G.; LE GODEC, Y.; GLAZKOV, V.P. (2007): Temperature- and pressure-driven spin-state transitions in $LaCoO_3$. Physical Review B 75, 064422

KOZLENKO, D.P.; DUBROVINSKY, L.S.; GONCHARENKO, I.N.; SAVENKO, B.N.; VORONIN, V.I.; KISELEV, E.A.; PROSKURNINA, N.V. (2007): Pressure-induced monoclinic distortion and charge and orbital ordering in $La_{0.5}Ca_{0.5}MnO_3$. Physical Review B 75, 104408

KOZLENKO, D.P.; DUBROVINSKY, L.S.; JIRAK, Z.; SAVENKO, B.N.; MARTIN, C.; VRATISLAV, S. (2007): Pressure-induced antiferromagnetism and compression anisotropy in $Pr_{0.52}Sr_{0.48}MnO_3$. Physical Review B 76, 094408

KUZNETSOV, A.Yu.; DMITRIEV, V.; VOLKOVA, Y.; KURNOSOV, A.; DUBROVINSKAIA, N.A.; DUBROVINSKY, L.S. (2007): *In situ* combined X-ray diffraction and electrical resistance measurements at high pressures and temperatures in diamond anvil cells. High Pressure Research 27 (2), 213-222

LI, Y.; QIN, S.; SEIFERT, F. (2007): Phase transitions in A-site substituted perovskite compounds: The $Ca_{1-2x}Na_xLa_x)TiO_3$ ($0 \leq x \leq 0.5$) solid solution. Journal of Solid State Chemistry 180, 824-833

LIU, L.; EL GORESY, A. (2007): High-pressure phase transitions of the feldspars and further characterization of lingunite. International Geology Review 49, 854-860

LOCHERER, T.; DUBROVINSKY, L.S.; FUESS, H. (2007): Isothermal compression of nitrogen doped zirconia/zirconium oxonitride $Zr_7O_{11}N_2$ and equation of states. Solid State Communications 143, 408-411

MACHEK, M.; ŠPAČEK, P.; ULRICH, S.; HEIDELBACH, F. (2007): Origin and orientation of microporosity in eclogites of different microstructure. Engineering Geology 89, 266-277

MARKS, M.A.; RUDNICK, R.L.; MCCAMMON, C.A.; VENNEMANN, T.; MARKL, G. (2007): Arrested kinetic Li isotope fractionation at the margin of the Ilímaussaq complex, South Greenland: Evidence for open system processes during final cooling of peralkaline igneous rocks. Chemical Geology 246, 207-230

MCENROE, S.A.; ROBINSON, P.; LANGENHORST, F.; FRANDSEN, C.; TERRY, M.P.; BOFFA BALLARAN, T. (2007): Magnetization of exsolution intergrowths of hematite and ilmenite: Mineral chemistry, phase relations, and magnetic properties of hemo-ilmenite ores with micron- to nanometer-scale lamellae from Allard Lake, Quebec. Journal of Geophysical Research 112, B10103, doi: 10.1029/2007JB004973

MCENROE, S.A.; CARTER-STIGLITZ, B.; HARRISON, R.; ROBINSON, P.; FABIAN, K.; MCCAMMON, C.A. (2007): Magnetic exchange bias of more than 1 Tesla in a natural mineral intergrowth. Nature Nanotechnology 2, 631-634

MIERDEL, K.; KEPPLER, H.; SMYTH, J.R.; LANGENHORST, F. (2007): Water solubility in aluminous orthopyroxene and the origin of Earth's asthenosphere. Science 315, 364-368

MIYAJIMA, N.; EL GORESY, A.; DUPAS-BRUZEK, C.; SEIFERT, F.; RUBIE, D.C.; CHEN, M.; XIE, X. (2007): Ferric iron in Al-bearing akimotoite coexisting with iron-nickel metal in a shock-melt vein in an L-6 chondrite. American Mineralogist 92, 1545-1549

NESTOLA, F.; LONGO, M.; MCCAMMON, C.A.; BOFFA BALLARAN, T. (2007): Crystal structural refinement of Na-bearing clinopyroxenes from mantle-derived eclogite xenoliths. American Mineralogist 92, 1242-1245

NESTOLA, F.; TRIBAUDINO, M.; BOFFA BALLARAN, T.; LIEBSKE, C.; BRUNO, M. (2007): The crystal structure of pyroxenes along the jadeite-hedenbergite and jadeite-aegirine joins. American Mineralogist 92, 1492-1501

NIWA, K.; YAGI, T.; OHGUSHI, K.; MERKEL, S.; MIYAJIMA, N.; KIKEGAWA, T. (2007): Lattice preferred orientation in $CaIrO_3$ perovskite and post-perovskite formed by plastic deformation under pressure. Physics and Chemistry of Minerals 34, 679-686

PALASYUK, T.; TKACZ, M.; DUBROVINSKY, L.S. (2007): Raman spectroscopy study of REH3 under pressure. Solid State Communications 142, 337-341

PIAZZONI, A.; STEINLE-NEUMANN, G.; BUNGE, H.-P.; DOLEJŠ, D. (2007): A mineralogical model for density and elasticity of the Earth's mantle. Geochemistry, Geophysics, Geosystems (G-cubed) 8, Q11010, doi: 10.1029/2007GC001697

RUBIE, D.C.; NIMMO, F.; MELOSH, H.J. (2007): Formation of Earth's core. – In: STEVENSON, D.J. (Ed.): Treatise on Geophysics Vol. 9: Evolution of the Earth, Elsevier, Amsterdam, pp. 51-90

SHIRYAEV, A.A.; FROST, D.J.; LANGENHORST, F. (2007): Impurity diffusion and microstructure in diamonds deformed at high pressures and temperatures. Diamond & Related Materials 16, 503-511

SMYTH, J.R.; MIERDEL, K.; KEPPLER, H.; LANGENHORST, F.; DUBROVINSKY, L.S.; NESTOLA, F. (2007): Crystal chemistry of hydration in aluminous orthopyroxene. American Mineralogist 92, 973-976

STEINBERGER, B. (2007): Effects of latent heat release at phase boundaries on flow in the Earth's mantle, phase boundary topography and dynamic topography at the Earth's surface. Physics of the Earth and Planetary Interiors 164, 2-20

STEINLE-NEUMANN, G. (2007): Ein Blick ins Innere der Erde, Spin-Paarung in (Mg,Fe)O. Physik Journal (Monthly Newsletter of the German Physical Society) 6 (11), 22-23

STOYANOV, E.; LANGENHORST, F.; STEINLE-NEUMANN, G. (2007): The effect of valence state and site geometry on Ti $L_{3,2}$ and O K electron energy-loss spectra of Ti_xO_y phases. American Mineralogist 92, 577-586

TALYZIN, A.; DZWILEWSKI, A.; DUBROVINSKY, L.S.; SETZER, A.; ESQUINAZI, P. (2007): Structural and magnetic properties of polymerized C_{60} with Fe. European Physical Journal B 55, 57-62

TALYZIN, A.V.; ANDERSSON, O.; SUNDQVIST, B.; KURNOSOV, A.; DUBROVINSKY, L.S. (2007): High-pressure phase transition in $LiBH_4$. Journal of Solid State Chemistry 180, 510-517

TERASAKI, H.; FROST, D.J.; RUBIE, D.C.; LANGENHORST, F. (2007): The interconnectivity of Fe-O-S liquid in polycrystalline silicate perovskite at lower mantle conditions. Physics of the Earth and Planetary Interiors 161, 170-176

TSUNO, K.; TERASAKI, H.; OHTANI, E.; SUZUKI, A.; ASAHARA, Y.; NISHIDA, K.; SAKAMAKI, T.; FUNAKOSHI, K.; KIKEGAWA, T. (2007): *In situ* observation and determination of liquid immiscibility in the Fe-O-S melt at 3 GPa using a synchrotron X-ray radiographic technique. Geophysical Research Letters 34, L17303, doi: 10.1029/2007GL030750

VAN DE MOORTÈLE, B.; REYNARD, B.; ROCHETTE, P.; JACKSON, M.; BECK, P.; GILLET, P.; MCMILLAN, P.F.; MCCAMMON, C.A. (2007): Shock-induced metallic iron nanoparticles in olivine-rich Martian meteorites. Earth and Planetary Science Letters 262, 37-49

WALTE, N.P.; BECKER, J.K.; BONS, P.D.; RUBIE, D.C.; FROST, D.J. (2007): Liquid-distribution and attainment of textural equilibrium in a partially-molten crystalline system with a high-dihedral-angle liquid phase. Earth and Planetary Science Letters 262, 517-532

WALTE, N.; HEIDELBACH, F.; MIYAJIMA, N.; FROST, D.J. (2007): Texture development and TEM analysis of deformed $CaIrO_3$: Implications for the D'' layer at the core-mantle boundary. Geophysical Research Letters 34, L08306, doi: 10.1029/ 2007GL029407

WENZEL, M.J.; STEINLE-NEUMANN, G. (2007): Nonequivalence of the octahedral sites of cubic Fe_3O_4 magnetite. Physical Review B 75, 214430

ZANAZZI, P.F.; COMODI, P.; NAZZARENI, S.; ROTIROTI, N.; VAN SMAALEN, S. (2007): Behavior of 10-Å phase at low temperatures. Physics and Chemistry of Minerals 34, 23-29

ZANAZZI, P.F.; MONTAGNOLI, M.; NAZZARENI, S.; COMODI, P. (2007): Structural effects of pressure on monoclinic chlorite: a single-crystal study. American Mineralogist 92, 655-661

5.2 Publications (submitted, in press)

ANTONANGELI, D.; BENEDETTI, L.R.; STEINLE-NEUMANN, G.; AUZENDE, A.-L.; BADRO, J.; HANFLAND, M.; KRISCH, M.; FARBER, D.L.: Anomalous pressure evolution of the axial ratio c/a in hcp cobalt: interplay between structure, magnetism and lattice dynamics. Physical Review Letters (submitted)

ASAHARA, Y.; RUBIE, D.C.; MIYAJIMA, N.; DUBROVINSKY, L.S.; FROST, D.J.; HOLZAPFEL, C.; OHTANI, E.; MIYAHARA, M.; SAKAI, T.: Oxygen content of the Earth's core. – In: OHTANI, E.; WANG, Y.; ANDRAULT, D.; STIXRUDE, L.; ASIMOW, P. (Eds.): Physics of the Earth and Planetary Interiors – Special Volume, 7th High Pressure Mineral Physics Seminar (submitted)

AUDÉTAT, A.; PETTKE, T.; HEINRICH, C.A.; BODNAR, R.J.: The composition of magmatic-hydrothermal fluids in barren versus mineralized intrusions. Economic Geology (submitted)

BAIER, J.; AUDÉTAT, A.; KEPPLER, H.: The origin of the negative niobium tantalum anomaly in subduction zone magmas. Earth and Planetary Science Letters (in press)

BALI, E.: ZAJACZ, Z.; KOVÁCS, I.; HALTER, W.; SZABÓ, Cs.; TÖRÖK, K.; VASELLI, O.: A quartz-bearing orthopyroxene-rich websterite xenolith from the Pannonian Basin, western Hungary: Evidence for release of quartz-saturated melts from a subducted slab. Journal of Petrology (in press)

BALI, E.; BOLFAN-CASANOVA, N.; KOGA, K.: Pressure and temperature dependence of H solubility in forsterite: an implication to water activity in the Earth interior. Earth and Planetary Science Letters (in press)

BESTMANN, M.; HABLER, G.; HEIDELBACH, F.; THÖNI, M.: Dynamic recrystallization of garnet and related diffusion processes. Journal of Structural Geology (submitted)

BROMILEY, G.D.; REDFERN, S.A.T.: The role of TiO_2 phases during melting of subduction-modified crust: implications for deep mantle melting. Earth and Planetary Science Letters (submitted)

CARACAS, R.: Elastic tensors and Raman spectra of mantle minerals from density functional perturbation theory. Physics of the Earth and Planetary Interiors (submitted)

CORGNE, A.; KESHAV, S.; WOOD, B.J.; MCDONOUGH, W.F.; FEI, Y.: Metal-silicate partitioning and constraints on the composition of the Earth's core and oxygen fugacity during Earth's accretion. Geochimica et Cosmochimica Acta (in press)

DECARLI P.S.; EL GORESY, A; XIE, Z.; SHARP, T.G.: Ejection mechanisms for Martian meteorites. Shock Physics (in press)

DOLEJŠ, D.; WAGNER, T.: Thermodynamic modeling of non-ideal mineral-fluid equilibria in the system Si-Al-Fe-Mg-Ca-Na-K-H-O-Cl at elevated temperatures and pressures: Implications for hydrothermal mass transfer in granitic rocks. Geochimica et Cosmochimica Acta (in press)

EL GORESY, A.; DERA, Z.; SHARP, T.G.; PREWITT, C.T.; CHEN, M.; DUBROVINSKY, L.S.; BOCTOR, N.Z.; WOPENKA, B.; HEMLEY, R.: Seifertite, a new dense orthorhombic polymorph of silica from the Martian meteorites Shergotty and Zagami. European Journal of Mineralogy (submitted)

FROST, D.J.; MCCAMMON, C.A.: The redox state of Earth's mantle. Annual Reviews of Earth and Planetary Sciences Letter (in press)

FROST, D.J.; MANN, U.; ASAHARA, Y.; RUBIE, D.C.: The redox state of the mantle during and just after core formation. Philosophical Transactions of the Royal Society of London, Series A (submitted)

FROST, D.J.: The upper mantle and transition zone. Elements (submitted)

HOLBIG, E.; DUBROVINSKY, L.S.; SWAMY, V.; WIRTH, R.; PRAKAPENKA, V.; KUZNETSOV, A.: Viscoelastic compression behavior of nanoscale anatase $Ti_{0.9}Zr_{0.1}O_2$. Journal of Physics and Chemistry of Solids (submitted)

HOLBIG, E.; GROVE, T.: Mantle melting beneath the Tibetan Plateau: Experimental constraints on ultra-potassic magmatism. Journal of Geophysical Research – Solid Earth (submitted)

HOLZAPFEL, C.; CHAKRABORTY, S.; RUBIE, D.C.; FROST, D.J.: Fe-Mg interdiffusion in wadsleyite: the role of pressure, temperature and composition and the magnitude of jump in diffusion rates at the 410 km discontinuity. Physics of the Earth and Planetary Interiors (submitted)

KANTOR, I.Yu.; KURNOSOV, A.; MCCAMMON, C.A.; DUBROVINSKY, L.S.: Monoclinic FeO at high pressures. Physical Review Letters (submitted)

KEGLER, P.; HOLZHEID, A.; FROST, D.J.; RUBIE, D.C.; DOHMEN, R.; PALME, H.: New Ni and Co metal-silicate partition data and their relevance for an early terrestrial magma ocean. Earth and Planetary Science Letters (submitted)

KESHAV, S.; GUDFINNSSON, G.H.; PRESNALL, D.C.: Widespread carbonatitic melts at depths of 400-600 km in the Earth. Science (submitted)

KLOTZ, S.; STEINLE-NEUMANN, G.; STRÄSSLE, Th.; PHILIPPE, J.; HANSEN, Th.; WENZEL, M.J.: Magnetism in Fe_3O_4 magnetite under pressure. Physical Review B (submitted)

KURNOSOV, A.; KANTOR, I.Yu.; BOFFA BALLARAN, T.; LINDHARDT, S.; DUBROVINSKY, L.S.; KUZNETSOV, A.; ZEHNDER, B.H.: The gas-loading system for mechanically closing of diamond anvil cells. Review of Scientific Instruments (submitted)

KURNOSOV, A.; DUBROVINSKY, L.S.; KUZNETSOV, A. DMITRIEV, V.: High-pressure melting curve of methane hydrates and implication to Titan's interior. Earth and Planetary Science Letters (submitted)

LEE, K.K.M.; STEINLE-NEUMANN, G.: *Ab initio* study of the effects of pressure and chemistry on the electron-capture radioactive decay constants of ^{7}Be, ^{22}Na and ^{40}K. Earth and Planetary Science Letters (submitted)

LEE, K.K.M.; STEINLE-NEUMANN, G.; AKBER-KNUTSON, S.: *Ab initio* predictions of potassium partitioning between Fe and Al-bearing $MgSiO_3$ perovskite and post-perovskite. Physics of the Earth and Planetary Interiors (submitted)

MANN, U.; FROST, D.J.; RUBIE, D.C.: The wetting ability of Si-bearing liquid Fe-alloys in a solid silicate matrix – Percolation during core formation under reducing conditions? Physics of the Earth and Planetary Interiors (in press)

MCCAMMON, C.A.; KANTOR, I.Yu.; NARYGINA, O.; ROUQUETTE, J.; PONKRATZ, U.; SERGUEEV, I.; MEZOUAR, M.; PRAKAPENKA, V.; DUBROVINSKY, L.S.: Intermediate-spin ferrous iron in lower mantle perovskite. Science (submitted)

MÉDARD, E.; MCCAMMON, C.A.; GROVE, T.L.: Oxygen fugacity, temperature reproducibility, and H_2O content for nominally dry piston-cylinder experiments using graphite capsules. American Mineralogist (submitted)

MIYAJIMA, N.; YAGI, T.; ICHIHARA, M.: Dislocation microstructures of $MgSiO_3$ perovskite at a high pressure and temperature condition. Physics of the Earth and Planetary Interior (submitted)

MIYAJIMA, N.; WALTE, N.; FROST, D.J.: Burgers vector determination on deformed perovskite and post-perovskite in $CaIrO_3$ using thickness-fringes in weak beam dark field images. Ultramicroscopy (submitted)

NAKASHIMA, D.; OTT, U.; HOPPE, P.; EL GORESY, A.: Search for extinct ^{36}Cl: Vigarano CAIs, the pink angel from Allende, and a Ningqiang chondrule. Geochimica et Cosmochimica Acta (submitted)

NAZZARENI, S.; COMODI, P.; BINDI, L.; SAFONOV, O.; PERCHUCK, L.; LITVIN, Y.: Synthetic hypersilicic Cl-rich mica in the phlogopite-celadonite join: A multi-methodic SCXRD, EMPA, and Raman characterization of the missing link between di- and tri-octahedral micas at high pressures, American Mineralogist (submitted)

NEUFELD, K.; RING, U.; HEIDELBACH, F.; DIETRICH, S.; NEUSER, R.D.: Omphacite textures in eclogites of the Tauern Window: Implications for the exhumation of the Eclogite Zone, Eastern Alps. Journal of Structural Geology (submitted)

OHGUSHI, K.; MATSUSHITA, Y.; MIYAJIMA, N.; KATSUYA, Y.; TANAKA, M.; IZUMI, F.; GOTOU, H.; UEDA, Y.; YAGI, T.: $CaPtO_3$ as a novel post-perovskite oxide. Physics and Chemistry of Minerals (in press)

PAVARINI, E.; ZEMA, M.; TARANTINO, S.C.; BOFFA BALLARAN, T.; GHIGNA, P.; CARRETTA, P.: Effect of high pressure on Li_2VOSiO_4 competing exchange coupling. Physics Review B (submitted)

PRESNALL, D.C.; GUDFINNSSON, G.H.: Origin of the oceanic lithosphere. Journal of Petrology, doi: 10.1093/petrology/egm052 (in press)

RIGBY, M.J.; DROOP, G.T.R.; BROMILEY, G.D.: Variations in fluid activity across the Etive thermal aureole, Scotland: evidence from cordierite volatile contents. Journal of Metamorphic Geology (in press)

ROSE-WESTON, L.A.; BRENAN, J.M.; FEI, Y.; SECCO, R.A.; FROST, D.J.: Perspectives on Earth differentiation from metal-silicate partitioning of Te, Se, and S. Geochimica et Cosmochimica Acta (submitted)

ROUQUETTE, J.; DOLEJŠ, D.; KANTOR, I.Yu.; MCCAMMON, C.A.; FROST, D.J.; DUBROVINSKY, L.S.: Iron-carbon interactions at high temperatures and pressures. Applied Physics Letters (in press)

ROUQUETTE, J.; KANTOR, I.Yu.; MCCAMMON, C.A.; DMITRIEV, V.; DUBROVINSKY, L.S.: High-pressure studies of olivine $(Mg_{0.9}Fe_{0.1})_2SiO_4$ using Raman spectroscopy, X-ray diffraction and Mössbauer spectroscopy. Inorganic Chemistry (in press)

SAIKIA, A.; FROST, D.J.; RUBIE, D.C.: Splitting of the 520 km seismic discontinuity and chemical heterogeneity in the mantle. Science (submitted)

SCHRINNER, M.; PROCH, S.; MEI, Y.; KEMPE, R.; MIYAJIMA, N.; BALLAUFF, M.: Stable bimetallic gold-platinum nanoparticles immobilized on spherical polyelectrolyte brushes: synthesis, characterization and application for the oxidation of alcohols. Advanced Materials (in press)

STEINLE-NEUMANN, G.: Magneto-elastic effects in dense cobalt. Physical Review B (submitted)

ŠTEMPROK, M.; DOLEJŠ, D.; MÜLLER, A.; SELTMANN, R.: Textural evidence of magma decompression, devolatilization and disequilibrium quenching: an example from the Western Krušné hory/Erzgebirge granite pluton. Contributions to Mineralogy and Petrology (in press)

SWAMY, V.; HOLBIG, E.; DUBROVINSKY, L.S.; PRAKAPENKA, V.; MUDDLE, B.C.: Mechanical properties of bulk and nanoscale TiO_2 phases. Journal of Physics and Chemistry of Solids (submitted)

SZABÓ, Cs.; HIDAS, K.; BALI, E.; ZAJACZ, Z.; KOVÁCS, I.; YANG, K.; GUZMICS, T.; TÖRÖK, K.: Mafic melt peridotite wall rock interaction as shown by silicate melt inclusions in upper mantle xenoliths from the central Pannonian Basin. Island Arc (submitted)

TARANTINO, S.C.; ZEMA, M.; BOFFA BALLARAN, T.; GHIGNA, P.: Room-temperature equation of state of Li_2VOSiO_4 up to 8.5 GPa. Physics and Chemistry of Minerals (in press) doi: 10.1007/s00269-007-0199-x

TERASAKI, H.; FROST, D.J.; RUBIE, D.C.; LANGENHORST, F.: Percolative core formation in planetesimals. Earth and Planetary Science Letters (submitted)

TERRY, M.P.; HEIDELBACH, F.; COUVY, H.; BROMILEY, G.D.; CARSWELL, D.A.: Deformation and metamorphism of the Kvalvika peridotite, Norway: Conditions and timing for olivine c-slip and exhumation at ultrahigh pressure. Journal of Metamorphic Petrology (submitted)

WALTER, M.J.; BULANOVA, G.; ARMSTRONG, L.S.; KESHAV, S.; BLUNDY, J.D.; LORD, O.; GUDFINNSSON, G.H.; LENNIE, A.; SMITH, C.; GOBBO, L.; Edinburgh Ion Microprobe Facility (EIMF): Primary carbonate melt in the mantle transition zone. Nature (submitted)

WOOD, I.G.; VOCADLO, L.; DOBSON, D.P.; PRICE, G.D.; FORTES, A.D.; COOPER, F.J.; NEALE, J.W.; MARSHALL, W.G.; TUCKER, M.G.; FRANCIS, D.J.; STONE, H.J.; MCCAMMON, C.A.: Thermoelastic properties of magnesiowüstite, $(Mg_{1-x}Fe_x)O$: Determination of the Anderson-Grüneisen parameter by time-of-flight powder neutron diffraction at simultaneous high pressures and temperatures. Journal of Applied Crystallography (submitted)

YUAN, J.; SCHMALZ, H.; XU, Y.; MIYAJIMA, N.; DRECHSLER, M.; MÖLLER, M.W.; SCHACHER, F.; MÜLLER, A.H.E.: Room-temperature growth of uniform tellurium nanorods and the assembly of tellurium or Fe_3O_4 nanoparticles on the nanorods. Advanced Materials (in press)

ZÖLLER, L.; BLANCHARD, H.; MCCAMMON, C.A.: The partial heat-longest plateau technique for TL dating of Middle and Upper Quaternary volcanic eruptions. Chemical Geology (submitted)

5.3 Presentations at scientific institutions and at congresses

ADJAOUD, O.; JAHN, S.; STEINLE-NEUMANN, G.: 01.-05.10.2007, 8th Silicate Melt Workshop, La Petite Pierre, Strasbourg, France: "Mg_2SiO_4 liquid under high pressure from Molecular dynamics"

AREFIN, M.L.; KLIMERA, A.; RAETHER, F.; DOLEJŠ, D.: 17.-21.06.2007, 10th International Conference and Exhibition of the European Ceramic Society, Berlin, Germany: "Liquid phase sintering of zinc oxide"

ARMSTRONG, L.S.; WALTER, M.J.: 19.-24.08.2007, Goldschmidt 2007, Cologne, Germany[*1]: "Mg-Fe^{2+}-Fe^{3+}-Al-Si-O phase relations at lower mantle conditions: Lack of evidence for Fe-disproportionation", Abstract Volume, A35

ARMSTRONG, L.S.; WALTER, M.J.; KESHAV, S.; BULANOVA, G.; PICKLES, J.; LORD, O.; LENNIE, A.: 10.-14.12.2007, AGU Fall Meeting, San Francisco, USA[*2]: "$Ca(Ti,Si)O_3$ inclusions in diamonds crystallized carbonate melts in the transition zone: experimental constraints", EOS Trans. AGU, 88(52), Fall Meet. Suppl., Abstract DI41B-08, 2007

ASAHARA Y.; RUBIE, D.C., FROST, D.J.: 08.-12.05.2007, HPMPS 7, 7th High Pressure Mineral Physics Seminar, Matsushima, Japan: "Oxygen content of the Earth's core"

ASAHARA, Y.; FROST, D.J.; RUBIE, D.C.; TERASAKI, T.; SAIKIA, A.; TSUNO, K.; NISHIDA, K.; OHTANI, E.; FUNAKOSHI, K.: 19.-24.05.2007, Japan Geoscience Union Meeting 2007, Makuhari, Japan: "*In situ* determination of solvus in the Fe-FeO system at 2-5 GPa", Abstract No. K131-021

ASAHARA, Y.; FROST, D.J.; RUBIE, D.C.; TERASAKI, T.; SAIKIA, A.; TSUNO, K.; NISHIDA, K.; OHTANI, E.; FUNAKOSHI, K.: 17.-21.09.2007, Joint 21st AIRAPT and 45th EHPRG International Conference on High Pressure Science and Technology, Catania, Italy: "*In situ* determination of solvus in the Fe-FeO system at 2-5 GPa up to 2800 K", Abstract No. 0194

AUDÉTAT, A.: 17.-20.07.2007, ECROFI XIX, European Current Research on Fluid Inclusions, Bern, Switzerland: "A new approach for measuring salinities of aqueous fluid inclusions that contain compressed gases", Abstract Volume, 278

AUDÉTAT, A.; PETTKE, T.; HEINRICH, C.A.: 19.-24.08.2007, Goldschmidt 2007, Cologne, Germany[*1]: "The role of fluid immiscibility in the formation of magmatic-hydrothermal ore deposits", Abstract Volume, A43

AUDÉTAT, A.: 24.-30.09.2007, Ores and Orogenesis Conference, Tucson, USA: "What makes the difference between porphyry-Mo and porphyry-Cu deposits? Insights by LA-ICP-MS analysis of fluid inclusions from Cave Peak and Santa Rita", Abstract Volume, 52

BALI, E.; AUDÉTAT, A.: 17.-20.07.2007, ECROFI XIX, European Current Research on Fluid Inclusions, Bern, Switzerland: "Synthetic fluid inclusions in rutile: a new technique to study mantle fluids". Abstract Volume, 142

BALI, E., AUDÉTAT, A.: 19.-24.08.2007, Goldschmidt 2007, Cologne, Germany[*1]: "Synthetic fluid inclusions in rutile: a new technique to study mantle fluids", Abstract Volume, A56

BALI, E.; ZAJACZ, Z.; KOVÁCS, I.; HALTER, W.; SZABÓ, Cs.; TÖRÖK, K.; VASELLI, O.: 29.-31.08.2007, European Mantle Workshop – Petrological Evolution of the European Lithospheric Mantle: from Archean to Present Day, Ferrara, Italy: "A quartz-bearing orthopyroxene-rich websterite xenolith from the Pannonian Basin, western Hungary: Evidence for release of Si-oversaturated melts from a subducted slab"

BALI, E.; BOLFAN-CASSANOVA, N.; KOGA, K.: 29.-31.08.2007, European Mantle Workshop – Petrological Evolution of the European Lithospheric Mantle: from Archean to Present Day, Ferrara, Italy: "Pressure and temperature dependence of H solubility in Forsterite: an implication to water activity in the Earth interior"

BINDER, B.; KEPPLER, H.: 19.-24.08.2007, Goldschmidt 2007, Cologne, Germany[*1]: "The speciation of sulfur in magmatic-hydrothermal fluids". Abstract Volume, A93

BOFFA BALLARAN, T.; TRØNNES, R.G.; FROST, D.J.: 08.-12.05.2007, HPMPS 7, 7th High Pressure Mineral Physics Seminar, Matsushima, Japan: "High-pressure single-crystal X-ray diffraction study of $CaIrO_3$ perovskite and post-perovskite phases"

BOFFA BALLARAN, T.; TRØNNES, R.G.; FROST, D.J.: 19.-24.08.2007, Goldschmidt 2007, Cologne, Germany[*1]: "High-pressure behaviour of $CaIrO_3$ perovskite and post-perovskite phases", Abstract Volume, A104

BOFFA BALLARAN, T.; 12.-14.09.2007, Geoitalia 2007, Rimini, Italy *(keynote lecture)*: "The help of high-pressure X-ray diffraction in understanding the deep Earth"

BOLFAN-CASSANOVA, N.; BALI, E.; KOGA, K.: 19.-24.08.2007, Goldschmidt 2007, Cologne, Germany[*1]: "Pressure and temperature dependence of water solubility in forsterite: implications for the activity of water in the Earth's mantle", Abstract Volume, A106

BUNGE, H.; STEINLE-NEUMANN, G.; PIAZZONI, A.; SCHUBERTH, B.; MODER, C.; OESER, J.: 10.-14.12.2007, AGU Fall Meeting, San Francisco, USA[*2] *(invited)*: "Global mantle circulation models with thermodynamically self consistent mineralogy: bridging the geodynamic/seismic gap", EOS Trans. AGU, 88(52), Fall Meet. Suppl., Abstract U34A-04, 2007

BUNGE, H.-P.; STEINLE-NEUMANN, G.; SCHUBERTH, B.; PIAZZONI, A.: 15.-20.04.2007, European Geosciences Union General Assembly 2007, Vienna, Austria *(invited)*: "Global models of mantle flow and density from geodynamic considerations", Geophysical Research Abstracts 9, 05451, 2007

CARACAS, R.; COHEN, R.E.: 11.-13.01.2007: 13th International Workshop on Computational Physics and Materials Science: Total Energy and Force Methods, Trieste, Italy: "New ferroelectric oxynitride perovskites with huge polarizations"

CARACAS, R.: 29.-31.01.2007, 3rd International ABINIT Developer Workshop, Liège, Belgium: "Elastic and spectroscopic properties of Earth and planetary materials"

CARACAS, R.: 29.-31.01.2007, 3rd International ABINIT Developer Workshop, Liège, Belgium: "New theoretical structures in high-pressure nitrogen"

CARACAS, R., COHEN, R.E.: 29.-31.01.2007, 3rd International ABINIT Developer Workshop, Liège, Belgium: "New ferroelectric oxynitride perovskites with huge polarizations"

CARACAS, R.; HEMLEY, R.J.: 05.-09.03.2007, 2007 APS March Meeting, Denver, USA: "Theoretical precursors to polymeric nitrogen"

CARACAS, R.: 08.-12.05.2007, HPMPS 7, 7th High Pressure Mineral Physics Seminar, Matsushima, Japan *(invited)*: "Elastic tensors and Raman spectra of mantle minerals from density functional perturbation theory"

CARACAS, R.: 19.-24.08.2007, Goldschmidt 2007, Cologne, Germany[*1]: "$(Mg,Fe,Al)(Si,Al)O_3$ post-perovskite and the D" layer", Abstract Volume, A143

CARACAS, R.: 20.09.2007, Institut de Ciencia de Materials de Barcelona, Universidad Autonoma de Barcelona, Spain: "*Ab initio* studies of major Earth and planetary materials"

CARACAS, R.: 23.10.2007, The Abdus Salam International Center for Theoretical Physics, Trieste, Italy *(invited)*: "*Ab initio* studies of major Earth and planetary materials"

COMODI, P.; NAZZARENI, S.; BINDI, L.; SAFONOV, O.; PERCHUCK, L.; LITVIN, Y.: 26.-28.06.2007, Frontiers in Mineral Sciences 2007, Cambridge, U.K.: "A Si and Cl-rich synthetic mica: new implications on phlogopite-celadonite miscibility at high pressure"

COMODI, P.; NAZZARENI, S.; ZANAZZI, P.F.: 12.-14.09.2007, Geoitalia 2007, Rimini, Italy: "A single-crystal X-ray study of gypsum at high pressure"

COMODI, P.; NAZZARENI, S.; ZANAZZI, P.F.: 22.-27.08.2007, 24th European Crystallographic Meeting, Marrakech, Morocco: "The high pressure behavior of gypsum: a single crystal X-ray study", Acta Crystallographica A63, 216

CORGNE, A.; WOOD, B.J.; MCDONOUGH, W.F.; KESHAV, S.; FEI, Y.: 19.-24.08.2007, Goldschmidt 2007, Cologne, Germany[*1]: "New metal-silicate partition coefficients and constraints on core composition and oxygen fugacity during Earth accretion", Abstract Volume, A189

DOLEJŠ, D.: 02.-04.05.2007, Department of Petrology and Structural Geology, Charles University, Prague, Czech Republic: "Physical-chemical principles of metamorphic, magmatic and hydrothermal processes"

DOLEJŠ, D.: 19.-24.08.2007, Goldschmidt 2007, Cologne, Germany[*1]: "Thermodynamic model for the simultaneous exsolution of two fluids from silicic magmas", Abstract Volume, A229

DOLEJŠ, D.: 08.-12.10.2007, Department of Geological Sciences, Masaryk University, Brno, Czech Republic: "Thermodynamics and chemical equilibria of metamorphic, magmatic and hydrothermal processes"

DOLEJŠ, D.: 25.-26.10.2007, EU c2c Working Meeting, Charles University, Prague, Czech Republic: "Dynamics of fluid flow in subduction zones"

DOLEJŠ, D.: 16.11.2007, Institut für Mineralogie und Petrographie, ETH Zürich, Switzerland: "Halogens in crustal magmatic systems: Experimental constraints and thermodynamic models"

DOLEJŠ, D.: 10.12.2007, Mineralogisch-Geochemisches Institut, Universität Freiburg, Germany: "Halogens at the magmatic-hydrothermal interface: Experimental and thermodynamic perspective"

DUBROVINSKY, L.S.; MCCAMMON, C.A.; NARYGINA, O.; KANTOR, I.Yu.; PRAKAPENKA, V.: 15.-20.04.2007, Study of Matter at Extreme Conditions, SMEC 2007, Miami Beach, USA *(invited)*: "Interplay between structural and electronic behaviour in iron bearing silicate perovskites at conditions of Earth's lower mantle"

DUBROVINSKY, L.S.; DUBROVINSKAIA, N.A.; KANTOR, I.Yu.; KURNOSOV, A.: 02.-07.09.2007, Gordon Research Conference 'Solid State Chemistry For Advanced Materials', Oxford, U.K. *(invited)*: "Chemistry in diamond anvil cells: from geosciences to synthesis of new materials"

DUBROVINSKY, L.S.; DUBROVINSKAIA, N.A.; NARYGINA, O.; KUZNETZOV, A.; PRAKAPENKA, V.; VITOS, L.; JOHANSSON, B.; MIKHAYLUSHKIN, A.S.; SIMAK, S.I.; ABRIKOSOV, I.A.: 03.-08.09.2007, IUCr High Pressure Meeting, Oxford, U.K. *(invited)*: "Iron alloys at extreme conditions: Experimental evidences for body-centred-cubic phase of Fe-Ni alloy in the Earth's core and chemistry of Fe-Mg, Fe-Si, and Fe-C systems"

DUBROVINSKY, L.S.; KANTOR, A.P.; KANTOR I.Yu.; KURNOSOV, A.; KRISCH, M.; BOSSAK, A.: 10.-14.12.2007, AGU Fall Meeting, San Francisco, USA[*2] *(invited)*: "Anelastic behaviour of FexO at high pressure", EOS Trans. AGU, 88(52), Fall Meet. Suppl., Abstract DI44A-05, 2007

DUBROVINSKY, L.S.; NARYGINA, O.; KANTOR, I.Yu.; PASCARELLI, S.; AQUILANTI, G.; MUNOZ, M.: 10.-14.12.2007, AGU Fall Meeting, San Francisco, USA[*2]: "2D micro-XAS mapping in diamond anvil cell: Application for post-spinel transition", EOS Trans. AGU, 88(52), Fall Meet. Suppl., Abstract MR31A-0136, 2007

EL GORESY, A.: 04.-13.05.2007, 3M (Magmatic-, Metamorphic-rocks and Meteorites) Symposium in Fez, Morocco *(invited)*: "High-pressure mineral inventory and their settings in shocked crystalline rocks in the Ries impact crater, Germany: A window to the Earth's mantle"

EL GORESY, A.: 04.-13.05.2007, 3M (Magmatic-, Metamorphic-rocks and Meteorites) Symposium in Fez, Morocco *(invited)*: "High-pressure minerals in shock-melt-veins in chondritic meteorites: Assemblages, textural relations and processes of phase transitions"

EL GORESY, A.; MIYAJIMA, N.; FERROIR, T.; GILLET, Ph.; DUBROVINSKY, L.S.; SIMIONOVICI, A.: 13.-17.08.2007, 70th Annual Meeting of the Meteoritical Society, Tucson, USA: "Two contrasting nucleation and growth settings induced by dynamic high-pressure phase transitions of olivine to ringwoodite and wadsleyite in shocked L6-chondrites"

EL GORESY, A.; GILLET, P.; DUBROVINSKY, L.S.: 19.-24.08.2007, Goldschmidt 2007, Cologne, Germany[*1] *(keynote lecture)*: "High-pressure mineral inventory in the Ries crater, Germany: A window to phase transformation processes in planetary interiors", Abstract Volume, A253

FROST, D.J.: 25.01.2007, ETH Zürich, Institut für Mineralogie und Petrographie, Zürich, Switzerland: "The redox state of the Earth during core formation"

FROST, D.J.: 08.02.2007, Freie Universität Berlin, Institut für Geologische Wissenschaften, Berlin, Germany: "The redox state of the Earth during core formation"

FROST, D.J.: 19.-24.08.2007, Goldschmidt 2007, Cologne, Germany[*1]: "Hydroxyl contents of deep mantle minerals coexisting with CH4-rich fluids: Implications for the focusing of fluids in the upper mantle by redox processes", Abstract Volume, A298

FROST, D.J.: 13.-14.09.2007, Royal Society Discussion Meeting 'Origin and differentiation of the Earth: from past to present', London, UK *(invited)*: "The redox state of the mantle during and just after core formation"

FROST, D.J.: 05.10.2007, Northwestern University, Department of Earth and Planetary Sciences, Evanston, USA: "Turning deep mantle seismic observations into petrological ones"

FROST, D.J.; SAIKIA, A.; RUBIE, D.C.: 10.-14.12.2007, AGU Fall Meeting, San Francisco, USA[*2]: "Calcium perovskite exsolution from majorite garnet and splitting of the 520 km seismic discontinuity: insights into mantle heterogeneity", EOS Trans. AGU, 88(52), Fall Meet. Suppl., Abstract DI51B-04, 2007

GANSKOW, G.; LANGENHORST, F.; POLLOK, K.; FROST, D.J.; RUBIE, D.C.; TARCEA, N.: 19.-20.02.2007, Colloquium, DFG Priority Programme 'Mars and the Terrestrial Planets', Berlin, Germany: "Stability and structures of hydrous minerals in the transition zone of the Martian mantle"

GAVRILENKO P.; KEPPLER H.: 19.-24.08.2007, Goldschmidt 2007, Cologne, Germany[*1]: "Water solubility in clinopyroxene", Abstract Volume, A312

GUDFINNSSON, G.H.; KESHAV, S.; PRESNALL, D.C.: 10.-14.12.2007, AGU Fall Meeting, San Francisco, USA[*2]: "Melting of hydrous, carbonate-bearing mantle peridotite", EOS Trans. AGU, 88(52), Fall Meet. Suppl., Abstract DI43A-04, 2007

HEIDELBACH, F.: 16.05.2007, FU Berlin, Germany: "Wechselwirkungen zwischen kristallographischen Texturen und Mineralreaktionen in natürlichen und experimentellen Metamorphiten"

HEIDELBACH, F.: 14.-15.06.2007, EBSD User Meeting, Zürich, Switzerland: "Interaction of deformation microstructures and chemical gradients"

HEIDELBACH, F.: 26.-28.06.2007, Frontiers in Mineral Sciences 2007, Cambridge, U.K.: "Experimental deformation of magnesiowüstite to high shear strains: the effect of iron content"

HEIDELBACH, F.: 25.-26.10.2007, EU c2c Working Meeting, Charles University, Prague, Czech Republic: "Rheology of mantle minerals – evidence from deformation experiments"

HOLBIG, E.; DUBROVINSKY, L.S.; SWAMY, V.; PRAKAPENKA, V.: 15.-20.04.2007, Study of Matter at Extreme Conditions, SMEC 2007, Miami Beach, USA: "Compression behaviour of Zr-doped nanoanatase"

HOLZHEID, A.; KEGLER, Ph.; FROST, D.J.; RUBIE, D.C.; PALME, H.: 12.-16.03.2007, 38th Lunar and Planetary Science Conference, Houston, USA: "Partitioning behaviour of copper and germanium: implications for terrestrial core formation scenarios", Abstract No. 2090

HUNT, S.A.; DOBSON, D.P.; WALTE, N.P.; WEIDNER, D.; LI, L.; VAUGHAM, M.: 10.-14.12.2007, AGU Fall Meeting, San Francisco, USA[*2]: "Transformational weakening during the perovskite – post perovskite phase transition in $CaIrO_3$", EOS Trans. AGU, 88(52), Fall Meet. Suppl., Abstract MR52A-08, 2007

KANTOR, I.Yu.; MCCAMMON, C.A.; DUBROVINSKY, L.S.: 10.-14.12.2007, AGU Fall Meeting, San Francisco, USA[*2]: "Spin crossover and short-range order in lower mantle (Mg,Fe)O", EOS Trans. AGU, 88(52), Fall Meet. Suppl., Abstract MR23D-03, 2007

KEGLER, Ph.; HOLZHEID, A.; FROST, D.J.; RUBIE, D.C.; PALME, H.: 19.-20.02.2007, Colloquium, DFG Priority Programme 'Mars and the Terrestrial Planets', Berlin, Germany: "Accretion and core formation of terrestrial planets: Insights from experimentally determined solubility behaviour of siderophile elements in silicate liquids"

KEPPLER, H.: 26.-29.03.2007, EuroMinSci Conference, La Colle-sur-Loup, France: "The origin of Earth's asthenosphere"

KEPPLER, H.: 08.05.2007, University of Erlangen, Germany: "Vulkane: Eruptionen, Auswirkungen, Vorhersagen"

KEPPLER, H.: 10.-15.06.2007, Gordon Research Conference 'Interior of the Earth', Mount Holyoke College, South Hadley, USA *(invited)*: "Water in the mantle and the origin of Earth's asthenosphere"

KEPPLER, H.: 05.-07.10.2007, Annual Meeting of Academy Leopoldina in Halle, Germany: "Migration geologischer Fluide"

KEPPLER, H.: 17.10.2007, Annual Meeting of the Friends of the Bavarian Academy of Sciences: "Vom Erdkern zu superharten Materialien: Hochdruckforschung am Bayerischen Geoinstitut"

KESHAV, S.; GUDFINNSSON, G.H.; PRESNALL, D.C.: 19.-24.08.2007, Goldschmidt 2007, Cologne, Germany[*1]: "Precipitous drop in the solidus of carbonated peridotite between 14-16 GPa: calcic carbonatites in the Earth's transition zone", Abstract Volume, A479

KESHAV, S.; GUDFINNSSON, G.H.: 10.-14.12.2007, AGU Fall Meeting, San Francisco, USA[*2]: "Carbonated eclogite solidus between 14 and 20 GPa: results from the model CMAS-CO_2 system and contrasting solidus behaviour to carbonated peridotite", EOS Trans. AGU, 88(52), Fall Meet. Suppl., Abstract DI41B-07, 2007

KONSCHAK, A.; KEPPLER, H.: 19.-24.08.2007, Goldschmidt 2007, Cologne, Germany[*1]: "The speciation of carbon dioxide in silicate melts from *in situ* infrared measurements", Abstract Volume, A511

KURNOSOV, A.: 15.-20.04.2007, European Geosciences Union General Assembly 2007, Vienna, Austria: "Methane hydrates in Titan's interior", Geophysical Research Abstracts 9, 08432, 2007

LEE, K.K.M.; NELSON, R.O.; RUNDBERG, R.; STEINLE-NEUMANN, G.: 10.-14.12.2007, AGU Fall Meeting, San Francisco, USA[*2]: "First measurements on how pressure affects the half-life of ^{22}Na: comparison to theory and analog to ^{40}K", EOS Trans. AGU, 88(52), Fall Meet. Suppl., Abstract V51E-0828, 2007

LONGO, M.; MCCAMMON, C.A.: 26.-28.06.2007, Frontiers in Mineral Sciences 2007, Cambridge, U.K.: "Iron oxidation state in (Mg,Fe)O: Calibration of the "flank method" using synthetic samples and application to natural diamond inclusions"

LONGO, M.; MCCAMMON, C.A.: 19.-24.08.2007, Goldschmidt 2007, Cologne, Germany[*1]: "$Fe^{3+}/\Sigma Fe$ in lower mantle (Mg,Fe)O: Calibration of the 'Flank Method'", Abstract Volume, A594

MANN, U.; FROST, D.J.; BECKER, H.; RUBIE, D.C.; SHEARER, C.K.; AGEE, C.B.: 12.-16.03.2007, 38th Lunar and Planetary Science Conference, Houston, USA: "Effect of pressure on the partitioning of highly siderophile elements between liquid Fe-alloy and peridotitic liquid", Abstract No. 1544

MANN, U.; FROST, D.J.; BECKER, H.; RUBIE, D.C.: 19.-24.08.2007, Goldschmidt 2007, Cologne, Germany[*1]: "Unequivocal evidence for a deep magma ocean from metal/silicate partitioning of Ta, V and Si during core formation", Abstract Volume, A619

MARKS, M.A.W.; RUDNICK, R.L.; MCCAMMON, C.A.; VENNEMANN, T.; MARKL, G.: 19.-24.08.2007, Goldschmidt 2007, Cologne, Germany[*1]: "Kinetic Li isotopic fractionation in the alkaline plutonic Ilímaussaq complex, South Greenland", Abstract Volume, A623

MCCAMMON, C.: 17.-18.04.2007, Université Claude Bernard Lyon 1, Lyon, France: "Oxygen fugacity"

MCCAMMON, C.A.: 24.-26.04.2007, DAC Workshop, Bayreuth, Germany: "Mössbauer spectroscopy (in house and synchrotron) with DACs"

MCCAMMON, C.A.; DUBROVINSKY, L.S.; KANTOR, I.Yu.; NARYGINA, O.; ROUQUETTE, J.; PONKRATZ, U.; CHUMAKOV, A.; SERGUEEV, I.; RÜFFER, R.: 08.-12.05.2007, HPMPS 7, 7th High Pressure Mineral Physics Seminar, Matsushima, Japan: "Iron behaviour in lower mantle phases derived from nuclear forward scattering experiments"

MCCAMMON, C.A.; KANTOR, I.Yu.; NARYGINA, O.; ROUQUETTE, J.; DUBROVINSKY, L.S.; PONKRATZ, U.; SERGUEEV, I.; MEZOUAR, M.; PRAKAPENKA, V.: 06.-10.08.2007, 2nd VLab Workshop, Minneapolis, USA: "Intermediate-spin ferrous iron in lower mantle perovskite"

MCCAMMON, C.A.: 01.-03.10.2007, 1. Berichtskolloquium of the SPP 1236, Hünfeld, Germany: "New results from *in situ* high P,T studies of lower mantle minerals"

MCCAMMON, C.: 23.11.2007, University of Oxford, Oxford, U.K.: "The paradox of mantle redox and consequences for the Earth's history"

MCCAMMON, C.A.; KANTOR, I.Yu.; NARYGINA, O.; ROUQUETTE, J.; PONKRATZ, U.; SERGUEEV, I.; MEZOUAR, M.; PRAKAPENKA, V.; DUBROVINSKY, L.S.: 10.-14.12.2007, AGU Fall Meeting, San Francisco, USA[*2] *(invited)*: "Intermediate-spin ferrous iron in lower mantle perovskite", EOS Trans. AGU, 88(52), Fall Meet. Suppl., Abstract MR22A-01, 2007

MELOSH, H.J.; RUBIE, D.C.: 12.-16.03.2007, 38th Lunar and Planetary Science Conference, Houston, USA: "Ni partitioning in the terrestrial magma ocean: a polybaric numerical model", Abstract No. 1593

MIYAJIMA, N.; WALTE, N.; HEIDELBACH, F.; FROST, D.J.: 08.-12.05.2007, HPMPS 7, 7th High Pressure Mineral Physics Seminar, Matsushima, Japan *(invited)*: "Burgers vector determination on deformed perovskite and post-perovskite in $CaIrO_3$"

MIYAJIMA, N.; WALTE, N.; HEIDELBACH, F.; FROST, D.J.: 19.-24.05.2007, Japan Geoscience Union Meeting 2007, Makuhari, Japan: "Burgers vector determinations on perovskite and post-perovskite in $CaIrO_3$"

MIYAJIMA, N.; WALTE, N.; HEIDELBACH, F.; FROST, D.J.: 12.-17.08.2007, 9th EMU School: Nanoscopic Approaches in Earth and Planetary Sciences, Munich, Germany: "Quantitative imaging of dislocations using weak-beam dark field technique – Determination of Burgers vector of perovskite and post perovskite"

MÜLLER, W.F.; WALTE, N.P.; MIYAJIMA, N.; FROST, D.J., KLEMD, R.: 27.09.-02.10.2007, 16th DRT Conference, Deformation Mechanisms, Rheology and Tectonics, Mailand, Italien: "TEM-study of experimentally deformed natural omphacite with primitive Bravais lattice"

NARYGINA, O.; KANTOR, I.Yu.; DUBROVINSKY, L.S.; DUBROVINSKAIA, N.A.: 26.-29.03.2007, EuroMinSci Conference, La Colle-sur-Loup, France: "Equation of state of bcc-, fcc, and hcp-structured phases of iron-nickel alloy $Fe_{0.9}Ni_{0.1}$"

NARYGINA, O.; KANTOR, I.Yu.; MCCAMMON, C.A.; DUBROVINSKY, L.S.: 10.-11.09.2007, PETRA III Workshop: Nuclear Resonant and Inelastic X-ray Scattering, Hamburg, Germany: "Iron behaviour in perovskite: a high pressure Mössbauer study"

PIAZZONI, A.S.; BUNGE, H.-P.; STEINLE-NEUMANN, G.: 15.-20.04.2007, European Geosciences Union General Assembly 2007, Vienna, Austria: "Linking mineral physics and geodynamic mantle models", Geophysical Research Abstracts 9, 02575, 2007

POLLOK, K.; HEIDELBACH, F.; LANGENHORST, F.; JOHN, T.: 19.-24.08.2007, Goldschmidt 2007, Cologne, Germany[*1]: "Textural and microstructural analysis of rapidly grown omphacite from eclogite facies pseudotachylites", Abstract Volume, A801

PRESNALL, D.C.; GUDFINNSSON, G.H.: 10.-14.12.2007, AGU Fall Meeting, San Francisco, USA[*2]: "Formation of the oceanic lithosphere from the upper asthenosphere", EOS Trans. AGU, 88(52), Fall Meet. Suppl., Abstract U21A-0007, 2007

ROSE-WESTON, L.A.; BRENAN, J.M.: 19.-20.02.2007, Colloquium, DFG Priority Programme 'Mars and the Terrestrial Planets', Berlin, Germany: "The behaviour of Te, Se, and S during terrestrial accretion and differentiation: the necessity of a late veneer"

ROSE-WESTON, L.A.; RUBIE, D.C.; BRENAN, J.M.: 19.-24.08.2007, Goldschmidt 2007, Cologne, Germany[*1]: "Late-stage removal of chalcophile elements from the mantle by sulfide liquid extraction to the core", Abstract Volume, A852

ROSE-WESTON, L.A.: 12.10.2007, University of Western Ontario, London, Canada: "Formation and differentiation of the terrestrial planets"

ROSE-WESTON, L.A.; BRENAN, J.M.; HENDERSON, G.: 30.10.2007, Ludwig-Maximilians-Universität München, Germany: "Element partitioning and solubility measurements as applied to Earth differentiation"

ROSE-WESTON, L.A.; FROST, D.J.; RUBIE, D.C.: 10.11.2007, Joint Workshop of SPP 1115 'Mars and the Terrestrial Planets', Cologne, Germany: "Consequences of a Hadean sulfide liquid in the aftermath of a Giant Impact on Earth"

RUBIE, D.C.; ASAHARA, Y.; FROST, D.J.; MELOSH, H.J.: 19.-20.02.2007, Colloquium, DFG Priority Programme 'Mars and the Terrestrial Planets', Berlin, Germany: "Element partitioning during core formation in terrestrial planets"

RUBIE, D.C.: 08.03.2007, University of Arizona, Tucson, USA: "Experimental constraints on core formation in the early Earth"

RUBIE, D.C.: 09.03.2007, Arizona State University, Tempe, USA: "Core formation in the early Earth"

RUBIE, D.C.: 04.05.2007, Symposium in Honour of Alan Thompson's 60th Birthday, ETH Zürich, Switzerland: "Composition of the Earth's core and kinetics of reactions at the core-mantle boundary"

RUBIE, D.C.; MANN, U.; FROST, D.J.: 19.-24.08.2007, Goldschmidt 2007, Cologne, Germany[*1]: "New constraints on conditions of core formation and the light element content of the Earth's core", Abstract Volume, A857

RUBIE, D.C.: 10.11.2007, Joint Workshop of SPP 1115 'Mars and the Terrestrial Planets', Cologne, Germany: "A new mass balance approach to constraining processes of terrestrial core formation"

RUBIE, D.C.; MANN, U.; FROST, D.J.; KEGLER, P.; HOLZHEID, A.; PALME, H.: 10.-14.12.2007, AGU Fall Meeting, San Francisco, USA[*2]: "Heterogeneous Earth accretion and incomplete metal-silicate re-equilibration at high pressure during core formation", EOS Trans. AGU, 88(52), Fall Meet. Suppl., Abstract U11A-0015, 2007

SAIKIA, A.; FROST, D.J.; BOFFA BALLARAN, T.; RUBIE, D.C.: 08.-12.05.2007, HPMPS 7, 7th High Pressure Mineral Physics Seminar, Matsushima, Japan: "A compressibility study of (Al,Fe)-$MgSiO_3$ perovskite single crystals of lower mantle composition"

SAIKIA A.; FROST D.J.; RUBIE, D.C.: 19.-24.08.2007, Goldschmidt 2007, Cologne, Germany[*1] *(invited)*: "The formation of calcium perovskite from majoritic garnet – Implications for splitting of the 520 km seismic discontinuity", Abstract Volume, A866

SAIKIA, A.; FROST, D.J.; RUBIE, D.C.: 10.-14.12.2007, AGU Fall Meeting, San Francisco, USA[*2]: "Calcium perovskite exsolution from majorite garnet and splitting of the 520 km seismic discontinuity: insights into mantle heterogeneity", EOS Trans. AGU, 88(52), Fall Meet. Suppl., Abstract DI51B-04, 2007

SAIKIA, A.; BOFFA BALLARAN, T.; FROST, D.J.; RUBIE, D.C.: 10.-14.12.2007, AGU Fall Meeting, San Francisco, USA[*2]: "The effect of iron concentration on the compressibility of (Fe,Mg)(Al,Si)O_3 perovskite", EOS Trans. AGU, 88(52), Fall Meet. Suppl., Abstract DI44A-08, 2007

SCHUBERTH, B.; PIAZZONI, A.; BUNGE, H.; IGEL, H.; STEINLE-NEUMANN, G.; MODER, C.; OESER, J.: 10.-14.12.2007, AGU Fall Meeting, San Francisco, USA[*2]: "Self-consistent synthetic mantle discontinuities from joint modeling of geodynamics and mineral physics and their effects on the 3D global wave field", EOS Trans. AGU, 88(52), Fall Meet. Suppl., Abstract DI51B-09, 2007

STEINLE-NEUMANN, G.; LEE, K.K.M.; AKBER-KNUTSON, S.: 08.-12.05.2007, HPMPS 7, 7th High Pressure Mineral Physics Seminar, Matsushima, Japan *(invited)*: "Potassium partitioning between perovskite and post-perovskite from *ab initio* computations"

STEINLE-NEUMANN, G.; LEE, K.K.M.; AKBER-KNUTSON, S.: 19.-24.08.2007, Goldschmidt 2007, Cologne, Germany[*1]: "Potassium partitioning in the lowermost mantle from *ab initio* computations", Abstract Volume, A971

TARANTINO, S.C.; ZEMA, M.; BOFFA BALLARAN, T.; PAVARINI, E.; CARRETTA, P.; GHIGNA, P.; TAZZOLI, V.: 12.-14.09.2007, Geoitalia 2007, Rimini, Italy: "Structural behaviour of Li_2VOSiO_4 as a function of temperature and pressure", Epitome 02, 1036, 2007

TARANTINO, S.C.; ZEMA, M.; BOFFA BALLARAN, T.; GHIGNA, P.: 22.-27.08.2007, 24th European Crystallographic Meeting, Marrakech, Morocco: "Thermoelastic behaviour of Li_2VOSiO_4", Acta Crystallographica A63, 293

TSUNO, K.; FROST, D.J.; RUBIE, D.C.: 10.-14.12.2007, AGU Fall Meeting, San Francisco, USA[*2]: "Partitioning of FeO between liquid Fe-Ni metal and magnesiowüstite at high pressures and temperatures", EOS Trans. AGU, 88(52), Fall Meet. Suppl., Abstract MR13A-0988, 2007

TSUNO, K.; TERASAKI, H.; OHTANI, E.; SUZUKI, A.; ASAHARA, Y.; NISHIDA, K.; SAKAMAKI, T.; FUNAKOSHI, K.; KIKEGAWA, T.: 06.-07.12.2007, International Workshop on Synchrotron High-Pressure Mineral Physics and Materials Science, Chicago, USA: "*In situ* observation of liquid immiscibility in the Fe-O-S melt at high pressure using an X-ray radiographic technique"

TSUNO, K.; FROST, D.J.; RUBIE, D.C.: 10.11.2007, Joint Workshop of SPP 1115 'Mars and the Terrestrial Planets' Subgroups 'Interior-Early Evolution-Core Formation' and 'SNC Meteorites', Cologne, Germany: "Element partitioning of oxygen between liquid Fe-Ni and magnesiowüstite up to 25 GPa and implications for the formation of planetary cores"

WALTE, N.P.; RUBIE, D.C.; HEIDELBACH, F.; FROST, D.J.: 26.-29.03.2007, EuroMinSci Conference, La Colle-sur-Loup, France: "Deformation and lattice preferred orientation of rock-forming minerals and analogues at a high pressure with the deformation-DIA"

WALTE, N.P.; HEIDELBACH, F.; RUBIE, D.C.; FROST, D.J.: 15.-20.04.2007, European Geosciences Union General Assembly 2007, Vienna, Austria: "LPO and perovskite − post-perovskite phase transition of $CaIrO_3$ during deformation with the D-DIA: Implications for the D" layer", Geophysical Research Abstracts 9, 09301, 2007

WALTE, F.; HEIDELBACH, N.; RUBIE, D.C.; FROST, D.J.: 19.-24.08.2007, Goldschmidt 2007, Cologne, Germany[*1]: "The perovskite – post-perovskite phase transition of $CaIrO_3$ during experimental deformation: Implications for the D" layer", Abstract Volume, A1083

WALTE, N.P.; HEIDELBACH, F.; FROST, D.J.: 27.09.-02.10.2007, 16th DRT Conference, Deformation Mechanisms, Rheology and Tectonics, Mailand, Italien: "Transition textures and deformation textures in $CaIrO_3$: Understanding deformation in the D" layer"

WALTER, M.J.; BULANOVA, G.; ARMSTRONG, L.S.; KESHAV, S.; BLUNDY, J.D.; HINTON, R.; LENNIE, A.: 10.-14.12.2007, AGU Fall Meeting, San Francisco, USA[*2] *(invited)*: "Primary Ca-rich carbonate melts in the transition zone", EOS Trans. AGU, 88(52), Fall Meet. Suppl., Abstract MR31D-07, 2007

WEIGEL, C.; CORMIER, L.; GALOISY, L.; CALAS, G.; MCCAMMON, C.A.: 01.-06.07.2007, XXI International Congress on Glass, Strasbourg, France: "Structural behaviour of Fe^{3+} in a $NaFeSi_2O_6$ glass determined by neutron diffraction with isotopic substitution coupled with numerical simulation"

WILLIAMS, H.M.; NIELSEN, S.G.; RENAC, C.; MCCAMMON, C.A.; GRIFFIN, W.L.; O'REILLY, S.Y.: 19.-24.08.2007, Goldschmidt 2007, Cologne, Germany[*1]: "Fractionation of Fe and O isotopes in the mantle: Implications for the origins of eclogites and the source regions of mantle plumes", Abstract Volume A1118

[*1] **Goldschmidt 2007: 17th Annual V.M. Goldschmidt Conference, 19.-24.08.2007, Cologne, Germany – Geochimica et Cosmochimica Acta 71, Issue 15, Supplement 1**

[*2] **AGU: American Geophysical Union Fall Meeting, 10.-14.12.2007, San Francisco, USA – EOS Transactions, American Geophysical Union, 88(52), AGU Fall Meeting 2007 Supplement**

5.4 Lectures and seminars at Bayerisches Geoinstitut

ABAKUMOV, A., University of Antwerp, EMAT: Electron Microscopy for Materials Science, Antwerp, Belgium: "New perovskite", 16.07.2007

ADJAOUD, O., Bayerisches Geoinstitut, Bayreuth, Germany: "First principles phase diagram calculations in group IV carbides and Mg_2SiO_4 liquid from molecular dynamics", 22.11.2007

ARMSTRONG, L., Bayerisches Geoinstitut, Bayreuth, Germany: "Mg-perovskite phase relations in the system Mg-Fe^{2+}-Fe^{3+}-Al^{3+}-Si-O at lower mantle conditions", 12.07.2007

AUDÉTAT, A., Bayerisches Geoinstitut, Bayreuth, Germany: "Practical aspects of LA-ICP-MS analysis at BGI", 25.01.2007

BERLIN, J., University of New Mexico, Department of Earth & Planetary Sciences, Albuquerque, USA: "Revisiting chondrite volatility trends and common reservoirs of chondritic components: More evidence for mixing and transport in the solar nebula?", 30.08.2007

BOYET, M., Université Jean Monnet, Saint-Etienne, France: "Geochemical evidences for early global differentiation of the silicate earth", 31.05.2007

CARACAS, R., Bayerisches Geoinstitut, Bayreuth, Germany: "Complexity in the phase diagram of a simple compound: Nitrogen", 24.05.2007

DACHS, E., Universität Salzburg, Geographie, Geologie und Mineralogie, Salzburg, Austria: "Low-temperature calorimetry on milligram-sized mineralogical samples: The method", 04.07.2007

DACHS, E., Universität Salzburg, Geographie, Geologie und Mineralogie, Salzburg, Austria: "Calorimetry of aluminosilicate minerals", 06.07.2007

DE KOKER, N., University of Michigan, Department of Geological Sciences, USA: "Mixing and melting of magnesiosilicate liquids in the mantle", 19.12.2007

DOBRZHINETSKAYA, L., University of California, Riverside, USA: "Terrestrial osbornite (TiN) and BN nanoinclusions in coesite: implication for nitrogen storage in Earth's interior", 17.09.2007

EL GORESY, A., Bayerisches Geoinstitut, Bayreuth, Germany: "Shock-induced high-pressure mineral inventory in chondritic meteorites: Evidence for diverse mechanisms of phase transformations", 18.10.2007

EREMETS, M., Max-Planck-Institut für Chemie, Mainz, Germany: "Choose of cells and materials", 24.04.2007

FARGES, F., Muséum National d'Histoire Naturelle de Paris, France: "Scanning transmission X-ray microscopy (STXM): a new tool for minerals, glasses and environmental samples", 07.05.2007

FARGES, F., Muséum National d'Histoire Naturelle de Paris, France: "Glass durability and its weathering", 09.05.2007

GAVRILENKO, P., Bayerisches Geoinstitut, Bayreuth, Germany: "Water solubility in diopside", 26.10.2007

GONZE, X., Université Catholique de Louvain, Louvain-la-Neuve, Belgium: "A first-principles study of Pb and Zr in SiO_2", 15.02.2007

HAYDEN, L., Rensselaer Polytechnic Institute, Troy, USA: "Grain boundary diffusion of metal and carbon in mantle rocks", 09.10.2007

HUI, H., University of Michigan, Department of Geological Sciences, Ann Arbor, USA: "Viscosity of silicate melts", 26.11.2007

JOCHYM, P., Polish Academy of Sciences, Institute of Nuclear Physics, Krakow, Poland: "Macroscopic properties of minerals from quantum-mechanical calculations", 21.06.2007

JUHIN, A., Université Paris 6, France: "First-principles investigation of Cr-incorporation in spinel and pyrope garnet: Structural relaxation and simulation of XANES spectra", 29.11.2007

JUNG, D., ETH Zürich, Laboratorium für Kristallographie, Zürich, Switzerland: "*Ab initio* treatment of minerals in the lower mantle", 01.03.2007

KESHAV, S., Bayerisches Geoinstitut, Bayreuth, Germany: "Everything you wanted to know about diamonds, but were afraid to ask", 16.05.2007

KONSCHAK, A., Bayerisches Geoinstitut, Bayreuth, Germany: "CO_2 in silicate melts at high temperature and pressure", 13.12.2007

KOPYLOVA, M., University of British Columbia, Department of Earth and Ocean Sciences, Vancouver, Canada: "Searching for parental kimberlite melt", 25.10.2007

LIANG, Y., Scuola Internazionale Superiore di Studi Avanzati (SISSA), Trieste, Italy: "Modelling structure, kinetics, and vibrational spectroscopy of silica at high pressure", 28.06.2007

LIBOUREL, G., CRPG-CNRS, Nancy, France: "Chondrule formation and the early history of the solar system", 27.06.2007

LIU, J., Bayerisches Geoinstitut, Bayreuth, Germany: "(Na,K) aluminosilicate hollandites: Solid solution structures, high-pressure behaviour and geochemical implication", 05.07.2007

MANN, U., Bayerisches Geoinstitut, Bayreuth, Germany: "Geochemical constraints on core - mantle differentiation in terrestrial planets", 20.12.2007

MANNING, C., University of California, Department of Earth & Space Sciences, Los Angeles, USA: "In Deep Water: On the novel chemistry of high-pressure fluids and their role in geologic processes", 26.02.2007

MANNING, C., University of California, Department of Earth & Space Sciences, Los Angeles, USA: "Are any elements immobile in high-pressure geologic fluids?", 28.02.2007

MÉDARD, E., Massachusetts Institute of Technology, Department of Earth, Atmospheric, and Planetary Sciences, Cambridge, USA: "Accretion and differentiation of Mars: Tales from the mantle and crust", 17.01.2007

MOOKHERJEE, M., Yale University, Department of Geology and Geophysics, New Haven, USA: "Water in Earth materials", 24.10.2007

MORARD, G., ESRF Grenoble, France: "Structure of liquid iron alloys at high pressure and high temperature: Implications for planetary cores", 18.01.2007

MUŇOZ JOLIS, E., Royal Holloway, University of London, U.K.: "Geochemistry of Húsafell central volcano, Iceland", 19.11.2007

NAGASEKI, H., Tohoku University, Graduate School of Science, Sendai, Japan: "Synchrotron radiation analysis of synthetic fluid inclusions: an application to the behaviour of metals in boiling hydrothermal solutions", 08.02.2007

NAVROTSKY, A. University of California at Davis, USA: "New adventures in mineral calorimetry: an overview", 02.04.2007

NAVROTSKY, A. University of California at Davis, USA: "Thermochemistry of environmentally important minerals", 04.04.2007

OVSYANNIKOV, S., University of Tokyo, Institute for Solid State Physics, Chiba, Japan: "High pressure properties of lead chalcogenides and other minerals", 26.07.2007

PARMAN, S., University of Durham, U.K.: "Helium isotopes and the punctuated evolution of the Earth", 19.07.2007

PONKRATZ, U., ESRF Grenoble, France: "High pressure studies of magnetism and lattice dynamics in lanthanide compounds by nuclear resonance scattering techniques", 10.01.2007

RIBEIRO, J., Universität Brest, France: "Adakitic magmas: Amphibole composition and geobarometric constraints", 17.07.2007

RICHET, P., Institut de Physique du Globe de Paris, France: "Water an elusive oxide in silicate melts?", 27.11.2007

RICHET, P., Institut de Physique du Globe de Paris, France: "Atomic dynamics in silicate melts: Effects of temperature and of the structural role of cations", 28.11.2007

ROSKOSZ, M., Université des Sciences et Technologies de Lille, France: "Experimental isotope geochemistry: Quantification of the fractionation of Fe isotopes during metal segregation from a silicate melt", 14.06.2007

STEVENSON, D., California Institute of Technology, Geological & Planetary Sciences, Pasadena, USA: "What is going on at the core-mantle boundary?", 20.09.2007

STIXRUDE, L., University of Michigan, Department of Geological Sciences, Ann Arbor, USA: "Silicate liquids in planetary interiors", 11.09.2007

WORTMANN, G., Universität Paderborn, Germany: "Phonons in iron at high pressure", 15.03.2007

WESTON, R., Strait Gold Corporation, Toronto, Canada: "Gold exploration in Peru: A field geologist's perspective", 22.03.2007

YUEN, D., University of Minnesota, Department of Geology and Geophysics, Minneapolis, USA: "How can the double crossings of the post-perovskite transition constrain the heat flux from the core?", 24.09.2007

YUEN, D., University of Minnesota, Department of Geology and Geophysics, Minneapolis, USA: "Interactive visualization and monitoring of 3-D mantle convection", 25.09.2007

Lectures and poster presentations during the EU RITA User Workshop 'The Structure and Properties of Materials at High Pressure', Bayreuth, Germany, 11.-12.10.2006

Lectures:

BOLFAN-CASANOVA, N.: "Incorporation of Al in perovskite"

BORGHINI, G.; FUMAGALLI, P.; RAMPONE, E.: "The subsolidus spinel to plagioclase transition in mantle peridotites: natural and experimental constraints"

COMODI, P.; NAZZARENI, S.; DUBROVINSKY, L.S.: "A multimethodic study of the high pressure behaviour of gypsum"

CRICHTON, W.: "Current status and future applications of the large-volume press project at the ESRF"

DOBSON, D.; DERONDE, A.; MEREDITH, P.G.; HEIDELBACH, F.: "Plastic weakening during the olivine-wadsleyite transition and delayed onset of deep seismicity"

HUNT, S.; DOBSON, D.; WEIDNER, D.; LI, L.; VAUGHN, M.: "Relative strength of the pyrope-majorite solid solution"

PETFORD, N.: "Deformation induced mechanical instabilities at the CMB"

RABIER, J.; DEMENET, J.-L.: "Plastic deformation of semiconductors under pressure: in pursuit of the dislocation mechanisms at the brittle to ductile transition"

SANLOUP, C.; SCHMIDT, B.; DEWAELE, A.; GUDFINNSSON, G.; MEZOUAR, M.: "Retention of heavy rare gases in silicates at high pressure and high temperature"

SKÁLA, R.; DRÁBEK, M.; BOFFA BALLARAN, T.: "Thermal expansion in Fe3P-Ni3P solid solution"

SOLOZHENKO, V.L.; KURAKEVYCH, O.O.; DUBROVINSKAIA, N.A.; DUBROVINSKY, L.S.: "HP-HT synthesis of nanocrystalline cubic boron nitride"

TALYZIN, A.: "High pressure phase transitions in borohydrides and alanates"

WALTE, N.; HEIDELBACH, F.; RUBIE, D.C.; FROST, D.J.: "Deformation and lattice preferred orientation of high-pressure phases and analogues with the deformation-DIA"

WALTER, M.; ARMSTRONG, L.; LORD, O.; MIYAJIMA, N.; CLARK, S.; LENNIE, A.: "Ironing out the mysteries of perovskite crystal chemistry"

YOSHINO, T.: "Electrical conductivity of mantle minerals, with implications for conductive structure of the mantle"

Poster presentations:

ARMSTRONG, L.: "TEM characterization of (Fe, Al)-bearing Mg-perovskite in diamond anvil cell experiments"

GATTA, G.D.; BOFFA BALLARAN, T.: "High-pressure behaviour of open-framework silicates: *in situ* single crystal diffraction experiments performed at the Bayerisches Geoinstitut"

MCCAMMON, C.A.; DUBROVINSKY, L.S.; KANTOR, I.Yu.; NARYGINA, O.; ROUQUETTE, J.; PONKRATZ, U.; SERGUEEV, I.: "High P,T *in situ* Mössbauer study of $(Mg,Fe)(Si,Al)O_3$ perovskite"

MCENROE, S.A.; FABIAN, K.; ROBINSON, P.; BURTON, P.B.; BOFFA BALLARAN, T.; MIYAJIMA, N.: "Low temperature phase diagram for ilmenite-hematite system"

KONSCHAK, A.; Keppler, H.: "*In situ* measurements of CO_2 speciation in silicate melts"

MIYAJIMA, N.; EL GORESY, A.; DUPAS-BRUZEK, C.; SEIFERT, F.; RUBIE, D.C.; CHEN, M.; XIE, X.: "Ferric iron in Al-bearing akimotoite coexisting with iron-nickel metal in a shock-melt vein in an L-6 chondrite"

NESTOLA, F.; BOFFA BALLARAN, T.: "High-pressure $C2/c - P2_1/c$ phase transitino along the $LiAlSi_2O_6 - LiGaSi_2O_6$ solid solution"

POMPILIO, M.: "Experimental constraints on the interaction between hydrous and anhydrous magmas at Stromboli volcano"

ROZENBERG, G.Kh.; KERTZER, M.; GREENBERG, E.; PASTERNAK, M.; KURNOSOV, A.; DUBROVINSKY, L.S.; HANFLAND, M.; MUNOZ, M.; PASCARELLI, S.: "Pressure induced Fe ↔ Cu intra cationic valence exchange in delaffosite ($CuFeO_2$)"

SAIKIA, A.; BOFFA BALLARAN, T.; FROST, D.J.; RUBIE, D.C.: "A compressibility study of (Al,Fe)-$MgSiO_3$ perovskite single crystals of lower mantle composition"

SERGHIOU, G.; GUILLAUME, C.; FROST, D.J.; MORNIROLI, J.P.: "Extreme conditions synthesis of alloys and ceramics"

SHINOVA, E.; YONCHEVA, M.; STOYANOVA, R.; ZHECHEVA, E.; MCCAMMON, C.A.: "Novel compositions in the $LiNi/FeO_2$-$Li[Li_{1/3}Ti_{2/3}]O_2$ system obtained under high-pressure"

TARANTINO, S.C.; ZEMA, M.; BOFFA BALLARAN, T.; PAVARINI, E.; CARRETTA, P.; GHIGNA, P.; TAZZOLI, V.: "Structural behaviour of Li_2VOSiO_4 as a function of temperature and pressure"

ZALITE, I.; FROST, D.J.: "Use of high pressure hot pressing equipment for fabricating of nanostructured ceramic materials"

5.5 Conference organization

17.-19.06.2007, ESF workshop on "Multiscale approach to alloys: advances and challenges", Stockholm, Sweden (Co-Organizer: DUBROVINSKY, L.S.)

19.-24.08.2007, 17th Annual V.M. Goldschmidt Conference, Coordinator of Theme 10: "Water in Planetary Systems", Cologne, Germany (KEPPLER, H.)

19.-24.08.2007, 17th Annual V.M. Goldschmidt Conference, Convenor of symposium "Earth's deep water cycle", Cologne, Germany (KEPPLER, H.)

19.-24.08.2007, 17th Annual V.M. Goldschmidt Conference, Special Session S25 "Mantle processes and properties on multiple scales: Observation, experiment, modeling", Cologne, Germany (Co-Organizer: STEINLE-NEUMANN, G.)

20.-24.08.2007, 17th Annual V.M. Goldschmidt Conference, Symposium S40: "From Field Observation to Experimental Petrology and Back – in Memory of Werner Schreyer", Cologne, Germany (Co-Organizer: SEIFERT, F.)

6. Visiting scientists

6.1 Visiting scientists funded by the Bayerisches Geoinstitut

AMIT, H., Institut de Physique du Globe de Paris, Equipe de Géomagnétisme, Paris, France: 10.-12.01.2007

ASAHARA, Y., JASRI, Hyogo, Japan: 02.-14.06.2007

BANIGAN, E., University of Pennsylvania, Philadelphia, USA: 10.-23.06.2007

BERLIN, J., University of New Mexico, Department of Earth & Planetary Sciences, Albuquerque, USA: 30.-31.08.2007

BERNINI, D., Università degli Studi di Pavia, Italy: 14.-17.02.2007

BOYET, M., Université Jean Monnet, Saint-Etienne, France: 28.05.-02.06.2007

DEGTYAREVA, V., Russian Academy of Sciences, Institute of Solid State Physics, Chernogolovka, Russia: 21.10.-03.11.2007

EVONUK, M., ETH Zürich, Institut für Geophysik, Zürich, Switzerland: 03.-05.04.2007

FERROIR, T., ENS Lyon, France: 20.-27.05.2007

GONZE, X., Université Catholique de Louvain, Louvain-la-Neuve, Belgium: 14.-16.02.2007

GRIGNÉ, C., ETH Zürich, Institut für Geophysik, Zürich, Switzerland: 09.-12.01.2007

HAYDEN, L., Rensselaer Polytechnic Institute, Troy, USA: 08.-11.10.2007

HUI, H., University of Michigan, Department of Geological Sciences, Ann Arbor, USA: 22.-29.11.2007

KOPYLOVA, M., University of British Columbia, Department of Earth and Ocean Sciences, Vancouver, Canada: 21.-28.10.2007

KOZLENKO, D.; Frank Laboratory of Neutron Physics, Joint Institute for Nuclear Research, Dubna, Russia: 04.11.-19.12.2007

LIBOUREL, G., CRPG-CNRS, Nancy, France: 26.-27.06.2007

MATIZAMHUKA, W.R., University of the Witwatersrand, School of Chemical & Metallurgical Engineering, Johannesburg, South Africa: 04.07.2007

MÉDARD, E., Massachusetts Institute of Technology, Department of Earth, Atmospheric, and Planetary Sciences, Cambridge, USA: 17.-18.01.2007

MOOKHERJEE, M., Yale University, Department of Geology and Geophysics, New Haven, USA: 22.-29.10.2007

MORARD, G., European Synchrotron Radiation Facility, Grenoble, France: 14.-20.01.2007

NAGASEKI, H., Tohoku University, Graduate School of Science, Sendai, Japan: 05.-12.02.2007

OVSYANNIKOV, S., University of Tokyo, Institute for Solid State Physics, Chiba, Japan: 24.-28.07.2007

PICKLES, J., University of Bristol, Department of Earth Sciences, Bristol, U.K.: 25.-29.09.2007

PONKRATZ, U., European Synchrotron Radiation Facility, Grenoble, France: 10.-11.01.2007

PRESNALL, D.C., University of Texas at Dallas, Department of Geosciences, Richardson, USA: 31.05.-31.07.2007, 01.-31.10.2007

RAUSCH, S., Universität Göttingen, Fakultät für Geowissenschaften, Göttingen, Germany: 16.-17.04.2007

RIBEIRO, J., Universität Brest, France: 15.-19.07.2007

ROSA, A., Universität Heidelberg, Mineralogisches Institut, Heidelberg, Germany: 19.02.-28.03.2007

ROSKOSZ, M., Université des Sciences et Technologies de Lille, France: 13.-17.06.2007

SAMUEL, H., ETH Zürich, Institut für Geophysik, Zürich, Switzerland: 09.-12.01.2007, 03.-05.04.2007

SCHIAVI, F., Università degli Studi di Pavia, Dipartimento di Scienze della Terra, Pavia, Italy: 06.-14.08.2007

SEIFERT, F., Berlin, Germany: 27.-28.09.2007

SHIRYAEV, A., Russian Academy of Sciences, Institute of Crystallography, Moscow, Russia: 06.-16.12.2007

STAGNO, V., Università degli Studi di Palermo, CFTA, Palermo, Italy: 04.-07.02.2007

WESTON, R., Strait Gold Corporation, Toronto, Canada: 21.02.-06.03.2007

WOODLAND, A., Johann Wolfgang Goethe-Universität Frankfurt/M., Institut für Geowissenschaften, Frankfurt/M., Germany: 11.10.-18.11.2007

YOSHINO, T., Okayama University, Institute for the Study of the Earth's Interior, Misasa, Japan: 04.-30.06.2007, 19.09.-30.10.2007

6.2 Visiting scientists supported by other externally funded BGI projects

ALARIO-FRANCO, M., Universidad Complutense de Madrid, Departamento de Quimica Inorganica I, Madrid, Spain: *"High pressure synthesis of perovskite based materials"*, 23.-25.10.2007 (RITA^{*A})

ARÉVALO, Á., Universidad Complutense de Madrid, Departamento de Quimica Inorganica I, Madrid, Spain: *"High pressure synthesis of perovskite based materials"*, 23.-27.10.2007, 20.-27.11.2007 (RITA^{*A})

ARMSTRONG, L., University of Bristol, Department of Earth Sciences, Bristol, U.K.: *"MgO-SiO_2-Fe_2-O_3-FeO phase relations and the Fe^{3+} substitution mechanism in Mg-perovskite: Implications for the lower mantle"*, 01.04.-01.10.2007 (AtG^{*B})

BERTHET, S., Université de Marne-la-Vallée, Laboratoire des Géomatériaux, Marne-la-Vallée, France: *"Evolution of the enstatite chondrite EH4 indarch at high pressure and temperature: New constraints for early planetary differentiation"*, 09.-24.07.2007 (RITA^{*A})

BOLFAN-CASANOVA, N., University of Clermont-Ferrand, Laboratoire Magmas et Volcans, Clermont-Ferrand, France: 10.-13.10.2007 (RITA^{*A})

BORGHINI, G., Università degli Studi di Genova, Dipartimento per lo Studio del Territorio e delle sue Risorse, Genova, Italy: 10.-12.10.2007 (RITA^{*A})

BROMILEY, G., University of Cambridge, Department of Earth Sciences, Cambridge, U.K.: *"The stability of TiO_2-rich phases during deep subduction of oceanic crust"*, 11.-19.06.2007 (RITA^{*A})

BUITER, S.J.H., Geological Survey of Norway, Trondheim, Norway: 12.-15.06.2007 (c2c[*C])

CADEK, O., Charles University, Department of Geophysics, Prague, Czech Republic: 10.-11.06.2007 (c2c[*C])

CALICCHIO, M., Istituto dei Materiali per l'Elettronica ed il Magnetismo, CNR, Fontanini-Parma, Italy: *"Densification of germanium dioxide"*, 28.10.-09.11.2007 (RITA[*A])

CASTILLO, E., Universidad Complutense de Madrid, Departamento de Quimica Inorganica I, Madrid, Spain: *"High pressure synthesis of perovskite based materials"*, 20.-27.11.2007 (RITA[*A])

CHAMORRO PEREZ, E., ENS-Lyon, Laboratoire Sciences Terre, Lyon, France: 10.-11.10.2007 (RITA[*A])

CERNIK, B., University of Manchester, School of Materials, Manchester, U.K.: *"Causes and effects of multiferroic behaviour in perovskite materials"*, 02.-09.07.2007 (RITA[*A])

COMBES, R., Université de Marne-la-Vallée, Laboratoire des Géomatériaux, Marne-la-Vallée, France: *"Evolution of the enstatite chondrite EH4 indarch at high pressure and temperature: New constraints for early planetary differentiation"*, 09.-16.07.2007 (RITA[*A])

COMODI, P., Università degli Studi di Perugia, Dipartimento di Scienze della Terra, Perugia, Italy: *"HP-HT behaviour of gypsum: a spectroscopic and diffractometric study"*, 09.-13.07.2007 (RITA[*A])

COMODI, P., Università degli Studi di Perugia, Dipartimento di Scienze della Terra, Perugia, Italy: 10.-12.10.2007 (RITA[*A])

CONNOLLY, J.: ETH Zürich, Institut für Mineralogie und Petrographie, Zürich, Switzerland: 06.-08.06.2007 (c2c[*C])

CORDIER, P., Université des Sciences et Technologies de Lille, Laboratoire de Structure et Propriétés de l'Etat Solide, Villeneuve d'Ascq, France: "*Plastic deformation experiments of garnets and pyroxenes at high pressure using the D-DIA*", 16.-28.07.2007 (RITA[*A])

DACHS, E., Universität Salzburg, Geographie, Geologie und Mineralogie, Salzburg, Austria: *"Low-temperature calorimetry on milligram-sized mineralogical samples: The method"*, *"Calorimetry of aluminosilicate minerals"*, 04.-06.07.2007 (ENB[*D])

DE KOKER, N., University of Michigan, Department of Geological Sciences, USA: 18.-23.12.2007 (c2c[*C])

DEMENET, J.-L., CNRS/University of Poitiers, UFR Sciences SP2MI, Chasseneuil Futuroscope, France: 10.-12.10.2007 (RITA[*A])

DOBRZHINETSKAYA, L., University of California at Riverside, Department of Earth Sciences, Riverside, USA: 16.-18.09.2008 (DFG[*E])

DOBSON, D., University College London, Department of Earth Sciences, London, U.K.: *"Synthesis of wadsleyite samples for hydrogen diffusion experiments"*, 08.-10.10.2007, 09.-15.12.2007 (RITA[*A])

DOBSON, D., University College London, Department of Earth Sciences, London, U.K.: 11.-13.10.2007 (RITA[*A])

EREMETS, M., Max-Planck-Institut für Chemie, Mainz, Germany: 23.-24.04.2007 (DFG[*E])

FAIT, A., Basell Poliolefine Italia srl, "Giulio Natta" Research Centre, Ferrara, Italy: *"High pressure crystallization of demicrystalline polypropylene"*, 17.-21.12.2007 (RITA[*A])

FARGES, F., Muséum National d'Histoire Naturelle de Paris, France: *"Scanning transmission X-ray microscopy (STXM): a new tool for minerals, glasses and environmental samples"*, *"Glass durability and its weathering"*, 07.-11.05.2007 (ENB[*D])

FORTUNATI, A., Università di Camerino, Dipartimento di Scienze della Terra, Camerino, Italy: *"Plagioclase growth kinetics during decompression of hydous basaltic melts and applications to magma dynamics within Stromboli and Etna"*, 27.08.-12.09.2007 (RITA[*A])

GATTA, G.D., Università degli Studi di Milano, Dipartimento di Scienze della Terra, Milano, Italy: *"Single crystal X-ray diffraction of magnetite Fe_3O_4 at high pressures"*, 15.-24.08.2007 (RITA[*A])

GATTA, G.D., Università degli Studi di Milano, Dipartimento di Scienze della Terra, Milano, Italy: *"Elastic behaviour and P-induced structure evolution of leucite, $K_{16}Al_{16}Si_{32}O_{96}$"*, 25.08.-04.09.2007 (RITA[*A])

GATTA, G.D., Università degli Studi di Milano, Dipartimento di Scienze della Terra, Milano, Italy: 10.-14.10.2007 (RITA[*A])

GKONTELITSAS, A., University of Athens, Department of Mineralogy and Petrology, Athens, Greece: *"Transmission electron microscopic and spectroscopic study of diamondiferous ultrahigh-pressure (UHP) rocks from northern Greece"*, 11.-22.12.2007 (RITA[*A])

GREENBERG, E., Tel Aviv University, School of Physics & Astronomy, Tel Aviv, Israel: *"The effect of pressure-induced electronic transitions upon the crystallographic structure of S=5/2 transition-metal compounds "*, 01.-21.07.2007 (RITA[*A])

GREENBERG, E., Tel Aviv University, School of Physics & Astronomy, Tel Aviv, Israel: 10.-13.10.2007 (RITA[*A])

HUNT, S., University College London, Department of Earth Sciences, London U.K.: *"Deformation of garnet at high pressure and temperature"*, 28.02.-16.03.2007, 09.-23.11.2007 (RITA[*A])

HUNT, S., University College London, Department of Earth Sciences, London U.K.: 10.-13.10.2007 (RITA[*A])

JOCHYM, P., Polish Academy of Sciences, Institute of Nuclear Physics, Krakow, Poland: 18.-22.06.2007 (c2c[*C])

JUHIN, A., IMPMC, CNRS - UMR, Paris, France: *"High pressure multianvil synthesis of $Mg_3Cr_2Si_3O_{12}$ garnet"*, 25.11.-03.12.2007 (RITA[*A])

JUNG, D., ETH Zürich, Laboratorium für Kristallographie, Zürich, Switzerland: 28.02.-02.03.2007 (c2c[*C])

KOSTOPOULOS, D., University of Athens, Department of Mineralogy and Petrology, Athens, Greece: *"Transmission electron microscopic and spectroscopic study of diamondiferous ultrahigh-pressure (UHP) rocks from northern Greece"*, 11.-22.12.2007 (RITA[*A])

KURAKEVYCH, O., Université Paris Nord, LPMTM-CNRS, Institut Galilée, Villetaneuse, France: *"High-pressure – high-temperature synthesis and studies of nanocrystalline superhard phases in the B-N system"*, 17.06.-05.07.2007 (RITA[*A])

LIANG, Y., Scuola Internazionale Superiore di Studi Avanzati (SISSA), Trieste, Italy: 27.-30.06.2007 (c2c[*C])

MANNING, C., University of California, Department of Earth & Space Sciences, Los Angeles, USA: *"In Deep Water: On the novel chemistry of high-pressure fluids and their role in geologic processes", "Are any elements immobile in high-pressure geologic fluids?"*, 25.02.-01.03.2007 (ENB[*D])

MARTIN, A., University of Otago, Department of Geology, Dunedin, New Zealand: *"Mantle redox conditions beneath Antarctica"*, 15.11.-31.12.2007 (AtG[*B])

MASSONNE, H.-J., Universität Stuttgart, Institut für Mineralogie und Kristallchemie, Stuttgart, Germany: 26.-28.10.2007 (c2c[*C])

MAZZULLO, S., Basell Poliolefine Italia srl, "Giulio Natta" Research Centre, Ferrara, Italy: *"High pressure crystallization of demicrystalline polypropylene"*, 17.-21.12.2007 (RITA[*A])

MCENROE, S., Geological Survey of Norway, Trondheim, Norway: *"The ilmenite-hematite solid solution, magnetic properties, exsolution and chemical ordering: constraints from synthetics samples"*, 11.-20.02.2007 (RITA[*A])

MCENROE, S., Geological Survey of Norway, Trondheim, Norway: 09.-13.10.2007 (RITA[*A])

MUŇOZ JOLIS, E., Royal Holloway, University of London, U.K.: *"Geochemistry of Húsafell central volcano, Iceland"*, 18.-21.11.2007 (ENB[*D])

NAVROTSKY, A. University of California at Davis, USA: *"New adventures in mineral calorimetry: an overview", "Thermochemistry of environmentally important minerals"*, 01.-06.04.2007 (ENB[*D])

NAZZARENI, S., Università degli Studi di Perugia, Dipartimento di Scienze della Terra, Perugia, Italy: *"HP-HT behaviour of gypsum: a spectroscopic and diffractometric study"*, 10.-27.07.2007 (RITA[*A])

NAZZARENI, S., Università degli Studi di Perugia, Dipartimento di Scienze della Terra, Perugia, Italy: 10.-12.10.2007 (RITA[*A])

NESTOLA, F., Università degli Studi di Padova, Dipartimento di Mineralogia e Petrologia, Padova, Italy: *"High-pressure phase transitions along the $LiAlSi_2O_6$-$LiGaSi_2O_6$ solid solution"*, 09.-31.07.2007 (RITA[*A])

PARMAN, S., Durham University, Department of Earth Sciences, Durham, U.K.: *"Piston cylinder, capsule gas-loading device, FEG-SEM"*, 23.06.-21.07.2007, 27.11.-05.12.2007 (RITA[*A])

PARVIAINEN, A., Helsinki University of Technology, Helsinki, Finland: *"Occurrence, mineralogy and geochemistry of heavy metals in the tailings of the Haveri mine, Southern Finland"*, 27.06.-03.07.2007 (RITA[*A])

PETFORD, N., Bournemouth University, Dorset, U.K.: 10.-12.10.2007 (RITA[*A])

PICKLES, J., University of Bristol, Department of Earth Sciences, Bristol, U.K.: *"Lower mantle to upper mantle: The back reaction and redox relations during mantle upwelling and avalanche"*, 01.11.-31.12.2007 (AtG[*B])

POE, B., Università degli Studi "G. d'Annunzio", Chieti, Italy: *"Effect of dissolved H_2O on the electrical conductivity of single crystal olivine"*, 26.02.-05.03.2007 (RITA[*A])

POMPILIO, M., Istituto Nazionale di Geofisica e Vulcanologia, Pisa, Italy: 10.-13.10.2007 (RITA[*A])

PRAKAPENKA, V., Argonne National Laboratory, Argonne, USA: 23.-27.04.2007 (AtG[*B])

RABIER, J., CNRS/University of Poitiers, UFR Sciences SP2MI, Chasseneuil Futuroscope, France: 10.-12.10.2007 (RITA[*A])

RABIER, J., CNRS/University of Poitiers, UFR Sciences SP2MI, Chasseneuil Futuroscope, France: *"Dislocations in elemental semi conductors below the Brittle to Ductile Transition (BDT) temperature"*, 09.-15.12.2007 (RITA[*A])

RICHET, P., Institut de Physique du Globe de Paris, France: *"Water an elusive oxide in silicate melts?"*, *"Atomic dynamics in silicate melts: Effects of temperature and of the structural role of cations"*, 27.-29.11.2007 (ENB[*D])

ROBINSON, P., Geological Survey of Norway, Trondheim, Norway: *"The ilmenite-hematite solid solution, magnetic properties, exsolution and chemical ordering: constraints from synthetics samples"*, 04.-10.02.2007 (RITA[*A])

ROZENBERG, G., Tel Aviv University, School of Physics & Astronomy, Tel Aviv, Israel: *"The effect of pressure-induced electronic transitions upon the crystallographic structure of S=5/2 transition-metal compounds "*, 01.-21.07.2007 (RITA[*A])

ROZENBERG, G., Tel Aviv University, School of Physics & Astronomy, Tel Aviv, Israel: 10.-13.10.2007 (RITA[*A])

SANLOUP, C., University of Edinburgh, Earth Sciences, Edinburgh, U.K.: 10.-12.10.2007 (RITA[*A])

SERGHIOU, G., University of Edinburgh, The School of Engineering and Electronics, Edinburgh, U.K.: 10.-13.10.2007 (RITA[*A])

SHEKHAR, S., Indian Institut of Technology, Kharagpur, India: 01.06.-15.07.2007 (RITA[*A])

SHINOVA, E., Bulgarian Academy of Sciences, Institute of General and Inorganic Chemistry, Sofia, Bulgaria: 10.-13.10.2007 (RITA[*A])

SKÁLA, R., Friedrich-Schiller-Universität Jena, Institut für Geowissenschaften, Bereich Mineralogie, Jena, Germany: 10.-13.10.2007 (RITA[*A])

SOLOZHENKO, V., Université Paris Nord, LPMTM-CNRS, Institut Galilée, Villetaneuse, France: *"High-pressure – high-temperature synthesis and studies of nanocrystalline superhard phases in the B-N system"*, 17.06.-05.07.2007 (RITA[*A])

SOLOZHENKO, V., Université Paris Nord, LPMTM-CNRS, Institut Galilée, Villetaneuse, France: 10.-13.10.2007 (RITA[*A])

STEVENSON, D., California Institute of Technology, Geological & Planetary Sciences, Pasadena, USA: *"What is going on at the core-mantle boundary?"*, 19.-21.09.2007 (ENB[*D])

STIXRUDE, L., University of Michigan, Department of Geological Sciences, Ann Arbor, USA: *"Silicate liquids in planetary interiors"*, 11.-12.09.2007 (ENB[*D])

TALYZIN, A., Umeå University, Experimental Physics, Umeå, Sweden: *"New carbon nanomaterilas by high-temperature high-pressure exfoliation"*, 08.-10.10.2007 (RITA[*A])

TALYZIN, A., Umeå University, Experimental Physics, Umeå, Sweden: 11.-13.10.2007 (RITA[*A])

TARANTINO, S., Università degli Studi di Pavia, Dipartimento di Scienze della Terra, Pavia, Italy: *"Pressure effect on the crystal structure of tapiolite $FeTa_2O_6$"*, 26.09.-09.10.2007 (RITA[*A])

TARANTINO, S., Università degli Studi di Pavia, Dipartimento di Scienze della Terra, Pavia, Italy: 10.-13.10.2007 (RITA[*A])

THRALL, M., University of Manchester, School of Materials, Manchester, U.K.: *"Causes and effects of multiferroic behaviour in perovskite materials"*, 02.-09.07.2007 (RITA[*A])

VAN MIERLO, W., Utrecht University, Faculty of Geosciences, Utrecht, The Netherlands: 09.-12.12.2007 (c2c[*C])

WALTER, M., University of Bristol, Department of Earth Sciences, Bristol, U.K.: 09.-12.10.2007 (RITA[*A])

WEIGEL, C., Institut de Minéralogie et de Physique des Milieux Condensés (IMPMC), Paris, France: 23.-27.04.2007 (AtG[*B])

WOOD, B., Oxford University, Department of Earth Sciences, Oxford, U.K.: *"The effects of core formation on the Pb- and Tl- isotopic composition of the silicate Earth"*, 16.-24.11.2007 (RITA[*A])

WORTMANN, G., Universität Paderborn, Department of Physics, Paderborn, Germany: 14.-16.03.2007 (DFG[*E])

YUEN, D., University of Minnesota, Department of Geology and Geophysics, Minneapolis, USA: *"How can the double crossings of the post-perovskite transition constrain the heat flux from the core?"*, *"Interactive visualization and monitoring of 3-D mantle convection"*, 23.-26.09.2007 (ENB[*D])

ZALITE, I., Riga Technical University, Institute of Inorganic Chemistry, Riga, Latvia: *"Use of high pressure hot pressing equipment for fabricating of nanostructured ceramics materials"*, 13.-26.05.2007 (RITA[*A])

ZALITE, I., Riga Technical University, Institute of Inorganic Chemistry, Riga, Latvia: 10.-13.10.2007 (RITA[*A])

ZARECHNAYA, E., Moscow State Institute of Steel and Alloys, Theoretical Physics Department, Moscow, Russia: *"Ab initio computations on B-doped diamonds"*, 01.01.-01.03.2007 (AtG[*B])

ZARECHNAYA, E., Moscow State Institute of Steel and Alloys, Theoretical Physics Department, Moscow, Russia: 22.-26.04.2007 (AtG[*B])

ZEMA, M., Università degli Studi di Pavia, Dipartimento di Scienze della Terra, Pavia, Italy: *"Pressure effect on the crystal structure of columbite minerals"*, 21.01.-11.02.2007 (RITA[*A])

ZEMA, M., Università degli Studi di Pavia, Dipartimento di Scienze della Terra, Pavia, Italy: 10.-12.10.2007 (RITA[*A])

[*A)] RITA: EU "Research Infrastructures: Transnational Access" Programme

[*B)] AtG: EU Marie Curie Actions "Atomic to Global" Training Programme

[*C)] c2c: EU Marie Curie Research Training Network - the fate of subducted material

[*D)] ENB: International Graduate School under the Elitenetzwerk Bayern

[*E)] DFG: Deutsche Forschungsgemeinschaft

6.3 Visitors (externally funded)

ABAKUMOV, A., University of Antwerp, EMAT: Electron Microscopy for Materials Science, Antwerp, Belgium: 15.-17.07.2007

ASAHARA, Y., JASRI, Hyogo, Japan: 22.-29.09.2007

BABUSHKIN, A., Ural State University, Russia: 19.11.-02.12.2007

BARSUKOVA, T., TU Bergakademie Freiberg, Germany: 06.-10.08.2007

BESTMANN, M., Universität Erlangen-Nürnberg, Lehrstuhl Geologie, Erlangen, Germany: 04.05.2007, 30.07.2007

ESCUDERO, A., Friedrich-Schiller-Universität Jena, Institut für Geowissenschaften, Bereich Mineralogie, Jena, Germany: 11.10.2007

FERROIR, T., ENS Lyon, France: 20.-27.05.2007

GANSKOW, G., Friedrich-Schiller-Universität Jena, Institut für Geowissenschaften, Bereich Mineralogie, Jena, Germany: 10.-12.01.2007, 05.-09.02.2007, 01.03.2007, 23.-27.04.2007, 18.-22.06.2007, 03.-07.12.2007

GROSS, T., Technische Universität Darmstadt, Fachbereich Materialwissenschaft, Darmstadt, Germany: 15.-19.01.2007, 23.-27.07.2007

HOPF, J., Friedrich-Schiller-Universität Jena, Institut für Geowissenschaften, Bereich Mineralogie, Jena, Germany: 23.-24.07.2007

JACOBSEN, S., Northwestern University, Department of Geological Sciences, Evanston, USA: 14.-21.03.2007

JUNG, A., Forschungszentrum Karlsruhe, Germany: 02.-04.05.2007

KEGLER, P., Universität Köln, Germany: 18.-21.05.2007

KLEIN, R., Gesellschaft für Schwerionenforschung mbH, Darmstadt, Germany: 15.-16.01.2007, 26.-28.02.2007, 02.-05.07.2007

KOMATSU, K., The University of Edinburgh, School of Physics, Edinburgh, U.K.: 30.05.-02.06.2007

KONRAD-SCHMOLKE, M., Universität Potsdam, Institut für Geowissenschaften, Germany: 25.-28.01.2007

KONZETT, J., Universität Innsbruck, Institut für Mineralogie und Petrographie, Innsbruck, Austria: 15.-28.02.2007, 24.09.-05.10.2007

LITVIN, Y.A., Russian Academy of Sciences, Institute of Experimental Mineralogy, Chernogolovka, Russia: 25.03.-16.04.2007

LOCHERER, T., Technische Universität Darmstadt, Fachbereich Materialwissenschaft, Darmstadt, Germany: 15.-19.01.2007, 23.-29.07.2007

MARQUARDT, H., GeoForschungsZentrum Potsdam, Germany: 03.12.2007

MILETICH, R., Universität Heidelberg, Mineralogisches Institut, Heidelberg, Germany: 23.-24.07.2007

NESTOLA, F., Università degli Studi di Padova, Dipartimento di Mineralogia e Petrologia, Padova, Italy: 28.02.-03.03.2007

NIKOLAEV, I., University of Antwerp, EMAT: Electron Microscopy for Materials Science, Antwerp, Belgium: 15.-17.07.2007

POLLOK, K., Friedrich-Schiller-Universität Jena, Institut für Geowissenschaften, Bereich Mineralogie, Jena, Germany: 01.03.2007, 12.-13.04.2007

REICHMANN, H.-J., GeoForschungsZentrum Potsdam, Germany: 03.12.2007

SANO, A., University of Tokyo, Japan: 30.05.-02.06.2007

SCHWARZ, M., TU Bergakademie Freiberg, Germany: 09.-10.08.2007, 12.-16.11.2007

SCHOLLENBRUCH, K., Johann Wolfgang Goethe-Universität Frankfurt/M., Institut für Geowissenschaften, Frankfurt/M., Germany: 02.07.2007, 22.10.-04.11.2007

SCHUSTER, B., Gesellschaft für Schwerionenforschung mbH, Darmstadt, Germany: 15.-16.01.2007, 26.-28.02.2007

SHEKHAR, S., Indian Institut of Technology, Kharagpur, India: 16.-28.10.2007

STOYANOV, E., Friedrich-Schiller-Universität Jena, Institut für Geowissenschaften, Bereich Mineralogie, Jena, Germany: 07.-08.02.2007

TALYZIN, A., Umeå University, Experimental Physics, Umeå, Sweden: 28.02.-06.03.2007

TERRY, M., South Dakota School of Mines & Technology, Rapid City, USA: 16.07.-04.08.2007

VOLKOVA, Y., Ural State University, Russia: 19.11.-02.12.2007

WIOSNA, I., Universität Köln, Germany: 18.-21.05.2007

WOODLAND, A., Johann Wolfgang Goethe-Universität Frankfurt/M., Institut für Geowissenschaften, Frankfurt/M., Germany: 02.07.2007

ZACHARIAS, J., Charles University, Prague, Czech Republik: 07.-08.11.2007

ZERR, A., Université Paris Nord, France: 17.-18.07.2007

ZEMA, M., Università degli Studi di Pavia, Dipartimento di Scienze della Terra, Pavia, Italy: 25.09.-09.10.2007

ZVORISTE, C., Technische Universität Darmstadt, Fachbereich Materialwissenschaft, Darmstadt, Germany: 17.-21.09.2007, 19.-23.11.2007

7. Additional scientific activities

7.1 Ph.D. theses

KANTOR, I.Yu.: High-pressure and high-temperature structural and electronic properties of (Mg,Fe)O and FeO

LIU, J.: (Na,K) Aluminosilicate Hollandites: Structures, crystal chemistry, and high-pressure behaviour

SCHMAUß-SCHREINER, D.: Experimental studies on the adsorption of SO_2 on volcanic ashes

7.2 Honours and awards

David DOLEJŠ	received the Albert Maucher award in geosciences of the German Science Foundation (Deutsche Forschungs-gemeinschaft) for outstanding scientific results
David DOLEJŠ	received the Innolec Lectureship award of the Masaryk University (Brno, Czech Republic) as an outstanding international visiting scientist
Innokenty KANTOR	received the E.ON Bavaria Cultural Award 2007 for his outstanding experimental work
Catherine MCCAMMON	was elected a *Geochemistry Fellow* of the Geochemical Society and the European Association for Geochemistry
Ashima SAIKIA	received the best poster award at the 7th Mineral Physics Seminar in Matshushima, Japan
Friedrich SEIFERT	was elected foreign member of the Italian Accademia Nazionale dei Lincei, Rome

7.3 Editorship of scientific journals

DOLEJŠ, D.	Editorial Advisory Board of "Journal of Geosciences"
DUBROVINSKY, L.S.	Member of the Editorial Board of the "High Pressure Research - International Journal"
FROST, D.J.	Associate Editor "Geophysical Research Letters"
HEIDELBACH, F.	Associate Editor "American Mineralogist"
KEPPLER, H.	Editorial Advisory Board "Elements"
	Editorial Board "Contributions to Mineralogy and Petrology"
MCCAMMON, C.A.	Editor "Physics and Chemistry of Minerals"
RUBIE, D.C.	Editor-in-Chief "Physics of the Earth and Planetary Interiors"

7.4 Membership of scientific advisory bodies

DUBROVINSKY, L.S.	Elected Chair of the Special Interest Group "Crystallography at extreme conditions" of the European Crystallography Union
KEPPLER H.	Chairman, Research Council of the German Mineralogical Society (Forschungskollegium Mineralogie der DMG) Member, Abraham Gottlob Werner Medal Committee, German Mineralogical Society (DMG) Member, Nominating Committee for Officers, Mineralogical Society of America Member, Commission for Research of Bayreuth University (Präsidialkommission für Forschung und wissenschaftlichen Nachwuchs)
MCCAMMON, C.A.	IMA Medal Committee of the International Mineralogical Association Fellows Committee of the Volcanology, Geochemistry & Petrology Section of the American Geophysical Union Executive Committee of the Mineral and Rock Physics Focus Group of the American Geophysical Union Advisory Board of "Mössbauer Information Exchange" International Advisory Board of the Mössbauer Effect Data Center
RUBIE, D.C.	Member of AGU Mineral and Rock Physics Executive Committee Chair of AGU Mineral and Rock Physics Awards Committee Member of Dana Medal Committee, Mineralogical Society of America Member of Forschungskollegium Physik des Erdkörpers (FKPE)

8. Scientific and Technical Personnel

Name		Position	Duration in 2007	Funding source
ADJAOUD, Omar	M.Sc. (Physics)	Wiss. Mitarbeiter		BGI/IGS
AREFIN, Mohammad Lutful	M.Sc. (Nanomaterials)	Wiss. Mitarbeiter		BGI/IGS[1]
AUDÉTAT, Andreas	Dr.	Wiss. Assistent		BGI
BALI, Enikö	Dr.	Wiss. Angestellte		BGI/VP
BAUMGARTNER, Alexander	Dipl.-Chem.	Wiss. Mitarbeiter		BGI/IGS[2]
BEHRINGER, Nicole	Reg. Inspektorin	Verwalt. Beamtin		BGI
BERNINI, Diego	Dipl.-Geol.	Gastwissenschaftler	from 07.05.	EU
BÖHM, Ulrich		Mechaniker		BGI
BOFFA BALLARAN, Tiziana	Dr.	Akad. Rätin		BGI
BUCHERT, Petra		Fremdsprachen-sekretärin		BGI
CARACAS, Razvan	Dr.	Wiss. Angestellter	to 31.03.	BGI/VP
DITTMANN, Uwe		Präparator	from 01.01.	BGI
DOLEJŠ, David	Dr.	Wiss. Angestellter		BGI/IGS
DUBROVINSKY, Leonid	PD Dr.	Akad. Oberrat		BGI
EL GORESY, Ahmed	Prof. Dr.			BGI/VP[3]
FISCHER, Heinz		Mechaniker		BGI
FROST, Daniel	Dr.	Akad. Direktor from 01.10.		BGI
GAVRILENKO, Polina	Dipl.-Geol.	Wiss. Mitarbeiterin		BGI/IGS
GOLLNER, Gertrud		Chem.-Techn. Assistentin		BGI
GUDFINNSSON, Gudmundur	Dr.	Wiss. Angestellter	01.01.-31.03. 01.04.-30.11. 01.12.-31.12.	EU BGI EU
HEIDELBACH, Florian	Dr.	Wiss. Mitarbeiter		EU
HERRMANN, Elisabeth	MTA	Chem.-Techn. Assistentin		BGI
HOLBIG, Eva	Dipl.-Min.	Wiss. Mitarbeiterin		BGI/IGS
HUANG, Xianliang	M.E. (Material Science)	Wiss. Mitarbeiter		BGI/IGS[1]
IRIFUNE, Tetsuo	Prof.	Foschungspreisträger	01.07.-23.09.	AvH
KANTOR, Anastasia	Cand. of Science	Wiss. Angestellte	01.01.-24.05. 25.05.-24.08. from 16.12.	DFG Industry DFG
KANTOR, Innokenty	Dr.	Wiss. Angestellter	01.01.-31.08. from 15.12.	DFG Industry
KEPPLER, Hans	Prof. Dr.	Leiter		BGI
KESHAV, Shantanu	Dr.	Wiss. Angestellter		BGI/VP

KEYSSNER, Stefan	Dr.	Akad. Oberrat		BGI
KISON-HERZING, Lydia		Sekretärin		BGI
KLASINSKI, Kurt	Dipl.-Ing. (FH)	Techn. Angestellter		BGI
KONSCHAK, Alexander	Dipl.-Geol.	Wiss. Angestellter	01.01.-28.02.	BGI/VP
			01.03.-30.09.	DFG
			01.10.-31.12.	BGI/VP
KRAUßE, Detlef	Dipl.-Inform. (FH)	Techn. Angestellter		BGI
KRIEGL, Holger		Haustechniker		BGI
KUMBAR, Suresh	M.Sc. (Inorg. Chem.)	Wiss. Mitarbeiter		BGI/IGS[2]
KURNOSOV, Alexander	Dr.	Wiss. Angestellter		BGI/VP
LEE, Kanani	Dr.	Stipendiatin	14.06.-11.08.	AvH[4]
LINHARDT, Sven		Elektrotechniker		BGI
LIU, Jun	Dipl.-Min.	Wiss. Angestellte	01.01.-31.07.	DFG
			01.08.-30.11.	BGI/VP
LONGO, Micaela	Dipl.-Min.	Gastwissenschaftlerin		EU
MANN, Ute	Dipl.-Geol.	Wiss. Mitarbeiterin		BGI/IGS
MCCAMMON, Catherine	Dr.	Akad. Oberrätin		BGI
MIYAJIMA, Nobuyoshi	Dr.	Akad. Rat a.Z.		BGI
NARYGINA, Olga	M.Sc. (Physics)	Wiss. Angestellte		DFG
POTZEL, Anke		Chem.-Techn. Assistentin		BGI
RAMMING, Gerd		Elektroniker		BGI
RAUSCH, Oliver		Mechaniker		BGI
ROSCHER Elisabeth		Wissensch. Techn. Assistentin		BGI
RUBIE, David C.	Prof. Dr.	Stellvertr. Leiter		BGI
SAIKIA, Ashima	M.Sc. (Geol.)	Wiss. Mitarbeiterin		BGI/IGS
SAMUEL, Henri	Prof. Dr.	Juniorprofessor	from 15.10.	Stiftung[5]
SCHIAVI, Federica	Dr.	Wiss. Mitarbeiterin	from 15.08.	BGI/VP
SCHULZE, Hubert		Präparator		BGI
SHCHEKA, Svyatoslav	Dr.	Wiss. Angestellter	01.01.-30.06.	DFG[4]
			01.07.-31.12.	BGI/VP
STAGNO, Vincenzo	Dipl.-Geol.	Stipendiat	12.03.-31.08.	SINTESI[6]
		Gastwissenschaftler	from 01.10.	EU
STEINLE-NEUMANN, Gerd	Dr.	Akad. Rat		BGI
TANG, Zhengning	M.E. (Material Science)	Gastwissenschaftler		EU
TSUNO, Kyusei	Dr.	Wiss. Mitarbeiter	from 19.03.	DFG/ BGI/VP
ÜBELHACK, Stefan		Mechaniker		BGI
WALTE, Nicolas	Dipl.-Geol.	Wiss. Angestellter	01.01.-31.05.	DFG
			01.06.-30.11.	BGI
			01.12.-31.12.	DFG
WEIGEL, Coralie	Dr.	Wiss. Angestellte	from 01.11.	DFG

WESTON, Lesley	Dr.	Wiss. Angestellte	01.03.-31.08. from 01.09.	DFG BGI/VP
WU, Xiang	Dr.	Forschungsstipendiat	from 23.08.	AvH
XIONG, Xiaolin	Ph.D.	Stipendiat	to 01.10.	China[7]
YELAMANCHILI, Ram Sai	Dipl.-Chem.	Wiss. Mitarbeiter		BGI/IGS[2]
ZARECHNAYA, Evgeniya	M.Sc.	Wiss. Mitarbeiterin	from 01.08.	BGI/VP

Abbreviations/explanations:

AvH	Alexander von Humboldt Foundation
BGI	Staff Position of Bayerisches Geoinstitut
BGI/VP	Visiting Scientists' Program of Bayerisches Geoinstitut
DFG	German Science Foundation
EU	European Union
IGS	International Graduate School under the Elitenetzwerk Bayern "Structure, Reactivity and Properties of Oxide Materials"

[1] Fraunhofer ISC Würzburg

[2] Chair of Inorganic Chemistry I, Prof. Breu

[3] partially funded by the Visiting Scientists' Program of Bayerisches Geoinstitut

[4] Summer Research Fellowship for U.S. Scientists and Scholars

[5] Juniorprofessorship for Geodynamic Modeling funded by Stifterverband für die Deutsche Wissenschaft

[6] funded by the Leonardo da Vinci programme of SINTESI (SINergie TEcnologiche in SIcilia) – Università degli Studi di Palermo

[7] Fellowship by the China Scholarship Council of the People's Republic of China

Index